UNIVERSITY OF SOUTHAMPTON

FACULTY OF NATURAL AND ENVIRONMENTAL SCIENCES

School of Chemistry

Preparation and Characterisation of Fluorescent Mesoporous Surfaces: Towards the Study of Extracellular Fluxes

by

Victor Lethuillier

Thesis for the degree of Doctor of Philosophy

September 2018

UNIVERSITY OF SOUTHAMPTON

ABSTRACT

FACULTY OF NATURAL AND ENVIRONMENTAL SCIENCES

Chemistry

Thesis for the degree of Doctor of Philosophy

PREPARATION AND CHARACTERISATION OF FLUORESCENT MESOPOROUS SURFACES: TOWARDS THE STUDY OF EXTRACELLULAR FLUXES

Victor Lethuillier

This thesis describes the efforts made toward developing new structured surfaces. These new structured and modified surfaces presented are of great potential interest in the detection of cellular flux. They also provide an interesting synthetic challenge due to the requirement for the synthesis of complex multi-functional molecules and their immobilisation on a surface. The project also presents a challenge in terms of multidisciplinarity, as many different techniques from different areas of science need to be understood and applied.

The structured surfaces were deposited using a method developed by Alain Walcarius: Electrochemically assisted self-assembly (EASA). Fluorescent dyes, chosen to respond to a typical cellular flux, were synthesised and covalently attached onto the deposited surface. This report presents the synthesis of nine dyes, which can respond to pH, K^+ or Zn^{2+}.

The nine dyes were attached on the structured surfaces, the surfaces were characterised (cyclic voltammetry, Raman spectroscopy, microscopy) and its properties determined (pK_a, quantum yield, selectivity). Ultimately, fluorescent microscopy will give numerous different possibilities for biological analysis. The future work will be to focus on growing cells on the surfaces and validate our methodology by studying the fluorescent response of the surface towards extracellular fluxes.

Table of Contents

Table of Contents ..... **i**
Table of Figures ..... **iii**
Academic Thesis: Declaration Of Authorship ..... **ix**
Acknowledgements ..... **xi**
Definitions and Abbreviations ..... **xiii**
Chapter 1 Introduction **1**
1.1 Overview on extracellular fluxes 1
1.1.1 Extracellular change of pH 2
1.1.2 Extracellular change of potassium ion 4
1.1.3 Extracellular change of zinc 6
1.2 Fluorescent probes 6
1.2.1 Basics of fluorescence 6
1.2.2 Carboxyfluorescein as a pH probe 8
1.2.3 Probes specific for potassium ion 11
1.2.4 Probe specific for zinc ion 15
1.3 Mesoporous silica 17
1.4 Aim of the project 18
Chapter 2 Results and Discussion **21**
2.1 Synthesis of the probes 21
2.1.1 Naphthalic anhydride derivative 21
2.1.1.1 Initial attempts to prepare napthalic anhydride probe 21
2.1.1.2 Revised synthetic approach 24
2.1.1.3 Alternative methods for fragment coupling 29
2.1.1.4 Conclusion 32
2.2 Synthesis of probes for pH, zinc and potassium based on 5(6)-carboxyfluorescein 33
2.2.1 Modification of 5(6)-carboxyfluorescein with a linker 33
2.2.2 Separation of the isomers 34
2.2.3 Preparation of dichlorocarboxyfluorescein 35
2.2.4 Mannich reaction 39

2.2.5 Preparation of the succinimidyl ester 42

2.3 Preparation and derivatisation of the mesoporous surface 46

2.3.1 Electrodeposition of silica on ITO 46

2.3.1.1 Grazing Incidence Small Angle X-ray Scattering (GISAXS) 49

2.3.1.2 Cyclic voltammetry of the silica surfaces 52

2.3.1.3 Microscopy study of the silica substrates 54

2.3.2 Addition of the linker on the silica substrates 56

2.3.3 Attachment of the probes on the silica substrates 60

2.3.3.1 Cyclic voltammetry of the modified substrates 62

2.3.3.2 Raman analysis of the modified silica substrates 68

2.3.3.3 Determination of pK_a of the modified substrates 72

2.3.3.4 Determination of the extinction coefficient of the modified substrates 75

2.3.3.5 Determination of the quantum yield of the modified substrates 80

2.3.3.6 Determination of the selectivity of the zinc probe 84

2.3.3.7 Conclusion 86

2.3.4 Fluorescence imaging 86

2.3.5 First biological tests on the modified substrates 90

Chapter 3 Conclusion and further work 93

Chapter 4 Experimental 97

Chapter 5 References 155

Table of Figures

Figure 1-1: Cellular respiration (adapted from Enger *et al.*).[10] 3

Figure 1-2: Adenosine triphosphate (ATP). 3

Figure 1-3: Calcification process of coccolithophores (adapted from Hutchins *et al.*).[15] 4

Figure 1-4: Ionic distribution at a cell membrane. 5

Figure 1-5: Jablonski diagram..... 8

Figure 1-6: Examples of pH probes: benzo[a]phenoxazine 1.02, pyrene 1.03, rhodamine 1.04, and bodipy 1.05. 9

Figure 1-7: Fluorescein 1.06, 6-carboxyfluorescein 1.07_a and 5-carboxyfluorescein 1.07_b. 9

Figure 1-8: Ionization equilibria of fluorescein **1.06**..... 10

Figure 1-9: Schematic representation of a potassium probe. 11

Figure 1-10: “Turn-on” photo-induced electron transfer (PET) by coordination of a metal ion. 12

Figure 1-11: Commercially available probes for Na^+ (SBFI) and K^+ (PBFI)..... 13

Figure 1-12: Examples of potassium ion probes. 14

Figure 1-13: Chelation of a potassium ion. 14

Figure 1-14: Proposed of potassium probe with the receptor (in blue), the linker (in red) and the fluorophore (in green). 15

Figure 1-15: Examples of zinc probes based on fluorescein. 15

Figure 1-16: Examples of zinc probes based on coumarin. 16

Figure 1-17: Schematic representation of possible complexation of Zn^{2+}.[74]..... 16

Figure 1-18: Examples of organosilanes that can react with silica supports. 18

Figure 2-1: First target as potassium probe..... 21

Figure 2-2: Amines selected for probing properties 39

Figure 2-3: Summary of the probes prepared. 45

Table of Figures

Figure 2-4: Electrochemically-assisted self-assembly (adapted from Walcarius *et al.*).[105] 47

Figure 2-5: EASA for the preparation of non-porous silica. 48

Figure 2-6: Chronoamperograms for the electrodeposition of TEOS on two different ITO substrates: small coverslips (1.5 mm × 1.5 mm × 0.55 mm with a surface resistivity of 70-100 Ω/sq) and large coverslips (2.5 mm × 2.5 mm × 1.1 mm with a surface resistivity of 70-100 Ω/sq), in the presence and absence of the surfactant. 49

Figure 2-7: Schematic representations of (a) conventional out-of-plane θ – 2θ mode XRD, and (b) grazing incident in-plane mode XRD. (c) An illustration of the geometry used for 2D GIXD measurements. 50

Figure 2-8: In-plane GISAXS pattern of a mesoporous silica film. 51

Figure 2-9: 3-Dimentional representation of a hexagonal lattice. 52

Figure 2-10: Voltammograms recorded at an ITO substrate (yellow) and an ITO/silica substrate (1.5 mm × 1.5 mm × 0.55 mm) before (blue) and after removal of surfactant (red). CVs were recorded in a solution of $NaNO_3$ (0.1 M) and $[Ru(NH_3)_6]^{3+}$ (1 mM) from 0.2 to −0.5 V vs. SCE at a scan rate of 0.05 $V.s^{-1}$. 53

Figure 2-11: Voltammograms recorded at an ITO/silica substrate (1.5 mm × 1.5 mm × 0.55 mm) before (red) and after (blue) the deposition of a flat silica surface. CVs were recorded in a solution of $NaNO_3$ (0.1 M) and $[Ru(NH_3)_6]^{3+}$ (1 mM) from 0.2 V to −0.5 V vs. SCE at a scan rate of 0.05 $V.s^{-1}$. 54

Figure 2-12: SEM pictures of mesoporous silica substrates prepared in this work. 55

Figure 2-13: Optical microscope pictures of the ITO/silica surfaces from above. 56

Figure 2-14: (3-Aminopropyl)triethoxysilane 2.66. 56

Figure 2-15: GISAXS of the ITO/silica surface after treatment with concentrated H_2SO_4. 57

Figure 2-16: In-plane GISAXS pattern of mesoporous silica surface on ITO after treatment with APTES in EtOH. 58

Figure 2-17: Voltammograms recorded at an ITO/silica substrate (1.5 mm × 1.5 mm × 0.55 mm) before (blue) and after (red) the addition of APTES. CVs were

recorded in a solution of $NaNO_3$ (0.1 M) and $[Ru(NH_3)_6]^{3+}$ (1 mM) from 0.2 V to −0.7 V vs. SCE at a scan rate of 0.05 $V.s^{-1}$. 59

Figure 2-18: Voltammograms recorded at an ITO/silica substrate (1.5 mm × 1.5 mm × 0.55 mm) after the addition of APTES at different times after washing. CVs were recorded in a solution of $NaNO_3$ (0.1 M) and $[Ru(NH_3)_6]^{3+}$ (1 mM) from 0.2 V to −0.7 V vs. SCE at a scan rate of 0.05 $V.s^{-1}$. 60

Figure 2-19: Résumé of the probes attached on the ITO/silica surface. 61

Figure 2-20: Voltammogram recorded at an ITO/silica substrate (1.5 mm × 1.5 mm × 0.55 mm) after the addition of the 6-carboxyfluorescein derivative 1.07_a. CVs were recorded in a solution of $NaNO_3$ (0.1 M) and $[Ru(NH_3)_6]^{3+}$ (1 mM) from 0.2 V to −0.7 V vs. SCE at a scan rate of 0.05 $V.s^{-1}$. 62

Figure 2-21: Voltammogram recorded at an ITO/silica substrate (1.5 mm × 1.5 mm × 0.55 mm) after the addition of the 6-carboxyfluorescein derivative 1.07_a. CVs were recorded in a tris buffer solution (pH 7.4, 50 mM) from 0.2 V to −1.0 V vs. SCE at a scan rate of 0.05 $V.s^{-1}$. Red: first cycle, blue: following cycles. 63

Figure 2-22: Voltammogram recorded at an ITO/silica substrate (1.5 mm × 1.5 mm × 0.55 mm) after the addition of the 6-carboxyfluorescein derivative 1.07_a without linker. CVs were recorded in a tris buffer solution (pH 7.4, 50 mM) from 0.2 V to −1.0 V vs. SCE at a scan rate of 0.05 $V.s^{-1}$. 64

Figure 2-23: Voltammogram recorded at an ITO/silica substrate (1.5 mm × 1.5 mm × 0.55 mm) after the addition of anthraquinone-2-carboxylic acid. CVs were recorded in a solution of $NaNO_3$ (0.1 M) and $[Ru(NH_3)_6]^{3+}$ (1 mM) from 0.2 V to −0.7 V vs. SCE at a scan rate of 0.05 $V.s^{-1}$. 66

Figure 2-24: Voltammogram recorded at an ITO/silica substrate (1.5 mm × 1.5 mm × 0.55 mm) after the addition of anthraquinone-2-carboxylic acid. CVs were recorded in tris buffer solution (pH 7.4, 50 mM) from 0.2 V to −0.7 V vs. SCE at a scan rate of 0.05 $V.s^{-1}$. 67

Figure 2-25: Raman spectra of the 6-carboxyfluorescein substrate 2.69_a at different stages of modification. 68

Figure 2-26: *Raman spectra of:* 1) 5(6)-carboxyfluorescein crystals $1.07_{a/b}$; 2) 6-succinimidyl ester of carboxyfluorescein crystals 2.38_a. 70

Table of Figures

Figure 2-27: *Raman spectra of the derivatives attached on the ITO/silica surface*: 1) 5-Carboxy-2´,7´-dichlorofluorescein 2.70_b; 2) 6-Carboxy-2´,7´-dichloro-fluorescein 2.70_a; 3) 5-Carboxy-4',5'-bis(morpholin)-2´,7´-dichlorofluorescein 2.71_b; 4) 6-Carboxy-4',5'-bis(morpholin)-2´,7´-dichlorofluorescein 2.71_a; 5) 5-Carboxy-4',5'-bis(dipicolylamine)-2´,7´-dichlorofluorescein 2.72_b; 6) 6-Carboxy-4',5'-bis (dipicolylamine)-2´,7´-dichlorofluorescein 2.72_a. 71

Figure 2-28: pK_a determination for the morpholine substrate 2.60_b..... 72

Figure 2-29: pK_a determination for 2.60_a and $1.07_{a/b}$. 73

Figure 2-30: pK_a determination for 2.45_a and 2.45_b. 73

Figure 2-31: pK_a determination for 2.61_a and 2.61_b. 74

Figure 2-32: pK_a determination for 2.62. 74

Figure 2-33: pK_a determination for the modified surface 2.60_a and 1.07_b. 75

Figure 2-34:Determination of $\boldsymbol{\varepsilon}$ for 5(6)-carboxyfluorescein $1.07_{a/b}$. 76

Figure 2-35: Determination of $\boldsymbol{\varepsilon}$ for the morpholine derivatives. 77

Figure 2-36: Determination of $\boldsymbol{\varepsilon}$ for the zinc probes. 78

Figure 2-37: Determination of $\boldsymbol{\varepsilon}$ for the zinc probe in the presence of $ZnCl_2$ (2 mM)... 79

Figure 2-38: Determination of $\boldsymbol{\varepsilon}$ for the potassium probe in the absence (left) and presence (right) of potassium (2 mM). 80

Figure 2-39: Determination of the optimal excitation wavelength. 81

Figure 2-40: Selectivity of the zinc probes toward several metals. 85

Figure 2-41: Picture of the modified surface with 6-carboxyfluorescein 2.69_a under basic conditions (fluorescence side). 86

Figure 2-42: Effect of pH on the modified surface with 6-carboxyfluorescein 2.69_a..... 87

Figure 2-43: Effect of photobleaching on the modified surface with 6-carboxyfluorescein 2.69_a. 88

Figure 2-44: Photobleaching of the surface under fluorescent light (red circles) and normal light (black squares)..... 89

Figure 2-45: Fluorescence images of the zinc substrate 2.72_a without (left) and with zinc (right). 90

Figure 2-46: Neurons cells on the pH probe substrate 2.69_a, with A the ITO non modified and B the modified surface 91

Figure 3-1: Summary of the probes prepared. 94

Academic Thesis: Declaration Of Authorship

I, Victor Lethuillier

declare that this thesis and the work presented in it are my own and has been generated by me as the result of my own original research.

PREPARATION AND CHARACTERISATION OF FLUORESCENT MESOPOROUS SURFACES: TOWARDS THE STUDY OF EXTRACELLULAR FLUXES

I confirm that:

1. This work was done wholly or mainly while in candidature for a research degree at this University;
2. Where any part of this thesis has previously been submitted for a degree or any other qualification at this University or any other institution, this has been clearly stated;
3. Where I have consulted the published work of others, this is always clearly attributed;
4. Where I have quoted from the work of others, the source is always given. With the exception of such quotations, this thesis is entirely my own work;
5. I have acknowledged all main sources of help;
6. Where the thesis is based on work done by myself jointly with others, I have made clear exactly what was done by others and what I have contributed myself;
7. None of this work has been published before submission:

Signed: .....

Date: .....

Acknowledgements

First I would like to thank my supervisor Richard Brown for giving me the opportunity to work on a new and exciting project. Richard's guidance throughout the project has enabled me to make this research.

A lot of this project was due to the insightful teachings of my second supervisors Peter Smith Phil Bartlett and Lynda Brown. I owe them a huge thank you for the guidance and advice about electrochemistry and biology, that I knew very little.

I would like to thank all the people I work with in the lab: Alex 1, Alex 2, Alex 3, Alex 4, Rob, Gareth, David, Kathy, Sean, Azzam, Firas, Marco, Joe and I hope I didn't forget someone. Thanks also to all the people from the third flour lab.

A special thanks needs to be given to the friends I met or already know when I arrive in England making the life in Southampton much nicer with all the night out.

Thank you to John Langley and Julie Herniman for their help with the mass spectroscopy analysis and Neil Wells for help with the NMR experiments.

A big thank you for a very helpful and supportive family with all my choice.

Finally, thank you to you Marta! I met you when I arrive in England, you are probably the best thing that happened to me in Southampton. A huge thank you for all your help during this thesis, thank you for all the support even when I am a bit stupid. I am happy to stay with you for the rest of my life.

Definitions and Abbreviations

aq.	Aqueous
atm	Atmosphere
br	Broad
d	Doublet
Da	Dalton
DCC	N,N'-dicyclohexyl-carbodiimide
DCM	Dichloromethane
DIPEA	N,N'-Diisopropylethylamine
DMF	Dimethylformamide
DMSO	Dimethylsulfoxide
EI	Electron Impact
eq.	Molar equivalents
ESI	Electrospray Ionisation
FT	Fourier Transform
h	Hour(s)
HPLC	High-Performance Liquid Chromatography
HRMS	High-Resolution Mass Spectrometry
IR	Infrared
ITO	Indium Tin Oxide
J	Coupling constant
LRMS	Low-Resolution Mass Spectrometry
m (NMR)	Multiplet
m (IR)	Medium
min	Minute(s)

Definitions and Abbreviations

MS	Mass Spectrometry
MW	Molecular Weight
NBS	N-Bromosuccinimide
NMR	Nuclear Magnetic Resonance
NOESY	Nuclear Overhauser Effect Spectroscopy
PET	photo-induced electron transfer
ppm	Parts per million
Py	Pyridine
q	Quartet
rt	Room temperature
RBF	Round Bottom Flask
s (IR)	Strong
s (NMR)	Singlet
Sat.	Saturated
SCE	Saturated calomel electrode
Spt	Septet
Sxt	Sextet
t	Triplet
t	Tertiary
THF	Tetrahydrofuran
TMS	Trimethylsilyl
TLC	Thin Layer Chromatography
UV	Ultraviolet
w	Weak

Chapter 1 Introduction

1.1 Overview on extracellular fluxes

The human body is continually exposed to internal and external changes due to, for example, infectious agents or diseases. To accommodate these fluctuations, the body is required to constantly adapt making adjustments in order to maintain a constant internal environment. The changes caused by the external and internal factors in the body can be monitored and studied. Nowadays researchers have developed many ways to study the origin of diseases, the science of epidemiology. An important area of research lies in the understanding of biological processes and how they are impacted by internal and external challenges, this includes all vital processes for living organisms, such as cell growth, reproduction and nerve transmission.

All biological processes consist of biological flux and chemical reactions. Therefore, probing these fluxes leads to a better understanding of cellular biology. In living organisms, the most important fluxes occur in the intracellular and extracellular fluids. Intracellular fluids are all the fluids inside the cells, whilst the extracellular fluids lie outside the cell (interstitial fluid, plasma, lymph, cerebrospinal fluid). It is important to be able to control and understand the changes occurring in both the fluids, however in this work our focus is on probing extracellular fluxes.

The extracellular fluid differs from the intracellular fluid as in general it has a higher concentration of sodium and lower concentration of potassium ions. Cells maintain a constant environment by releasing specific substances in order to perform cellular operations. The cations (sodium, potassium, calcium and magnesium) and anions (chloride and bicarbonate) present in the body are not equally distributed. As mentioned, the intracellular fluid contains a high concentration of potassium ions, while the extracellular fluid contains large quantities of sodium and chloride ions. These solutes and ion gradients contribute to maintaining the balanced equilibrium of the fluids and the electrical potential of the cell membranes. Moreover, the extracellular fluid allows the exchange of substances between cells. Studying the fluxes occurring within this fluid and the substances released by the cells could lead to a better understanding of how biological processes are impacted by disease, leading to a better knowledge of the disease itself.

Techniques already applied to study the intracellular fluxes include: electrophysiology (using microelectrodes),[1] fluorescent indicators[2-4] and fluorescent proteins.[5] In this project we will focus on the study of the extracellular fluxes. Of the techniques that have already been developed to study extracellular flux, most are adapted from methods employed to

study intracellular fluxes such as: microelectrodes or fluorescent indicators attached to different surfaces. This work describes the use of fluorescent dyes attached to a solid surface to enable the detection of particular extracellular fluxes. The aim of this work is to grow cells on surfaces specifically designed to detect changes in extracellular pH or cations (K^+ or Zn^{2+}), to gain a better understanding of the biological processes that cause change. The following sections describe these types of fluxes in more details.

1.1.1 Extracellular change of pH

The conservation of a constant environment is very important for the body and one of the main variables to control is pH. In fact, most biological processes need a specific pH to function properly, whilst even small changes can provoke important dysfunctions. Much research has been carried out to study the influence of extracellular pH on processes or cell components such as intracellular pH,[6] cells growth[7] and potassium channels.[8]

The following examples give a better understanding of the importance of studying extracellular conditions and changes. Lardner has reviewed the effect of pH on immune functions,[9] reporting many different studies on the effect of pH and the immune system proving the direct influence of pH on immunological functions. Claiming how important these studies are, he concludes: “Hopefully, an increasing awareness of the relevance of the environmental pH surrounding immune cells and organs will encourage more research in what is undoubtedly a field ripe with research possibilities.”

Another example where the ability to study cellular pH would be important is in cellular respiration (**Figure 1-1**). Cellular respiration takes place in the cells and consists of the conversion of energy (derived from nutrient) into adenosine triphosphate (ATP, shown in **Figure 1-2**). Respiration consists of metabolic reactions and processes that break large molecules into smaller ones, releasing the energy necessary to fuel the cellular activity.

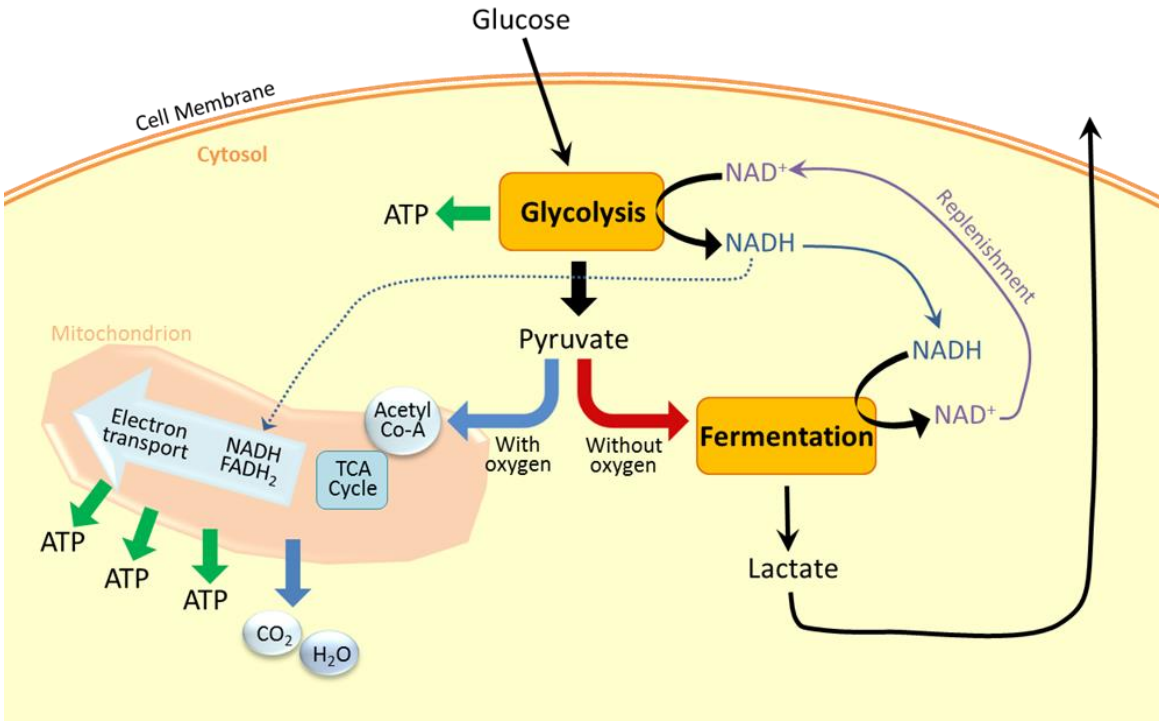

Figure 1-1: Cellular respiration (adapted from Enger *et al.*).[10]

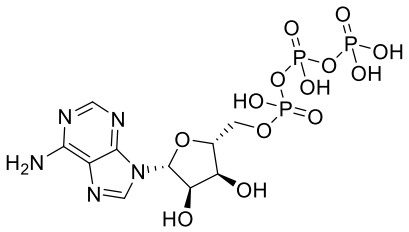

1.01

Figure 1-2: Adenosine triphosphate (ATP).

Cellular respiration is an exothermic redox reaction that releases energy (in the form of ATP), and CO_2 and lactic acid as by-products. Carbonic acid is produced by the reaction of the CO_2 with water, and lactate is formed, both these products have an influence on the surrounding pH. To maintain the environment at constant pH the body responds by releasing the excess of CO_2 for example. When all internal processes are functioning properly, the body self regulates, however when there is a problem all processes are affected and the surrounding pH around cells can change.

Finally, it could be possible to use the surfaces developed during this work to study a phenomenon linked with climate change. A type of calcifying phytoplankton organism present in the sea, called coccolithophores, are able to perform calcification. During this calcification process the cells form a coccolith made of $CaCO_3$ using atmospheric CO_2 dissolved in sea water, as shown in **Figure 1-3**. Climate change causes an increase in the acidity of the seas due to the increase of CO_2 in the atmosphere, and this will have a direct

impact on coccolithophores.[11, 12] Coccolithophores are one of the main and more abundant primary producers of organic compounds in the ocean, synthesising organic compounds from atmospheric or aqueous CO_2.[13] As such, coccolithophores play a very important role as they are part of the base of the food chain and therefore it is essential to understand how climate changes will impact on them. Techniques already exist to understand the calcification process,[14] however the surfaces produced in this work could be used to study, in real time, how coccolithophores react to pH changes, how they use the surrounding CO_2 and how the external pH is impacted.

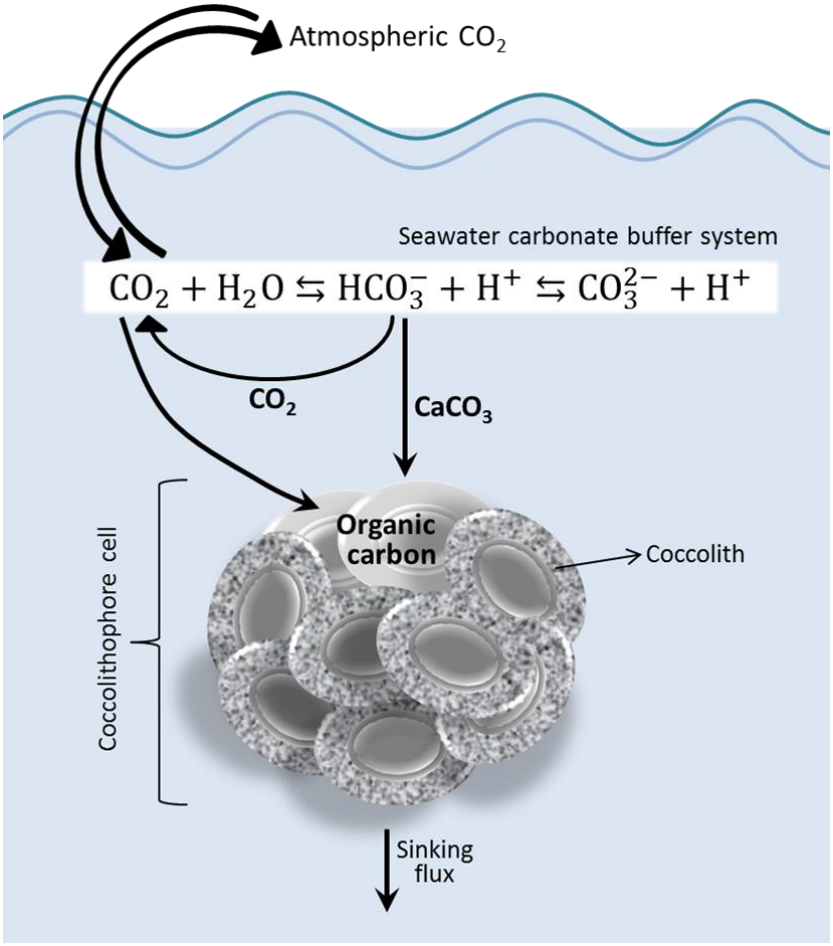

Figure 1-3: Calcification process of coccolithophores (adapted from Hutchins *et al.*).[15]

1.1.2 Extracellular change of potassium ion

The second flux of interest to this project is extracellular potassium. Most of the potassium in the human body is dispersed in the intracellular fluid, and only the 2% is present in the extracellular region. The exchange of potassium ion between intra- and extracellular space is performed by membrane transporters (K^+ channels and Na^+/K^+ -ATPase) to maintain homeostasis of potassium within the body. External agents (e.g. poisons, diseases, drugs) can interact with this process and deregulate the extracellular potassium ion concentration. A recent review presents how important optimum homeostasis is and the possible agents

impacting on a good distribution the potassium.[16] The authors describe that the movement of the ions across the membrane between the intra- and extracellular space creates the electrical properties of an excitable cell, which is what defines the membrane potential. The ability of an ion to cross the cellular membrane (called permeability) depends on the ion species and this difference has some physiological consequences. As discussed above, the ionic composition inside the cell varies from the extracellular fluid: this creates concentration gradients that contribute to the movement of ions, or flux.

The concentration of potassium ion in the extracellular fluid is normally in a range between 3.5 and 5 mM and is essential to the well-being of the membrane potential. On the other hand, the intracellular potassium has a concentration of about 160 mM. The concentrations are inverted for sodium, and there is a continuous exchange of sodium and potassium ions between the external and internal fluid in order to maintain homeostasis. The aim of this work would be to use the surfaces developed to study how the potassium ions behave in the extracellular fluid and how the cells react to external challenges. The process is depicted in **Figure 1-4**. It is immediately obvious that one of the biggest challenges will be to develop a selective probe for potassium as the concentration of sodium is about 40 times higher in the extracellular fluid.

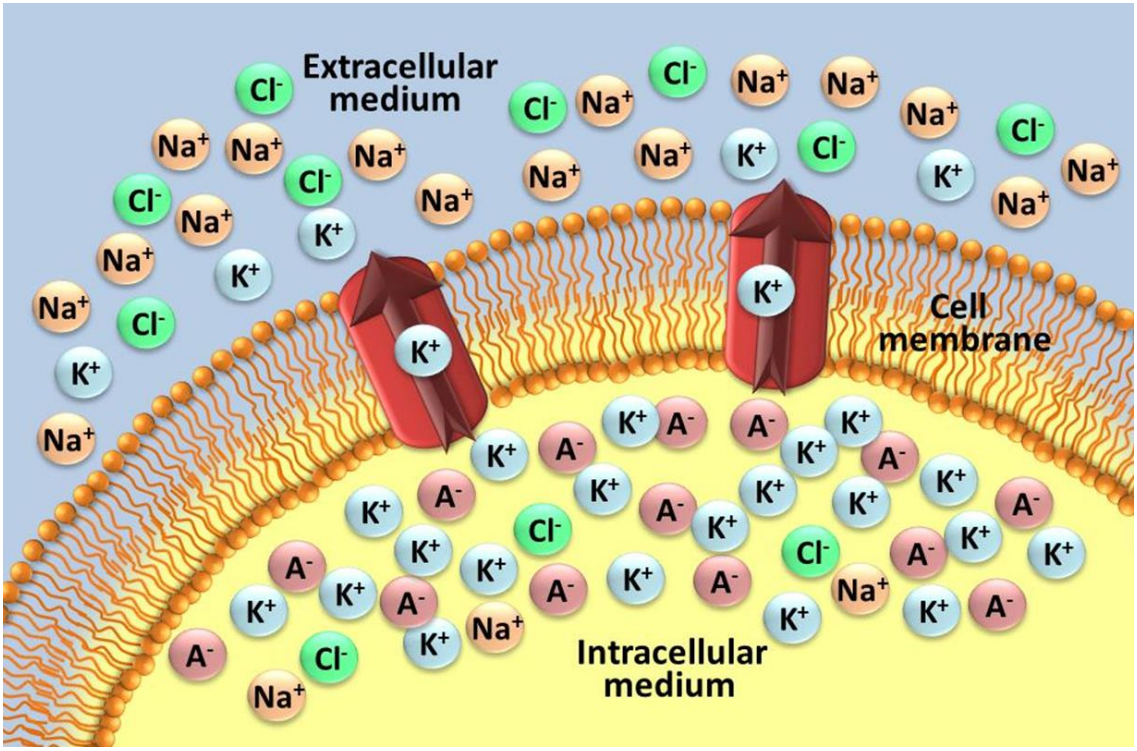

Figure 1-4: Ionic distribution at a cell membrane.

1.1.3 Extracellular change of zinc ion

A further type of flux considered important for study is extracellular zinc (Zn^{2+}). As with potassium, zinc plays an important role in particular processes in the body. In the brain, for example, zinc homeostasis is important for memory and good learning capacities.[17, 18] Most of the zinc is located inside a specific subcategory of glutamatergic neurons (neurotransmitters that produce glutamate) and, in some particular cases, zinc is released in order to provide an answer to an unwanted change. For example, in the case of acidosis due to a neurological disorder such as ischemia, epileptic seizure or stroke, zinc ions are released to increase its extracellular concentration. Some researchers have shown that the zinc is playing a protective role in case of acidosis.[19] However, the exact role of the zinc is more difficult to define. A potential application of our modified surfaces would be to grow cells on them, and it should then be possible to study how the zinc interacts in the extracellular space. This discussion includes only one of the possible applications for extracellular zinc, however this element plays a role in many other biological processes such as: microglial activation,[20] or ischemia.[21] Another important observation will be the concentration of extracellular zinc and which other metal ions present in the extracellular fluid that could interfere with the detection of zinc. It is reported that the sensitivity and selectivity of our future probe. In a recent paper we found that to detect physiological Zinc we will need a sensitivity of the order of µM will be required,[21] and that possible interference could arise from other metal ions including transition metals and Ca^{2+}.

The following section provides an overview of fluorescent dyes typically employed to study pH and metals ions (K^+ or Zn^{2+}).

1.2 Fluorescent probes

The use of fluorescence has been of great interest in biological research over the last century, and can be considered to be a fundamental tool in the study of biological processes and sensing. Improvements in fluorescence chemistry, along with technical discoveries, have allowed the development of many different kinds of fluorophores.[22-26] Nowadays the large selection of available fluorophores provides greater flexibility, variation and performance for research applications. In the following section we will describe the operating principles of fluorescent probes, and how they can be employed to study cellular flux.

1.2.1 Basics of fluorescence

Fluorescence is a three-stage process that occurs in certain molecules known as fluorophores or fluorescent dyes. A fluorescent probe is designed to respond to a specific

stimulus or to localise within a specific region of a biological specimen. The process of fluorescence is illustrated using a Jablonski diagram (**Figure 1-5**), and can be divided in three main stages:

Stage 1: Excitation

A photon of energy ($h\nu_{EX}$) is supplied by an external source and absorbed by the fluorophore, promoting it from the ground state (S_0) to an excited electronic singlet state (S_1').

Stage 2: Excited-State Lifetime

The excited state exists for a finite time. During this time, the fluorophore undergoes conformational and vibrational changes and is subject to possible interactions with its molecular environment. These processes have two important consequences. First, the energy of S_1' is partially dissipated, yielding a relaxed singlet excited state (S_1) from which fluorescence emission originates. Secondly, not all the molecules initially excited by absorption (Stage 1) return to the ground state (S_0) by fluorescence emission but other processes may depopulate S_1 such as relaxation where the excitation energy is dissipated as heat. The fluorescence quantum yield (Φ), which is the ratio of the number of fluorescence photons emitted (Stage 3) to the number of photons absorbed (Stage 1), is a measure of the relative extent to which these processes occur.

Stage 3: Fluorescence Emission

A photon of energy ($h\nu_{EM}$) is emitted, returning the fluorophore to its ground state S_0. Due to energy dissipation during the excited-state lifetime, the energy of this photon is lower and possesses a longer wavelength than ($h\nu_{EX}$). The difference in energy or wavelength represented by ($h\nu_{EX} - h\nu_{EM}$) is called the Stokes shift. The Stokes shift is fundamental to the sensitivity of fluorescence techniques because it allows emission of photons to be detected against a low background, isolated from excitation photons.

Fluorescent dyes have the property of absorbing in a broad range and emitting in the visible range of the colour spectrum. Each fluorescent dye has its own unique properties that are suitable for use in various applications.[27] The first objective of the current research will be to investigate fluorescent dyes that are suitable to sense differences of pH.

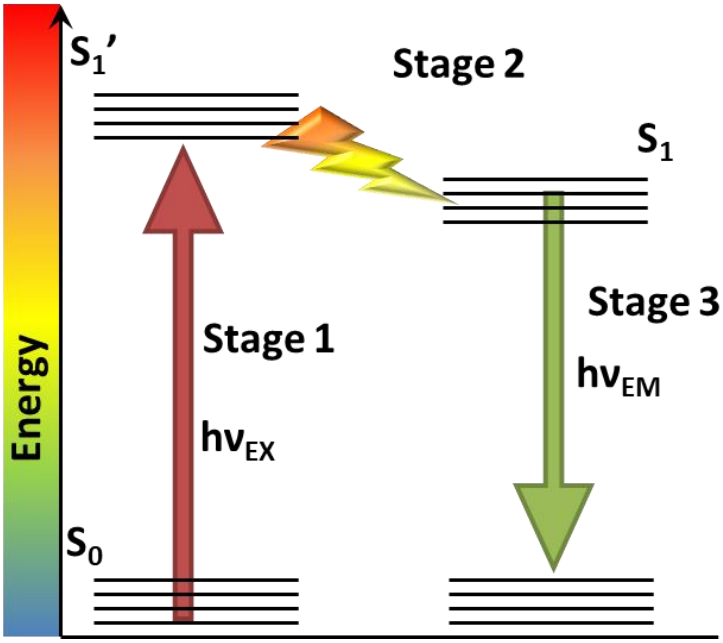

Figure 1-5: Jablonski diagram.

1.2.2 Carboxyfluorescein as a pH probe

In this part of the project we will discuss the development of a sensor dye to study pH cellular flux.[4] Fluorescent indicators are particularly valuable tools for measuring changes in intracellular and extracellular proton concentration.[28] To be used for pH measurements in a biological system, a fluorescent probe should be non-toxic, have a pK_a within the physiological range to allow detection of small pH changes typical in a cell, whilst having excitation and emission wavelengths suitable for detection by flow cytometry, fluorescence microscopy or other techniques suitable for cell fluorescence analysis. Moreover, fluorescence of the probe should be stable over time. Literature reports demonstrate many different probes specifically synthesised to study intracellular and extracellular pH. Most of these probes are based on a main skeleton that can be modified synthetically in order to produce small controllable changes of characteristic properties. Some of the skeletons employed include: benzo[a]phenoxazine **1.02**,[29] pyrene **1.03**,[30] rhodamine **1.04**,[31-33] and bodipy **1.05** (**Figure 1-6**).[34-36] Several other skeletons and derivatives have been reviewed.[2, 37, 38] In most examples described, it is evident that fluorescent pH probes are based on a highly photo-active moiety that can be activated by an acid-base reaction at a specific position (e.g. phenol, amine or *N*-heterocycle) or by a nucleophilic addition of hydroxide ion.

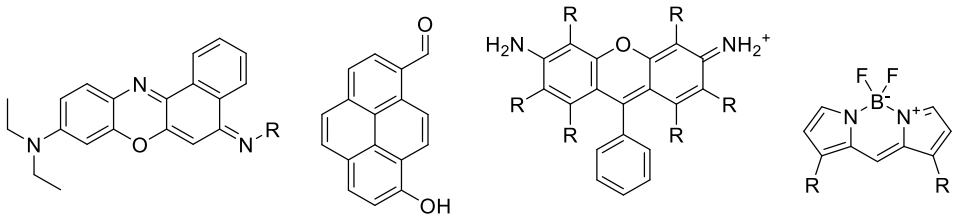

1.02 **1.03** **1.04** **1.05**

Figure 1-6: Examples of pH probes: benzo[a]phenoxazine **1.02**, pyrene **1.03**, rhodamine **1.04**, and bodipy **1.05**.

Of the probes numerous reported in the literature one attracted our interest: fluorescein, or more specifically, one of its derivatives 5(6)-carboxyfluorescein (**Figure 1-7**). A number of typical fluorescent probes used for pH measurements are based on fluoresceins,[39-42] a group of dyes that exhibits multiple pH-dependent equilibria.

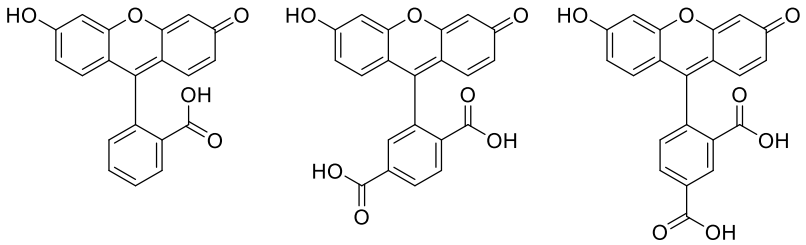

1.06 **1.07$_a$** **1.07$_b$**

Figure 1-7: Fluorescein **1.06**, 6-carboxyfluorescein **1.07$_a$** and 5-carboxyfluorescein **1.07$_b$**.

Fluorescein is one of the most common dye reagents, exhibiting some useful and interesting properties such as high extinction coefficients, excellent fluorescence quantum yield, good water solubility and low toxicity. Fluorescein can be used to detect oxygen,[43] but its sensitivity to pH has been utilised most frequently. It displays pH-dependent ionic equilibria; above pH 9 the phenol and carboxylic acid functional groups are almost totally ionized in aqueous solutions (**Figure 1-8**). Then, formation of the monoanion by acidification of the fluorescein dianion results in the first protonation on the phenol (pK_a = 6.4), followed by the carboxylic acid (pK_a = 5) to produce neutral fluorescein. Further acidification generates a cation (pK_a = 2.1).

The monoanion and the dianion are fluorescent, with quantum yields of 0.37 and 0.93, respectively, whereas the neutral and cationic species need excitation to produce emission, with effective quantum yields of 0.31 and 0.18, respectively.[44] A further equilibrium involves the formation of a colourless, non-fluorescent lactone. The lactone is not formed in aqueous solutions above pH 5, but may be the dominant form of neutral fluorescein in solvents such as acetone. However, the fluorescence emission spectrum of most fluorescein derivatives, even in acidic solution, is dominated by the dianion, with only small contributions from the monoanion. Consequently, the wavelength and shape of the resulting emission spectra are

relatively independent of the pH, but the fluorescence intensity is dramatically reduced in acidic pH. This is important to obtain a gradient of intensity in the fluorescence near a physiological pH.

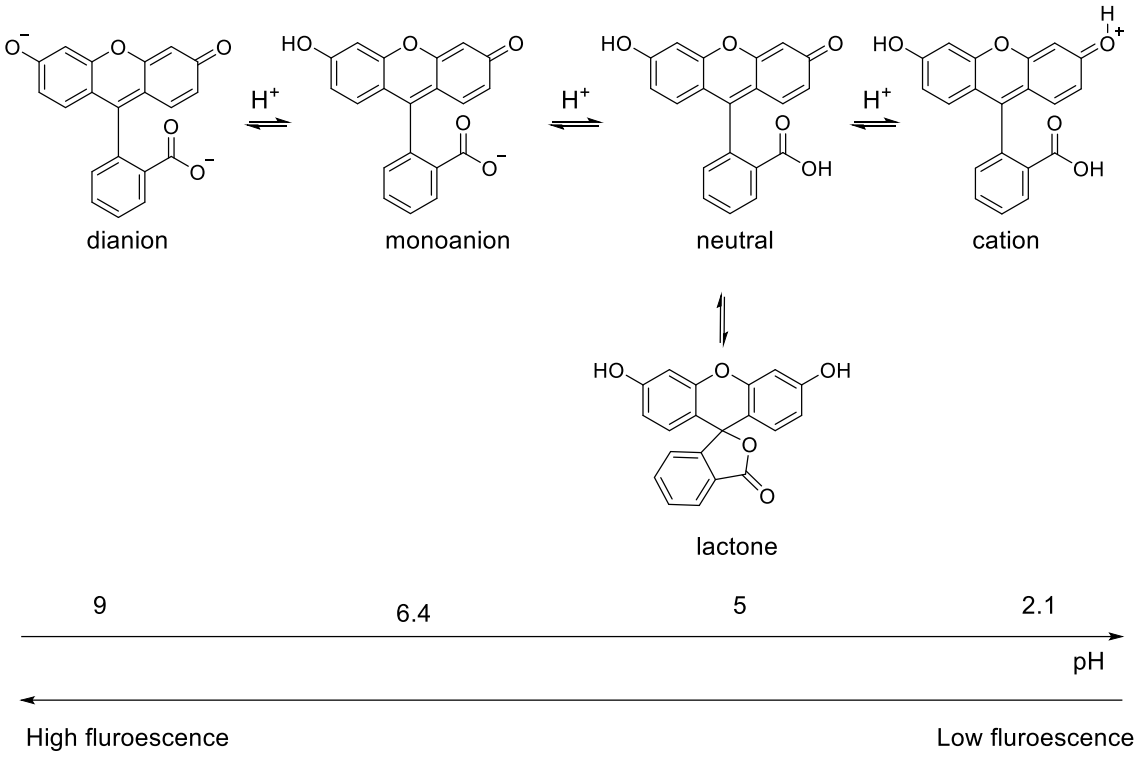

Figure 1-8: Ionization equilibria of fluorescein **1.06**.

Despite all the advantages described here above, the use of fluorescein still presents a significant issue, which is due to its rapid leakage from the cells, making the quantification of changes in pH challenging. This problem could be overcome by attaching the molecular probe to a solid surface as described by Bradley *et al*.,[45] who covalently linked fluorescein to polystyrene microspheres to monitor in real time pH changes within cells. The authors use a carboxyfluorescein derivative presenting a carboxyl group that can be modified in order to be attached on a surface. Moreover, other groups described encapsulation of the probe in silica nanoparticles to reduce leakage.[46, 47] Therefore, covalent binding of our dyes to silica substrates should eliminate leakage of the dyes into the cells and ensure a highly localised dye that could allow extracellular detection. Additionally, the pores of the silica substrates labelled with the probe should be easily visualised by microscopy. Finally, the incorporation of reference dyes could allow ratiometric measurements to be performed, which take into account any fluctuation in light source intensity and enable the sensors to be calibrated *ex-vitro* and used *in-vitro* as the same fluorescent response is obtained in both environments.

5(6)-Carboxyfluorescein presents the same type of fluorescence characteristics as fluorescein, whilst having the advantage of processing a functional group suitable for

covalent modification. The only disadvantage of 5(6)-carboxyfluorescein is that the synthesis involves the preparation of the molecule as a mixture of region isomers (synthesis is discussed in the results and discussion chapter).

1.2.3 Probes specific for potassium ions

Another part of this project consisted in the development of a fluorescent dye suitable for detection of potassium flux. Detection of potassium in extracellular flux is challenging and it is important to have good selectivity between extracellular K^+ (4 mM) and Na^+ (140 mM) with a resolution of <0.1 mM.[48] A probe for K^+ needs to have good stability and a fast response. Different methods of detection exist, such as: ion-selective microelectrodes,[49] aptamers[50-52] or fluorescent sensors.[38, 53, 54] In this work we will focus on fluorescent sensors, which are mostly based on the generalised structure represented in **Figure 1-9**.

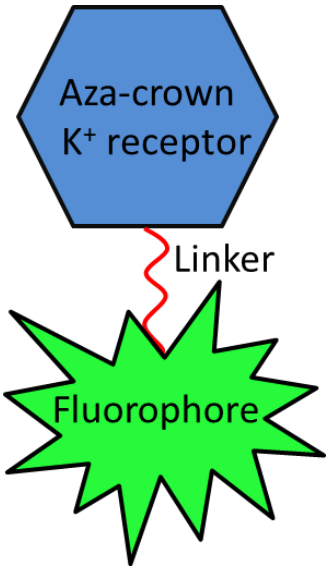

Figure 1-9: Schematic representation of a potassium probe.

In this system a receptor specific for a targeted metal is linked to a fluorophore. In many cases, these probes work through a process call photo-induced electron transfer (PET) emission quenching (**Figure 1-10**).[38, 55, 56] During the PET process an excited electron is transferred from a donor to an acceptor. In the case of the potassium probe, PET quenches the fluorescence in the absence of the metal ion. However, when the receptor chelates the target metal cation, PET cannot occur due to lowering of the energy of the donor electron pair, and strong fluorescence is observed.

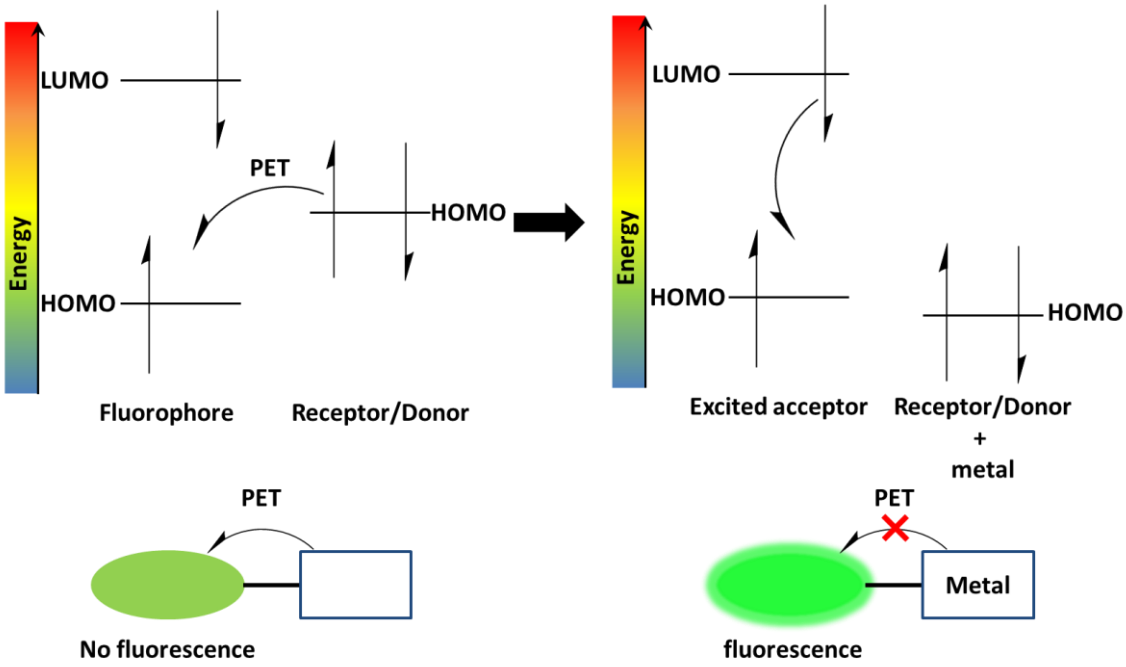

Figure 1-10: "Turn-on" photo-induced electron transfer (PET) by coordination of a metal ion.

A second important mechanism of fluorescence for this type of probe is the internal charge transfer (ICT): this consists of a direct transfer of charge to the fluorophore (resulting in quenching of the fluorophore). However, chelation of a metal ion prevents the direct transfer (no quenching of the fluorophore) allowing the fluorophore to retain its fluorescence properties.

Azacrown ethers are described in the literature as having excellent affinity for alkali and alkaline earth metal cations.[57] The crown ether moiety would act as the receptor and the nitrogen as the donor. Intercalation of a metal ion in the cavity results in a blockage of the PET mechanism so that the fluorophore retains its strong fluorescence properties. As previously discussed, an important consideration in the preparation of a potassium probe is to ensure selectivity toward the target metal cation, even in the presence of high concentrations of similar metal ions. Control of selectivity towards K^+ or Na^+ is provided by the size of the crown ether.[58, 59] This is exemplified in **Figure 1-11**: the two commercial molecules reported, SBFI[60] and PBFI,[61] display selectivity towards sodium or potassium just by removing one heteroatom from the crown ether. SBFI (K_d = 11.3 mM in solutions with a combined Na^+ and K^+ concentrations of 135 mM), with five heteroatoms in the crown ether, is selective for Na^+ and PBFI (K_d = 44 mM in solutions with a combined Na^+ and K^+ concentrations of 135 mM), with six heteroatoms, is selective for K^+. SBFI is ~18-fold more selective for Na^+ than for K^+.

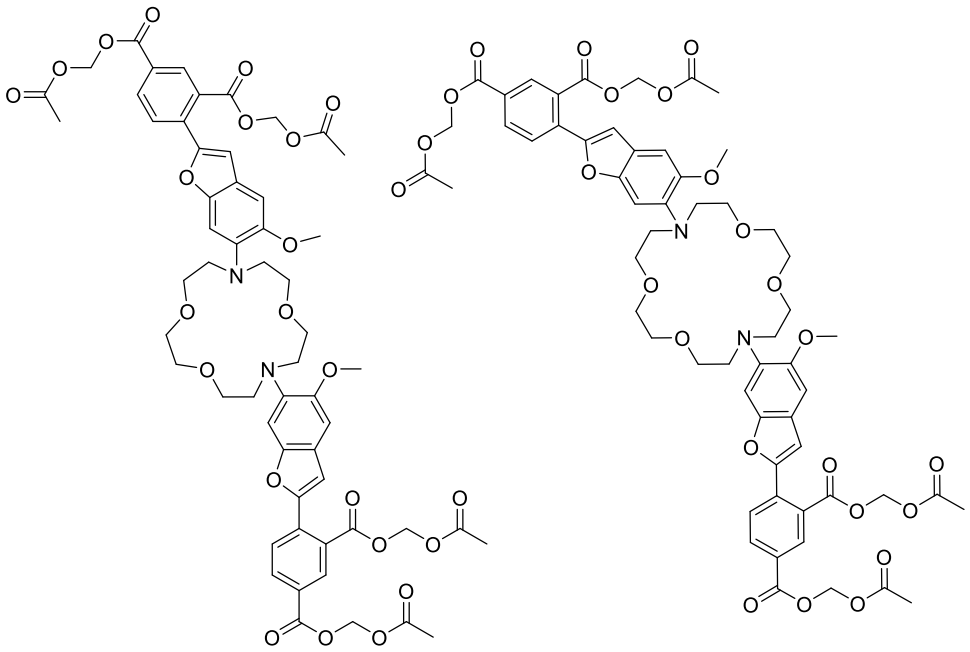

1.08 SBFI **1.09 PBFI**

Figure 1-11: Commercially available probes for Na^+ (SBFI) and K^+ (PBFI).

PBFI is the only probe commercially available for potassium ion, but this displays a relatively poor selectivity. In this work, we will synthesise a probe with a very high selectivity for potassium ion, essential for applications in an environment with a high concentration of sodium ions such as exists in the extracellular fluid. The target probe should also allow a means of covalent attachment to silica surface.

In **Figure 1-12** two different types of potassium probe are presented. Macrocycle **1.10** is a triazacryptand-based receptor with a naphthalic anhydride fluorophore,[62, 63] which offers the advantage of very good selectivity for K^+ at physiological concentration. Moreover, 4-amino-1,8-naphthalic its thermally and photochemically stable, has desirable spectral properties (high aqueous quantum yield, LED-compatible λ-max near 450 nm, high Stokes' shift > 50 nm) and a good pH stability.[64] The main issue with this type of molecule is the challenge of synthesising the triazacryptand moiety due to the complex nature of the ring system.[65]

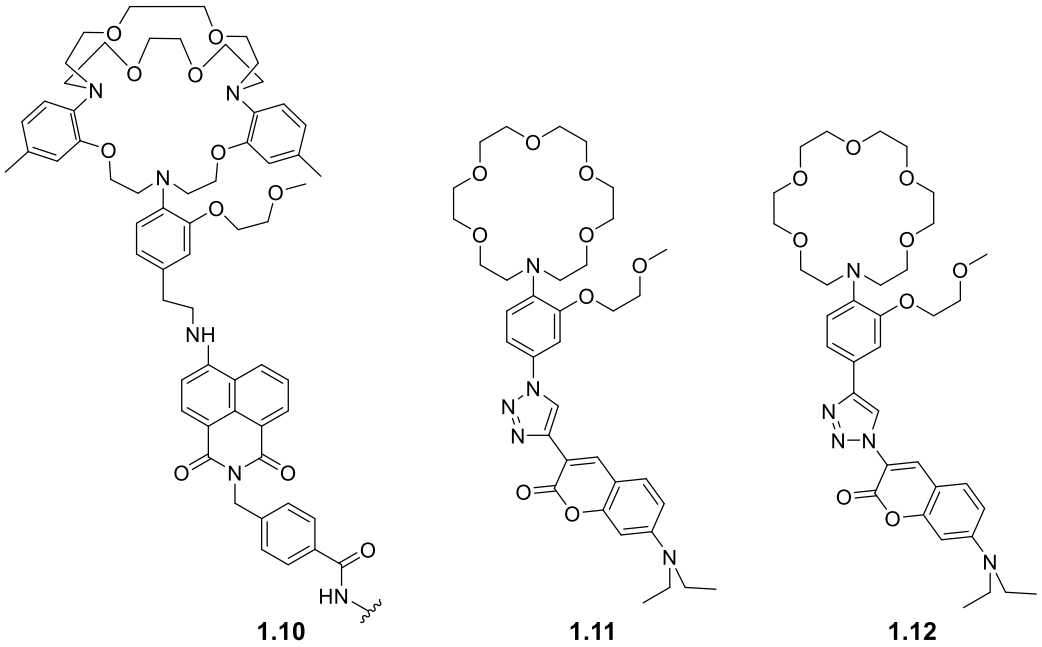

Figure 1-12: Examples of potassium ion probes.

Molecules **1.11** and **1.12** are reported in the literature,[66, 67] synthesised in four steps according from commercial starting materials. Even though these molecules present a more simplified structure for the receptor, the authors discovered that the combination of the 2-methoxyethoxy lariat group with a simple phenlyaza-[18]crown-6 receptor allowed selective complexation of K^+ at physiological concentrations. The lariat presumably aids chelation of the ion potassium as shown in **Figure 1-13**. In almost all cases, literature reports utilised one of the two types of potassium receptors shown in **Figure 1-12**, the only difference being the choice of fluorophore.[38]

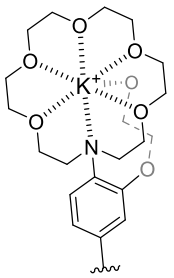

Figure 1-13: Chelation of a potassium ion.

Building on knowledge developed from the previous research, our work targets new probes for potassium, taking some elements from the different sensors previously described. The molecule shown in **Figure 1-14**, was designed for synthesis. The phenlyaza-[18]crown-6 receptor was selected as it is relatively easy to prepare and showed some good results when combined with the lariat. By linking naphthalic anhydride as a fluorophore, all the important properties of the probe will be incorporated and it will be possible to link this molecule onto the silica surface after addition of a suitable linker.

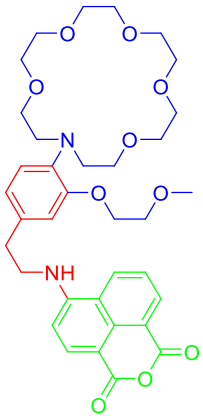

Figure 1-14: Proposed of potassium probe with the receptor (in blue), the linker (in red) and the fluorophore (in green).

1.2.4 Probe specific for zinc ion

As described for the potassium probe, the development of a probe that is specific for zinc is challenging as it needs to be sensitive and selective. To achieve high selectivity for zinc sensing in media such as extracellular fluids is complicated due to the fact that this environment is rich in many different metal ions. Moreover, detection of concentrations of zinc at levels of the order of µM is required. To accomplish this selectivity, researchers have developed numerous types of probe for zinc. These probes work in a different way than those employed for potassium sensing, having a receptor able to complex with Zn^{2+} leading to activation of the fluorophore.[68, 69] Some examples of zinc probes based on fluorescein are shown in **Figure 1-15**,[70] and probes based on coumarin are shown in **Figure 1-16**.[13, 71]

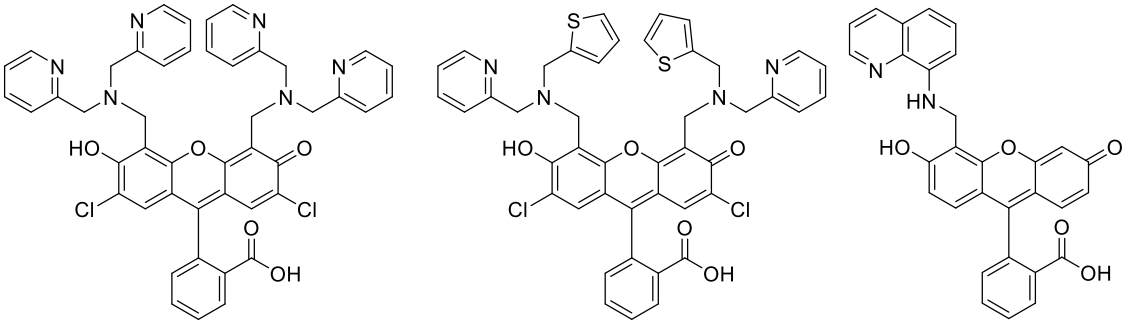

1.13 ZP1 **1.14 ZS6** **1.15 QZ1**

Figure 1-15: Examples of zinc probes based on fluorescein.

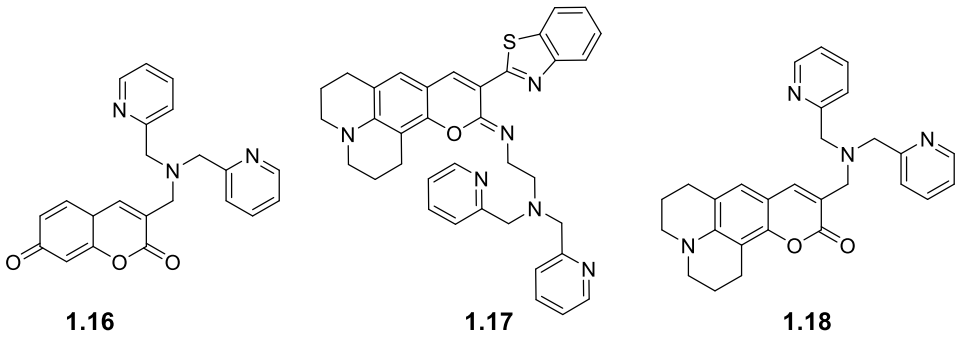

1.16 **1.17** **1.18**

Figure 1-16: Examples of zinc probes based on coumarin.

The range of receptors available that are specific for zinc is wider than for potassium, the fluorescence process is based on the complexation (**Figure 1-17**). Moreover, the presence of nitrogen is very important in zinc receptors as it chelates the zinc ion. Many of the zinc receptors are based on pyridine/pyrazine containing structures. Our choice of zinc probe, again required a molecule that would be relatively easy to prepare synthetically, with good sensing properties that could be conveniently attached on a surface. The probe that particularly attracted our attention, was the ZP1 (**Figure 1-15**), as the carboxyfluorescein based molecule has been previously synthesised and characterised.[72-74] The carboxylic group of carboxyfluorescein could serve for the attachment to the silica surface. Overall, this probe presented the highly desirable characteristics to develop different probes for the detection of zinc based on different receptors. The synthesis of the probe and its attachment will be described in the results and discussion chapter.

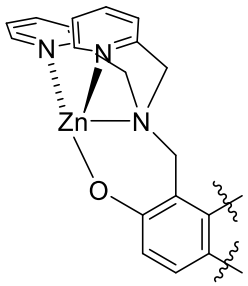

Figure 1-17: Schematic representation of possible complexation of Zn^{2+}.[74]

Following development of suitable method to synthesise three ion specific fluorescent probes, further interest will lie in extending the approach to different probes suitable for the study other types of cellular flux (calcium,[75] sodium,[76] etc.[77]). Since the aim of this work is to immobilise the fluorescent probes onto solid supports, as mentioned above, the following section will describe the material chosen for this purpose, mesoporous silica.

1.3 Mesoporous silica

Porous materials can be defined as a combination of solid phases and the pores formed in the solid phases. The position and structure of the pores determines how a porous material can be used. Therefore, to define these materials, basic parameters are used such as: porosity, pore size, pore shape or specific surface area. According to the IUPAC system porous materials are classified depending on the diameter of their pores so that we can talk of micropores (< 2 nm), [78-80] mesopores, (2 to 50 nm), and macropores (> 50 nm).[81, 82] In this work we will focus on silicate mesoporous materials for a number of reasons; firstly, these materials can be easily prepared and characterised, and they have good stability over a range of conditions. We also believe that the mesoporous silica surfaces will provide a good environment for growing cells. Furthermore, mesoporous silica layers on a conductive substrate (e.g. ITO) will allow electrochemistry experiments, which may be useful for this work.

The term “mesoporous” refers to a diameter of pores in the region between 2 and 50 nm. The small mesopores limit the kind of ions and molecules that can be admitted inside the pores of the material. In fact, control over the pore size offers the possibility of molecular sieving or molecular selectivity. Mesoporosity can also endow a material with a high surface area exceeding 1000 m^2/g and pore volume greater than 1 cm^3/g. This greatly expands the potential of the materials for applications such as adsorption, where the mesoporous structure can be modified by immobilising catalysts or sensing molecules. These important properties make mesoporous materials our materials of choice, providing, pores large enough to be accessible, allowing modification and future experiments such as cyclic voltammetry study. Furthermore, the pores provide a high specific surface area giving the possibility to attach a higher concentration of probe molecules. Mesoporous surfaces can be prepared by a number of different methods,[83] and utilising different materials such as ordered mesoporous carbon,[84-88] mesoporous metal oxides,[89-92] or mesoporous silica.[93-97]

In general, silica is an attractive material for many sensing applications because of its stability over a fairly wide range of pH, relative inertness in many environments, and transparency in the UV-visible spectrum. For these beneficial reasons, it was chosen for the preparation of our surfaces. Many routes exist for designing hybrid inorganic-organic mesoporous silicates.[76] The silica can be prepared in different forms such as particles or films. Silica particles include a very important family of mesoporous silicates such as the Mobil Composition of Matter (MCM) synthesised in 1992,[98, 99] or the Hiroshima Mesoporous Material (HMM), first prepared in 2009.[100] Despite the advantageous properties presented by mesoporous silica particles, mesoporous silica films are used for this work, as they provide a surface for cells to grow.

Numerous techniques exist for the preparation of stable well-ordered silica films,[101] however the most common process to prepare mesoporous silica materials is by sol-gel.[102] This process leads to the formation of a solid material from small molecule units. Small particles are suspended in a liquid (sol), followed by a polymerisation phase (usually initiated by evaporation of solvent or addition of an initiator) leading to the formation of the "gel". The resulting gel is then heated at high temperature to dry and give the final product. A recently published variation of this technique: the electrochemically assisted self-assembly (EASA),[103-105] developed by Alain Walcarius is utilised during this work.[106-108] All details of this technique will be fully described in the results and discussion chapter.

The mesoporous surfaces once prepared, are covered with many silanol moieties that can be reacted with organosilanes, common examples are 3-aminopropyltrimethoxysilane **1.19** (APTMS),[109] 3-mercaptopropyltrimethoxysilane **1.20** (MPTMS),[110] and hexamethyldisilazane **1.21** (HMDS) (**Figure 1-18**).[111] This possibility of grafting on alternative functional groups opens up wide opportunities for further derivatisation of the surface.

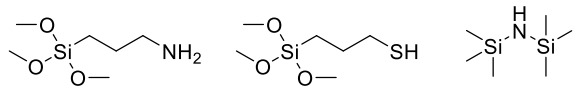

1.19 APTMS **1.20 MPTMS** **1.21 HMDS**

Figure 1-18: Examples of organosilanes that can react with silica supports.

1.4 Aim of the project

This project aims to develop novel modified surfaces to study cellular fluxes by luminescence switching of fluorescent dyes. Fluorescent probes are normally used to detect particular components of complex biomolecular assemblies, such as living cells, with high sensitivity and selectivity. An interesting aspect of this work is the use of modified surfaces, which opens a large field of new possibilities for the use of fluorescent probes.

The objectives of this work can be divided in four main steps. First of all, the most suitable dyes to respond to particular cellular fluxes will be selected and the synthesis of all the probes will be presented. Secondly, a new and effective technique to produce ordered mesoporous silica films onto solid surfaces, electrochemically assisted self-assembly (EASA),[112] will be tested and used. Then, a synthetic methodology to link the fluorescent probe of choice to the silica substrates will be developed. Finally, all the substrates will be characterised and tested to evaluate their ability to detect changes of pH or metals ions (K^+ or Zn^{2+}) leading to the key objective of the project: the application of the surfaces in biological studies with cells.

The first section will describe the synthesis of the new potassium probe, followed by a description of the synthesis of the carboxyfluorescein derivative probes (for pH, zinc and potassium). In the second section the EASA techniques will be explained in detail, and the methods used to characterise the created surfaces will be described. The newly prepared surface will be modified by an organosilane followed by an addition of the synthesised fluorescent probes. The new fluorescent probes will be characterised and tested in initial biology tests.

Chapter 2 Results and Discussion

2.1 Synthesis of the probes

This first section presents the synthesis of the fluorescent probes. Firstly, the design and synthesis of a new potassium probe will be described, followed by preparation of a second probe based on carboxyfluorescein.

2.1.1 Naphthalic anhydride derivative

2.1.1.1 Initial attempts to prepare napthalic anhydride probe

This section will describe our first attempts to synthesise a modified naphthalic anhydride as a potassium ion probe. The importance of having a crown ether with a specific size for selective detection potassium ions was previously described (see introduction). Other key features are the requirement to have a fluorescent fragment, and a means for attachment of the probe to a surface. The first target towards a potassium probe is the molecule shown in **Figure 2-1**.

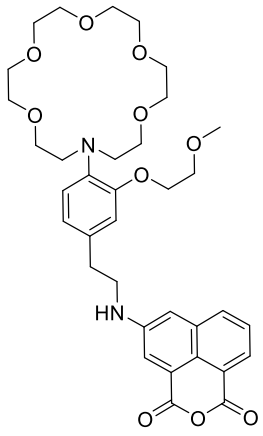

2.01

Figure 2-1: First target as potassium probe.

The aza-crown **2.01** can be divided in two moieties: an aza-crown ether derivative (receptor) and a naphthalic anhydride (fluorophore). A lariat was added alpha to the crown ether; a recent paper from Ast *et al.*[66] described how the sensitivity for potassium was increased by ten times through addition of a lariat. The main challenges to be addressed in the preparation of the potassium probe **2.01** are the synthesis of the crown ether and a method to link the two components together.

Scheme 2-1 shows our retrosynthetic analysis to **2.01**, the idea being to link the two main parts of the molecule in the last step through a reliable coupling methodology. Nitrophenol **2.07** is commercially available and affordable as a starting material. The retrosynthesis identifies disconnection of the fluorophore in **2.01** (**Scheme 2-1**), by disconnection of the C—N bond. The aminoethyl chain present in **2.02** can be disconnected back to the aza-crown ether **2.05**, which can be prepared by a macrocyclization from diol **2.06**. Finally, diol **2.06** can be derived from reduction of the nitro group and three substitutions on the starting material **2.07**.

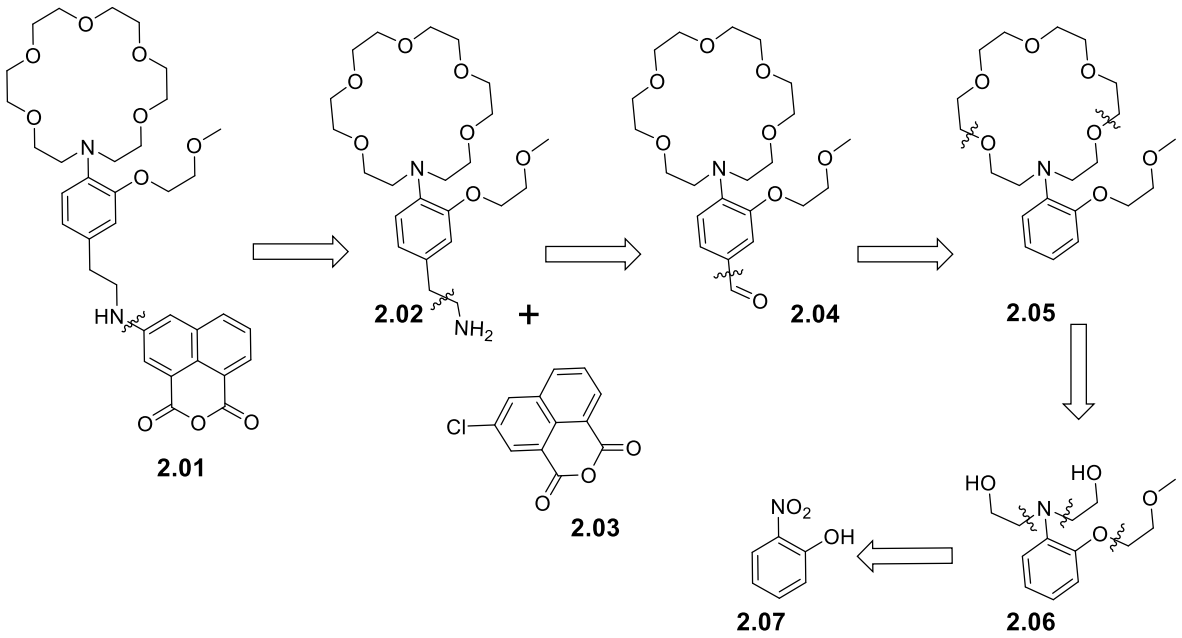

Scheme 2-1: Retrosynthesis for the first target.

The synthesis of **2.06** is described in **Scheme 2-2**, starting with a quantitative S_N2 reaction of bromoethyl methyl ether with 2-nitrophenol. The reduction of the nitro group was firstly attempted with Pd/C and H_2 but only the starting material **2.08** was recovered after an overnight reaction. The problem was solved by using a classical reduction method,[113] which reduces the nitro group with Fe powder activated in the presence of HCl Di-substitution of the amine **2.09** was carried out with 2 equivalents of bromoethanol in very good yield, to give the diol **2.06** containing the required functionality for the formation of the crown ether (**Scheme 2-2**).

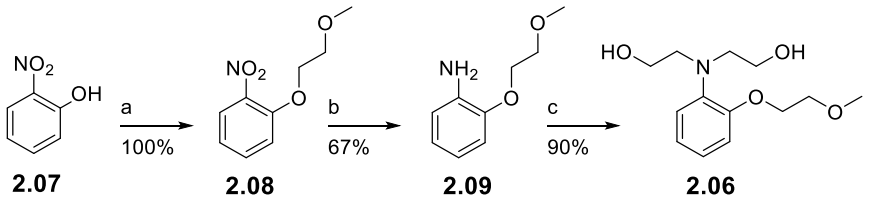

Scheme 2-2: ***Reagents and conditions***: a) bromoethyl methyl ether, KI, K_2CO_3, DMF, 110 °C; b) i) EtOH, Fe, conc. HCl, 65 °C; ii) aq. NH_4Cl, **2.08**, 60 °C; c) 2-bromoethanol, $CaCO_3$, water, 60 °C.

Before the preparation of the aza-crown ether **2.05**, it was necessary to prepare a suitable alkylating species **2.11** for the macrocyclization (**Scheme 2-3**). Tosylation of tetraethylene glycol **2.10** gave the bis-tosylate **2.11** in quantitative yield.

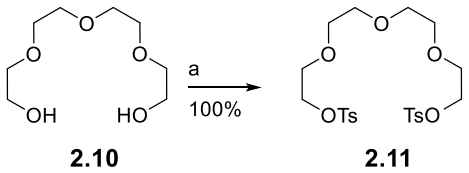

Scheme 2-3: ***Reagents and conditions***: a) 4-toluenesulfonyl chloride, THF, KOH, 0 °C to rt.

The aza-crown ether **2.05** was prepared by double deprotonation of diol **2.06** with a strong base, followed by addition of ditosylate **2.11** (**Scheme 2-4**). The first attempts to perform this reaction were not satisfactory, with poor yields of between 5 and 20%. Preparation of macrocycles is often highly challenging due to competing polymerisation, which can be difficult to avoid. A workable solution was found that afforded a suitable yield of **2.05** to allow continuation of the synthesis, by using a syringe pump to add **2.11** at a slow rate it proved possible to obtain the desired macrocycle in yield of 41%. The purification of **2.05** also proved quite challenging due to its high polarity.

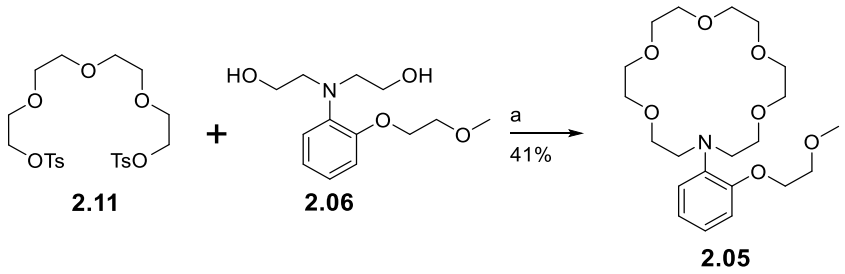

Scheme 2-4: ***Reagents and conditions***: a) NaH (60%), THF, N_2, rt to 70 °C.

The next step was a Vilsmeier formylation of the electron-rich aryl group in with $POCl_3$ and DMF (**Scheme 2-5**). Unfortunately, NMR showed a mixture of aldehyde regioisomers were formed (see also mechanism **Scheme 2-6**), which were impossible to separate by silica gel

column chromatography due their similarity as well as their high polarity. Therefore, it was concluded that the current route needed to be changed.

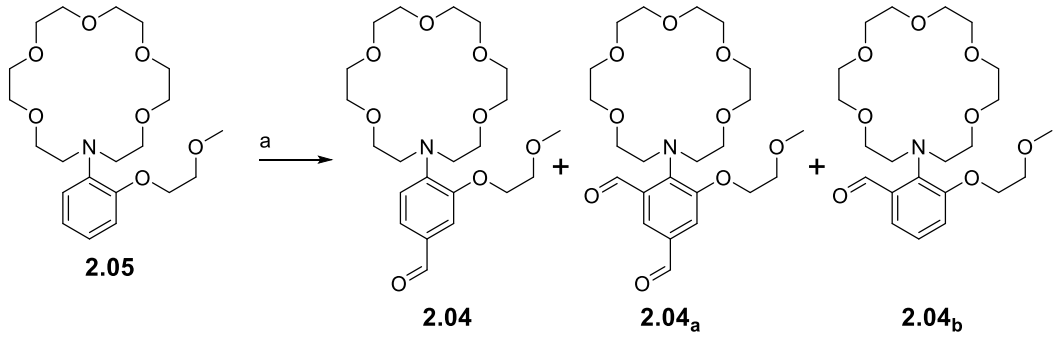

Scheme 2-5: ***Reagents and conditions***: a) $POCl_3$, DMF, 0 °C to rt.

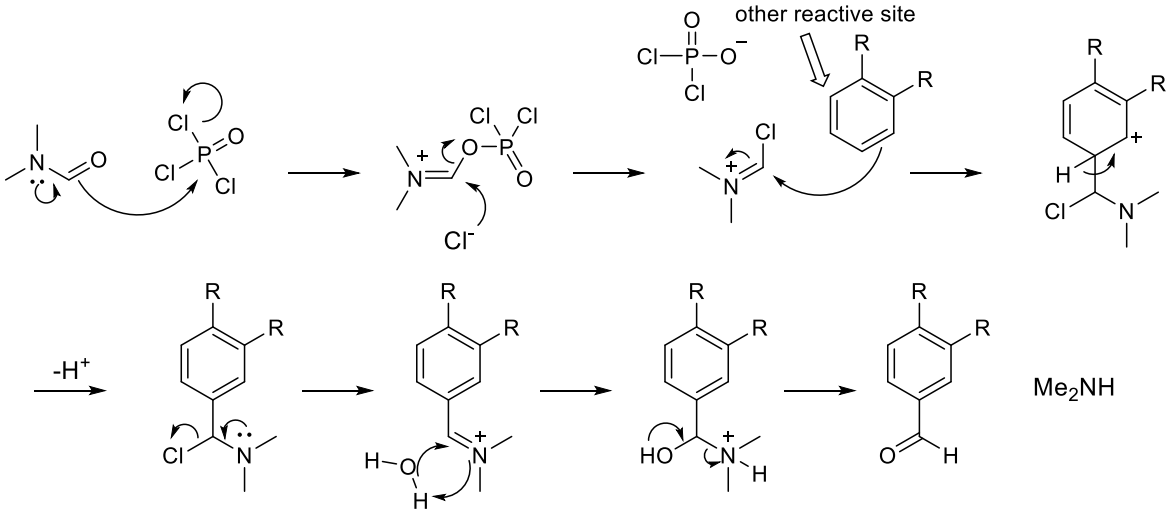

Scheme 2-6 : Mechanism of the Vilsmeier formylation

2.1.1.2 Revised synthetic approach

A revised route was proposed (**Scheme 2-7**), where the method of linking the receptor and fluorophore was changed, to be carried out through a metal-catalysed cross-coupling reaction. For this, it was necessary to brominate to the aza-crown derivative and introduce an amine group to the naphthalic anhydride, prior to enable the coupling reaction. The brominated aza-crown fragment **2.13** was to be prepared by the route previously established.

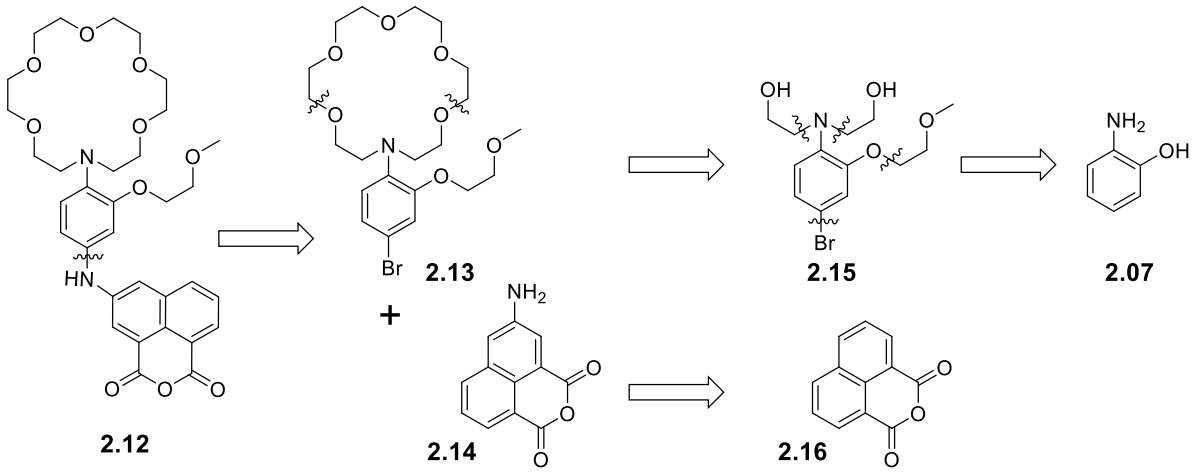

Scheme 2-7: Retrosynthetic analysis for the revised potassium probe.

The addition of bromine to **2.09** was performed through aromatic electrophilic substitution with *N*-bromosuccinimide (NBS). Due to use of excess NBS during the first bromination reaction, the di-bromo product **2.16** (**Scheme 2-8**) was obtained. However, we decided to continue to prepare the probe with this compound, as it could be interesting to study the response of the probe with different types of substitution. However, the diol **2.17** could not be obtained due to insolubility of the dibromide, even when the reaction temperature was increased. The di-brominated derivative **2.16** was therefore not investigated further.

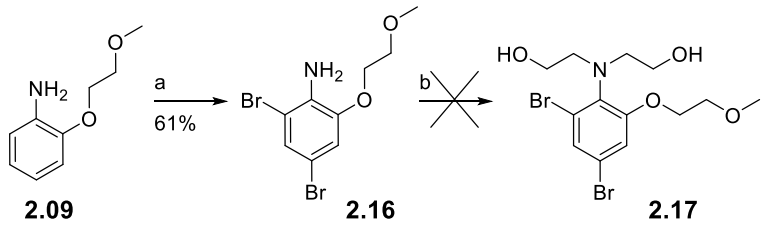

Scheme 2-8: ***Reagents and conditions***: a) CH_3CN, NBS, N_2, 0 °C to rt; b) 2-bromoethanol, $CaCO_3$, water, 60 °C.

Starting from **2.09**, the bromide **2.15** was prepared using two different routes (**Scheme 2-9**). In the first route the bromide **2.18** was obtained in a yield of 57% over two steps, by the addition of the bromine followed by double alkylation of **2.18** to give the diol **2.15**. Again, poor solubility of **2.18** was likely to be responsible for the lower yield of the diol **2.15**. To obtain a higher yield, the two steps were reversed, solving the problem of solubility and providing a yield of 77% over two steps for the second route.

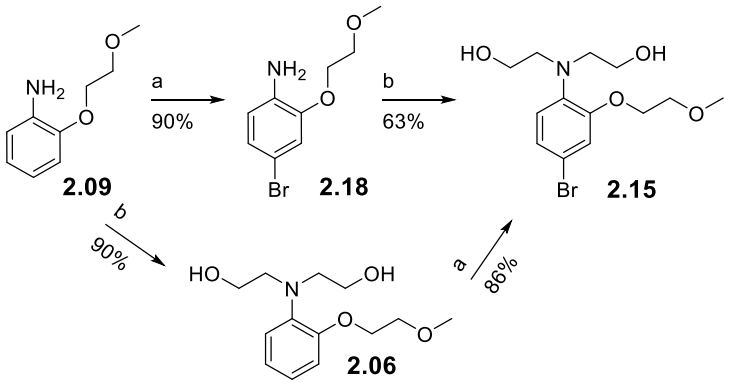

Scheme 2-9: ***Reagents and conditions***: a) CH_3CN, NBS, N_2, 0 °C to rt; b) 2-bromoethanol, $CaCO_3$, H_2O, 60 °C.

The macrocyclisation was performed as described before, using a syringe pump to slowly add ditosylate **2.11** to diol **2.15**, achieving a 52% yield of aza-**crown 2.13** (**Scheme 2-10**).

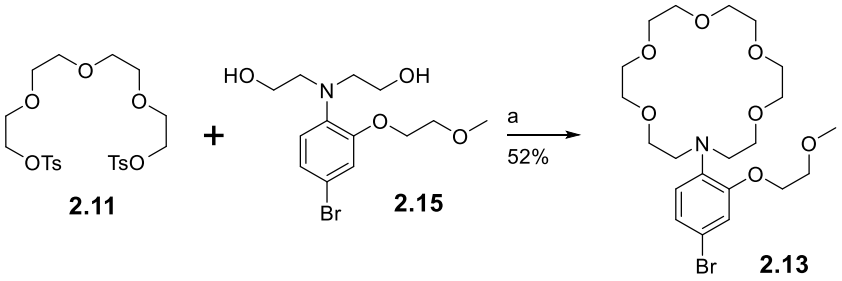

Scheme 2-10*: **Reagents and conditions***: a) NaH (60% in oil), THF, N_2, 0 °C to rt.

Meanwhile, the naphthalic anhydride derivative was prepared (**Scheme 2-11**). Naphthalic anhydride **2.16** was treated with a solution of H_2SO_4 and HNO_3 to form the nitro compound **2.19** in good yield. Reduction of the nitro group was investigated using different methods; the first attempt involved reduction over palladium in MeOH, however the reaction did not work due to the poor solubility of **2.19** in MeOH. Attempted reduction using Fe activated in HCl, gave the same problem as again **2.19** was not soluble under the reaction conditions. Finally, using $SnCl_2$ in concentrated HCl,[114] we managed to reduce nitroaromatic **2.19** in a yield of 72%. However, this reaction was not ideal as it required a large excess of $SnCl_2$ (4.0 g for the reduction of only 1.0 g of **2.19**) making it difficult to scale up. For that reason, we reinvestigated reduction of **2.19** over palladium in different solvents. Ultimately, the best conditions for the hydrogenation were found to be 5 wt % palladium in CH_3CN, obtaining the product with a good yield of 71%.

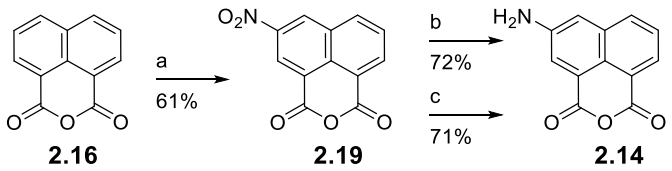

Scheme 2-11*: **Reagents and conditions:*** a) H_2SO_4, HNO_3, 5 °C to rt; b) $SnCl_2$, HCl, EtOH, rt; c) 5 wt % Pd/C, H_2, CH_3CN, rt.

With the two fragments successfully prepared on 5 g scale, the final step involved linking them together. After macrocyclisation, this was the second biggest challenge of the synthesis, to be accomplished by cross-coupling. Our first approach explored direct metal-catalysed cross-coupling using Ullmann or Buchwald-Hartwig reactions (**Scheme 2-12**).[115-117]

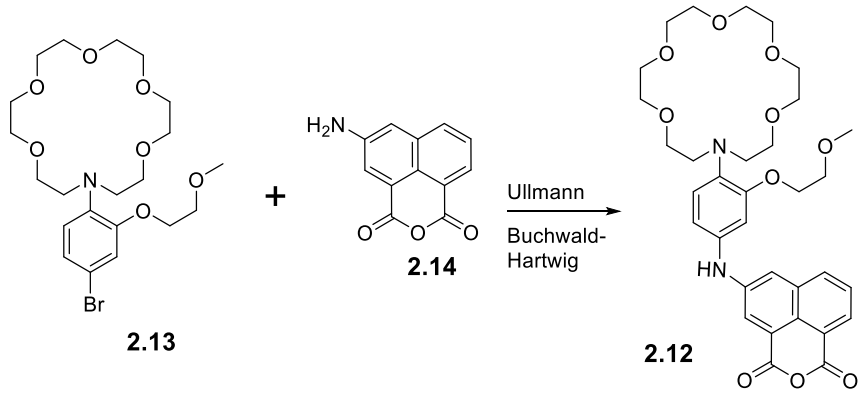

Scheme 2-12: Attachment of the fragments.

The Ullmann condensation involves a copper-catalysed aromatic substitution, between a nucleophile and an aryl halide (**Scheme 2-13**). In our system (**Scheme 2-12**) we were expecting the aniline **2.14** to be sufficiently nucleophilic to substitute the bromoaromatic **2.13**.

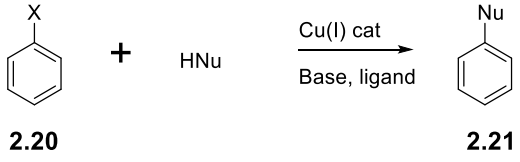

Scheme 2-13: Ullmann reaction.

The Buchwald-Hartwig cross-coupling is a palladium-catalysed synthesis of aryl amines, consisting of the reaction between an aryl halide and a primary or a secondary amine (**Scheme 2-14**).

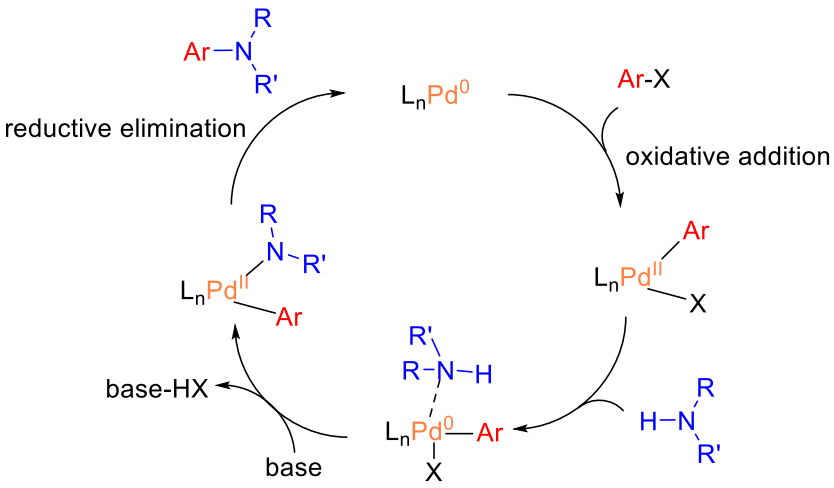

Scheme 2-14: Buchwald-Hartwig cross coupling reaction.

Firstly, the Ullmann condensation was attempted using conditions described in a recent paper.[118] In this work, CuI was used as catalyst, K_2CO_3 as base, pipecolinic acid as ligand and DMF as solvent. Unfortunately, there was not reaction. Moreover, it was difficult to follow the reaction by mass spectrometry, and all attempts to isolate products were inconclusive.

To ensure that the amine **2.14** was indeed reactive towards nucleophilic substitution we utilised a simple aryl halide **2.23** as a model (to prevent wasting the precious crown ether **2.13**) and the reactivity of **2.14** was tested (**Scheme 2-15**) using bromobenzene. The Ullmann condensation was tested using two different sets of conditions; the first conditions were as already described using the CuI catalyst, the second using CuBr as a catalyst, KOH as the base and 1,10-phenantroline as a ligand.

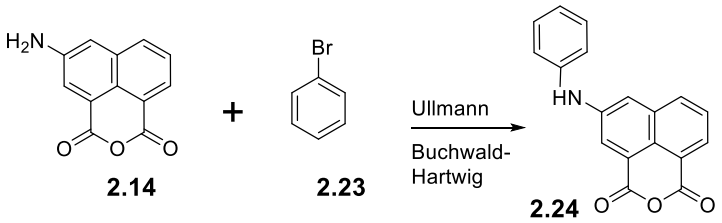

2.14 **2.23** **2.24**

Scheme 2-15: Test for amine reactivity.

The results (**Table 2-1**) indicate that the reaction cannot occur with our amine. We believe that the major issue was the solubility of the 3-Amino-1,8-naphthalic anhydride fragment **2.14**. For most of the reactions we observed disappearance of **2.14** by mass spectrometry, but we did not observe any product ion that was consistent with formation of our target product. Purification was also difficult due to the characteristics of the product **2.24**.

Reaction	Catalyst	Base	Ligand	Solvent	Results
Ullmann	CuI	K_2CO_3	Pipecolinic acid	DMF	No formation of desired product
Ullmann	CuBr	KOH	1,10-Phenantroline	Toluene	No formation of desired product
Buchwald-Hartwig	$Pd(PPh_3)_4$	Cs_2CO_3		Toluene	No formation of desired product

Table 2-1: Results for attachment of the fragments.

2.1.1.3 Alternative methods for fragment coupling

In view of the failure of the cross-coupling strategy, two new ways of linking the fragments were investigated, one consisting of a click reaction and the second involving a double Sonogashira coupling (**Scheme 2-16**). The Sonogashira reaction couples terminal alkynes with aryl or vinyl halides, typically using a palladium catalyst, a copper co-catalyst and an amine base. Click reactions involve the synthesis of 1,2,3-triazoles through a copper-catalysed 1,3-dipolar cycloaddition between an azide and an alkyne. For these two syntheses we first had to prepare the alkyne **2.27** and the two 1,8-naphthalic anhydride derivatives **2.26** and **2.28**.

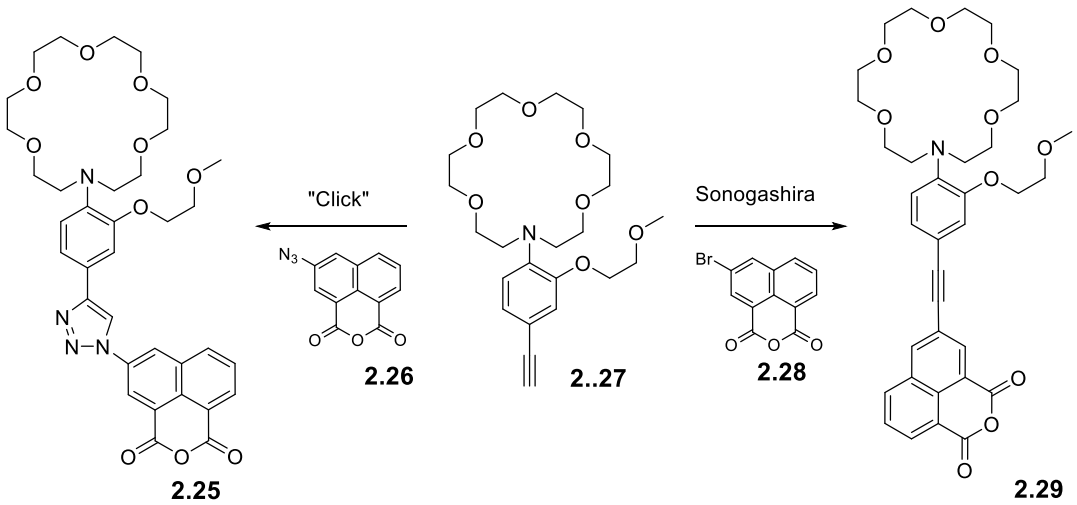

Scheme 2-16: New routes to coupling the fragments.

To prepare the alkyne **2.27** in good yield, we believed that the cyclic crown ether should be introduced at a late stage to prevent any loss of material during purification due to its high polarity. The alkyne macrocyclization precursor **2.31** was successfully obtained by Sonogashira coupling of the diol **2.15** (**Scheme 2-17**). However, subsequent

macrocyclisation was not successful and the alkyne starting materials was lost on all attempts

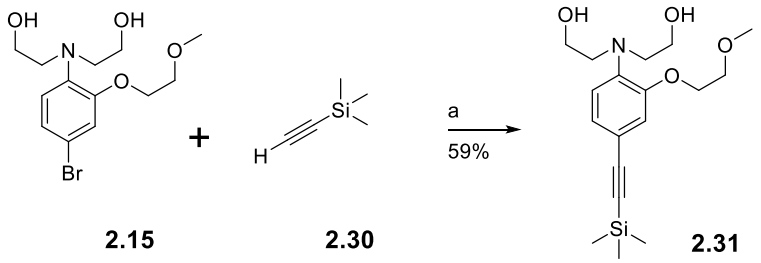

2.15 **2.30** **2.31**

Scheme 2-17: ***Reagents and conditions***: a) $PdCl_2(PPh_3)$, Et_3N, CuI, THF, 70 °C.

Therefore, the alkyne was added to the crown ether derivative **2.13**, first and then subsequent Sonogashira coupling was achieved with a yield of 48% after some optimisation of the conditions (**Scheme 2-18**). Different catalysts and solvents were investigated, along with different orders of addition of the components.[119] The catalyst $PdCl_2(PPh_3)_2$ gave better results than $Pd(PPh_3)_4$, also removing THF and using only Et_3N as solvent substantially increased the yield. Finally, considering the mechanism of the Sonogashira coupling, it was decided that trimethylsilylacetylene should be added last.

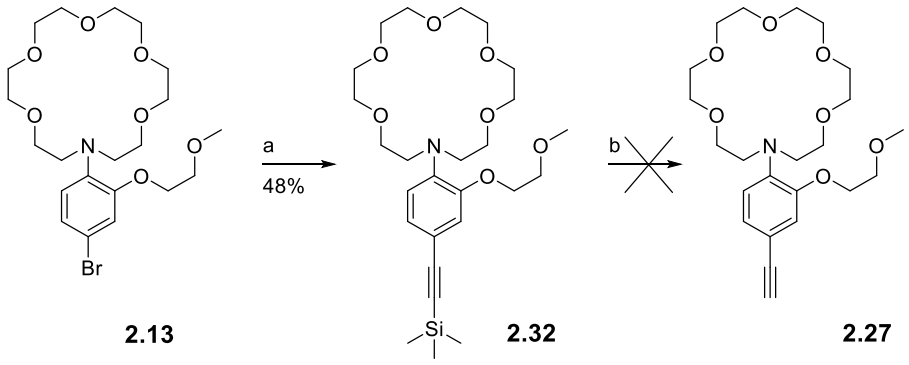

2.13 **2.32** **2.27**

Scheme 2-18: ***Reagents and conditions:*** a) $PdCl_2(PPh_3)$, Et_3N, CuI, 70 °C; b) K_2CO_3, MeOH, rt.

The main problem encountered was the purification of the unprotected alkyne **2.27**: addition of the TMS alkyne was successful and subsequent TMS deprotection proceeded but all purification attempts were unsuccessful. During purification different problems occurred such as polymerisation of the product, loss of the alkyne and product sticking to the silica column. At this point, and in view of the difficulties encountered attempting to purifying **2.27**, it was therefore decided to continue the synthesis with the crude product.

The required 1,8-naphthalic anhydride derivatives were prepared for coupling to **2.27**. Firstly, 1,8-naphthalic anhydride **2.16** underwent bromination using *N*-bromosuccinimide.

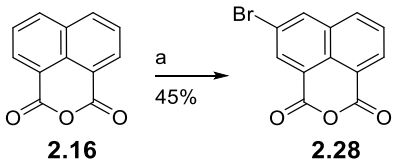

Scheme 2-19: ***Reagents and conditions:*** a) NBS, H_2SO_4 (conc.), 0 °C.

The reaction was first attempted using acetonitrile as the solvent but there was no reaction, replacing acetonitrile with conc. H_2SO_4 gave the product **2.28** with a mediocre yield under the harsh conditions (**Scheme 2-19**). Secondly, the azide **2.26** was synthesised from amine **2.14** using known methodology[120] via *in-situ* diazotization followed by substitution with sodium azide. The reaction proceeded well and gave a satisfying yield by crude NMR (**Scheme 2-20**), but all attempts to purify the azide **2.26** were unsuccessful due to its apparent poor stability. Therefore, this product was used crude in the following "click" reaction.

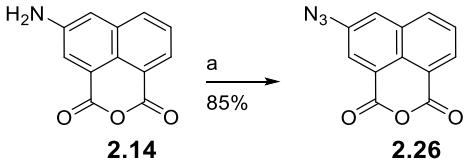

Scheme 2-20: ***Reagents and conditions***: a) HCl, AcOH, $NaNO_2$, NaN_3, H_2O, 0 °C to rt.

Our first attempt to link two fragments together was via a Sonogashira coupling. Different conditions were investigated using different catalysts, bases and solvents (**Scheme 2-21**).

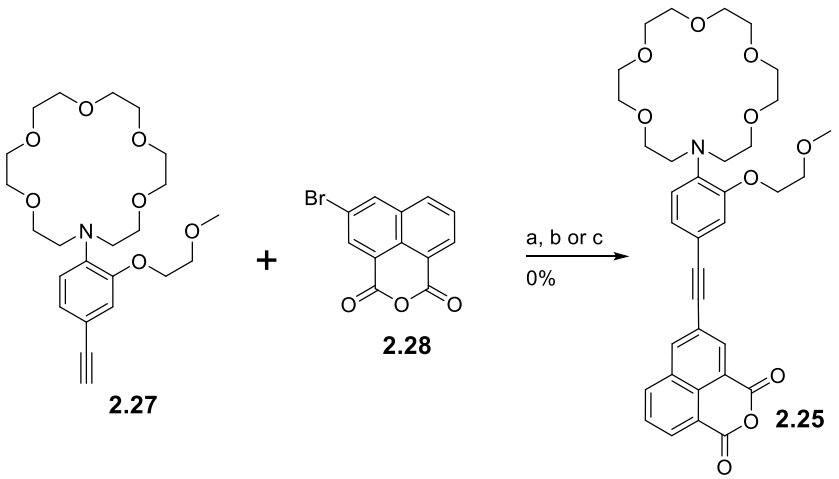

Scheme 2-21: ***Reagents and conditions***: a) $PdCl_2(PPh_3)_2$, PPh_3, DIPEA, toluene, 70 °C; b) $Pd(PPh_3)_4$, CuI, DIPEA, toluene, 70 °C; c) $Pd(PPh_3)_4$, CuI, Et_3N, THF, 70 °C.

The reaction failed to produce the desired product under any of the conditions investigated, as confirmed by mass spectrometry or NMR analysis of the crude reaction mixture. We believed that the problem resided in the naphthalic anhydride fragment. To confirm this theory, we tried to add the alkyne **2.30** to the naphthalic anhydride fragment **2.28** using the

previously successful conditions. However, the reaction failed, and in view of the growing number of failed attempts to couple naphthalic anhydride derivatives using metal-catalysed cross-coupling, we moved our attention to alternative coupling strategies.

We turned our attention to the click reaction of azide **2.26**. Several methods shown in **Scheme 2-22** were investigated,[67] but in all cases there was no reaction. As before, it was very difficult to detect anything by mass or NMR spectrometry and the purification was almost impossible, again due to solubility issues mainly associated with the 1,8-naphthalic anhydride system.

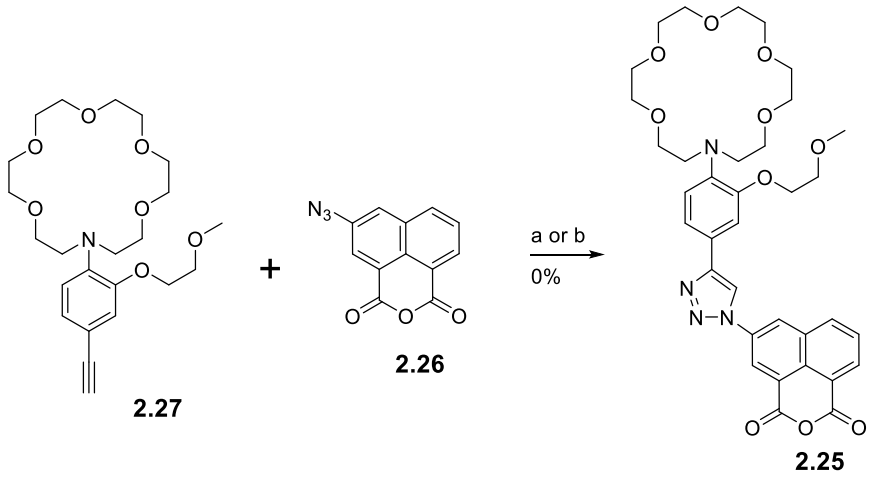

2.27 **2.26** **2.25**

Scheme 2-22: ***Reagents and conditions:*** a) CuI, THF, 60 °C; b) $CuSO_4.5H_2O$, sodium ascorbate, THF, H_2O, 60 °C.

2.1.1.4 Conclusion

Despite all our attempts to couple different aza-crown receptor and 1,8-naphthalic anhydride fluorophore fragments, we never managed to successfully prepare the target probe molecules such as **2.25**. An efficient synthesis of the aza-crown fragment was successfully achieved, but all our attempts of linking it to the fluorescent 1,8-naphthalic anhydride fragment were ineffective. After all our attempts we can conclude that the fluorescent fragment (1,8-naphthalic anhydride) was the main issue, mainly due to its poor solubility. We believed that the solution lay in identifying a suitable fluorophore, with improved solubility. A successful route to a fluorescent sensor will be presented in the following chapter.

2.2 Synthesis of probes for pH, zinc and potassium based on 5(6)-carboxyfluorescein

2.2.1 Modification of 5(6)-carboxyfluorescein with a linker

As presented in the introduction, fluorescein derivatives are molecules of great interest in extracellular interaction. In this chapter we will discuss the synthesis of carboxyfluorescein derivatives suitable for attachment to a surface. For that, we will need to add a linker to the fluorescein derivative, capable of reaction with a silica / functionalised silica surface.

The first step of the synthesis was the preparation of 5(6)-carboxyfluorescein as a mixture of isomers.[121] The reaction involved condensation of resorcinol **2.34** with 4-carboxyphthalic anhydride **2.33**, which gave the desired products as a mixture of regioisomers with a good yield (**Scheme 2-23**).

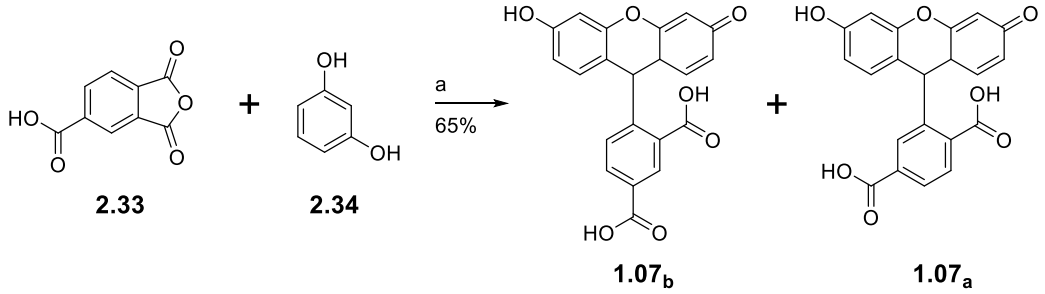

Scheme 2-23: ***Reagents and conditions:*** a) CH_3SO_3H, 80 °C.

5(6)-Carboxyfluorescein **1.07$_{a/b}$** was protected by acetylation of both hydroxyl groups (**Scheme 2-24**). The protection provides a derivative with better solubility and ensures that its fluorescent properties are not affected by the derivatisation, when protected carboxyfluorescein is less sensitive to light excitement making it more resistant to degradation.

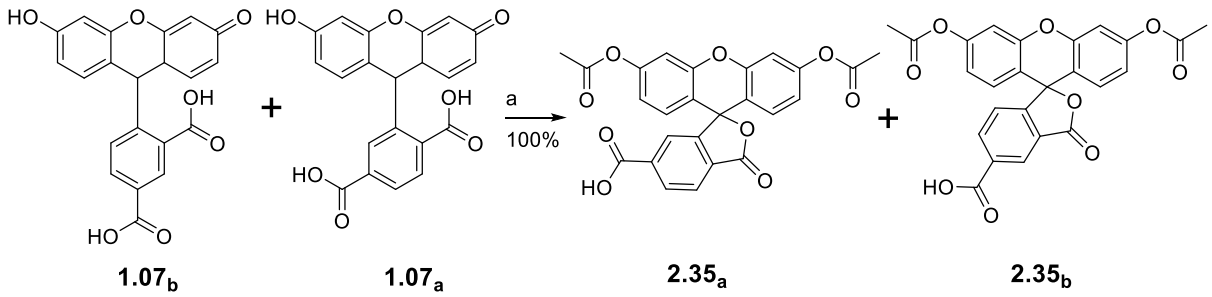

Scheme 2-24: ***Reagents and conditions:*** a) Ac_2O, pyridine, 110 °C.

Scheme 2-25 shows the first attempt at derivatisation of the carboxylic acid via formation of the acid chloride **2.36$_{a/b}$** prior to the reaction with (3-amino)triethoxysilane (APTES), which

would serve as a linker. Although the reaction may well have worked, this approach was unsuccessful as it was not possible to purify and characterise the product **2.37$_{a/b}$** due to low stability of the triethoxysilane function and the poor solubility of the molecule.

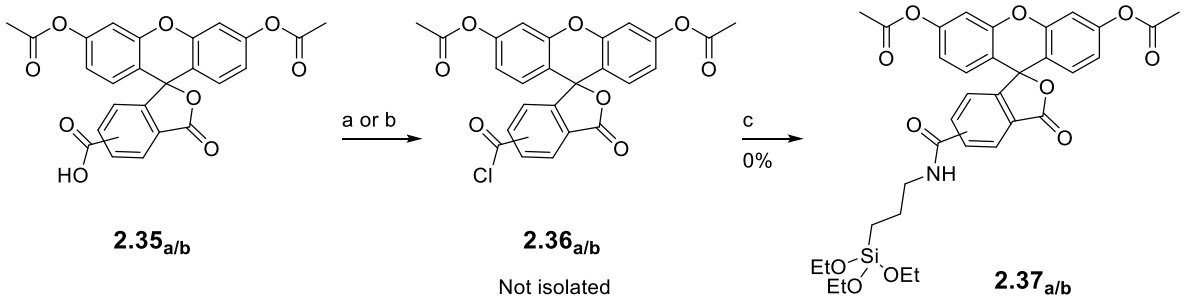

2.35$_{a/b}$ **2.36$_{a/b}$** Not isolated **2.37$_{a/b}$**

Scheme 2-25: ***Reagents and conditions:*** a) Oxalyl chloride, CH_2Cl_2, DMF, -78 °C; b) $SOCl_2$, reflux; c) APTES, toluene, Et_3N, rt.

The same problems occurred when a one-step synthesis was attempted using EDC/DMAP coupling conditions (**Scheme 2-26**). It was difficult to isolate and characterise the product by NMR spectroscopy as it was a mixture of inseparable isomers. The situation was further complicated due to the reactivity of triethoxysilane, which can readily polymerise and lead to products that are difficult to solubilise or characterise.

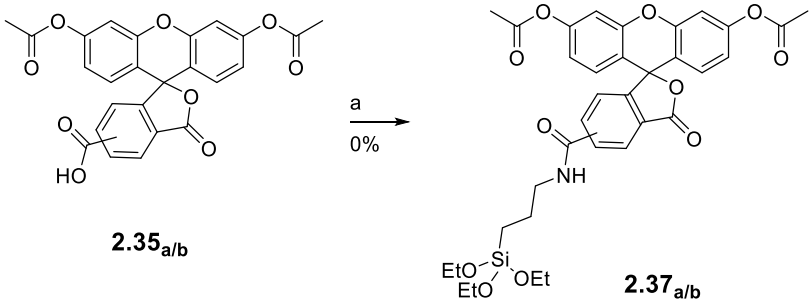

2.35$_{a/b}$ **2.37$_{a/b}$**

Scheme 2-26: ***Reagents and conditions:*** a) EDC.Cl, DMAP, APTES, CH_3CN, rt.

2.2.2 Separation of the isomers

In order to overcome the problem described above, a new strategy was developed to attach the linker directly onto the silica surface and then react the dye with the surface using a solid-phase coupling reaction. The modification of the silica surface with the linker will be described later in section **2.3.2**.

In order to attach the dye, the carboxylic function needed to be converted to a good leaving group. A recent paper describes a simple method to form a *N*-hydroxysuccinimide ester,[122] which is a good leaving group and also facilitates the separation of the two isomers (**Scheme 2-27**).

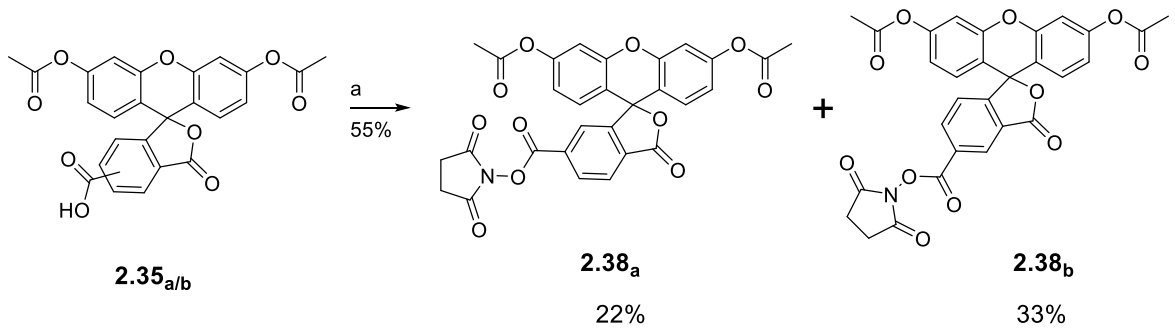

2.35$_{a/b}$ **2.38$_{a}$** 22% **2.38$_{b}$** 33%

Scheme 2-27: ***Reagents and conditions:*** a) NHS, CH_2Cl_2, DIC, rt.

The regioisomers **2.38$_{a}$** and **2.38$_{b}$** should be easily attached to the silica surface, and separation of the isomers would facilitate characterisation of the products. Having established a suitable method developed for activation and attachment of carboxyfluorescein to the silica surface, it was decided to synthesis modified carboxyfluorescein derivatives to prepare different probes appropriate for monitoring different extracellular fluxes.

2.2.3 Preparation of dichlorocarboxyfluorescein

In a recent paper, fluorescein was modified in order to vary its pK_a.[123] The authors modified fluorescein at the alpha position to the hydroxyl group with different functionalities (**Scheme 2-28**).

As previously described, the fluorescent properties of fluorescein are due to the different protonated forms of the molecule, and strong fluorescence is exhibited in the basic pH region. Therefore, modification at the alpha position modifies the fluorescence properties. For instance, the addition of a benzylic amine causes the molecule to exhibit strong fluorescence in the acidic region. This change can be explained by the photo-induced electron transfer (PET) process from the benzylic amine, at acidic pH protonation of the amine can block the PET process inducing high fluorescence at acidic pH.

This changes in pH-fluorescence properties provides wider possibilities to study extracellular flux. It has been reported that benzylic amine derivatised fluorescein can be used as chemosensor for metal ions and anions.[123] With this information in hand, we decided to modify carboxyfluorescein derivatives as probes useful for the detection of different fluxes.

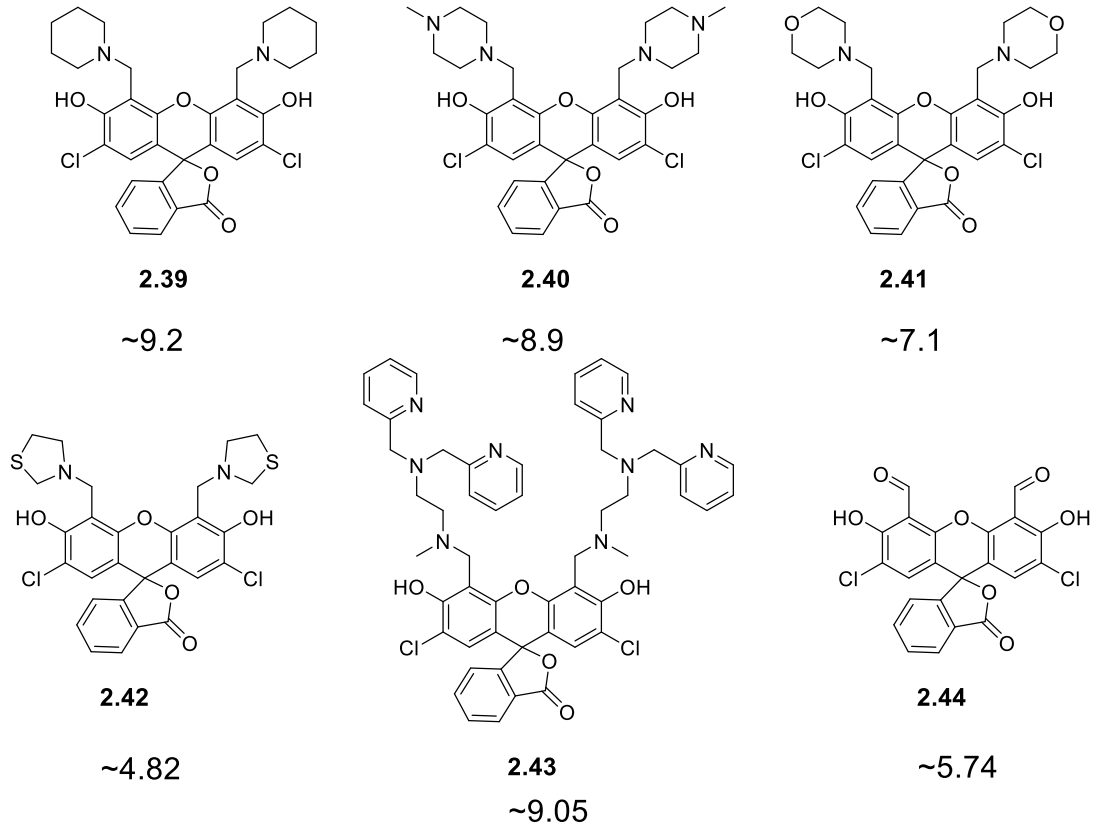

Scheme 2-28: pK_a of fluorescein derivatives.

The benzylic amine derivatives can be prepared through a Mannich reaction of fluorescein. In order to control the reaction, we first needed to block two other reactive positions, therefore 5(6)-carboxy-2′,7′-dichlorofluorescein **2.45$_{a/b}$** was prepared.

5(6)-Carboxy-2′,7′-dichlorofluorescein **2.45$_{a/b}$** was synthesised in the same way as 5(6)-carboxyfluorescein through a condensation with CH_3SO_3H (**Scheme 2-29**).

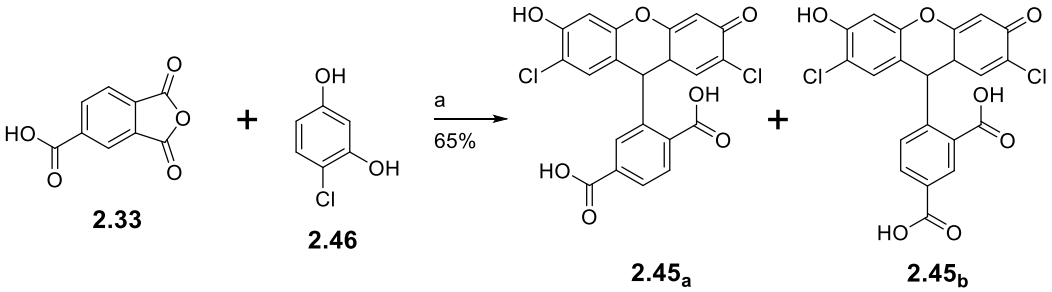

Scheme 2-29: ***Reagents and conditions:*** a) CH_3SO_3H, 80 °C.

At this point in the synthesis we wanted to separate the two regioisomers prior to the Mannich reaction, mainly to facilitate the characterisation of novel compounds. A purification performed in the same way as with 5(6)-carboxyfluorescein was not possible, as the *N*-hydroxysuccinimide ester would not survive the Manich reaction. A recent paper describes the preparation of 5- and 6-carboxyfluorescein on large scale: in this synthesis, the authors

prepared two benzophenone intermediates that can be easily separated by crystallisation (**Scheme 2-30**).[121] A further equivalent of resorcinol can be added to the separated intermediates in order to form the pure corresponding isomer.

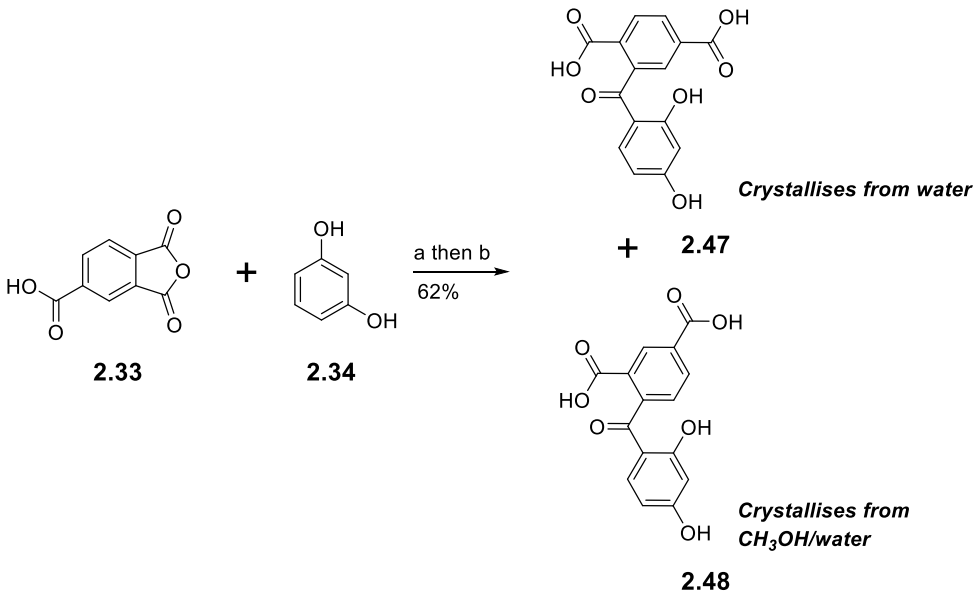

Scheme 2-30: ***Reagents and conditions***: a) CH_3SO_3H, 80 °C; b) 50% NaOH (aq.), 80 °C.

The reaction was first tested with 5(6)-carboxyfluorescein **1.07$_{a/b}$** in order to verify the method. It worked well and we managed to isolate the two benzophenones **2.47** and **2.48**. The method was then applied to the synthesis of 5(6)-carboxy-2′,7′-dichlorofluorescein **2.45$_{a/b}$**, but unfortunately it was not possible to separate the isomers after trying many crystallisation solvents.

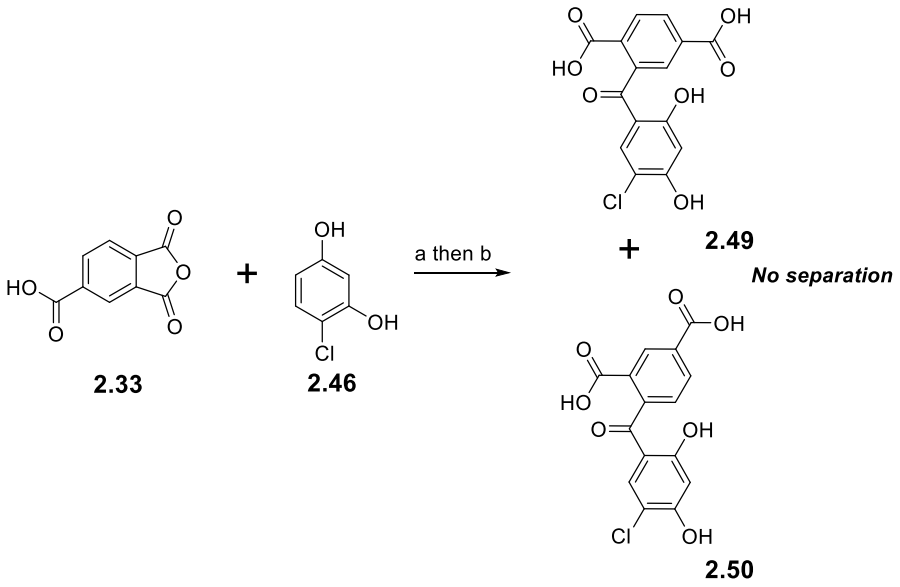

Scheme 2-31: ***Reagents and conditions:*** a) CH_3SO_3H, 80 °C; b) 50 % NaOH (aq.), 80 °C.

In this synthesis we wanted to avoid protection of **2.45$_{a/b}$** in the same way as for 5(6)-carboxyfluorescein as the acetylation of the two hydroxyl groups is undesirable for the Mannich reaction. However, a recent paper describing the separation of the two isomers via the acetylation of 5(6)-carboxy-2′,7′-dichlorofluorescein **2.45$_{a/b}$** led us to reconsider this approach.[73] The reaction of **2.45$_{a/b}$** with Ac_2O and pyridine facilitates the formation of the pyridinium salt of the 6-isomer **2.51$_a$**, therefore the salt can be easily isolated by filtration. The 5-isomer **2.51$_b$** does not form its corresponding pyridinium salt and can be easily isolated by extraction and subsequent recrystallisation. The reaction worked well producing the two pure isomers with acceptable yields (**Scheme 2-32**).

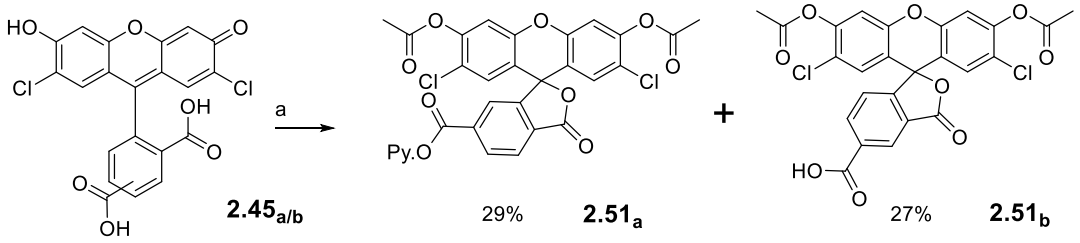

2.45$_{a/b}$ **2.51$_a$** **2.51$_b$**

Scheme 2-32*: Reagents and conditions:* a) Ac_2O, pyridine, reflux.

Both the isomers were then modified to allow surface attachment. The same procedure applied to 5(6)-carboxyfluorescein was used for the formation of the succinimide ester, giving the two final products in quantitative yields (**Scheme 2-33**).

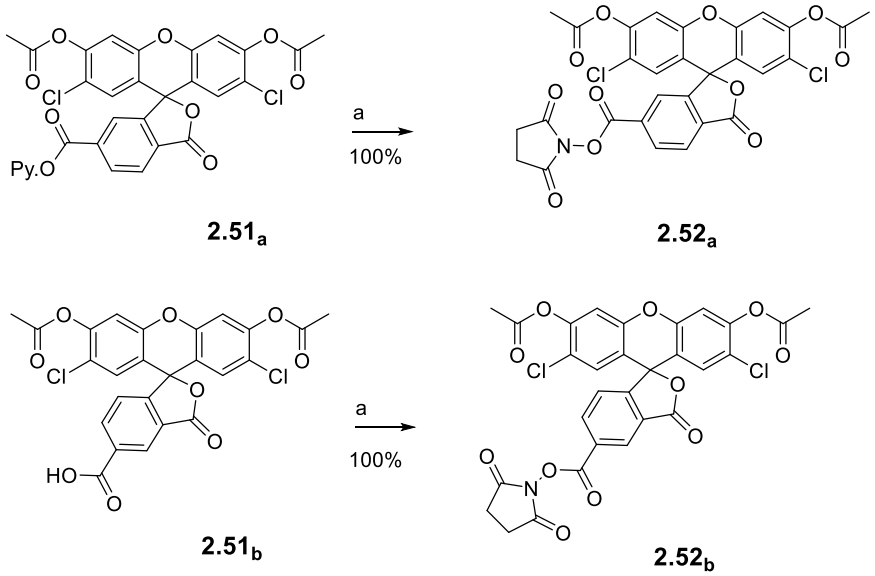

2.51$_a$ **2.52$_a$**

2.51$_b$ **2.52$_b$**

Scheme 2-33*: Reagents and conditions*: a) NHS, CH_2Cl_2, DIC, rt.

To conclude, four fluorescein-based probes have been successfully synthesised, containing functionality suitable for anchoring to a surface, which can be used to study cellular fluxes over a wide pH range; 5(6)-carboxyfluorescein **1.07$_{a/b}$** presents a pK_a of 6.5 and 5(6)-carboxy-2′,7′-dichlorofluorescein **2.45$_{a/b}$** a pK_a of 4.52. These probes are suitable for further

structural modification with different sensor functionalities, to extend their application to other species of interest or pH ranges as described below.

2.2.4 Mannich reaction

Before further derivatisation of the carboxyfluorescein derivatives, we needed to select the benzylic amine that would be most useful for detection of particular extracellular fluxes. Three amines were selected (**Figure 2-2**), which each possessed different characteristics. The morpholine **2.53**, with a pK_a around 7.1 and a strong fluorescence in the acidic region, could be useful to study extracellular pH fluxes in a completely different range from those accessible with fluorescein. Additionally, morpholine can interact with silver so that it could also be used as a probe for this metal.[124] The amine **2.54** is a well-known ligand used to bind zinc ions: carboxyfluorescein modified with this amine is a well-known probe for zinc. However, it has never been attached onto a surface, which could stimulate new interest and applications. Finally, fluorescein modified with the crown ether **2.55** would provide a new probe for potassium ion.

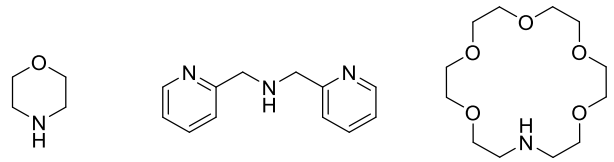

2.53 **2.54** **2.55**

Figure 2-2: Amines selected for probing properties

As previously described, a Mannich reaction was to be applied in order to introduce benzylic amine functionality into the the fluorescein probe. The classical Mannich reaction consists of a multi-component condensation of an aldehyde, an amine and an enolizable carbonyl (**Scheme 2-34**).

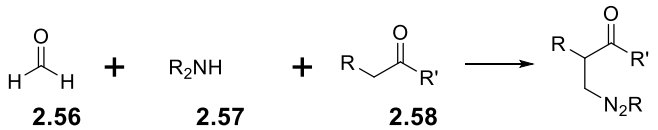

2.56 **2.57** **2.58** **2.59**

Scheme 2-34: Mannich reaction.

In our case, the carbonyl compound is replaced by the electron-rich aromatic ring of the fluoresceien derivatives, and the reaction should proceed through addition to the highly electrophilic iminium ion (**Scheme 2-35**).

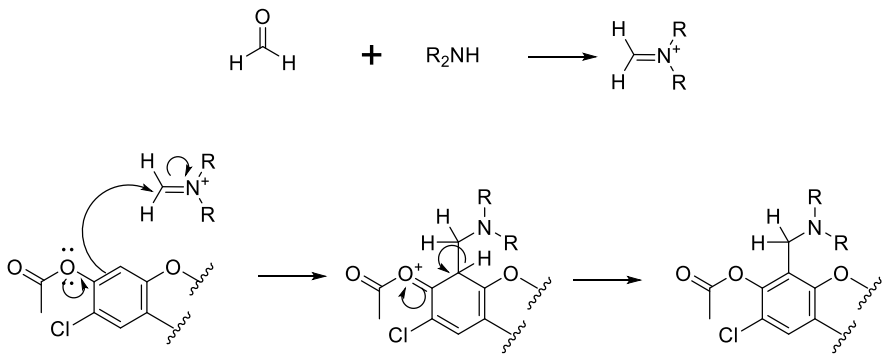

Scheme 2-35: Proposed mechanism for the Mannich of fluorescein derivatives

In the proposed mechanism, the importance of chlorine substitution at one of the activated positions is clear. Without it, the reaction would lead to a mixture of regioisomers with reaction at the two positions ortho to the acetoxy group. Furthermore, reaction meta to the acetoxy is unlikely as it is sterically blocked and is not activated by the lone pairs on the oxygen substituents.

Our first attempt was with the addition of morpholine, following a literature procedure using a mixture of water and CH_3CN as solvent.[73] The reaction worked, but with a low isolated yield due to solubility problems with the product. By removing the water, we could easily remove all the solvent and purify the product by recrystallisation obtaining both isomers with excellent yield (**Scheme 2-36**). It is worth noting that during the reaction the acetyl protecting groups were lost, presumably due to the nucleophilicity of the amine used in excess. The loss of the acetyl group could present problems during the later stages of the synthesis, however as it changed the solubility of the product, it simplified the purification process.

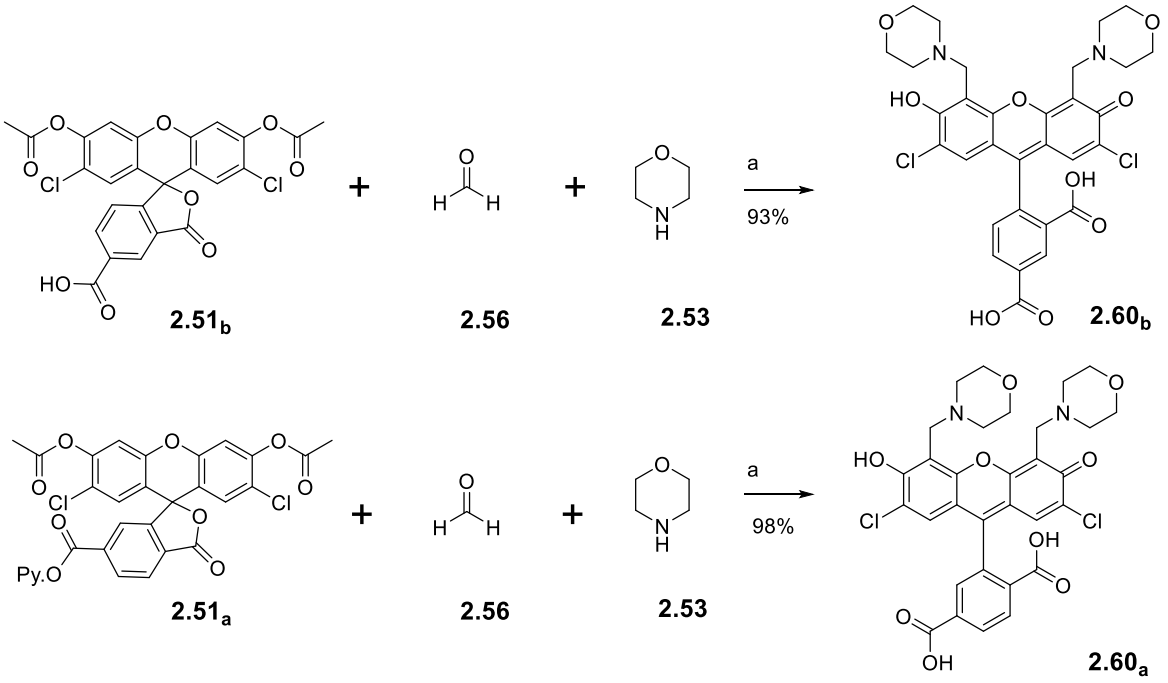

Scheme 2-36: ***Reagents and conditions:*** a) CH_3CN, reflux.

Fluorescein derivatives **2.61$_a$** and **2.61$_b$** are well-known probes for zinc, and were prepared following a known procedure.[73] This type of probe displays good results in terms of selectivity and sensitivity for zinc, and has been previously applied to quantify biological zinc.[72, 74] Different versions of this molecule, with different aromatic rings such as pyrazine and pyridine, are known but we decided to focus on the di-pyridine derivatives (**Scheme 2-37**). Here we modified the synthesis by removing the water, leading to increased yields. Both the isomers were prepared in good yield (**Scheme 2-37**).

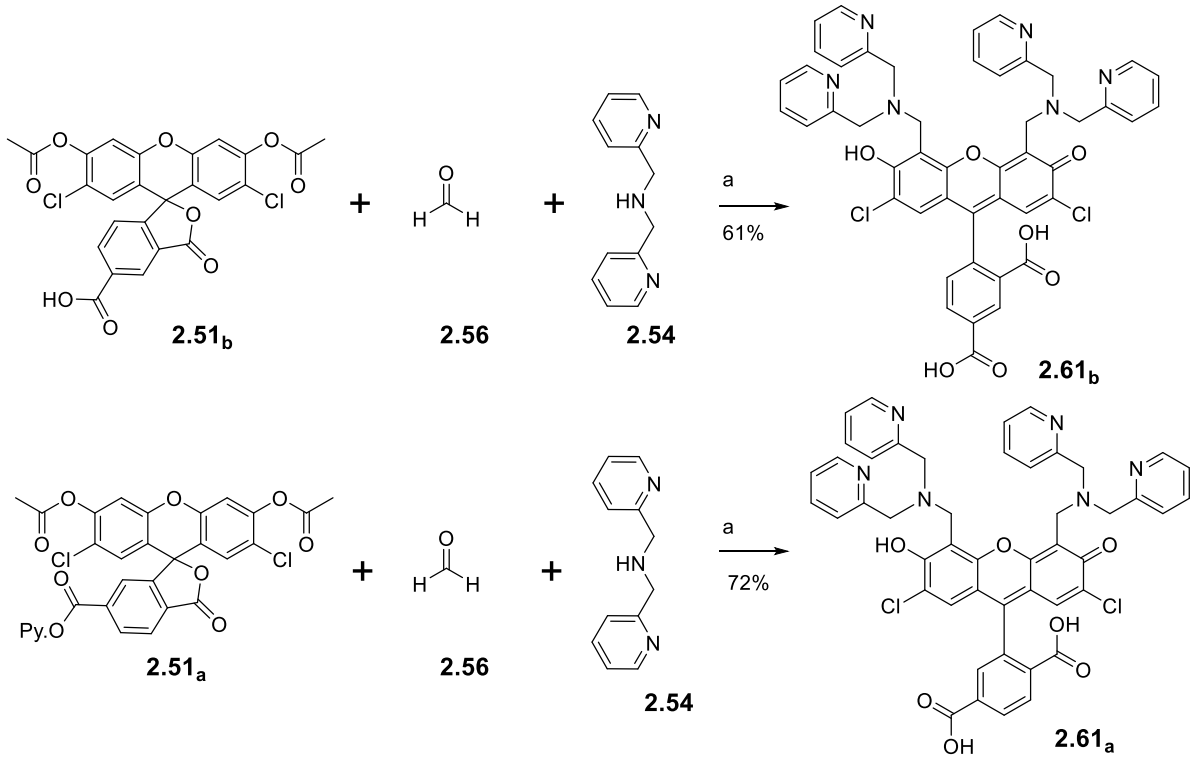

Scheme 2-37: ***Reagents and conditions***: a) CH_3CN, reflux.

Finally, the carboxyfluorescein was modified in the same way with an aza-crown ether. This molecule could offer a new type of probe for potassium. The synthesis avoided the difficult macrocyclisation step, facilitating scale up of the procedure and increasing the overall efficiency of the synthesis. The presence of two crown ethers on one molecule could also increase the sensitivity for potassium. This new derivative was synthesised using the 6-isomer only in order to perform preliminary studies (**Scheme 2-38**).

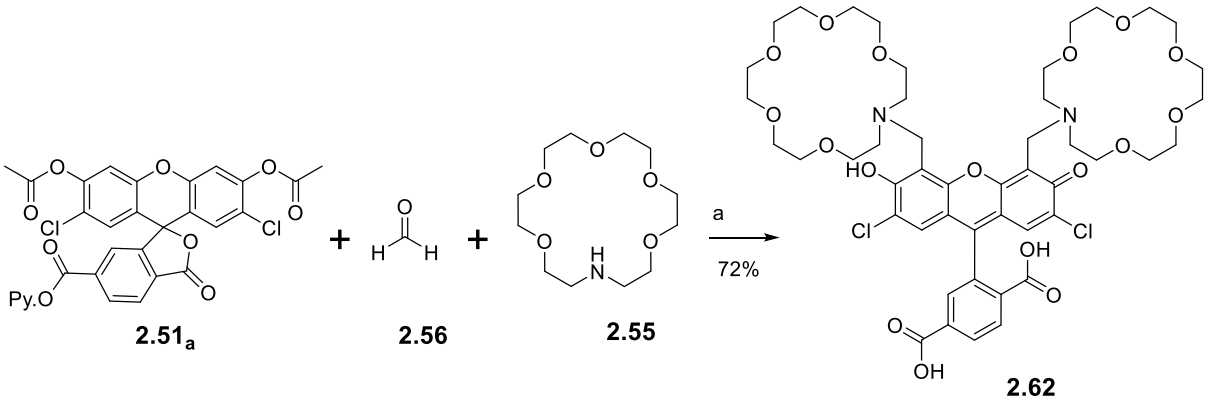

Scheme 2-38: ***Reagents and conditions:*** a) CH_3CN, reflux.

2.2.5 Preparation of the succinimidyl ester

The next step was the preparation of the *N*-hydroxy succinimide ester. Before performing this reaction we required protection of the carboxyfluorescein phenolic hydroxyls groups to ensure the closed ring lactone structure, ensuring only one carboxylic group is accessible for reaction with the *N*-hydroxy succinimide (**Scheme 2-39**).

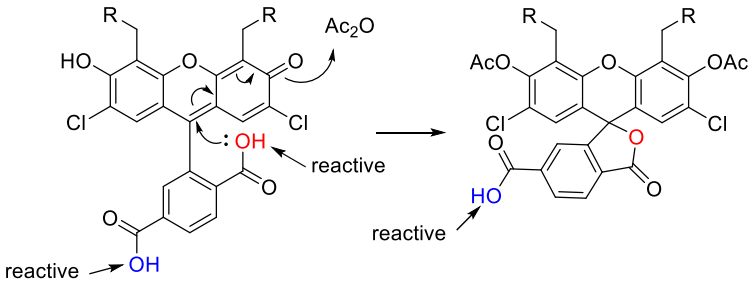

Scheme 2-39: Effect of protection on carboxyfluorescein.

The reaction did not work, probably as a consequence of the benzylic amino group sterically blocking these positions. We attempted to form the succinimidyl ester without protection expecting the desired carboxylic group to be more reactive as it is more accessible.

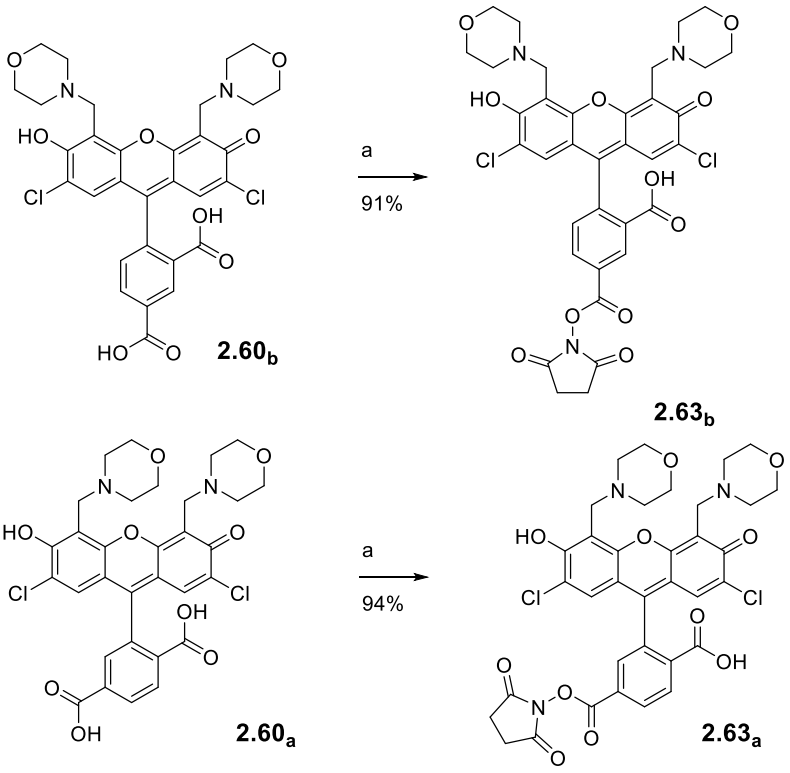

Scheme 2-40: ***Reagents and conditions***: a) NHS, CH_2Cl_2, DIC, rt.

The reaction was performed under the conditions that allowed control of the reactivity: one equivalent of *N*-hydroxysuccinimide was used in one portion. After a short time, the solvent was removed and the product was purified by recrystallisation from EtOH. The reaction worked well on the morpholine derivative (**Scheme 2-40**) and the zinc probe carboxyfluorescein derivative (**Scheme 2-41**).

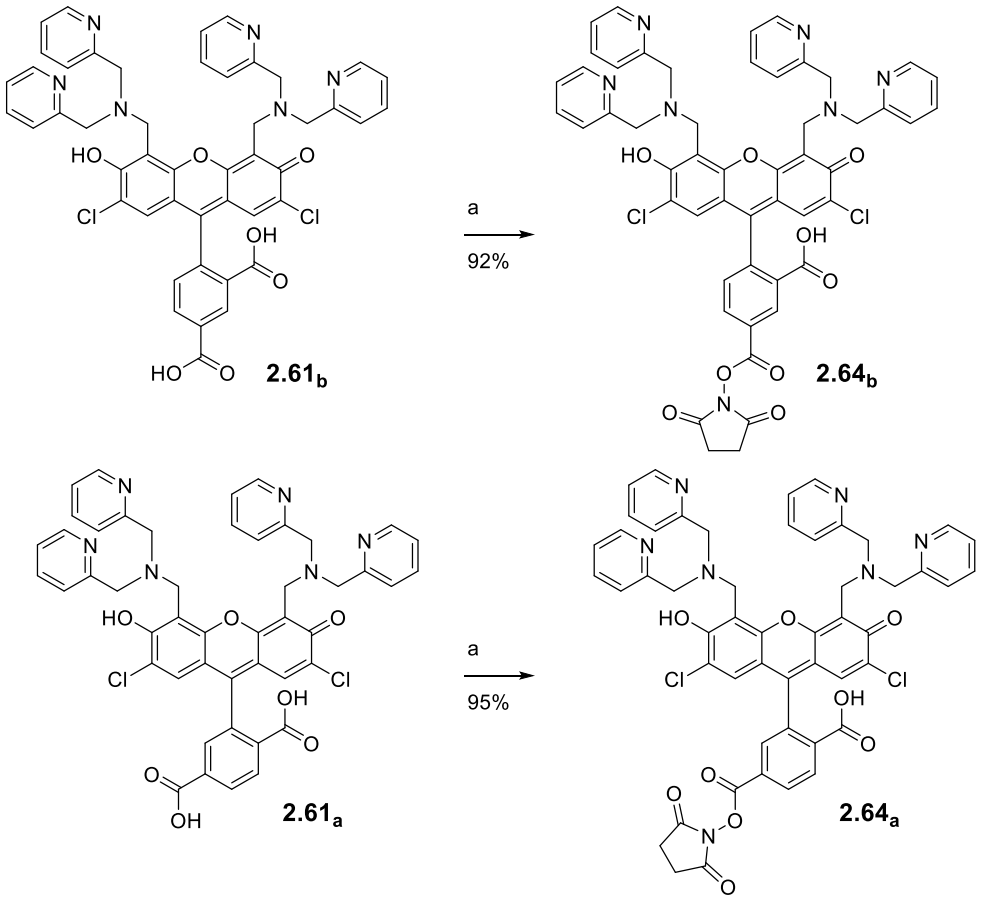

Scheme 2-41: ***Reagents and conditions:*** a) NHS, CH_2Cl_2, DIC, rt.

In conclusion, in this section the successful synthesis of nine new probes, suitable for attachment to surfaces, has been described (**Figure 2-3**). All the probes possess different characteristics and can be used to study different cellular fluxes. The next stage of the research involved preparation of the solid surface and attachment of the probes to the surface. Following that the modified surface will be characterised to ensure it has the required properties for biological applications.

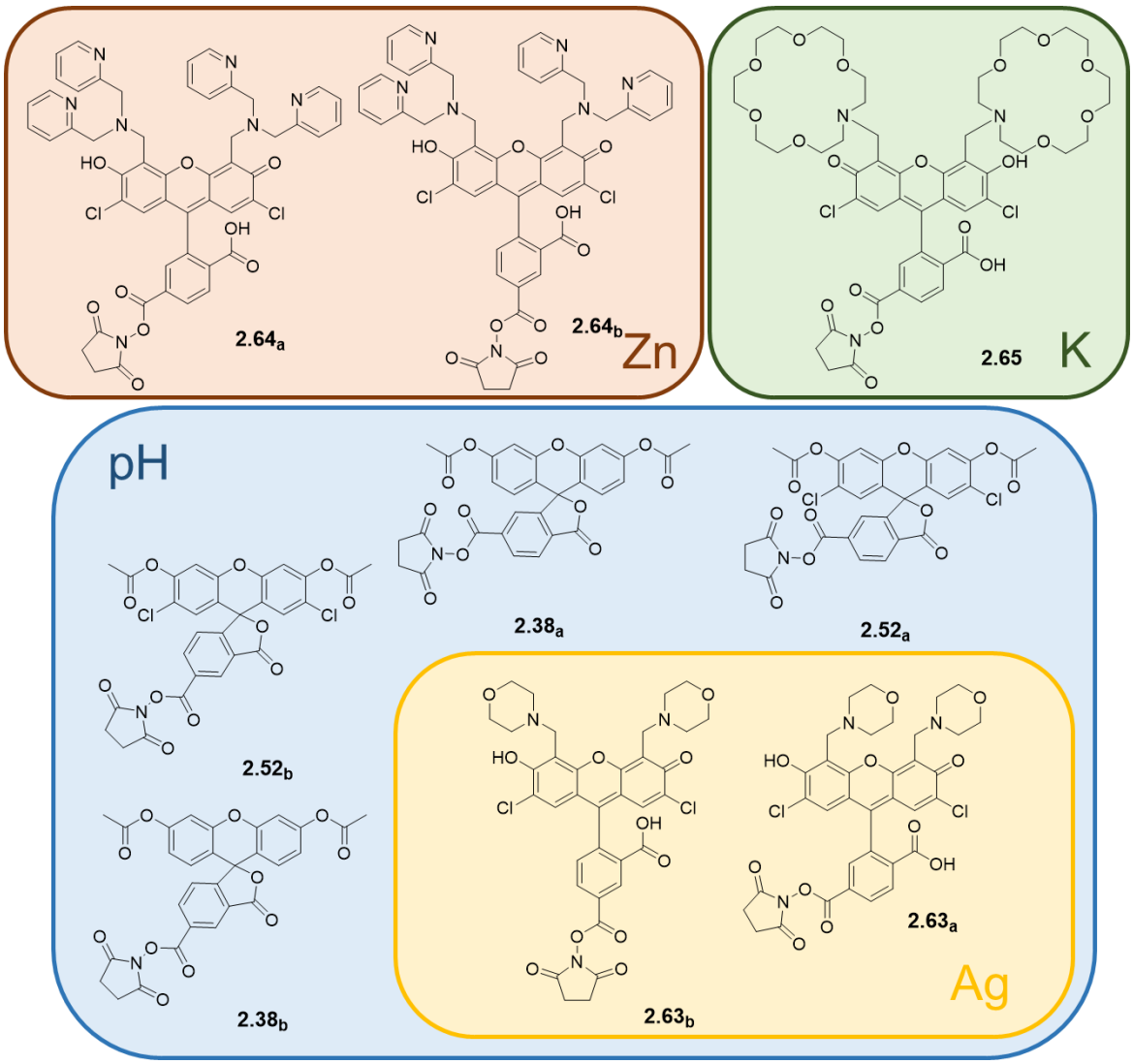

Figure 2-3: Summary of the probes prepared.

2.3 Preparation and derivatisation of the mesoporous surface

As discussed in the introductory chapter, an innovative aspect of this project involved attachment of our probes to a solid surface. Numerous types of surface and techniques of preparation exist, but our interest focused in growing mesoporous silica surfaces onto a conductive substrate. We have already presented the advantages of such surfaces. The following section will describe the technique employed to prepare such surfaces, Electrochemically-Assisted Self-Assembly (EASA), developed by Alain Walcarius in 2007.[103]

2.3.1 Electrodeposition of silica on ITO

The procedure described by Walcarius[103] consists of growing a mesoporous silicate surface onto a conductive substrate through the application of a negative potential (**Figure 2-4**). The first step is the preparation of an aqueous solution containing a surfactant, a supporting electrolyte and tetraethyl orthosilicate (TEOS). The surfactant is usually a long linear carbon chain with an ammonium salt polar head group, which can self-assemble on the surface thanks to the electric field. This will serve as a template for the deposition of TEOS, which creates the silica channels on the surface.

The pH of the solution must be decreased to pH 3 to activate the TEOS by protonation. An indium tin oxide (ITO) substrate is then placed in the solution and a negative potential is applied to the substrate for a specific amount of time. This negative potential reduces water to hydrogen and hydroxide ion, which increases the pH at the surface of the electrode, inducing the condensation of TEOS resulting in gelation on the surface. At the same time the surfactant forms micelles, so that the gelation of TEOS will occur around them providing the pore structure. The final step involves an acidic washing of the surface that removes the surfactant leaving a mesoporous silica on the substrate.

Walcarius explored a range of conditions, and he reported that parameters can be changed depending on required surface. For example, the choice of the surfactant plays a role in determining the size of the pores, the time of application of the negative potential allows control over the thickness of the silica layer deposited on the ITO. He also studied different surfaces as well as the use of different counter and reference electrodes. In our case, the optimum conditions chosen were: cetrimonium bromide as surfactant, ITO as working electrode and a potential of –1.3 V *vs.* SCE applied for 20 seconds.

Two different types of ITO substrate were used. In the intial stages we worked with ITO slides, as this is a cheap material, and therefore it was used in all trial surface reactions. Later work employed ITO coverslips, which are relatively expensive. The ITO coverslips are

very thin, which is important in order to obtain good results for the imaging of biological systems. The procedure described above was applied on the ITO slides and we were able to see a small amount of deposition on the surface even with the naked eye. However, different analytical techniques were applied to confirm the integrity of the deposition and study the porosity of the surface.

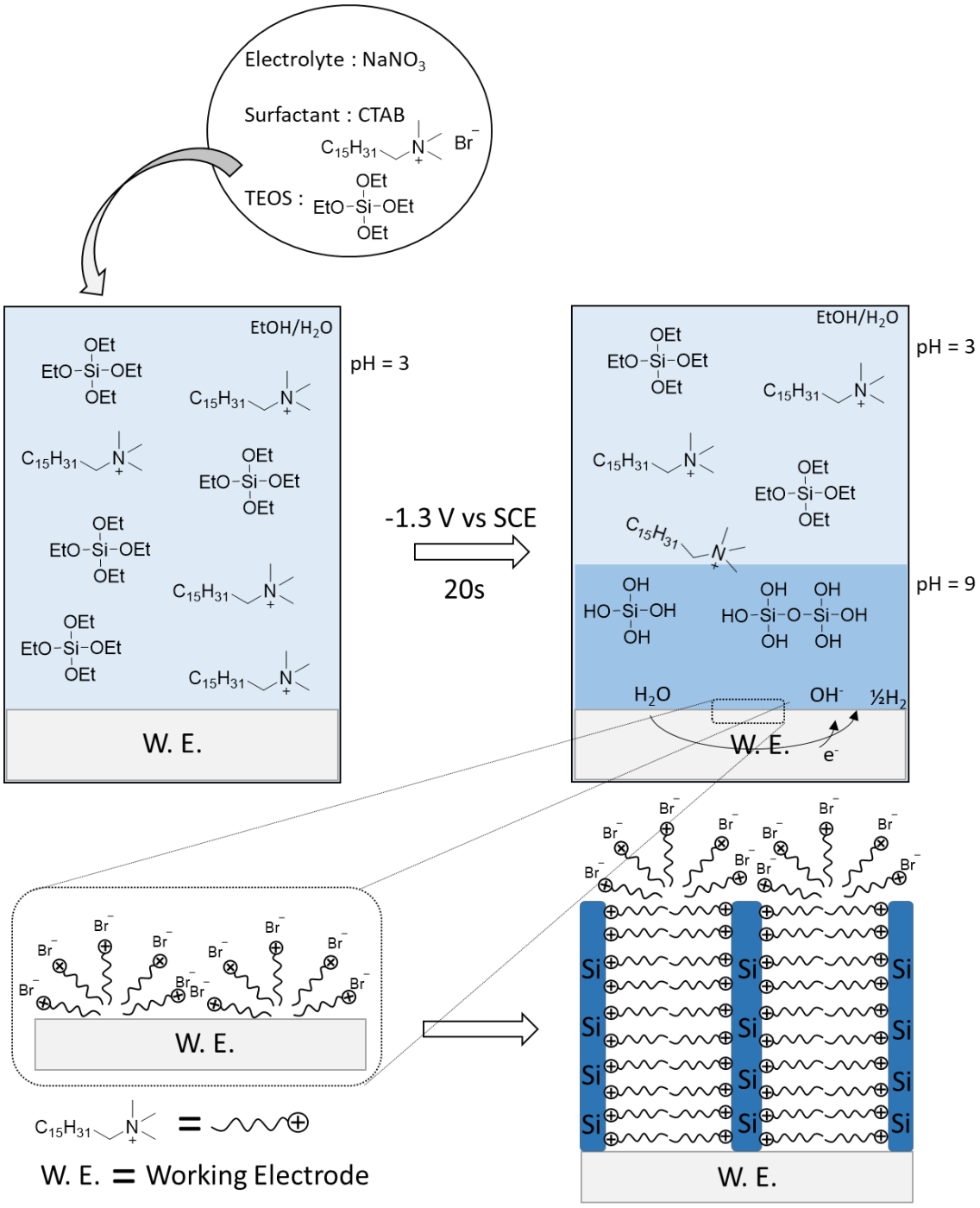

Figure 2-4: Electrochemically-assisted self-assembly (adapted from Walcarius *et al.*).[105]

An important part of this work was to validate the reason for using a mesoporous surface, and to establish that the pores were more beneficial than simply using a non-porous

material. We have already described the proposed benefits of such surfaces above (e.g. larger active surface area, potential for growing cells etc.). Therefore, as a control experiment we also prepared a non-porous silica surface and performed all the same experiments with it for direct comparison. The preparation of the non-porous surface was essentially the same as for the porous, only the surfactant was removed (**Figure 2-5**).

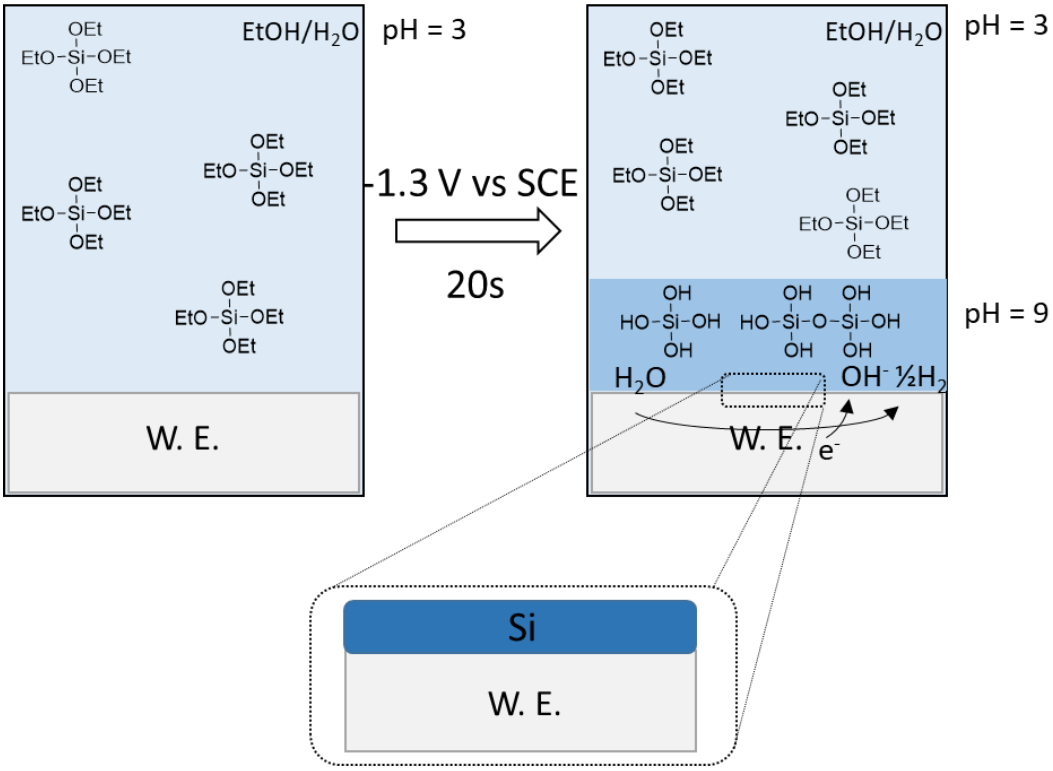

Figure 2-5: EASA for the preparation of non-porous silica.

As shown in **Figure 2-6** the chronoamperograms recorded for the electrodeposition of silica on three different substrates (a large coverslip, a small coverslip and another small coverslip without the surfactant) are quite similar. The small and large coverslips in the presence of the surfactant (red and blue curves) present a constant current slightly decreasing with time, which is consistent with previous work.[103] This pattern is due to the formation of the silica on the surface that slightly reduces the current, as the resistance is increased. However, when the surfactant is absent (yellow curve), the current starts at higher values and then rapidly decreases in the first couple of seconds. This is explained with the electrode surface being less crowded and therefore more accessible in the absence of surfactant, at least until the silica surface is formed.

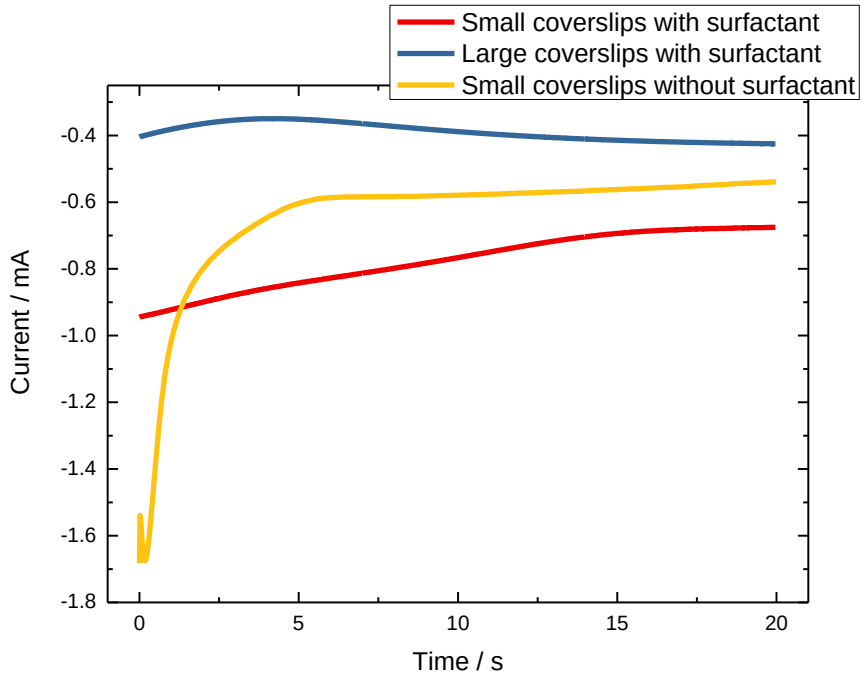

Figure 2-6: Chronoamperograms for the electrodeposition of TEOS on two different ITO substrates: small coverslips (1.5 mm × 1.5 mm × 0.55 mm with a surface resistivity of 70-100 Ω/sq) and large coverslips (2.5 mm × 2.5 mm × 1.1 mm with a surface resistivity of 70-100 Ω/sq), in the presence and absence of the surfactant.

When a new type of surface is synthesised it is always challenging to find methods to accurately characterise them. Different characterisation techniques will be presented in the following sections. The first technique is used widely for characterisation of many types of surface, and is based on X-ray scattering.[125]

2.3.1.1 Grazing Incidence Small Angle X-ray Scattering (GISAXS)

The first technique used to characterise the porous surface was grazing incidence small angle X-ray scattering (GISAXS). This technique is based on the X-ray specular reflectivity (XRR), a non-destructive technique to measure thin film properties such as film thickness, laterally averaged electron density distribution normal to the surface and interfacial roughness.

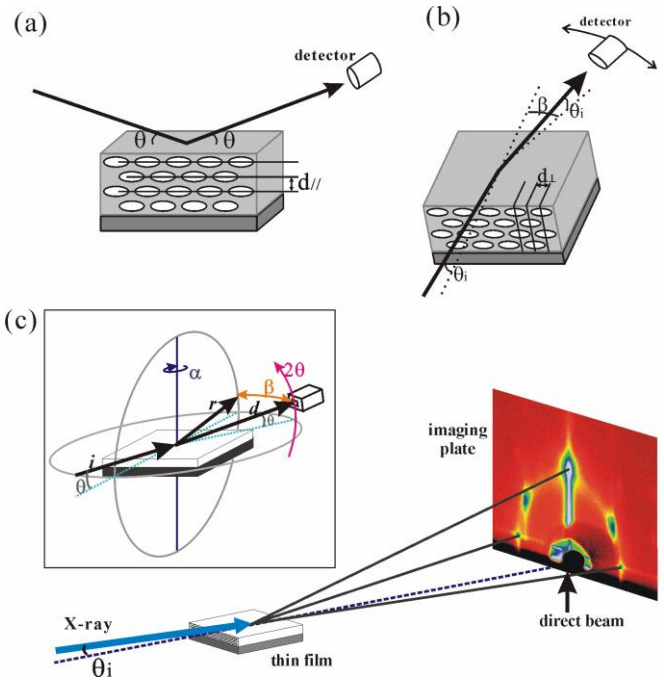

Figure 2-7: Schematic representations of (a) conventional out-of-plane θ – 2θ mode XRD, and (b) grazing incident in-plane mode XRD. (c) An illustration of the geometry used for 2D GIXD measurements.

The X-ray refractive index of air is 1, while for dense matter it is less than 1. When the X-ray beam impinges from air to a flat surface with an incident angle *θi* below the critical angle *θc*, the beam is totally reflected. However, at an incident angle higher than *θc*, X-rays penetrate into the film and the intensity of the reflected beam drops sharply. The larger the incident angle, the deeper the X-rays penetrate.

Reflection mode X-ray diffraction (XRD) is a well-established technique for the characterisation and identification of structures of powdery mesoporous samples. However, the pores in mesoporous silica films are usually expected to pack and align in a specific and preferred orientation at the air-solution interface or on a flat substrate. With such ordering of pores, only lattice planes parallel to the surface, *d//s,* can be detected by XRD patterns in *θ – 2θ* scan (**Figure 2-7**).

In order to acquire information beyond the out-of-plane periodic lattice in the film, grazing incidence X-ray diffraction (GIXD) was employed. The incident beam impinges on the surface with an angle *θi,* which is often set at *θc* in GIXD. A beam-stopper is used to shield the direct and total reflection beams in order to avoid signal saturation of the 2D image plate detector, while the point detector can scan either vertically (*2θ*) or horizontally (*β*). The diffraction patterns of GIXD provide the bulk average information about lattice parameters of 2D structures in thin films.

In the case of mesoporous thin films prepared by EASA, grazing incidence small angle X-ray scattering (GISAXS) provided the results shown in **Figure 2-8**.

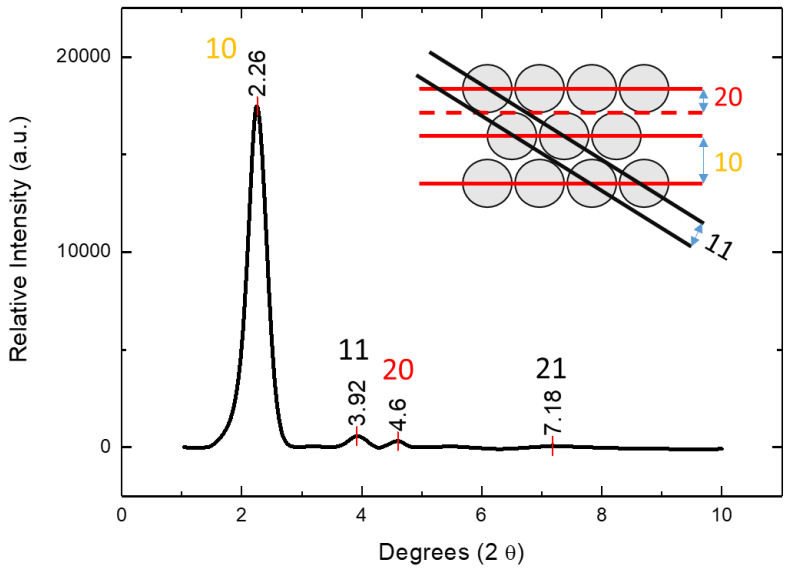

Figure 2-8: In-plane GISAXS pattern of a mesoporous silica film.

Each peak in the spectrum can be indexed as the 10, 11 and 20 reflections of a hexagonal lattice of cylinders with a lattice parameter to determine. The 10, 11 and 20 reflections of a hexagonal lattice refer to the different planes in the structure, and each plane is indexed with the Miller indices. The Miller indices are linked to the repetition within the structure of a material: for mesoporous silica with a hexagonal structure where each circle represents a pore and a, b and c are the lattice parameters. In a hexagonal structure with a = b and ϒ = 120 °, each peak of the X-ray analysis is linked to the distance between two similar Miller planes. This provides a method to determine the diameter of the pores or the distance between them. In **Figure 2-9** a 3-dimensional pattern of a hexagonal lattice is shown, giving an idea of the 3-dimensional structure of the surface.

With this technique the dimensions of the surface can be calculated. In accordance with to the work of Walcarius,[104] this procedure produced surfaces with the following characteristics:

Thickness = ~ 60 nm

Pore size = ~ 2 nm

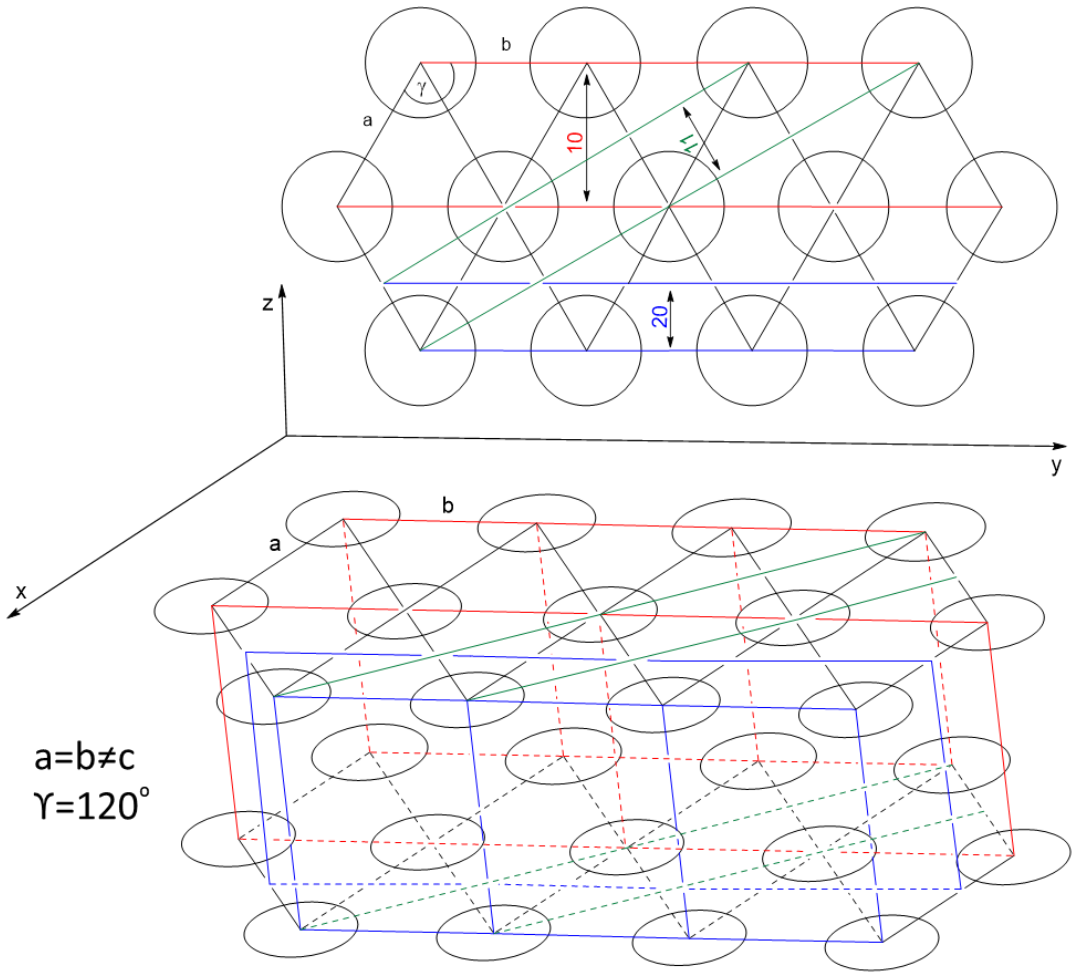

Figure 2-9: 3-Dimentional representation of a hexagonal lattice.

2.3.1.2 Cyclic voltammetry of the silica surfaces

One of the advantages of our porous surfaces on a conductive substrate is the possibility of carrying out electrochemical experiments. Therefore, it was necessary to prove that the surfaces would function as electrodes. A cyclic voltammetry (CV) study of $Ru^{2+/3+}$ was carried out (**Figure 2-10**). This experiment consisted of the reduction of Ru^{3+} and oxidation of Ru^{2+} using the modified ITO substrates as a working electrode.[97] This redox process is only possible if there is access to the working electrode.

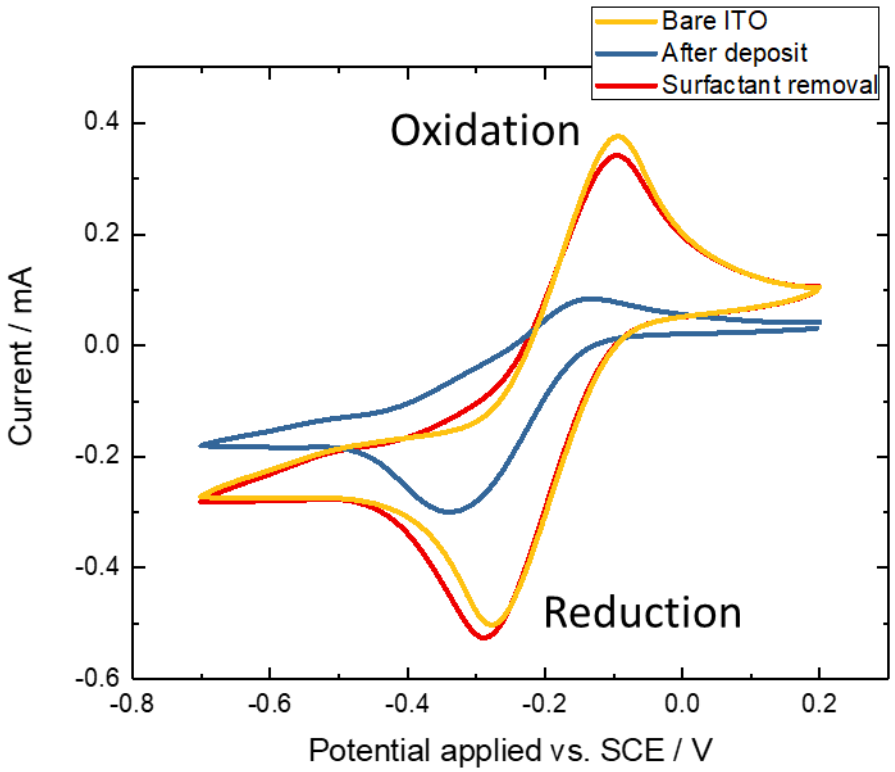

Figure 2-10: Voltammograms recorded at an ITO substrate (yellow) and an ITO/silica substrate (1.5 mm × 1.5 mm × 0.55 mm) before (blue) and after removal of surfactant (red). CVs were recorded in a solution of $NaNO_3$ (0.1 M) and $[Ru(NH_3)_6]^{3+}$ (1 mM) from 0.2 to −0.5 V vs. SCE at a scan rate of 0.05 $V.s^{-1}$.

The experiment was performed at each stage during the formation of the surface. In yellow, the CV trace obtained at a bare ITO substrate, shows both reduction and oxidation peaks of ruthenium, as expected. In blue, the CV trace recorded after EASA, there is a loss in the intensity of the redox peaks. However, as the surfactant is still in the pores access to the electrode surface is blocked making the reduction/oxidation of ruthenium more difficult. Finally, after washing and removing the surfactant, the red CV trace is almost back to that of bare ITO showing that the pores are now clean and accessible to the electrolyte.

The same CV study was performed on the flat silica (**Figure 2-11**), the CV recorded at a bare ITO substrate before the deposition of silica (red curve) displayed nice redox peaks as before. After the deposition of a flat silica surface, the CV trace showed much smaller peaks for the reduction/oxidation of ruthenium (blue curve), confirming our proposition that the ITO/silica mesoporous surface was suitable for electrochemistry experiments, but the flat silica surface was not.

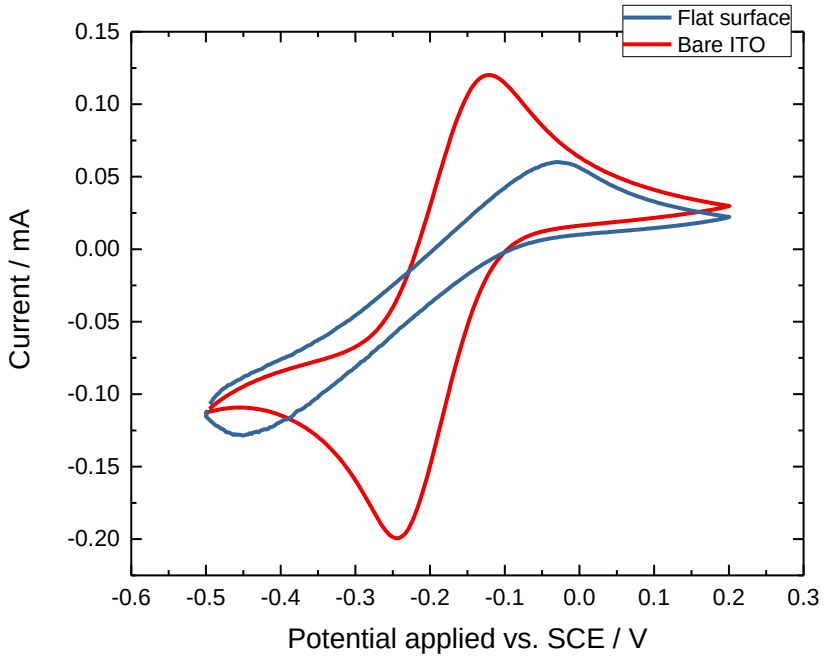

Figure 2-11: Voltammograms recorded at an ITO/silica substrate (1.5 mm × 1.5 mm × 0.55 mm) before (red) and after (blue) the deposition of a flat silica surface. CVs were recorded in a solution of $NaNO_3$ (0.1 M) and $[Ru(NH_3)_6]^{3+}$ (1 mM) from 0.2 V to −0.5 V vs. SCE at a scan rate of 0.05 $V.s^{-1}$.

2.3.1.3 Microscopy study of the silica substrates

A good method to characterise a surface is simply by close examination using microscopy techniques, such as Scanning Electron Microscopy (SEM). For these studies a SEM Philips XL30 environmental scanning electron microscope (ESEM) using a 30 kV accelerating voltage was used (**Figure 2-12**). With this technique we cannot actually see the pores of the surface as the resolution of this microscope is too low. However, SEM can still provide us with useful information. Pictures 1 and 3 (**Figure 2-12**), show the surface after the removal of the surfactant, we note aggregates of silica all over the surface (white in the picture). These are common feature, they form in solution and precipitate on the surface.

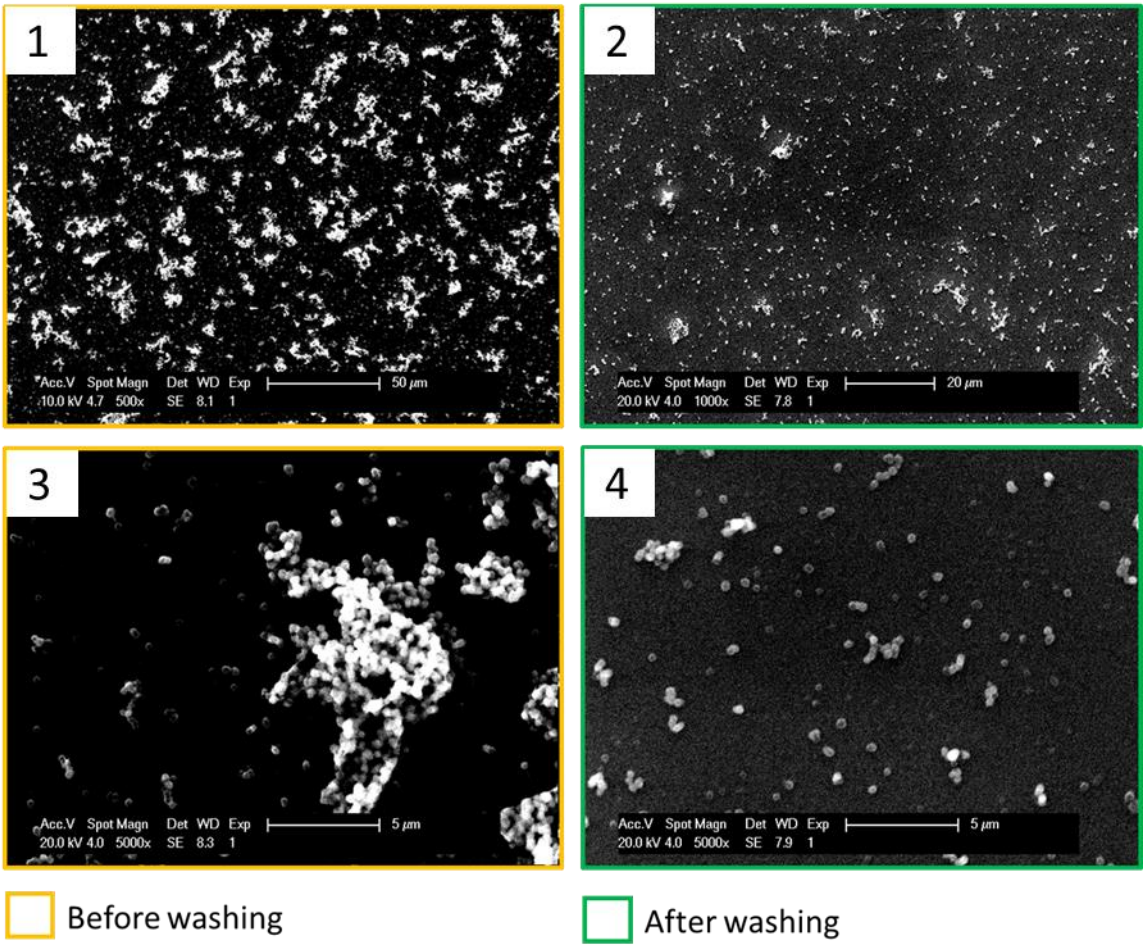

Figure 2-12: SEM pictures of mesoporous silica substrates prepared in this work.

The aggregates formed during the deposition process could be an issue when attaching the probes to the surface and subsequent biological tests. We would prefer a clean surface to avoid such complications. To remove the aggregates, a second acidic washing with 0.1 M HCl in EtOH was performed, followed by a basic washing with 0.1 M NaOH in water. The surfaces were then dried overnight and the new pictures obtained by SEM (2 and 4 in **Figure 2-12**) show the surfaces with reduced aggregates confirming that most were removed by washing leaving only some very small clusters of silica (< 1 µm). The acidic and basic washing produced a clean surface for the next steps.

An optical microscope was also used, model: Eclypse LV 100ND optical microscope with an integrated camera, both purchased from Nikon. The software used to control the microscope is NIS element Eclipse. With this microscope we can easily see the border between the silica and the ITO (**Figure 2-13**). The surface is not uniform, but this should not prove problematic for future work.

To conclude, in this section we characterised the ITO/silica substrates using two different microscopic techniques. The main finding was the discovery of the silica aggregates, leading us to develop an appropriate washing procedure to eliminate them from the surface.

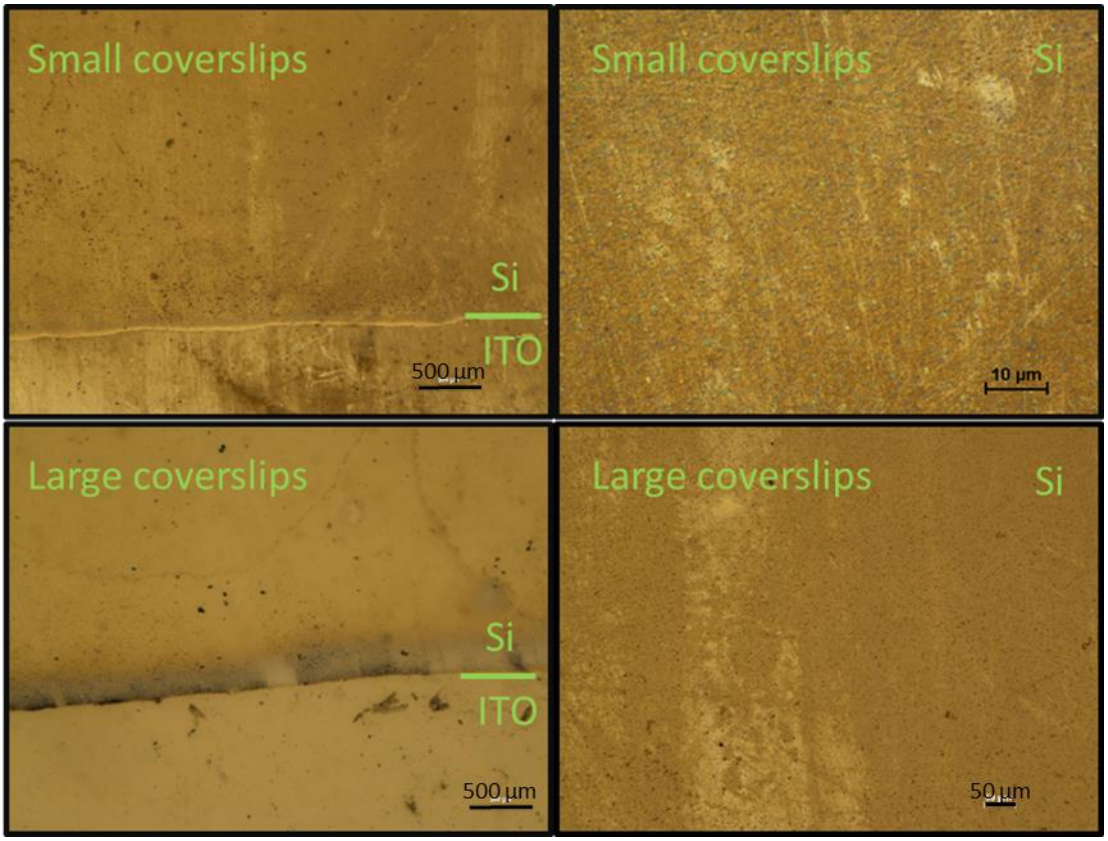

Figure 2-13: Optical microscope pictures of the ITO/silica surfaces from above.

2.3.2 Addition of the linker on the silica substrates

The next stage of the project was to add a linker to the ITO/silica surface in order to attach the probes. At the ITO/silica surface the reactive chemical functional group is silanol, therefore it was necessary to use a linker bearing a functionality able to covalently bind to the silanol groups of the surface but also possessing a further functionality that could react with the succinimidyl ester of the probes. We chose (3-aminopropyl)triethoxysilane **2.66** (APTES) for this purpose (**Figure 2-14**), which is a well established linker for use with silica based materials.[126]

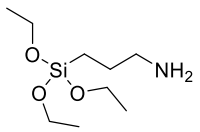

2.66

Figure 2-14: (3-Aminopropyl)triethoxysilane **2.66**.

The advantages of APTES are, firstly, the known reactivity of the triethoxysilane towards the condensation reaction with silanol groups and, secondly, the reactivity of the amine with succinimidyl ester. It is almost impossible to know how many silanol groups were present on the surface, making it difficult to estimate the concentration of APTES needed. At the

same time, it was important to not destroy the structure of the surface under the reaction conditions selected. It was observed that the surface was destroyed with strong acid, such as concentrated H_2SO_4**,** since all the characteristic peaks of ITO/silica at the GISAXS disappeared, as shown in **Figure 2-15**.

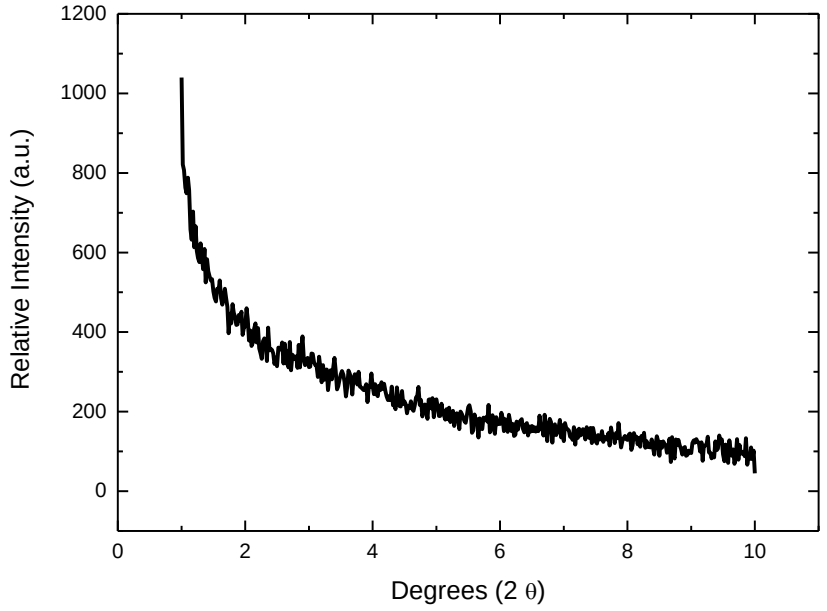

Figure 2-15: GISAXS of the ITO/silica surface after treatment with concentrated H_2SO_4.

However, it was found that triethoxysilane can react with a silica surface in EtOH without destroying the surface.[127] Therefore, the reaction was performed with 0.01 mM APTES in EtOH overnight at rt. Given that the area of our substrates was about 5 cm^2, APTES should be in large excess (**Scheme 2-42**).

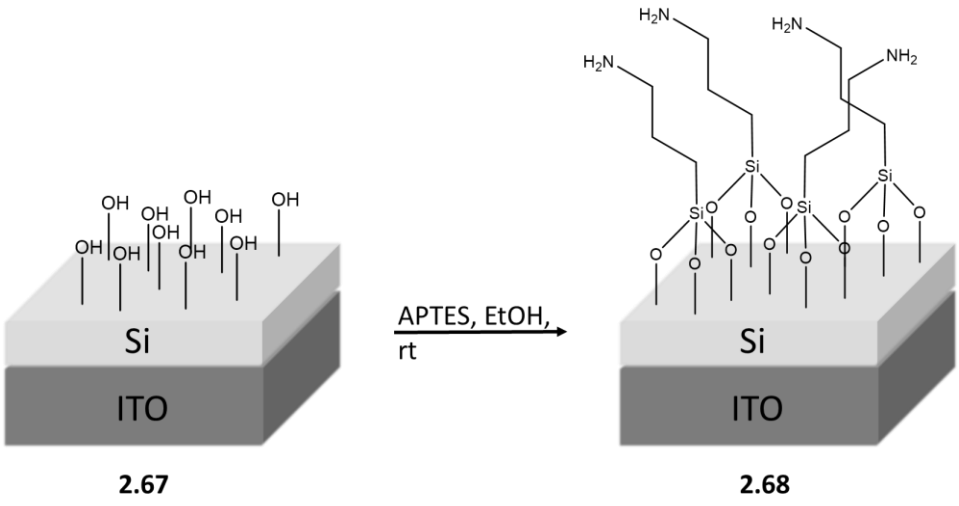

2.67 **2.68**

Scheme 2-42: Reaction of APTES with the ITO/silica surface.

In **Scheme 2-42** only one of the possible methods of attachment is represented, it is difficult to estimate how many bonds APTES would form with the silanol groups on the surface, given that each molecule of APTES has three reactive ethoxysilanes. After the addition of the linker, we ran X-ray diffraction to ensure that the material was still porous (**Figure 2-16**).

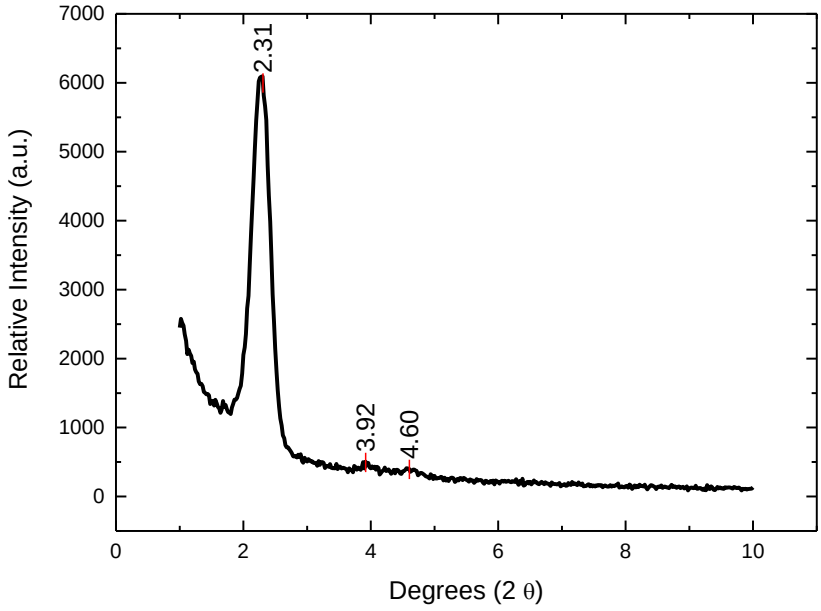

Figure 2-16: In-plane GISAXS pattern of mesoporous silica surface on ITO after treatment with APTES in EtOH.

In **Figure 2-16** some differences in the intensity of the characteristic peaks are evident, from comparison with the GISAXS spectrum of the surface recorded before the addition of the linker (**Figure 2-8**). One explanation for this is that the addition of APTES slightly modified the structure of the mesoporous surface.

The second analysis performed was cyclic voltammetry, again employing the reduction/oxidation of ruthenium performed on the substrate just after deposition of the silica (**Figure 2-17**).

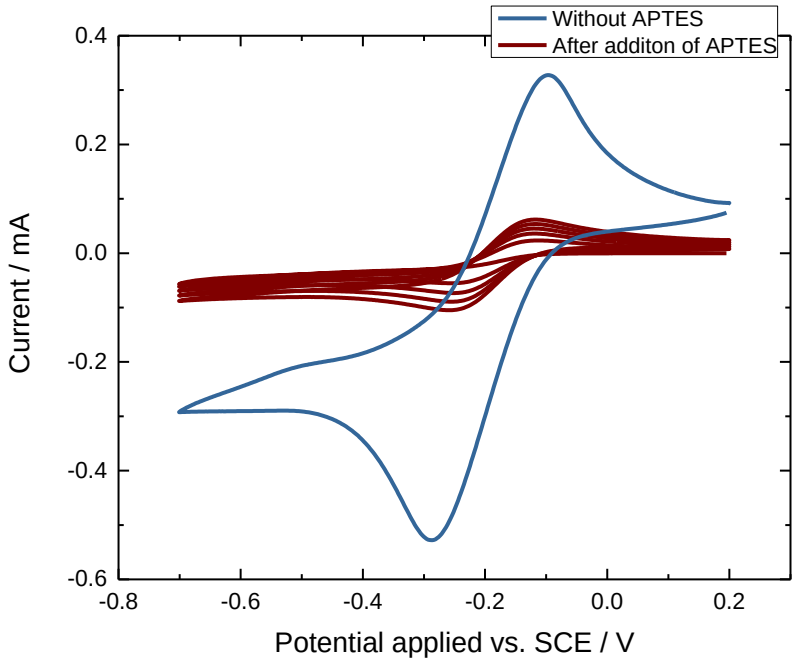

Figure 2-17: Voltammograms recorded at an ITO/silica substrate (1.5 mm × 1.5 mm × 0.55 mm) before (blue) and after (red) the addition of APTES. CVs were recorded in a solution of $NaNO_3$ (0.1 M) and $[Ru(NH_3)_6]^{3+}$ (1 mM) from 0.2 V to −0.7 V vs. SCE at a scan rate of 0.05 $V.s^{-1}$.

After the addition of APTES (red CV in **Figure 2-17**), the first scans presented very small redox peaks that slightly increased after each scan. This implied that the pores of the silica surface were blocked so that ruthenium could not easily access the electrode surface. Our conclusion was that the pores were initially blocked by some non-specifically absorbed APTES molecules. After leaving the substrate in solution, the APTES slowly diffused out of the pores leading to the observed increasing peak currents.

The electrode was left in the same electrolyte solution containing ruthenium salts and was stirred at rt. Then new CVs were recorded at different time intervals (**Figure 2-18**). The results of this experiment confirmed our first thoughts: there were APTES molecules non-covalently bound to the surface that were blocking the pores, and a simple washing was sufficient to remove them and clear the pores. The peaks reached their maximum after 30 min of stirring, they were slightly lower than the ones recorded at the surface without APTES (red CV in **Figure 2-18**): this was expected as the APTES was also covalently attached within the pores.

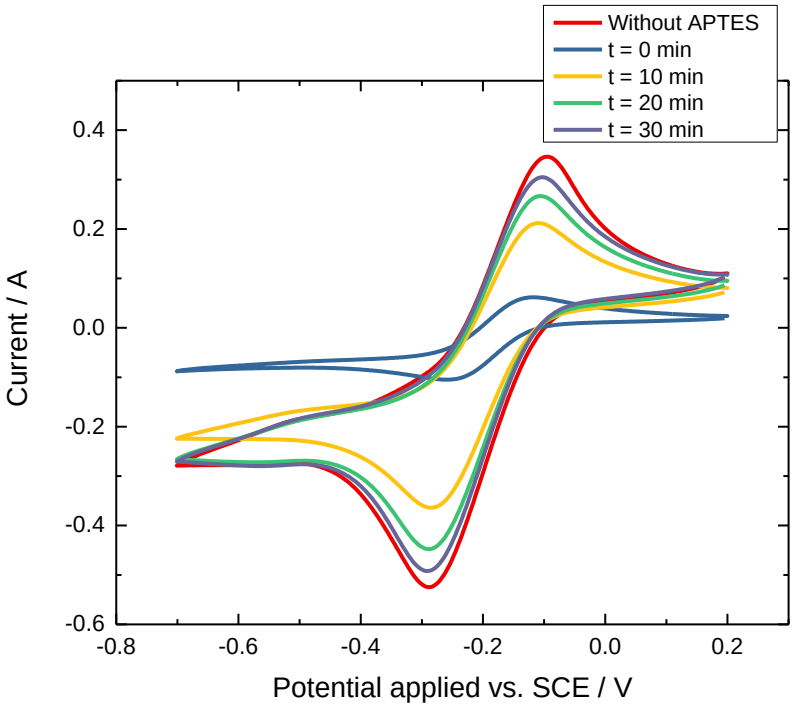

Figure 2-18: Voltammograms recorded at an ITO/silica substrate (1.5 mm × 1.5 mm × 0.55 mm) after the addition of APTES at different times after washing. CVs were recorded in a solution of $NaNO_3$ (0.1 M) and $[Ru(NH_3)_6]^{3+}$ (1 mM) from 0.2 V to −0.7 V vs. SCE at a scan rate of 0.05 $V.s^{-1}$.

Following these experiments, we concluded that the attachment of the linker was successful, although it was not possible to determine the surface coverage of the linker as there are no known techniques to observe this. However, more data can be gained to prove the attachment of the linker after addition of the probes. The probes providing us with more possibilities for analysis.

2.3.3 Attachment of the probes on the silica substrates

For the attachment of the probes to the surface, it was decided to apply identical conditions for each type of probe. The desired reaction was between the amine attached to the silica surface with the succinimidyl ester of the probes, and concurrent deprotection of carboxyfluorescein when required. The reaction was performed with a 0.01 mM aqueous solution of probe in 0.05 M aqueous NaOH at rt overnight. **Figure 2-19** shows all the different probes attached to the ITO/silica surface through this reaction.

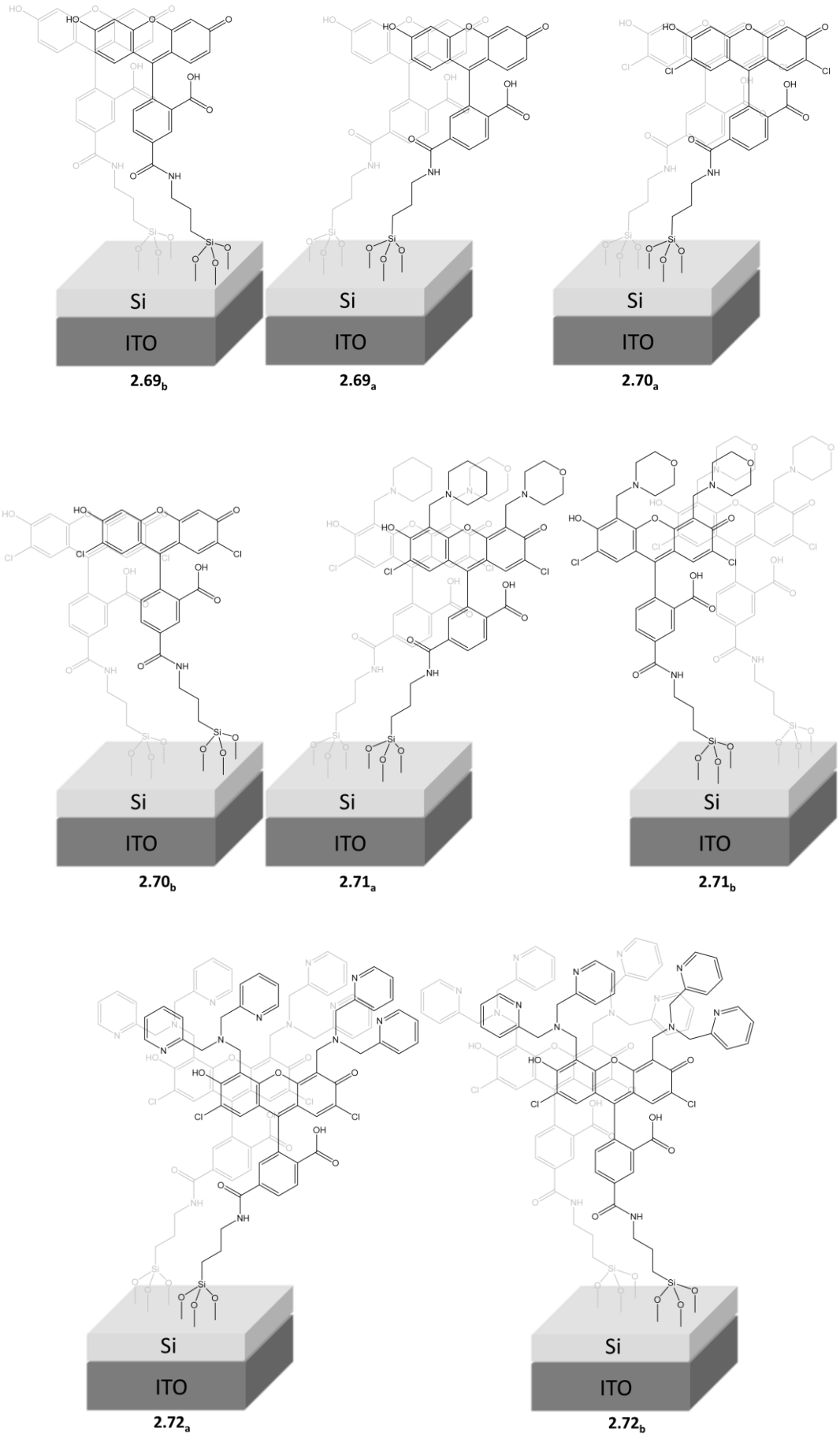

Figure 2-19: Résumé of the probes attached on the ITO/silica surface.

2.3.3.1 Cyclic voltammetry of the modified substrates

Prior to any bio-sensory application of the probes, it was necessary to prove the attachment of the probe and fully characterise the modified surface. Our first approach was to characterise the surface by cyclic voltammetry, we envisaged the we could to reduce and oxidise the carboxyfluorescein attached to the surface and to use the resulting voltammogram to determine its presence. The first experiment was performed employing a solution of ruthenium and a substrate modified with the 6-carboxyfluorescein probe **2.69$_a$** as working electrode (**Figure 2-20**).

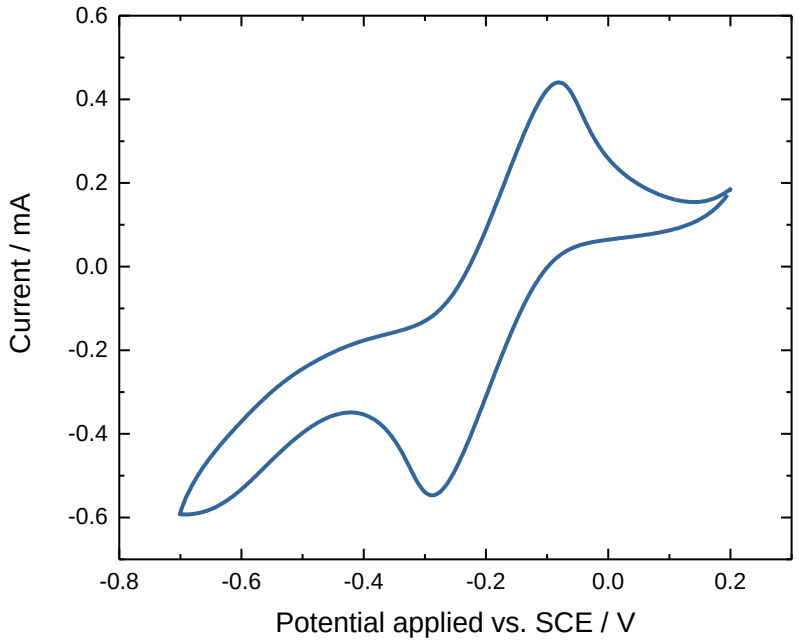

Figure 2-20: Voltammogram recorded at an ITO/silica substrate (1.5 mm × 1.5 mm × 0.55 mm) after the addition of the 6-carboxyfluorescein derivative **1.07$_a$**. CVs were recorded in a solution of $NaNO_3$ (0.1 M) and $[Ru(NH_3)_6]^{3+}$ (1 mM) from 0.2 V to −0.7 V vs. SCE at a scan rate of 0.05 $V.s^{-1}$.

On the voltammogram we can clearly see the two peaks of ruthenium at −0.1 V and −0.3 V, proving that the pores are accessible. However, this could imply that the coupling reaction did not work and there is only the linker on the surface. However, unlike in the previous voltammograms (**Figure 2-10**), there is big difference on the voltammogram at potentials more negative than −0.4 V: we also observe a new peak around −0.6/−0.7 V that could be due to the reduction of carboxyfluorescein. As a consequence, we ran another CV without ruthenium in order to try to detect the redox peaks of the carboxyfluorescein on the surface.

The voltammograms were recorded in a Tris buffer solution (pH 7.4, 50 mM) with the substrate modified with the 6-carboxyfluorescein probe **2.69$_a$** as working electrode (**Figure 2-21**). The first scan (red curve) showed a reduction peak at −0.6 V, which was no longer present in the following scans (blue curves). Moreover, no oxidation peaks were observed in the backwards scans. From this result we concluded that the carboxyfluorescein under these conditions is reduced and destroyed after the first scan. Nevertheless, these two experiments indicated successful attachment of the probes.

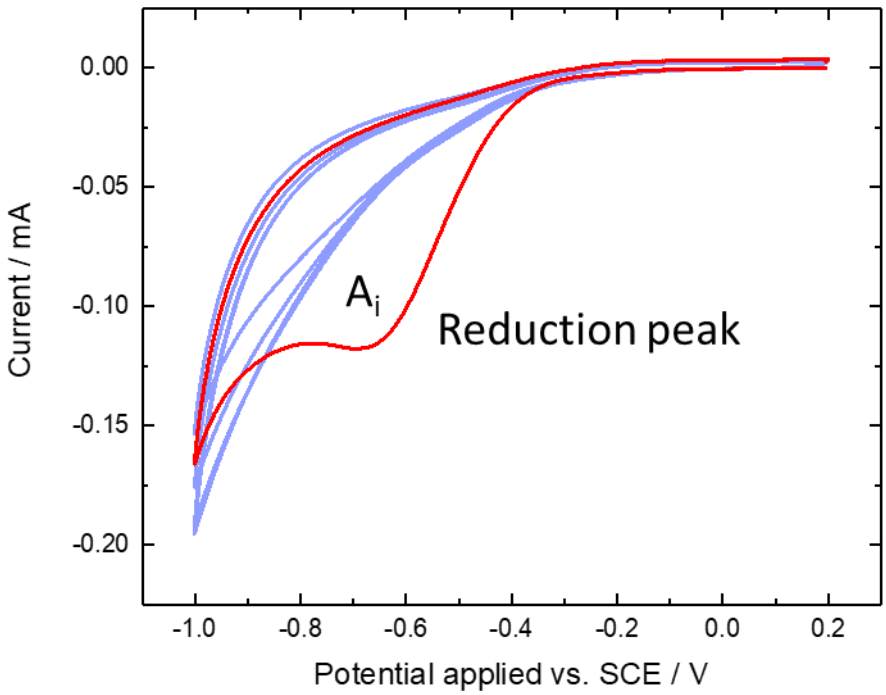

Figure 2-21: Voltammogram recorded at an ITO/silica substrate (1.5 mm × 1.5 mm × 0.55 mm) after the addition of the 6-carboxyfluorescein derivative **1.07$_a$**. CVs were recorded in a tris buffer solution (pH 7.4, 50 mM) from 0.2 V to −1.0 V vs. SCE at a scan rate of 0.05 V.s^{-1}. Red: first cycle, blue: following cycles.

It was important to prove that the above result was specific for covalent attachment of the probe to the surface and not just due to electrostatic or other non-specific binding of carboxyfluorescein in the pores. Therefore, a further experiment was performed as a control. The probe was added to an ITO/silica substrate not modified with the linker under the same conditions previously used for its attachment on the amino-modified surfaces. The surface was washed and the CV was performed, this time, no redox peaks were observed in the region of −0.6 V (**Figure 2-22**). This confirmed that covalent attachment of the probe had occurred by reaction with the linker on the surface modified using APTES.

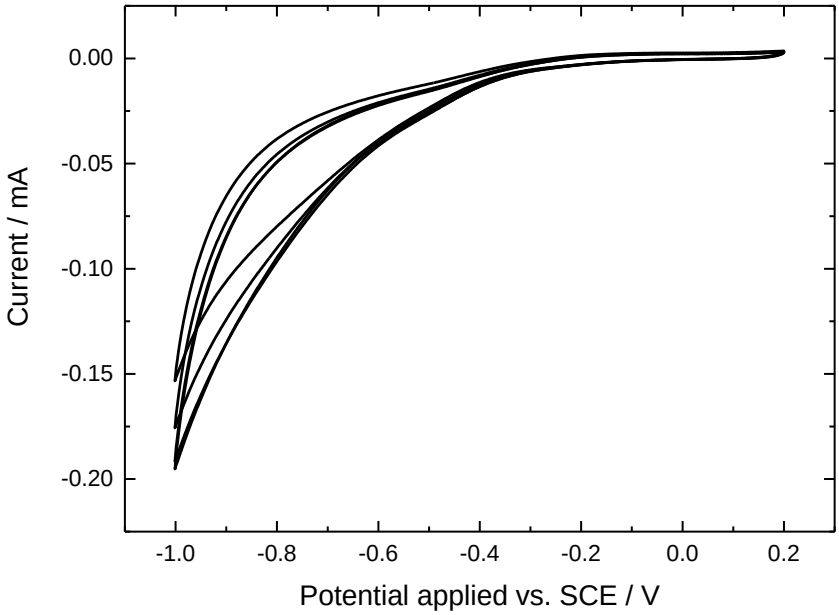

Figure 2-22: Voltammogram recorded at an ITO/silica substrate (1.5 mm × 1.5 mm × 0.55 mm) after the addition of the 6-carboxyfluorescein derivative **1.07$_a$** without linker. CVs were recorded in a tris buffer solution (pH 7.4, 50 mM) from 0.2 V to −1.0 V vs. SCE at a scan rate of 0.05 V.s^{-1}.

From the CV scan (**Figure 2-21**) it was possible to determine the quantity of carboxyfluorescein attached on the surface by a simple known method. The integration of the area of the reduction peak (A_i) that is related to the charge through the following equation:

$$Q = \frac{A_i}{v}$$

Equation 2-1: Q = charge (C); A_i = integration area (A.V); v = scan rate (V.s^{-1}).

With a scan rate of 0.05 V.s^{-1} and an integrated area of 9.3 µA.V, the charge was 185 µC. Using the Faraday law (**Equation 2-2**) the number of moles of carboxyfluorescein can be calculated.

$$Q = nmF \rightarrow m = \frac{Q}{nF}$$

Equation 2-2: Q = charge (C); n = number of electrons; m = number of moles (mol); F = Faraday constant (C.mol^{-1}).

The charge was previously calculated and Faraday constant is known (96 485 C.mol^{-1}). As described by Compton,[128] the reduction of fluorescein in aqueous media should be a 2e$^-$/1H$^+$ process. Using the **Equation 2-2**, the number of moles of carboxyfluorescein

immobilised on the substrate was found to be 0.96 nmol. Finally, with an estimated geometrical area of 5 cm^2 for the substrate used in this experiment, we calculated a surface coverage without the pores area of 0.19 $nmol.cm^{-2}$. This is the amount of compound that can react at the electrode surface, there could be more material that is unable to be reduced.

It was then decided to attach another redox probe, anthraquinone, onto the surface. Anthraquinone is a molecule often used to prove possible attachment of organic functionalities onto electrode surfaces and to calculate the surface coverage as it presents a very specific voltammogram with well-defined redox peaks. In addition, its carboxylic acid derivative can be easily attached to an amino-modified surface.[129-131] Therefore, anthraquinone-2-carboxylic acid was attached using a coupling reaction with DCC and NHS (**Scheme 2-43**).

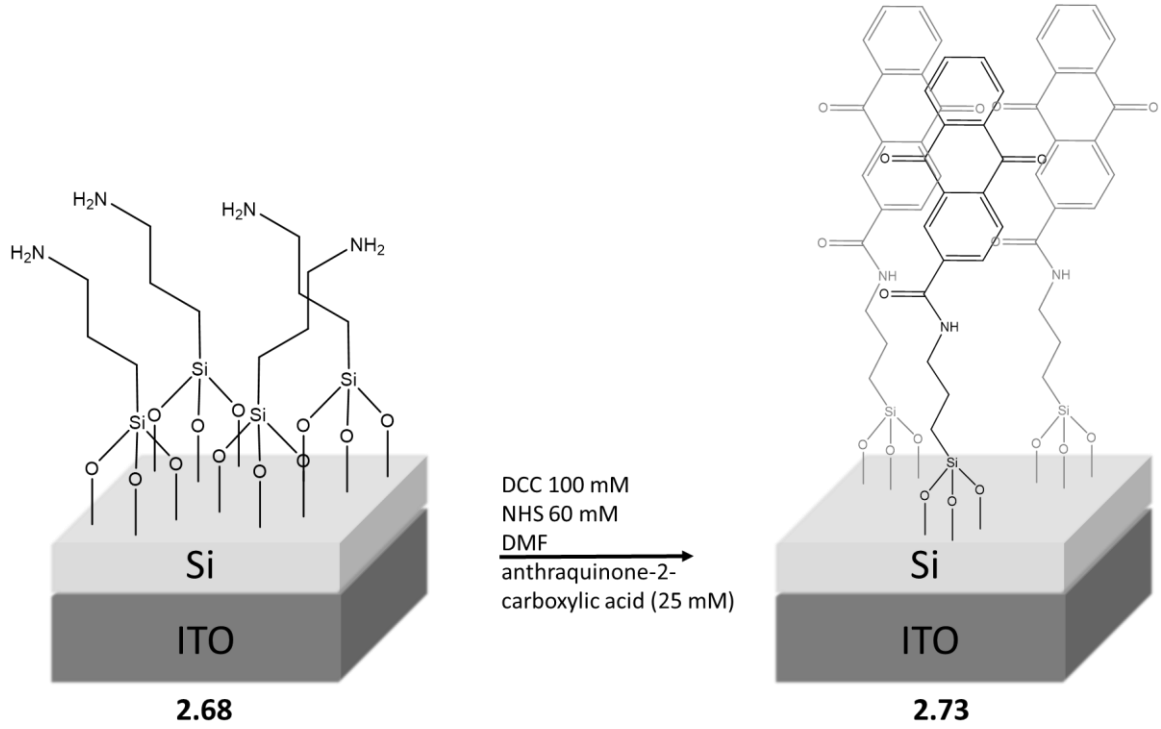

Scheme 2-43: Attachment of anthraquinone on the amino-modified ITO/silica surface.

The redox experiment was performed on this surface involving the reduction/oxidation of ruthenium under the same conditions previously described (**Figure 2-23**). The voltammogram shows the two redox peaks for ruthenium at around −0.2 V and a reduction peak at −0.6 V due to the anthraquinone, as expected. This voltammogram is proof of the attachment of anthraquinone.

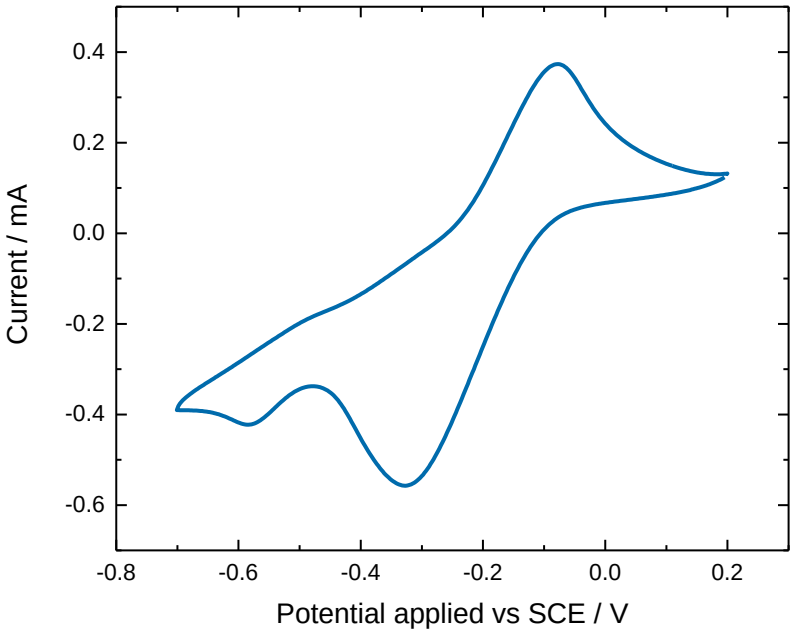

Figure 2-23: Voltammogram recorded at an ITO/silica substrate (1.5 mm × 1.5 mm × 0.55 mm) after the addition of anthraquinone-2-carboxylic acid. CVs were recorded in a solution of $NaNO_3$ (0.1 M) and $[Ru(NH_3)_6]^{3+}$ (1 mM) from 0.2 V to −0.7 V vs. SCE at a scan rate of 0.05 $V.s^{-1}$.

The cyclic voltammetry was then performed in a Tris buffer solution (pH 7.4, 50 mM) (**Figure 2-24**). Here we can see that a few scans were needed to have a stable CV, presumably due to the initial presence of anthraquinone non-covalently bound in the pores that diffused away over time. The CV has a very particular shape with a clearly visible reduction peak at −0.5 V and another unexpected peak in the backward scan at −0.6 V, not characteristic of a normal scan of anthraquinone.

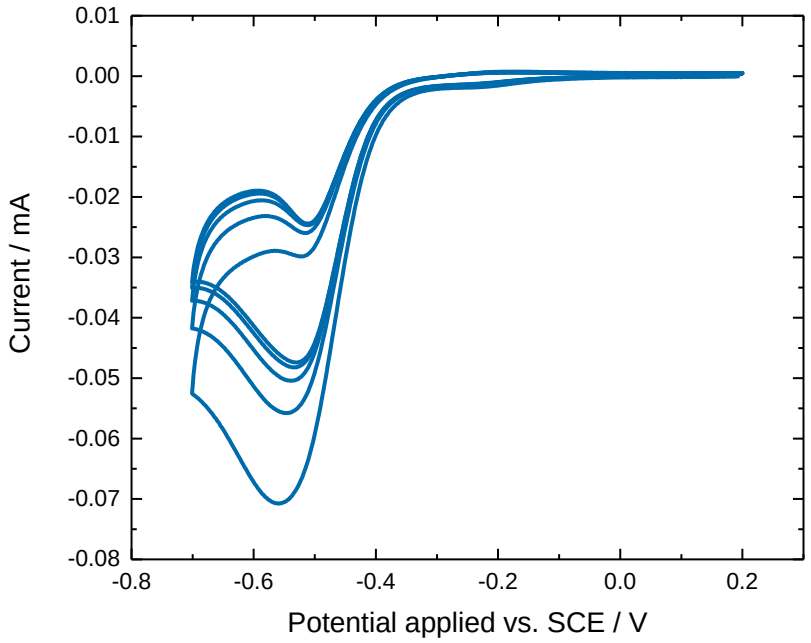

Figure 2-24: Voltammogram recorded at an ITO/silica substrate (1.5 mm × 1.5 mm × 0.55 mm) after the addition of anthraquinone-2-carboxylic acid. CVs were recorded in tris buffer solution (pH 7.4, 50 mM) from 0.2 V to −0.7 V vs. SCE at a scan rate of 0.05 $V.s^{-1}$.

This difference could be due to the particular shape of the surface structure or by the reaction of reduced anthraquinone with O_2 but that conclusion is difficult to prove. However, using the last scan (**Figure 2-24**) of the CV, the surface coverage of anthraquinone was determined with the same method previously decribed. The integrated area of the reduction peak was 3.7 µA.V and with a scan rate of 0.05 $V.s^{-1}$, the charge was calculated as 74 µC. Since reduction of anthraquinone is a two electron process (n = 2), the number of moles immobilised on the substrate was found to be 0.38 nmol with a surface coverage of 0.08 $nmol.cm^{-2}$.

The surface coverage of carboxyfluorescein was estimated to be approximately ten times higher that of the anthraquinone. This can be accounted for by the different methods employed for attachment of the redox active species. Carboxyfluorescein succinimidyl ester was purified, and should react cleanly with the amine linker. The activated anthraquinone carboxylic acid intermediate, which is generated *in* situ, reacted directly with the linker. Ideally, the same immobilisation method should be used for both species. In conclusion, the surface coverage of the probes found here must be considered as an approximation, more experiments are needed to conclusively prove the exact level coverage. However, these results are proof of the attachment of the probes on the surface, while providing a guide to the amount present on the surface.

2.3.3.2 Raman analysis of the modified silica substrates

The next technique used to characterise the modified surface was Raman spectroscopy. In this technique the surface is excited by a laser beam and the vibrational modes of the molecules near the surface can be observed. All the prepared modified surfaces and also the free probes were analysed by Raman spectroscopy.

Figure 2-25 shows the spectra of the 6-carboxyfluorescein substrate **2.69$_a$** at different stages of preparation. The bare ITO substrate and the mesoporous silica (red and yellow curves) do not present significant peaks, however, many peaks were observed after the addition of the carboxyfluorescein (black curve). A study of this type of surface with Raman has never be report and for a molecule of this size it is difficult to identify all the peaks.

A paper published in 2001[132] reporting the Raman spectra of fluorescein in solution was used to identify specific peaks. The peaks between 1238 and 1416 cm^{-1} are characteristic of the xanthene ring with the C−C stretching and the C−C bending, and the peak at 1567 cm^{-1} is characteristic of the C=O and C−C stretching. A control experiment was also carried out with the addition of the carboxyfluorescein to the surface without the linker, the surface was washed and a Raman spectrum was taken, the obtained spectrum did not display any peaks.

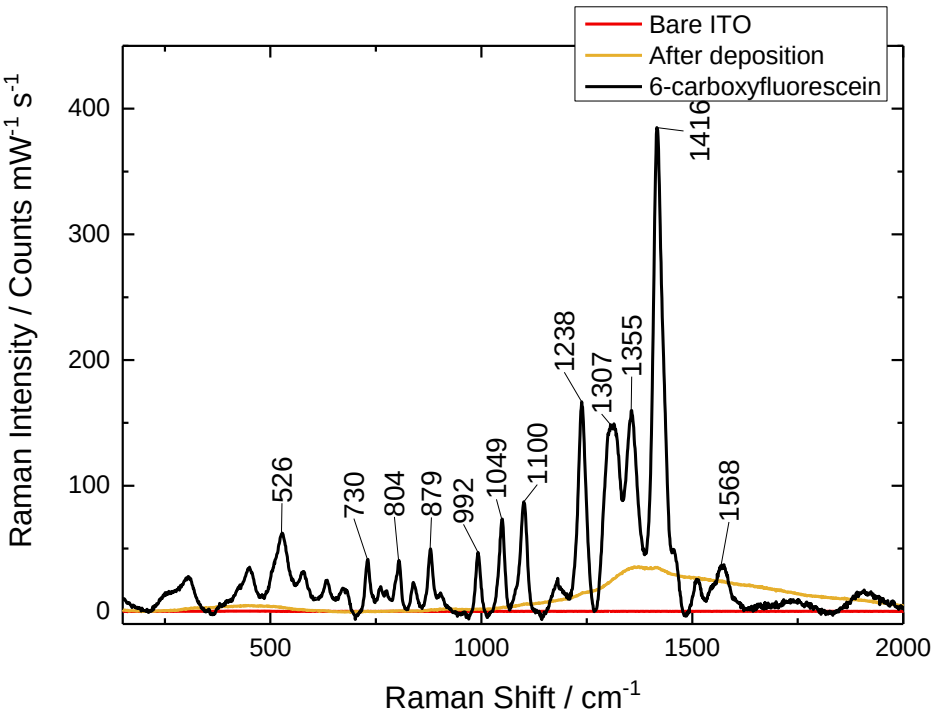

Figure 2-25: Raman spectra of the 6-carboxyfluorescein substrate **2.69$_a$** at different stages of modification.

To gain more information, a powdered sample of 6-carboxyfluorescein **1.07$_a$** was also analysed by Raman spectroscopy (**Figure 2-26**, spectrum 1). We can observe peaks at similar wavelengths to the modified surface **2.69$_a$** but with different intensities due to the difference between the pure crystals and the probe attached on the surface. A second observation is the collection of three peaks present in both the surface and powder spectra around 1000 cm^{-1}, this appears to be a characteristic pattern for carboxyfluorescein.

The spectrum of the succinimidyl derivative of carboxyfluorescein was also recorded (**Figure 2-26**, spectrum 2). In this spectrum we can observe the usual peaks of the xanthene ring and the three peaks around 1000 cm^{-1} observed in the previous two spectra. Two new peaks appeared at 1617 and 1779 cm^{-1} that are due to the succinimidyl ester moiety, and confirmed by the fact that these two peaks disappeared when the probe was added to the surface. Again, this supports the reaction of the linker with the activated ester. Furthermore, we are expecting peaks in the region 1500-1700 cm^{-1} for the amide formed after the surface modification with the probes.

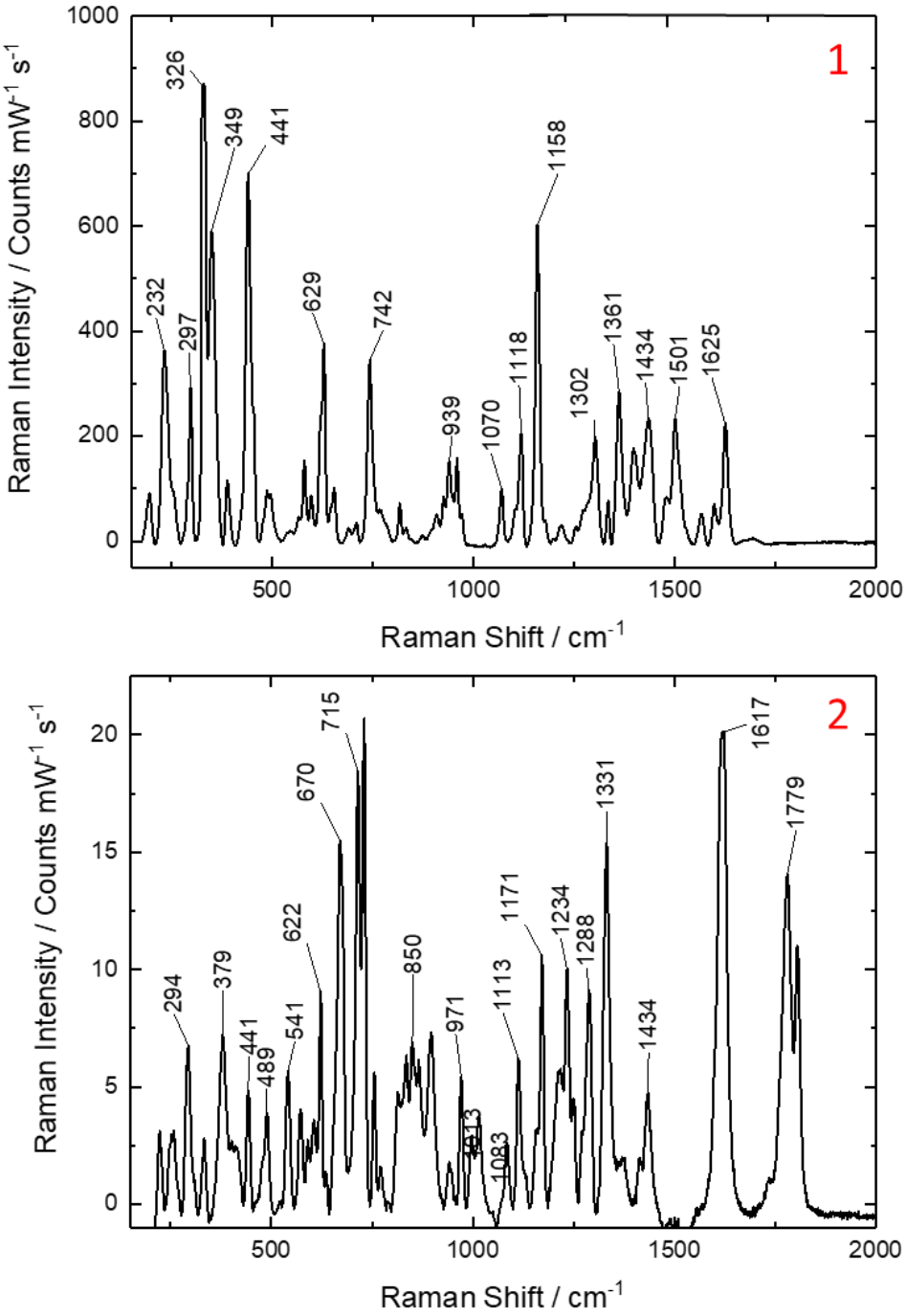

Figure 2-26: ***Raman spectra of:*** 1) 5(6)-carboxyfluorescein crystals **1.07$_{a/b}$**; 2) 6-succinimidyl ester of carboxyfluorescein crystals **2.38$_{a}$**.

A spectrum for each probe attached on the ITO/silica surface was recorded (**Figure 2-27**). They all present peaks in the region of the xanthene and the three peaks between 990 and 1100 cm^{-1}. Between all the different modified surfaces we can also notice some differences as expected as each surface is modified by a different probe molecule.

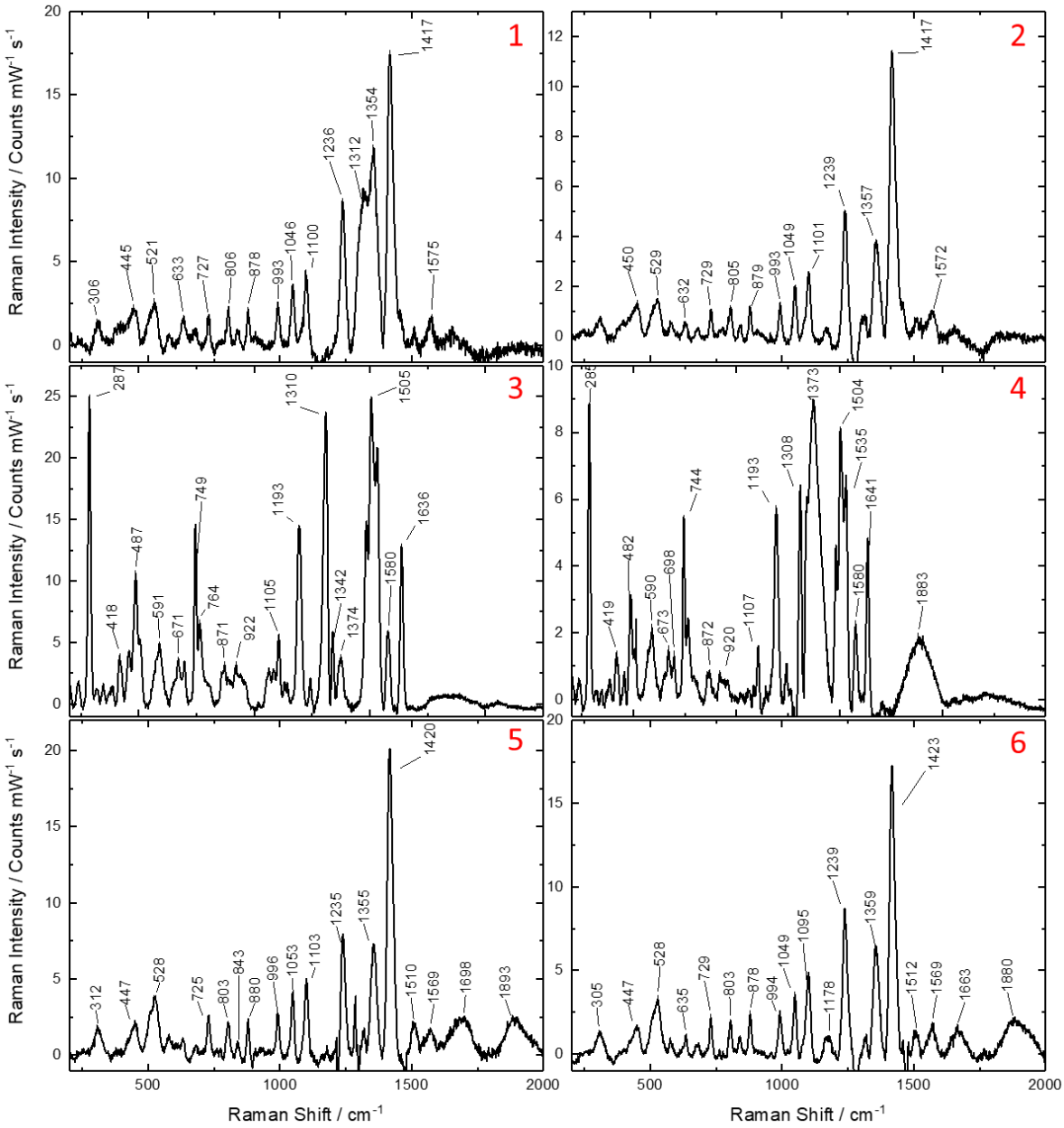

Figure 2-27: ***Raman spectra of the derivatives attached on the ITO/silica surface***: 1) 5-Carboxy-2´,7´-dichlorofluorescein **2.70$_b$**; 2) 6-Carboxy-2´,7´-dichloro-fluorescein **2.70$_a$**; 3) 5-Carboxy-4',5'-bis(morpholin)-2´,7´-dichlorofluorescein **2.71$_b$**; 4) 6-Carboxy-4',5'-bis(morpholin)-2´,7´-dichlorofluorescein **2.71$_a$**; 5) 5-Carboxy-4',5'-bis(dipicolylamine)-2´,7´-dichlorofluorescein **2.72$_b$**; 6) 6-Carboxy-4',5'-bis (dipicolylamine)-2´,7´-dichlorofluorescein **2.72$_a$**.

In conclusion, there is a clear evidence that probes have been attached to the surface and they present some characteristic peaks of carboxyfluorescein derivative. The next stage was to use the surfaces in fluorescence experiments, in particular to determine the fluorescence parameters such as quantum yield and extinction coefficient, and also the probes response to changes in pH (pK_a measurements).

2.3.3.3 Determination of pK_a of the modified substrates

The first experiment was performed to determine the pK_a of all the molecules synthesised. Solutions of the fluorophores were prepared at different pH, but otherwise, under the same conditions (see experimental for full details). The fluorescence spectra were recorded at each pH, see below (**Figure 2-28**) for an example with the derivative **2.60b**. The peak at about 540 nm for each spectrum was integrated and the integration area was plotted vs. the pH. Data were then fitted using Origin 2017 with a Boltzmann sigmoidal function that allowed us to determine the inflection point, which corresponds to the pK_a of the fluorophore.

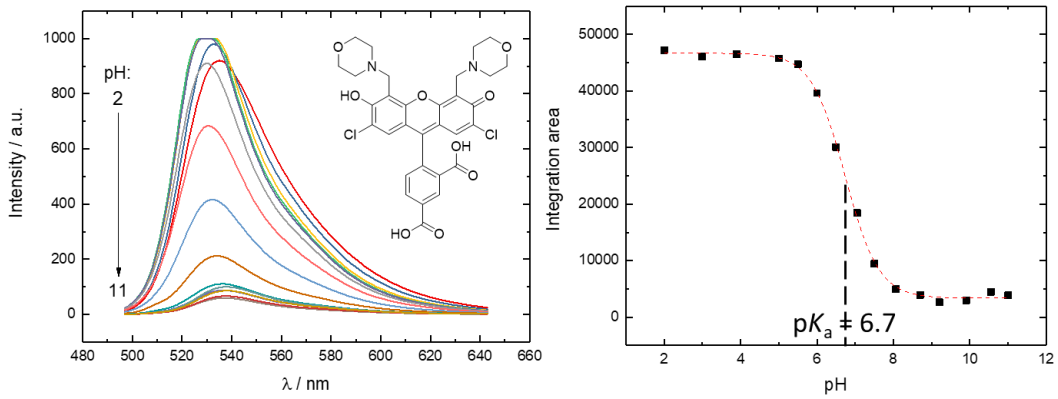

Figure 2-28: Fluorescence spectra in aqueous solution (EDTA 1 mM + KCl 100 mM) of the morpholine substrate **2.60b** from pH 11 to 2 (left) and pH profile of the morpholine substrate **2.60b** (right).

The first analysis (**Figure 2-28**) was performed for the determination of the pK_a of the 5-isomer of the morpholine derivative **2.60b**. The pK_a obtained was of 6.73: as previously described (section **2.2.4**), the addition of a benzylic amine causes the fluorescence to be strongest at acidic pH. **Figure 2-29** shows a comparison between the 6-isomer of carboxyfluorescein morpholine derivative **2.60a** and 5(6)-carboxyfluorescein **1.07a/b**, from this the two different kinds of pK_a profile for different fluorescent probes can be seen, which is of interest for use in biosensing. It is worth noting the difference in pK_a of 0.5 units for the two regioisomeric morpholine derivatives (the 5-isomer a pK_a of 6.7 and the 6-isomer a pK_a of 6.2), showing the influence on pK_a of the position of the carboxylic group.

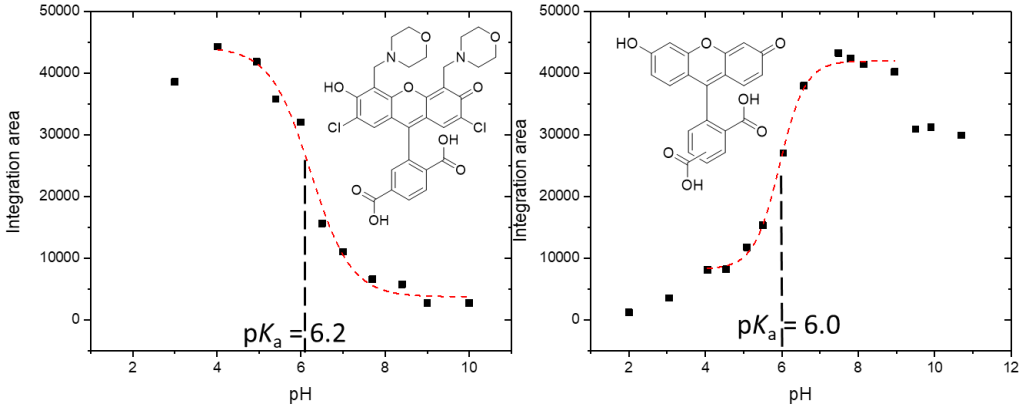

Figure 2-29: pH profile of the morpholine substrate **2.60$_a$** (left) and 5(6)-carboxyfluorescein substrate **1.07$_{a/b}$** (right).

The results for the two isolated isomers of dichlorofluorescein are presented (**Figure 2-30**). The fluorescence analysis was performed after leaving the succinimidyl derivative in a solution at pH 11 (aqueous NaOH) to deprotect the acetates and hydrolyse the succinimidyl ester back to the acid, subsequently the pH was decreased to 2. The profile is similar to that of 5(6)-carboxyfluorescein (**Figure 2-29**, right) but the pK_a has decreased to 3.9 or 3.7 offering new pH ranges for sensing applications of these probes.

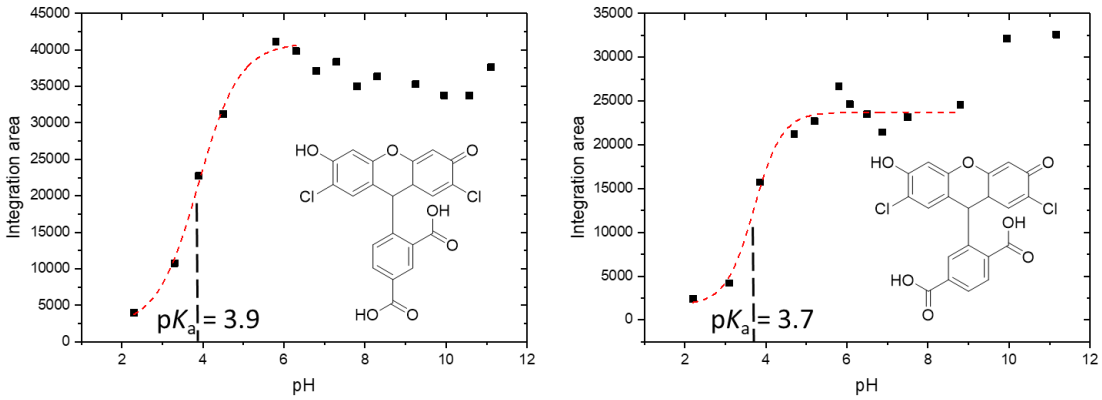

Figure 2-30: pH profile of substrate **2.45$_a$** (left) and substrate **2.45$_b$** (right).

The pK_a for the two zinc probes was also determined (**Figure 2-31**). We did not consider these probes as pH probes, however, it is important to verify their pH profile with the literature. In this case we can see the impact of the benzylic amine moiety on fluorescence properties indicating that it is preferential to avoid working at acidic pH when sensing Zn^{2+} as the probes already present strong fluorescence at acidic pH.

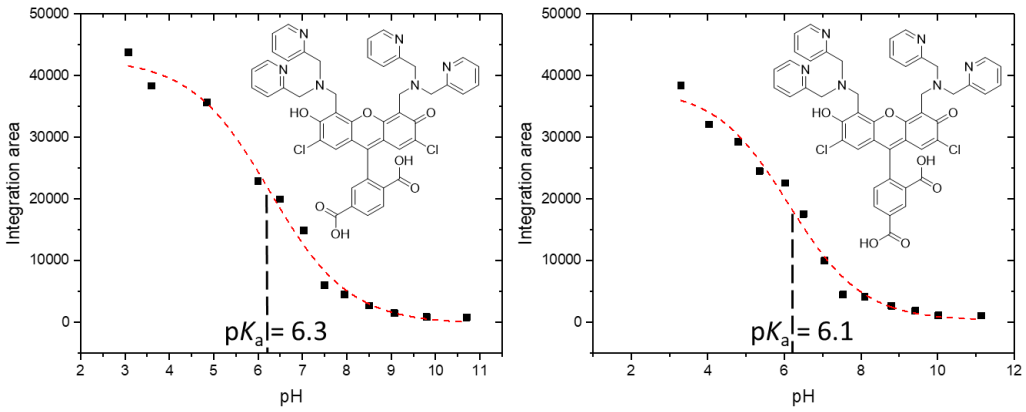

Figure 2-31: pH profile of substrate **2.61$_a$** (left) and substrate **2.61$_b$** (right).

Finally, we characterised the pH profile of the potassium probe. This a completely novel molecule and therefore the pK_a was not known. The pK_a was found to be 9.1 (**Figure 2-32**). This indicated that this probe will be fluorescent until this high pH, thus unfortunately reducing the possibilities of the biological applications of this probe. For the future, it would be interesting to modify the main skeleton of the molecule in an attempt to reduce its pK_a, for example by adding more halogen groups.

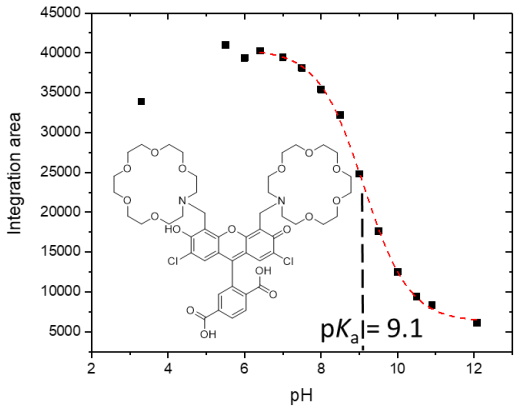

Figure 2-32: pH profile of substrate **2.62**.

It was then necessary to obtain the pK_a for the modified surfaces. **Figure 2-33** presents the determination of pK_a for the morpholine derivative **2.60$_a$** and carboxyfluorescein **1.07$_b$** attached on the ITO/silica surface.

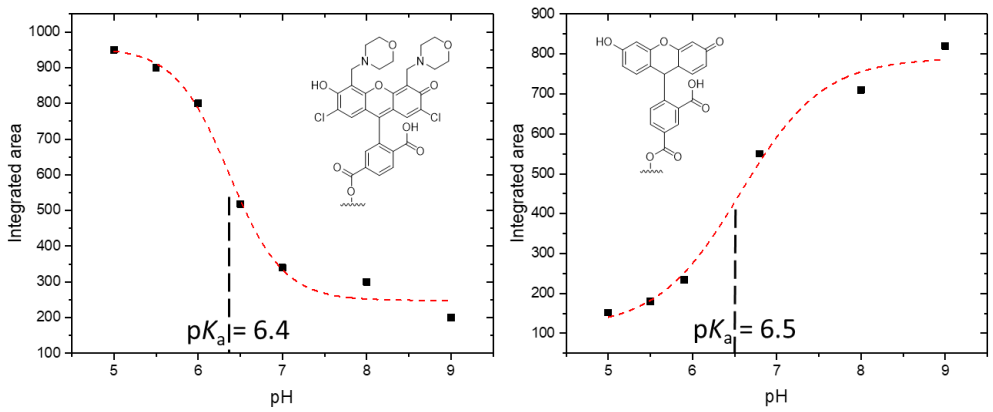

Figure 2-33: pH profile of the modified surface **2.60$_a$** and **1.07$_b$** fluorescence spectra in aqueous solution (EDTA 1 mM + KCl 100 mM) from pH 5 to 9 were measured, integrated and plotted with pH.

2.3.3.4 Determination of the extinction coefficient of the modified substrates

The extinction coefficient, or molar attenuation coefficient, is one of the parameters that define a fluorophore. It is a property that describes how strongly a chemical species attenuates the light at a particular wavelength. With the Beer-Lambert law (**Equation 2-3**) this coefficient can be easily related to absorbance and the concentration of a solution.

$$A = \varepsilon C l$$

Equation 2-3: Beer Lambert law with A = absorbance; $\boldsymbol{\varepsilon}$ = extinction coefficient (M^{-1} cm^{-1}); C = concentration (M); l = path length (cm).

With *l* constant for our cell and equal to 1 cm, the determination of ε was performed by recording the absorbance spectra of a fluorophore at the same wavelength but at different concentrations. The absorbance maximum was plotted vs. the concentration (**Figure 2-34**) and the data were fitted with a linear function using Origin 2017. The slope of the linear fitting was used to determine ε using the Beer-Lambert law (**Equation 2-3**).

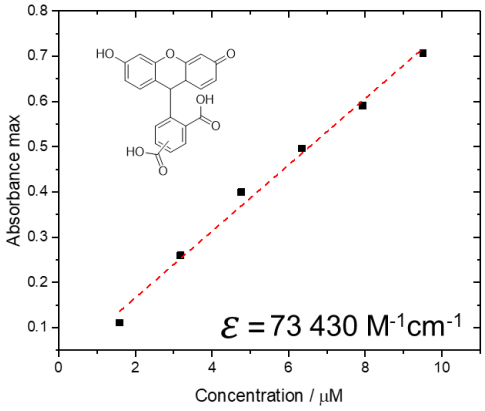

Figure 2-34: Determination of ε for 5(6)-carboxyfluorescein substrate **1.07$_{a/b}$** in HEPES buffer (50 mM, pH 7.5, KCl 100 mM) at 492 nm.

The first coefficient determined was for 5(6)-carboxyfluorescein **1.07$_{a/b}$**. All the fluorescent parameters for this molecule are well known, but comparison of our experimental measurements to calculate ε and those reported in the literature would validate our method. The coefficient was found to be equal to 74 430 M^{-1} cm^{-1}, which was in good agreement for carboxyfluorescein in the literature (75 000 M^{-1} cm^{-1}),[133] confirming accuracy in our method and readings.

The extinction coefficients were not calculated for dichlorocarboxyfluorescein. As the values for these molecules are well-known and we wanted to avoid unnecessary deprotection of our molecule. The coefficient was calculated for all the other fluorophores with and without the succinimidyl ester to determine its influence. It is important to characterise the succinimidyl ester for two reasons, first the fluorescence response of these molecules can help model the probe that ends up attached to the surface. Secondly, they are new fluorescent molecules and they could be use in other biological application. The first results shown are for the morpholine derivatives (**Figure 2-35**), the two isomers have similar coefficients and we notice, in both cases, an increase of 30 000 M^{-1} cm^{-1} after the addition of the succinimidyl ester. This is due to the succinimidyl ester absorbing more the light, presumably due to its increased electron delocalisation.

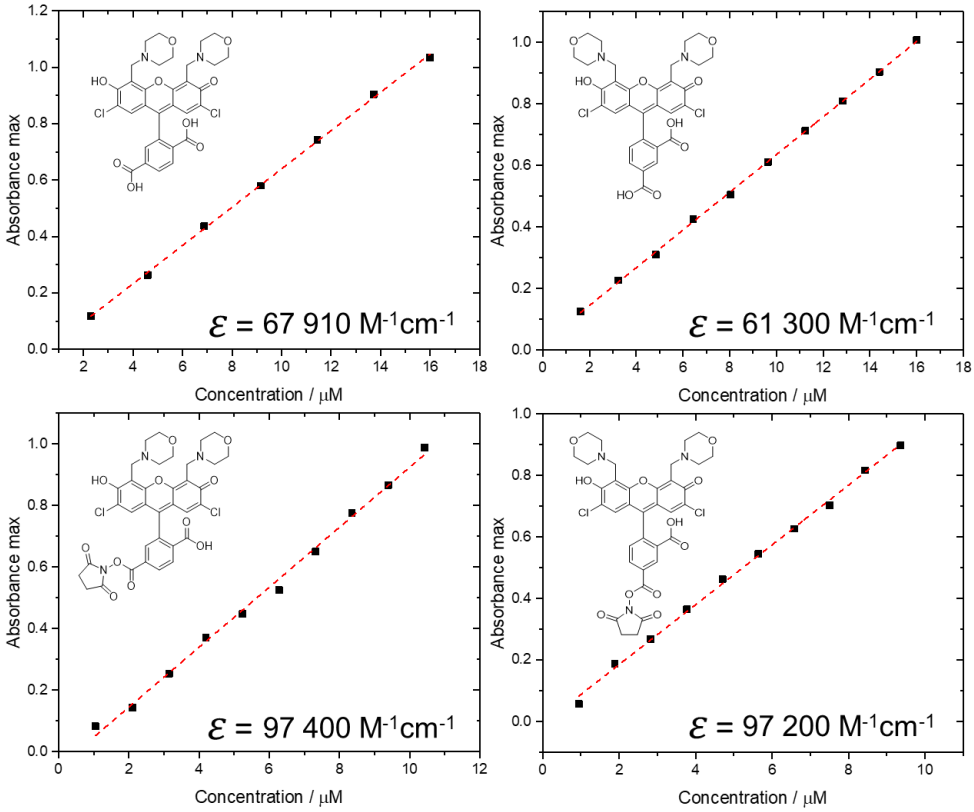

Figure 2-35: Determination of ε in HEPES buffer (50 mM, pH 7.5, KCl 100 mM) for the morpholine derivatives **2.60$_a$** at 514 nm (top left), **2.60$_b$** at 514 nm (top right), **2.63$_a$** at 515 nm (bottom left) and **2.63$_b$** at 515 nm (bottom right).

Measurements for the zinc probes were taken (**Figure 2-36**). The extinction coefficient for the molecules **2.63$_a$** and **2.63$_b$** has been reported in recent work,[73] these two molecules being well known probes for the determination of zinc ion concentration. However, the succinimidyl ester derivatives are not known or characterised in the literature. We observed a small difference between our measurements of extinction coefficient (66 280 and 67 450 M^{-1} cm^{-1}) and those from the literature (81 000 and 76 000 M^{-1} cm^{-1}) but within experimental error. There is also an increase in the extinction coefficient after the addition of the succinimidyl ester.

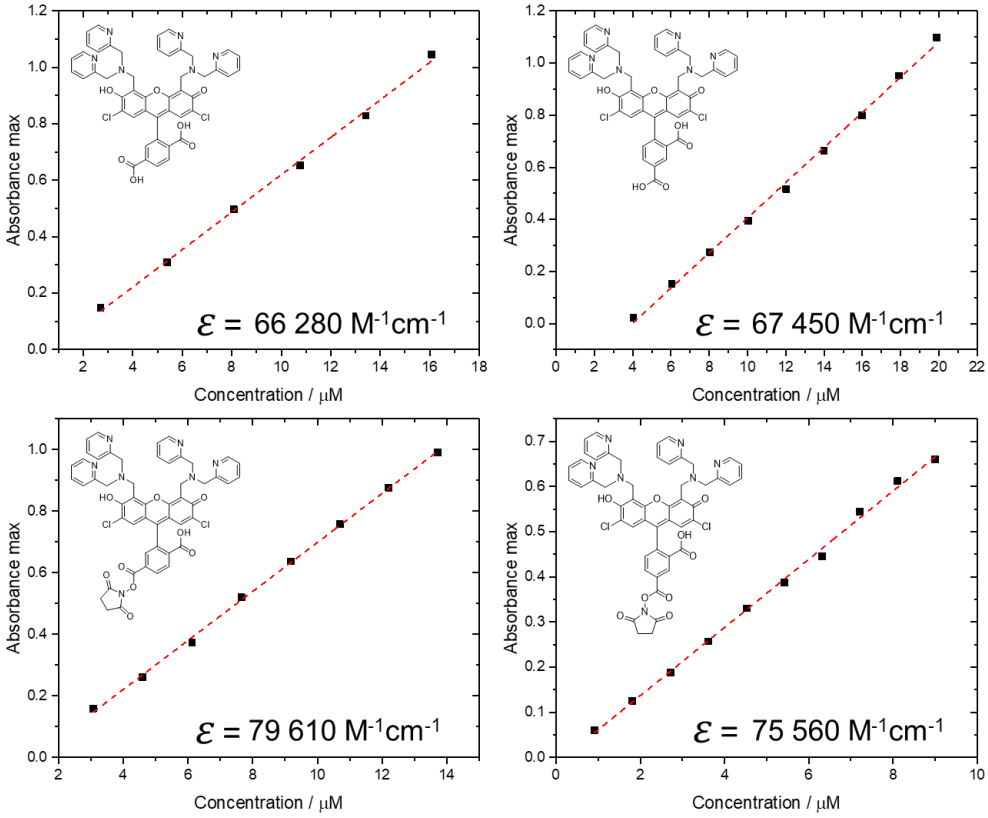

Figure 2-36: Determination of ε in HEPES buffer (50 mM, pH 7.5, KCl 100 mM) for the derivatives **2.61$_a$** at 522 nm (top left), **2.61$_b$** at 522 nm (top right), **2.64$_a$** at 522 nm (bottom left) and **2.64$_b$** at 522 nm (bottom right).

The experiment was repeated in the presence of zinc in order to study the effect of the zinc on the probes **(Figure 2-37**). We were expecting to see a difference as the zinc would interact with the probes increasing the fluorescence and so the ability of the solution of attenuate the light. The results were as expected except for the 5-isomer without the ester, which presented no increase in the extinction coefficient. The simplest explanation would be that this was experimental error and this experiment should be repeated in the future to provide confirmation. However, all the other results showed an increase when zinc was added as expected due to the increase of fluorescence and light absorption when the zinc interacts with the probes.

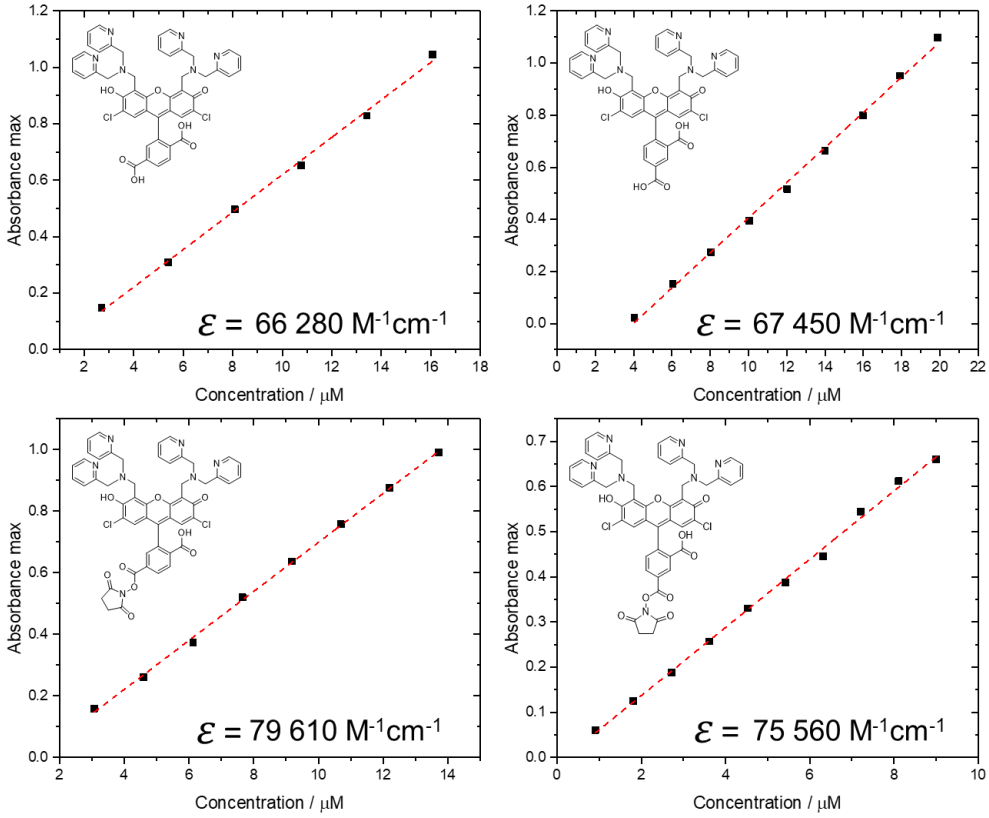

Figure 2-37: Determination of ε in HEPES buffer (50 mM, pH 7.5, KCl 100 mM) + $ZnCl_2$ 2 mM for the derivatives **2.61$_a$** at 522 nm (top left), **2.61$_b$** at 522 nm (top right), **2.64$_a$** at 522 nm (bottom left) and **2.64$_b$** at 522 nm (bottom right).

Finally, the experiment was repeated with the potassium probe **2.62** (**Figure 2-38**) in the presence and absence of potassium ion. We can see that this new probe presents a good coefficient confirming that it can be used as a fluorescent probe. However, when we added the potassium, we did not observe any increase in the extinction coefficient, due to the fact the we were working at pH 7.5. At this pH the probe is already at the maximum of its fluorescence emission so therefore adding potassium, even if it interacts with the probe, would not lead to any increase in fluorescence emission.

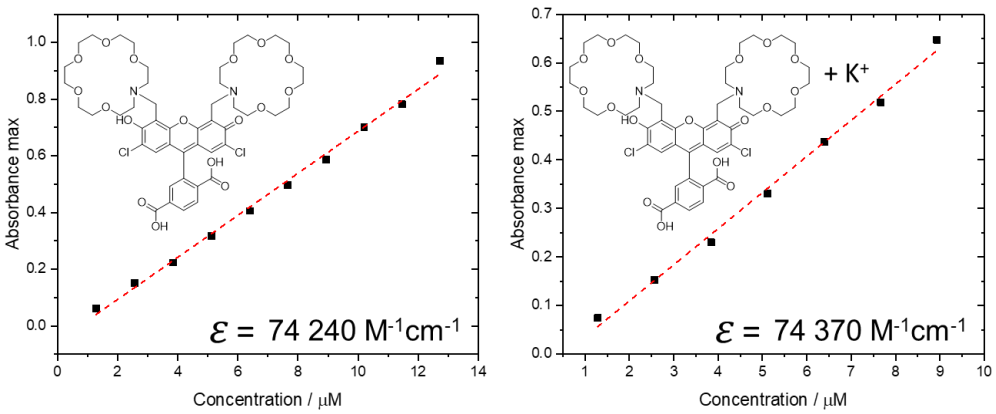

Figure 2-38: Determination of ε for the potassium probe **2.62** in HEPES buffer (50 mM, pH 7.5) at 513 nm (left) and in HEPES buffer (50 mM, pH 7.5) + KCl (2 mM) at 513 nm (right).

The next step would be to measure the extinction coefficient of the modified surfaces, however to do this we need to plot the concentration of the probes against the absorbance maxima. We attempted to measure the absorbance spectrum but the instrument was not sensitive enough to see any response. The concentration of the fluorophore immobilised on the surface is quite low and therefore we would require an instrument with greater sensitivity.

2.3.3.5 Determination of the quantum yield of the modified substrates

In fluorescence the quantum yield (Φ) defines how efficient a fluorophore is, it can be define using the **Equation 2-4**. There are two ways to measure it: by an absolute or a relative measurement. The absolute method is more complicated and would require an instrument that was not available to us (an integrating sphere setup), while for the relative method a normal fluorescence spectrometer is sufficient.

$$\Phi = \frac{photons\ emitted}{photons\ absorbed}$$

Equation 2-4: Definition of the quantum yield.

In order to calculate the quantum yield with a relative measurement, it is necessary to have a standard reference with a known Φ, similar to the fluorophores studied. In our case fluorescein is a very common standard used for the calculation of quantum yield and it is very similar to our fluorophores. We used the method described by Würth *et al,*[134] which can be summarised using the **Equation 2-5**.

$$\Phi_{f,X} = \Phi_{f,st} * \frac{F_X}{F_{st}} * \frac{f_{st}}{f_X} * \frac{n_X^2(\lambda_{em})}{n_{st}^2(\lambda_{em})}$$

Equation 2-5: $\boldsymbol{\Phi_f}$ = fluorescence quantum yield; X = studied fluorophore; st = standard; F = relative integrated photon flux; f = absorption factor; n = refractive index of the solvent at a specific emission wavelength ($\boldsymbol{\lambda_{em}}$).

The details of the method are described in the experimental chapter, fluorescein with a known quantum yield equal to 0.95 was used as standard. The same solvent was used so that the refractive indices remain equal and can be ignored in the equation. The absorption factors (**Equation 2-6**) can be removed from the equation as the ratio f_{st}/f_X can be approximated to 1.

$$f = 1 - 10^{-A(\lambda_{ex})}$$

Equation 2-6: Absorption factor with A = absorbance at $\boldsymbol{\lambda_{ex}}$.

As described by Würth *et al*, the absorption spectra of the standard and the fluorophore studied were recorded and the intersection of the curves was used to choose the absorbance of excitation to record the fluorescence emission spectra (**Figure 2-39**). Using this technique, the absorption factors are equal and can therefore be ignored.

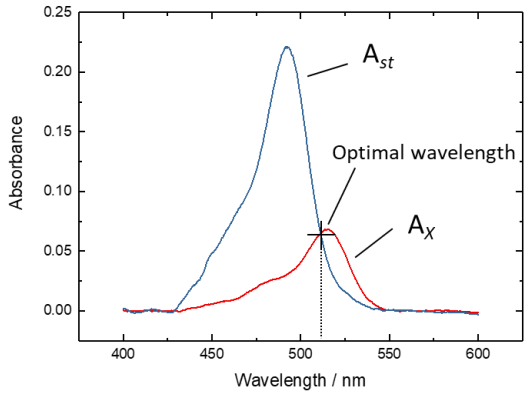

Figure 2-39: Determination of the optimal excitation wavelength.

After having simplified the **Equation 2-5**, it was only necessary to integrate the fluorescence spectra to obtain the relative photon flux (F) for both the standard and the fluorophore studied. All the absorption and fluorescence spectra were recorded as needed and integrated and all the parameters are summarized in **Table 2-2**. In general, the quantum yields of the fluorophores are as expected. We can compare the fluorophores with each other: the morpholine derivatives (in green) present the best efficiency, followed by the zinc probes (in red) and, lastly, the potassium probe (in yellow) with a low quantum yield. The loss in efficiency for the potassium probe could be due to the size of the new groups added

to the structure that does not reemit light efficiently after absorbing it. However, having a low quantum yield when the fluorophore is not activated could be advantageous as it can lead to a large increase in fluorescence after the addition of the respective “activator” (zinc or potassium).

Comparing the fluorophores with their respective ester derivatives, we can see that there is no real difference in quantum yield for the zinc probes (red), we can see a significant decrease for the morpholine derivatives (green). The addition of the ester in the morpholine derivatives makes the molecule a less efficient fluorophore however the extinction coefficient increased. Given that the fluorophore will be attached on the surface via an amide and not as this ester, we hope that this loss in efficiency will not impact future use of this derivative as a biological probe.

Finally, we repeated the experiment in the presence of zinc for the two zinc probes and with potassium for the potassium probe. With the zinc probes there is a significant increase in the quantum yield of 0.20 after addition of the metal ion, confirming that the fluorophore was activated and more efficient. However, with the potassium probe we did not observe any change in quantum yield and the value was always very low. It is still unclear why the quantum yield is so low, but the lack of change indicates there is no activation of the fluorophore in the presence of potassium ion.

X	F_X	$\Phi_{f,X}$	ε ($M^{-1}cm^{-1}$)	pK_a
5(6)-carboxyfluorescein		0.95	73430	6.0
6-Carboxy-4',5'-bis(dipicolylamine)-2´,7´-dichlorofluorescein **2.61$_a$**	11627	0.28	66280	6.3
5-Carboxy-4',5'-bis(dipicolylamine)-2´,7´-dichlorofluorescein **2.61$_b$**	11963	0.29	67450	6.1
6-Carboxy-4',5'-bis(morpholin)-2´,7´-dichlorofluorescein **2.60$_a$**	29304	0.72	67910	6.2
5-Carboxy-4',5'-bis(morpholin)-2´,7´-dichlorofluorescein **2.60$_b$**	27858	0.68	61300	6.7
6-Carboxy-4',5'-bis(1-aza-18-crown-6)-2´,7´-dichlorofluorescein **2.62**	3077	0.07	74240	9.1
6-Carboxy-4',5'-bis(dipicolylamine)-2´,7´-dichlorofluorescein, succinimidyl ester **2.64$_a$**	10220	0.25	79610	
5-Carboxy-4',5'-bis(dipicolylamine)-2´,7´-dichlorofluorescein, succinimidyl ester **2.64$_b$**	9708	0.24	75560	
6-Carboxy-4',5'-bis(morpholin)-2´,7´-dichlorofluorescein, succinimidyl ester **2.63$_a$**	16268	0.40	97400	
5-Carboxy-4',5'-bis(morpholin)-2´,7´-Dichlorofluorescein, succinimidyl ester **2.63$_b$**	12169	0.30	97200	
6-Carboxy-4',5'-bis(dipicolylamine)-2´,7´-dichlorofluorescein **2.61$_a$** + Zn^{2+}	20431	0.50	80540	
5-Carboxy-4',5'-bis(dipicolylamine)-2´,7´-dichlorofluorescein **2.61$_b$** + Zn^{2+}	21578	0.53	67740	
6-Carboxy-4',5'-bis(1-aza-18-crown-6)-2´,7´-dichlorofluorescein **2.62** + K^+	2953	0.07	74370	

Table 2-2: Résumé of the fluorescence parameters.

To study the quantum yield of the surface modified with probes the absorbance spectra of the modified surface would need to be measured, this was not possible due to the low sensitivity of the spectrometer available to us during this work. As an approximation, we used the absorption wavelength of the corresponding fluorophore and ran an emission spectrum of the surface at this wavelength, and used this to calculate the quantum yield of the surface. These results should be taken as an approximation; the experiments were performed to establish a rough idea of how fluorescent the surface is. We were expecting low quantum yields using this method as it is not a fair correlation to compare the concentration of fluorophore in a solution with that of the fluorophore on a surface (**Table 2-3**).

X	F_X	$\Phi_{f,X}$
6-Carboxy-4',5'-bis(morpholin)-2´,7´-dichlorofluorescein on surface **2.71$_a$**	4409	0.11
6-Carboxy-4',5'-bis(dipicolylamine)-2´,7´-dichlorofluorescein on surface **2.72$_a$**	2621	0.06
6-Carboxy-4',5'-bis(dipicolylamine)-2´,7´-dichlorofluorescein on surface **2.72$_a$** + Zn^{2+}	3038	0.07

Table 2-3: Estimated quantum yield of modified surfaces with **2.71$_a$** and **2.72$_a$**.

As expected, the quantum yields are low but these results show that the surface provided a response to a light excitation. In order to obtain better results, we would need to determine the absolute quantum yield for a surface.[134] Unfortunately we did not have access to a suitable instrument.

2.3.3.6 Determination of the selectivity of the zinc probe

When a probe is prepared to be specific for a certain species it is important to determinate its selectivity, and interference from other species likely to be present in the system to be studied. It was not necessary to study the selectivity for the pH probes, but it was important for the zinc and potassium probes. The zinc probe is a well-known probe and there are reports in the literature of such experiments. We set about repeating these methods to evaluate the selectivity for our probe and then to also study the succinimidyl derivative and the modified surface for comparison. The process is explained in detail in the experimental section. In brief, it consists of taking an emission spectrum of the fluorophore in solution

before and after the addition of a known quantity of a metal ion. The results are shown in **Figure 2-40**.

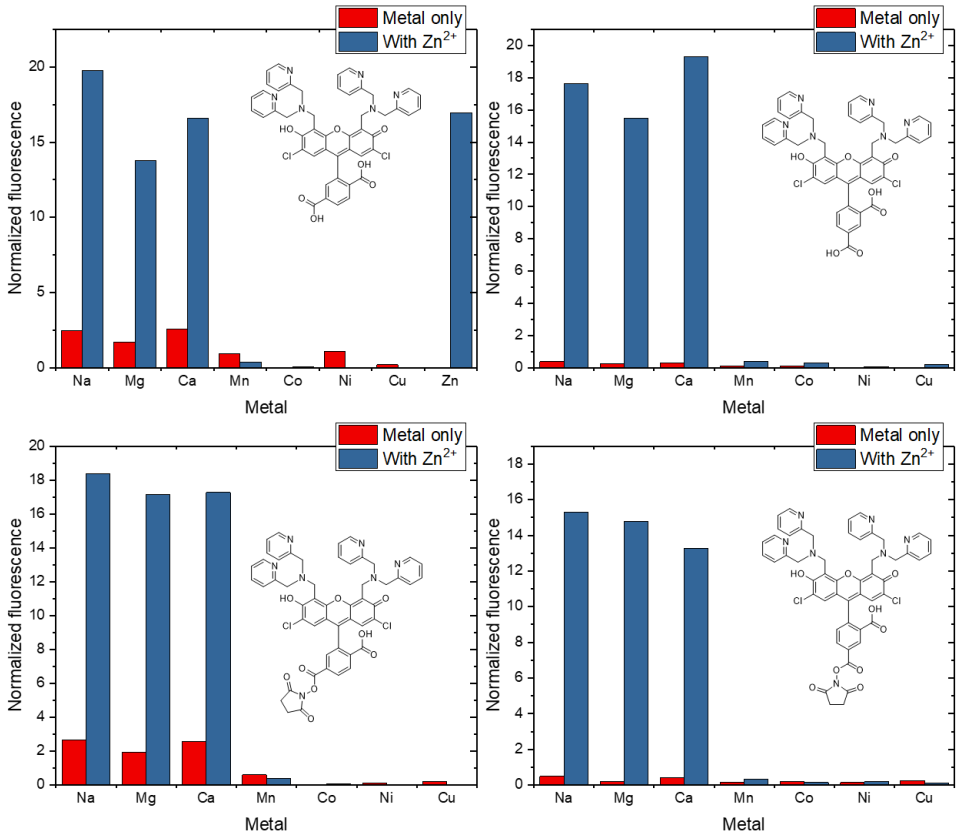

Figure 2-40: Selectivity of Zn^{2+} response: treatment of 1 µM dye with 50 µM-2mM shown metal ion (red bars) followed by addition of 50 µM $ZnCl_2$ (blue bars) for the substrates **2.61$_a$** (top left), **2.61$_b$** (top right), **2.64$_a$** (bottom left) and **2.64$_b$** (bottom right).

These results are similar to those reported in the literature except with the manganese. In our hands the manganese quenched the fluorescence of the zinc probes and any addition of $ZnCl_2$ did not change the result, while the cited authors report that the addition of the zinc did increase the fluorescence.[72] This difference could be an experimental error, however, it is significant that all four probes gave the same result. It is possible that the result could arise from the manganese we used. However, we can conclude that the first-row transition metal ions (Mn^{2+}, Co^{2+}, Ni^{2+}, Cu^{2+}) quenched the fluorescence irreversibly, while the biologically relevant metal ions (Ca^{2+}, Na^{+}, Mg^{2+}) did not significantly affect the fluorescence of the zinc probes. Gratifyingly, we can see that there is no difference between the fluorophores and the succinimidyl ester modified probes, which was expected and confirmed to us that attachment of the probes onto the surface should not impact the sensory properties of the molecules.

2.3.3.7 Conclusion

In conclusion the attachment of the probes to the silica/ITO surface has been proved by a range of techniques. The Raman analysis clearly showed that carboxyfluorescein derivatives were attached onto the surface proving that our method of attachment was successful. Cyclic voltammetry provided further proof of the modification but also gave us some information about the quantity of fluorophore attached on the surface. However, to further investigate the properties of the surface, a full study focusing on the electrochemistry would be needed. The calculation of the fluorescence parameters was more problematic, especially due to the insensitivity of the instrumentation available to us, making it difficult to detect some of the required parameters of the modified surface. Further work would require complete characterisation of the surfaces. We have proven that the surfaces are fluorescent emitters and we have determined the pK_a for some of the surfaces. However, some other parameters such as detection limit, quantum yield and extinction coefficient could not be calculated precisely. The following section will describe how to use these novel modified surfaces in actual fluorescence experiments in order to validate this new concept.

2.3.4 Fluorescence imaging

After having calculated most of the main fluorescence parameters, it was necessary to test our surface in a real application. A simple test for our surface was to observe it in the non-fluorescent and fluorescent and fluorescent states. Our first experiment was performed using a surface modified with carboxyfluorescein, and studied the impact on the fluorescence emission of the surface of the addition of a basic solution, using a fluorescence microscope.

Figure 2-41: Picture of the modified surface with 6-carboxyfluorescein **2.69$_a$** under basic conditions (fluorescence side).

Figure 2-41 shows an image taken under a fluorescence microscope where a drop of a basic solution (NaOH) pH 10 is placed on the surface. We can clearly see that there is a major difference between the dry surface and the wet surface. As expected, under alkaline

conditions carboxyfluorescein provided a very bright fluorescence response when activated.

The next step was to study the effect of a solutions at different pH. The result are presented in **Figure 2-42**: four solutions at different pH (5.4, 6.4, 7.4 and 8.4) were placed on the surface and images recorded. We can see that there is a clear increase in the fluorescence with increasing pH, with a pK_a around 6, this is similar to the observed result for carboxyfluorescein in solution.

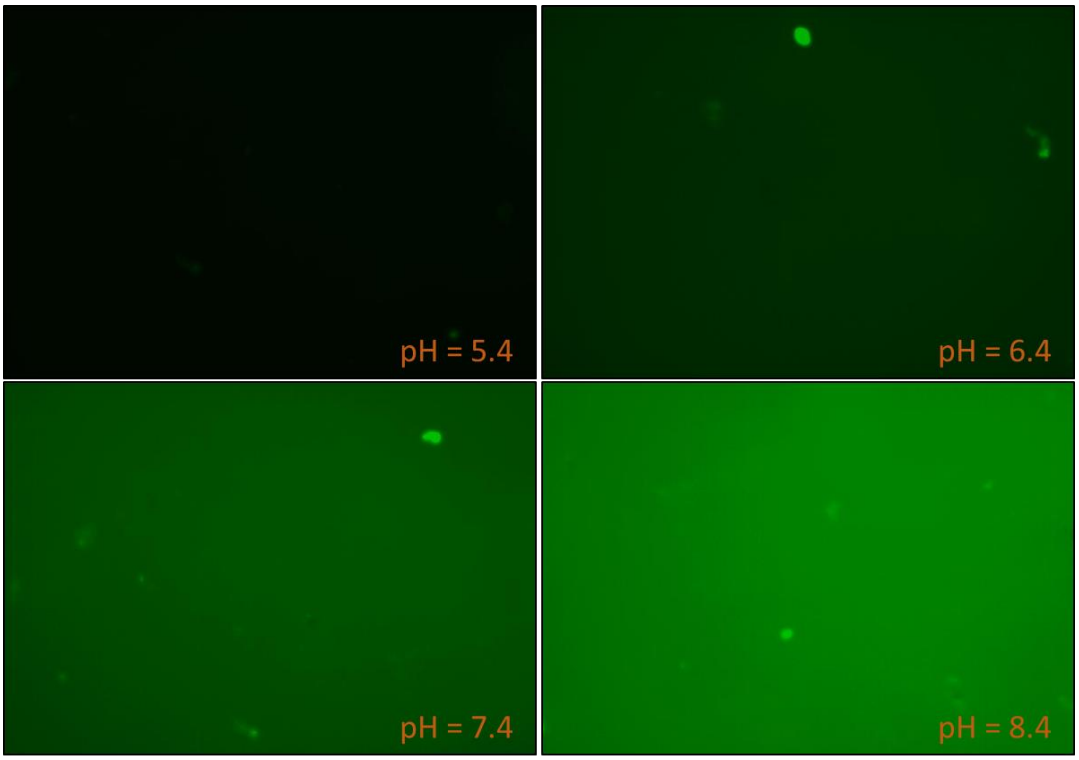

Figure 2-42: Effect of pH on the modified surface with 6-carboxyfluorescein **2.69a**.

One of the main issue with the probes in fluorescence microscopy is photobleaching. It arises from the alteration of the dye through cleavage of the covalent bonds caused by the transition from the singlet state to the triplet state of the fluorophore. This photobleaching is problematic as it leads to a loss of fluorescence over time, reducing the level of fluorescence observable. It has been shown that fluorescein can photobleach under intense light. To examine this, the surface was analysed by microscopy under strong fluorescence activation in a very basic solution (NaOH, 0.1 M). The results are shown in **Figure 2-43**.

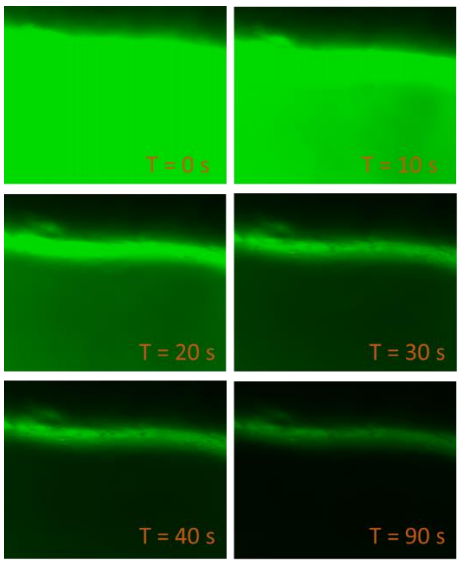

Figure 2-43: Effect of photobleaching on the modified surface with 6-carboxyfluorescein **2.69$_a$**.

We can see that there is a clear drop in intensity after a few seconds of strong light exposure, indicating that the fluorophore is not stable under these conditions. This result is not surprising as it is a well-documented phenomenon for such fluorophores.[135] To avoid this problem would require reducing the exposure time and the intensity of the light during microscopy.

The same experiment was repeated to study how a normal light impacted on the fluorescence intensity of the surface over time. By taking the mean fluorescence intensity of the images and plotting it against time we were able to demonstrate the reduced effect under normal light conditions. **Figure 2-44** shows the results of photobleaching on the surface at λ_{ex} = 492 nm (red circles) and under the light of the fume hood (black squares).

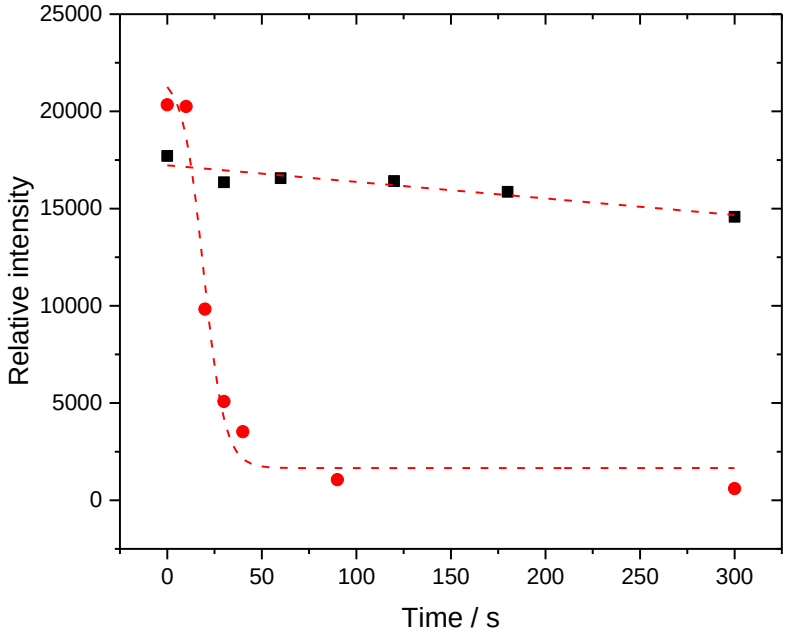

Figure 2-44: Photobleaching of the surface at λ_{ex} = 492 nm (red circles) and under the light of the fume hood (black squares).

Figure 2-44 clearly illustrates the rapid reduction in fluorescent intensity under strong fluorescent light (red circles). However, under normal light there is only a slight drop in intensity over time (black squares). From these results we can conclude that the surface needs to be protected from light as much as possible, and that the surfaces should be stored in the dark. Also care must be taken using fluorescence microscopy to not destroy the fluorophore on the substrates, by careful choice of lamp intensity.

Finally, the solid supported zinc probe was also analysed by taking two pictures of the surface with and without zinc (**Figure 2-45**). The pictures were taken under identical conditions, only the presence of zinc was changed. As expected, we can see that there is a clear increase in the fluorescence intensity when $ZnCl_2$ was added. This proves the ability of the surface to detect this specific metal.

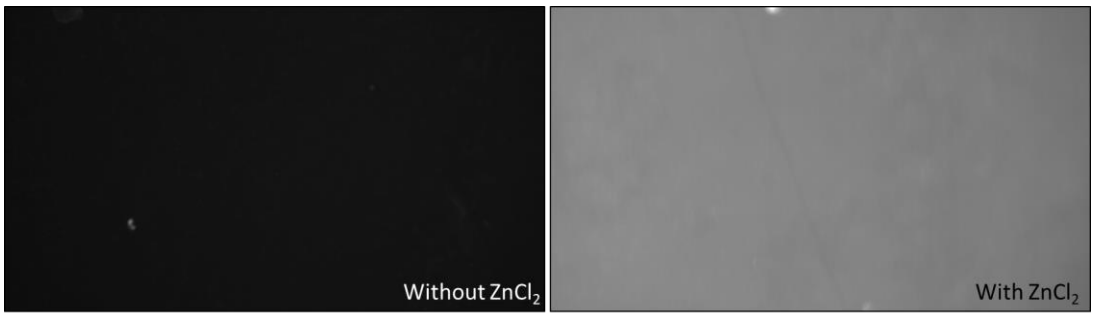

Figure 2-45: Fluorescence images of the zinc substrate **2.72$_a$** without (left) and with zinc (right).

This section describes how the probe modified surfaces behave under the fluorescence microscope. From these results we can conclude that: i) our surfaces behave as fluorescence sensors, responding to the change of conditions (change of pH, presence of zinc); ii) the surface needs to be protected from the light as much as possible; iii) using too strong light intensity in microscopy can easily destroy the dye and lead to a loss of fluorescence. The next important stage is to grow cells on the modified surfaces and test the surface sensory properties. To enable these experiments, it was necessary to ensure that cells could grow and survive on the surface.

2.3.5 First biological tests on the modified substrates

It was important to determine if live cells could grow and survive on our modified surfaces or that indeed they could adhere to it. Therefore, the surface modified with the 6-carboxyfluorescein **2.69$_a$** pH probe was placed in a media containing neuron cells. The cells were allowed to grow, under the correct conditions for three days. After this the cells were visualised under an optical microscope and photographed. The images in **Figure 2-46** show, side **A** , the cells grown as a control on the unmodified ITO surface. It is clear to see that on the ITO surface the cells did not grow properly and aggregated into multiple agglomerates (one shown by red circle). This aggregation occurs when cells cannot grow effectively and the cells “stick” together and form connections. However, when the cells were grown on our probe modified surface, side **B**, **Figure 2-46** it is clear that the cells have grown successfully and formed the desired connections between each other. This presents clear evidence that the cells are able to grow on at least some of our modified surfaces. This is the first evidence we gained to show that our surfaces are suitable for biological tests. Unfortunately, due to the timescales of the project and access to correct equipment we were unable to test the cells further. We are optimistic that these preliminary experiments demonstrate the possibility of utilising our surfaces in biosensory applications, however more experiments are clearly needed.

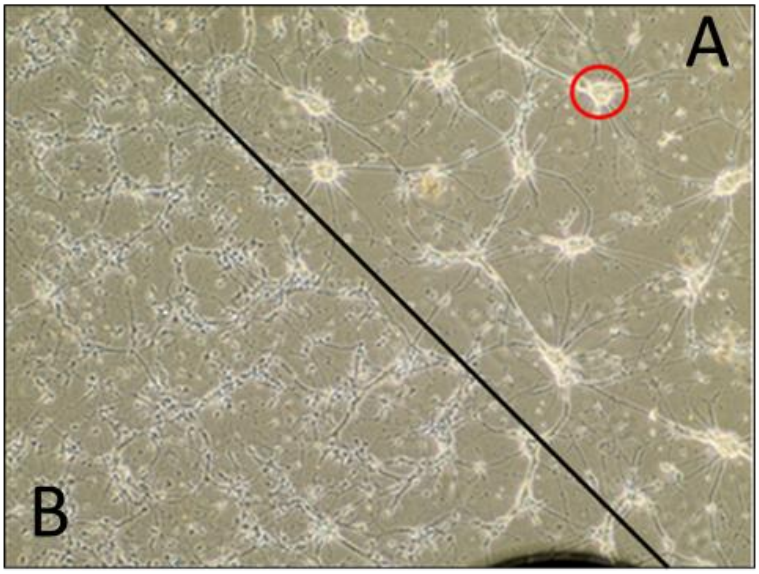

Figure 2-46: Neurons cells on the pH probe substrate **2.69$_a$**, with **A** the ITO non modified and **B** the modified surface

Chapter 3 Conclusion and further work

Significant progress has been made towards the preparation and characterisation of new fluorescent surfaces that can be used for applications in biology, particularly in the study of extracellular fluxes. Fluorescent probes were prepared, in a form suitable for direct attachment to a surface. The first route designed for the synthesis of a probe based on a naphthalic anhydride fluorescent moiety failed at the stage of coupling the fluorophore with the receptor. This led to change our plan: an efficient second route based on carboxyfluorescein allowed us to prepare nine fluorescent probes targeted to be specific towards different types of extracellular fluxes. Those probes were prepared through the synthesis and separation of the two isomers of carboxyfluorescein, followed by addition of a specific receptor through a Mannich reaction. The receptors were chosen according to the target molecules we wanted to detect, as it was decided to focus on three main extracellular fluxes: pH, potassium ions and zinc ions, even though two of the pH probes synthesised have been found able to detect silver too (for a summary of the nine probes prepared in this work see **Figure 3-1**). In the last step of the preparation of the probes, the free carboxylic group in the carboxyfluorescein moiety was modified into a succinimidyl ester, which is a functional group more suitable for ease attachment onto the silica surfaces modified with a linker bearing amino groups.

The substrates used for the immobilization of the probes, mesoporous silica surfaces, were successfully prepared by Electrochemical-Assisted Self-Assembly (EASA), a method developed by the group of Alain Walcarius.[103] This method is inspired by the sol-gel deposition: it consists in applying a negative potential to a working electrode, which activates the deposition of the silica on the surface. The presence of a surfactant (CTAB in this work) in the solution leads to the formation of micelles, around which the silica grows producing a porous surface. The surfaces were then successfully modified with a linker (APTES), bearing a terminal amino group. At this stage the surfaces were characterised by X-ray spectroscopy and cyclic voltammetry, proving the successful formation of a porous surface.

After that, the surfaces were modified with the fluorescent probes previously prepared, using the reaction between the amino groups introduced at the silica surface and the succinimidyl ester of the probes. Therefore, the modified surfaces were characterised using different techniques, such as Raman spectroscopy and cyclic voltammetry, providing experimental data to support the attachment of the probes. The fluorescence parameters (quantum yield, extinction coefficient and selectivity) were determined for all the probes, both in solution and immobilised on the surface. The fluorescence experiments allowed us

to prove that the surfaces can respond to specific external changes. Finally, cells (in particular, neurons) were successfully grown on one of the surfaces modified with a fluorescein probe, proving that our substrates are suitable to be used with living microorganisms.

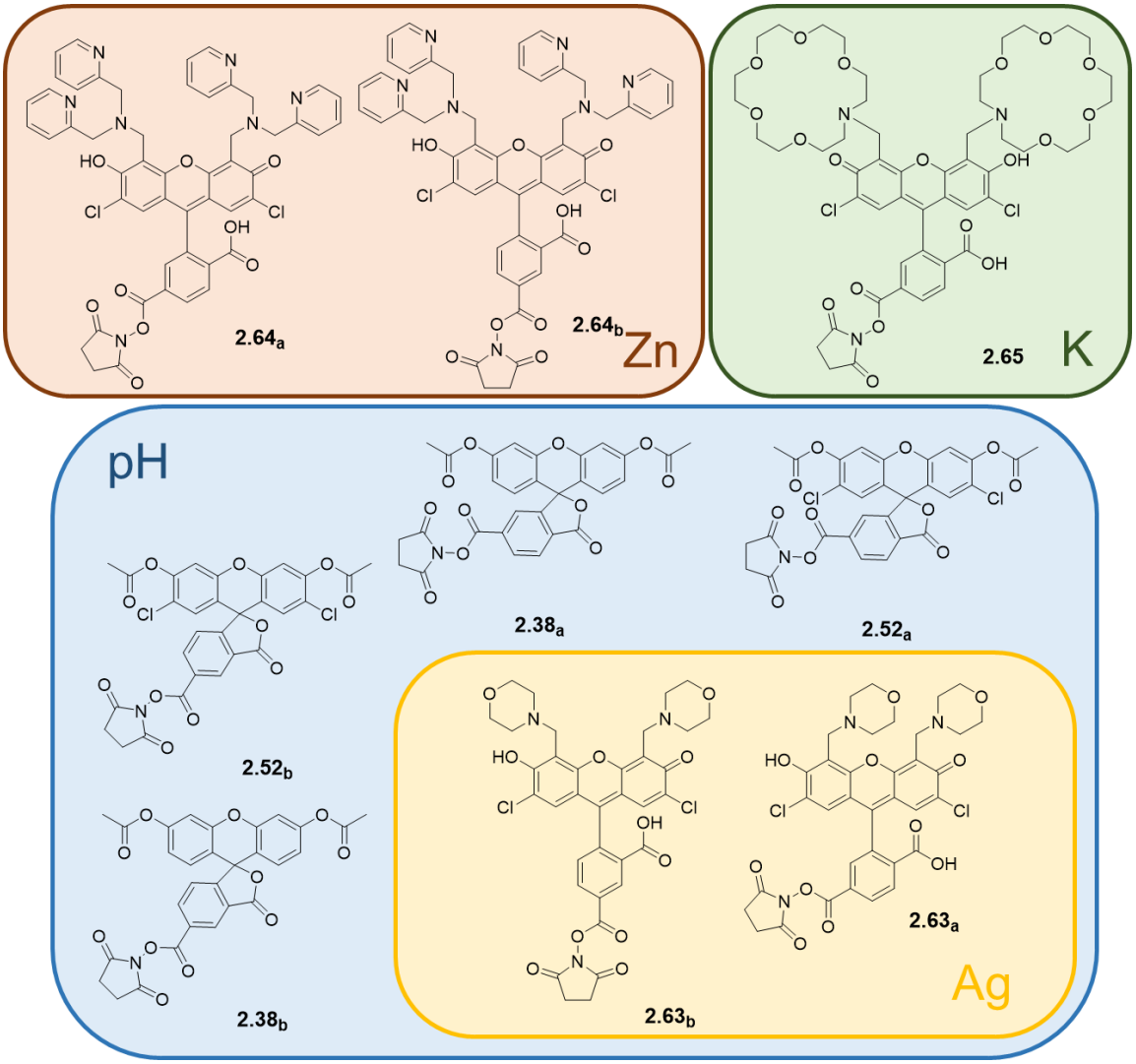

Figure 3-1: Summary of the nine probes prepared in this work.

The work presented here is intended to be a first study for the application of solid surfaces to the detection of extracellular fluxes. However, further work needs to be carried out to confirm the applicability of our modified surfaces. First of all, some of the experiments already performed should be repeated, especially to confirm all the fluorescence parameters of the probes in solution. Then, further fluorescence studies need to be performed on the surfaces themselves to understand better how they react to external changes.

In this work, we have established the methods for the preparation of fluorescent mesoporous surfaces and, once the surfaces will be fully characterised, future work needs to focus on growing specific types of cells on them. Furthermore, we should study how the

surfaces respond when the cells are subject to external changes, such as change of pH or modification of the media. For example, the surface modified with the pH probe could be used to understand better the cell respiration process, as presented in the introduction, or the one modified with the potassium probe could help to understand how neurons interact between each other. The nine fluorescent probes prepared in this work could have a wide range of applications to study changes in pH, zinc and potassium ions, at or near the surface of the cells. If preliminary biology tests with our surfaces will be successful, new probes could be prepared based on carboxyfluorescein, in order to study different types of extracellular fluxes such as the ones of calcium, sodium or magnesium.

Chapter 4 Experimental

General methods

Chemicals were purchased from Sigma-Aldrich, Fisher Scientific or Alfa Aesar. NaH was used as a 60% dispersion in oil. All air/moisture sensitive reactions were carried out under an inert atmosphere, in oven-dried or flame-dried glassware. The solvents THF (from Na/benzophenone), CH_3CN and CH_2Cl_2 (from CaH_2) and MeOH (from $Mg(OMe)_2$) were distilled before use, and where appropriate, other reagents and solvents were purified by standard techniques.[136] TLC was performed on aluminium-precoated plates coated with silica gel 60 with an F254 indicator; visualised under UV light (254 nm) and/or by staining with anisaldehyde, ceric ammonium molybdate, iodine, phosphomolybdic acid, potassium permanganate or vanillin. Flash column chromatography was performed using high purity silica gel, pore size 60 Å, 230-400 mesh particle size, purchased from Merck. ^{1}H NMR and ^{13}C NMR spectra were recorded in $CDCl_3$ and DMSO-d_6 (purchased from Cambridge Isotope Laboratories) at 298 K using Bruker DPX400 (400 and 101 MHz respectively) spectrometers. Chemical shifts are reported on the δ scale in ppm and were referenced to residual solvent ($CDCl_3$: 7.27 ppm for ^{1}H NMR spectra and 77.0 ppm for ^{13}C NMR spectra; DMSO-d_6: 2.50 ppm for ^{1}H NMR spectra and 39.52 ppm for ^{13}C NMR spectra). All spectra were reprocessed using ACD/Labs software version 2015 or ACD/Spectrus. Coupling constants (*J*) were recorded in Hz. The following abbreviations for the multiplicity of the peaks are s (singlet), d (doublet), t (triplet), q (quartet), quin (quintet), sxt (sextet), spt (septet), br (broad), and m (multiplet). Electrospray (ES) low resolution mass spectra were recorded on a Waters TQD quadrupole spectrometer. Electron impact (EI) low resolution mass spectra were recorded on a Trace 2000 Series GC-MS. High resolution mass spectra were recorded on a Bruker APEX III FT-ICR mass spectrometer. Fourier-transform infrared (FT-IR) spectra are reported in wavenumbers (cm^{-1}) and were collected as solids or neat liquids on a Nicolet 380 fitted with a Smart Orbit Goldengate attachment using OMNIC software package. The abbreviations s (strong), m (medium), w (weak) and br (broad) are used when reporting the spectra. Melting points were obtained using a Gallenkamp Electrothermal apparatus. Electrochemical measurements were performed in glass or plastic cells using the software Nova 1.10 with a standard three-electrode arrangement, connected with either a μAutolab type III or an Autolab PGSTAT 302 (Ecochemie, Netherlands). The counter electrode was a platinum gauze and the reference was a home-made saturated calomel electrode (SCE). Working electrodes were ITO (Indium Tin Oxide) coated glass slides and coverslips purchased from NANOCS. Raman spectra of modified SSV substrates were acquired using a Renishaw inVia Raman microspectrometer equipped with a 50x objective and a 785 nm He-Ne laser. About 100 mW is the maximum power

output of the laser, but usually lower powers were used, and Raman spectra were acquired for 20-30 s accumulation time, under extended mode from 2500 cm^{-1} to 100 cm^{-1}. Spectra were then normalised in respect to the laser power and accumulation time using Origin 9.1 software. Characterisation by grazing incidence small angle x-ray scattering was performed with a Rigaku SmartLab thin film and materials diffractometer.

2-(2-Methoxyethoxy)nitrobenzene (2.08)

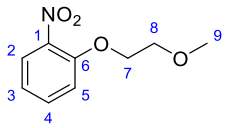

$C_9H_{11}NO_4$

197.19 $gmol^{-1}$

A suspension of 2-nitrophenol (14.0 g, 101 mmol), bromoethyl methyl ether (10.0 mL, 106 mmol), KI (8.40 g, 50.6 mmol), K_2CO_3 (15.3 g, 111 mmol) in DMF (50 mL) was heated at 110 °C. After 2 h, the solvent was evaporated and the brown oil dissolved in CH_2Cl_2 (50 mL) and water (50 mL). The organic phase was separated, then washed with aqueous Na_2CO_3 (2.5%, 2 × 50 mL), brine (50 mL) and dried (Na_2SO_4). The solvent was evaporated to afford the aryl ether as a yellow oil (19.5 g, 98.9 mmol, 98%). The product was of sufficient purity to be used in the next reaction without further purification. Spectroscopic and physical data were consistent with reported values.[62]

FT-IR (neat) ν_{max} = 2930 (w), 2882 (w), 1606 (m), 1520 (s), 1349 (m), 1275 (m), 1125 (m), 1031 (m), 924 (w), 850 (m), 742 (s) cm^{-1}

^{1}H NMR ($CDCl_3$, 400 MHz) δ = 7.81 (dd, *J* = 8.3, 1.7 Hz, 1H, **2**), 7.50 (ddd, *J* = 8.5, 7.2, 1.7 Hz, 1H, **4**), 7.10 (dd, *J* = 8.5, 1.0 Hz, 1H, **5**), 7.02 (ddd, *J* = 8.3, 7.2, 1.0 Hz, 1H, **3**), 4.24–4.27 (m, 2H, **7**), 3.77–3.81 (m, 2H, **8**), 3.43 (s, 3H, **9**) ppm

^{13}C NMR ($CDCl_3$, 101 MHz) δ = 152.29 (C, **6**), 140.15 (C, **1**), 134.11 (CH, **4**), 125.54 (CH, **3**), 120.66 (CH, **2**), 115.10 (CH, **5**), 70.62 (CH_2, **7**), 69.55 (CH_2, **8**), 59.43 (CH_3, **9**) ppm

LRMS (ES^+) *m/z* = 198 $[M+H]^+$

2-(2-Methoxyethoxy)aniline (2.09)

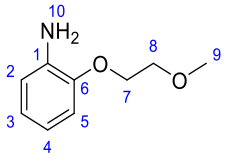

$C_9H_{13}NO_2$

167.21 $gmol^{-1}$

To a three-necked RBF containing EtOH (125 mL) under an atmosphere of N_2, Fe powder (13.8 g of <10 µm, 250 mmol,) was added followed by conc. HCl (36 M, 0.90 mL, 25.0 mmol) and the suspension was stirred at 65 °C for 2 h. After cooling to 55 °C, aqueous NH_4Cl (1.30 M, 40.0 mL, 52.0 mmol) was added followed by a slow addition of 2-(2-methoxyethoxy)nitrobenzene (**2.08**, 10.0 g, 50.7 mmol), and the mixture was then stirred at 60 °C for 3 h. After cooling to rt, EtOH (100 mL) and celite (20 g), were added prior to filtration. The filter cake was washed with EtOH and the filtrate concentrated under reduced pressure. The brown residue was dissolved in EtOAc (100 mL), the organic layer was washed with saturated $NaHCO_3$ (50 mL), brine (50 mL), dried (Na_2SO_4) and concentrated under vacuum to give a black oil. Purification by silica gel column chromatography (EtOAc, 100%) afforded 2-(2-methoxyethoxy)aniline (**2.09**) as a brown oil (5.70 g, 34.1 mmol, 66%). Spectroscopic and physical data were consistent with reported values.[62]

FT-IR (neat) ν_{max} = 3457 (w), 3357 (w), 2927 (w), 2879 (w), 1614 (m), 1503 (s), 1457 (m), 1275 (m), 1216 (s), 1222 (m), 1053 (m), 927 (w), 735 (s) cm^{-1}

^{1}H NMR ($CDCl_3$, 400 MHz) δ = 6.68–6.88 (m, 4H, **2**, **3**, **4** & **5**), 4.14–4.19 (m, 2H, **7**), 3.75–3.80 (m, 2H, **8**), 3.46 (s, 3H, **9**) ppm

^{13}C NMR ($CDCl_3$, 101 MHz) δ = 146.41 (C, **6**), 136.87 (C, **1**), 121.81, 118.40, 115.37 and 112.81 (CH, **2**, **3**, **4** & **5**), 71.20 (CH_2, **8**), 68.18 (CH_2, **7**), 59.10 (CH_3, **9**) ppm

LRMS (ES^+) *m/z* = 168 $[M+H]^+$

_N_,_N_-Di(2-hydroxyethyl)-2-(2-methoxyethoxy)aniline (2.06)

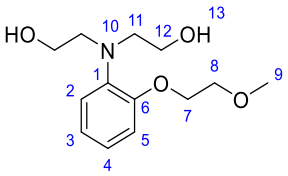

$C_{13}H_{21}NO_4$

255.31 gmol^{-1}

A mixture of 2-(2-methoxyethoxy)aniline (**2.09**, 5.01 g, 29.9 mmol), 2-bromoethanol (7.50 mL, 106 mmol) and $CaCO_3$ (5.01 g, 49.9 mmol) in water (100 mL) was stirred 12 h at 60 °C. After cooling at rt, Na_2CO_3 (3.75 g, 35.4 mmol) was added and the mixture was stirred 40 min at 60 °C. The resulting solid was then removed by filtration, and the aqueous layer was saturated with NaCl prior to extraction with CH_2Cl_2 (3 × 50 mL). The combined organic phases were dried ($MgSO_4$) and concentrated under vacuum to give a brown oil. Purification by silica gel column chromatography (EtOAc 100%) afforded *N*,*N*-di(2-hydroxyethyl)-2-(2-methoxyethoxy) aniline (**2.06**) as a dark red oil (6.95 g, 27.2 mmol, 91%). Spectroscopic and physical data were consistent with reported values.[66]

FT-IR (neat) ν_{max} = 3385 (w), 2929 (w), 2877 (w), 1593 (w), 1498 (m), 1449 (m), 1235 (m), 1050 (s), 927 (m), 746 (s) cm^{-1}

^{1}H NMR ($CDCl_3$, 400 MHz) δ = 7.23 (dd, *J* = 7.8, 1.7 Hz, 1H, **2**), 7.13 (td, *J* = 7.8, 1.7 Hz, 1H, **4**), 7.00 (td, *J* = 7.8, 1.3 Hz, 1H, **3**), 6.92 (dd, *J* = 7.8, 1.3 Hz, 1H, **5**), 4.0.9–4.14 (m, 2H, **7**), 3.73–3.76 (m, 2 H, **8**), 3.44–3.50 (m, 4H, **12**), 3.45 (s, 3H, **9**), 3.13–3.18 (m, 4 H, **11**) ppm

^{13}C NMR ($CDCl_3$, 101 MHz) δ = 155.20 (C, **6**), 139.18 (C, **1**), 126.09 (CH, **4**), 125.48 (CH, **2**), 122.28 (CH, **3**), 113.37 (CH, **5**), 70.75 (CH_2, **8**), 67.82 (CH_2, **7**), 59.67 (CH_2,**12**), 58.97 (CH_3, **9**), 57.92 (CH_2, **11**) ppm

LRMS (ES$^+$) *m/z* = 278 [M+Na]$^+$, 256 [M+H]$^+$

Tetraethylene glycol di(*p*-toluenesulfonate) (2.11)

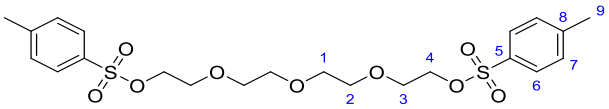

$C_{22}H_{30}O_9S_2$

502.59 gmol^{-1}

Tetraethylene glycol (10.0 g, 51.5 mmol) and 4-toluenesulfonyl chloride (30.0 g, 157 mmol) were dissolved in THF (200 mL), the mixture was cooled at 0 °C. A solution of KOH (20.5 g, 365 mmol) in water (50 mL) was added dropwise, and the resulting two-phase mixture was stirred 2 h at rt. The mixture was poured into water (100 mL) and Et_2O (300 mL). The organic layer was washed with saturated NH_4Cl (150 mL), water (100 mL), brine (100 mL), dried ($MgSO_4$) and then concentrated under vacuum to afford the title disulfonate **2.11** as a colourless oil (25.9 g, 51.4 mmol, 100%). Spectroscopic and physical data were consistent with reported values.[137]

FT-IR (neat) ν_{max} = 2871 (w), 1597 (w), 1451 (w), 1351 (m), 1173 (s), 1095 (m), 1011 (m), 913 (s), 814 (m), 772 (m), 661 (s), 552 (s) cm^{-1}

^{1}H NMR ($CDCl_3$, 400 MHz) δ = 7.78 (d, *J* = 8.2 Hz, 4H, **6**), 7.33 (d, *J* = 8.2 Hz, 4H, **7**), 4.15 (t, *J* = 4.9 Hz, 4H, **4**), 3.67 (t, *J* = 4.9 Hz, 4H, **3**), 3.53–3.58 (m, 8H, **1** & **2**), 2.44 (s, 6H, **9**) ppm

^{13}C NMR ($CDCl_3$, 101 MHz) δ = 144.83 (C, **5**), 132.99 (C, **8**), 129.84 (CH, **7**), 127.96 (CH, **6**), 70.71 (CH_2, **1**), 70.54 (CH_2, **2**), 69.28 (CH_2, **3**), 68.67 (CH_2, **4**), 21.63 (CH_3, **9**) ppm

LRMS (ES$^+$) *m/z* = 525 [M+Na]$^+$, 503 [M+H]$^+$

1,4,7,10,13-Pentaoxa-16-azacyclooctadecane, 16-[2-(2-methoxyethoxy) phenyl] (2.05)

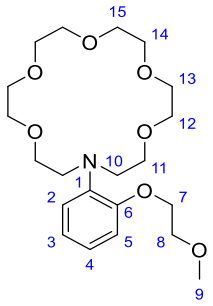

$C_{21}H_{35}NO_7$

413.51 $gmol^{-1}$

NaH (100 mg of a 60 % dispersion in mineral oil, 2.50 mmol) was slowly added to a solution of *N*,*N*-di(2-hydroxyethyl)-2-(2-methoxyethoxy)aniline (**2.06**, 300 mg, 1.18 mmol) in dry THF (15 mL) under N_2 atm. The mixture was heated at reflux and tetraethylene glycol di(*p*-toluenesulfonate) (**2.11**, 600 mg, 1.19 mmol) in dry THF (10 mL) was added dropwise using a syringe pump at 0.3 mL/min. The reaction was heated under reflux 12 h. After cooling to rt, the precipitate was removed by filtration, then the solvent was then removed under vacuum to give a brown oil. Purification by silica gel column chromatography (CH_2Cl_2/MeOH, 85:15) afforded the pure product as a pale brown oil (200 mg, 48.4 mmol, 41%). Spectroscopic and physical data were consistent with reported values.[66]

FT-IR (neat) ν_{max} = 2867 (w), 1495 (w), 1242 (w), 1118 (m), 936 (w), 842 (w) cm^{-1}

^{1}H NMR ($CDCl_3$, 400 MHz) δ = 6.83–7.15 (m, 4H, **2**, **3**, **4** & **5**), 4.08–4.20 (m, 2H, **7**), 3.53–3.81 (m, 26H, **8**, **10**, **11**, **12**, **13**, **14** & **15**), 3.43 (s, 3H, **9**) ppm

^{13}C NMR ($CDCl_3$, 101 MHz) δ = 152.37 (C, **6**), 137.97 (C, **1**), 129.82 and 127.99 (CH, **2** & **4**), 121.37 (CH, **3**), 114.18 (CH, **5**), 70.10–71.04 (CH_2, **11**, **12**, **13**, **14** & **15**), 69.60 (CH_2, **8**), 67.85 (CH_2, **7**), 59.00 (CH_3, **9**), 52.51 (CH_2, **10**) ppm

LRMS (ES^+) *m/z* = 414 $[M+H]^+$

2,4-Dibromo-2-(2-methoxyethoxy)aniline (2.16)

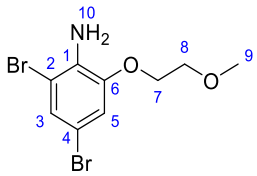

$C_9H_{11}Br_2NO_2$

325.00 $gmol^{-1}$

To a solution of 2-(2-methoxyethoxy)aniline (**2.09**, 100 mg, 0.60 mmol) in dry CH_3CN (5 mL) at 0 °C under N_2 was added *N*-bromosuccinimide (213 mg, 1.20 mmol) in one portion. The mixture was then stirred at rt for 12 h. The reaction was quenched with water (5 mL) and extracted with CH_2Cl_2 (3 × 10 mL). The combined organic layers were washed with brine (15 mL), dried (Na_2SO_4) and concentrated under vacuum to afford the product **2.16** as a dark red oil (120 mg, 0.37 mmol, 61%).

FT-IR (neat) ν_{max} = 3343 (w), 2912 (w), 2865 (w), 1570 (w), 1486 (w), 1404 (w), 1211 (w), 1126 (w), 1059 (w), 946 (w), 826 (w), 669 (w) cm^{-1}

^{1}H NMR ($CDCl_3$, 400 MHz) δ = 7.21 (d, *J* = 2.0 Hz, 1H, **3**), 6.87 (d, *J* = 2.0 Hz, 1H, **5**), 4.11–4.14 (m, 2H, **9**), 3.73–3.75 (m, 2H, **8**), 3.44 (s, 3H, **9**) ppm

^{13}C NMR ($CDCl_3$, 101 MHz) δ = 146.75 (C, **6**), 134.87 (C, **1**), 126.91 (CH, **3**), 114.70 (CH, **5**), 108.44 (C, **2**), 108.34 (C, **4**), 70.78 (CH_2, **8**), 68.88 (CH_2, **7**), 59.12 (CH_3, **9**) ppm

LRMS (ES^+) *m/z* = 328 $[M(^{81}Br^{81}Br)+H]^+$, 326 $[M(^{79}Br^{81}Br)+H]^+$, 324 $[M(^{79}Br^{79}Br)+H]^+$

4-Bromo-2-(2-methoxyethoxy)aniline (2.18)

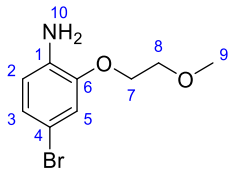

$C_9H_{12}BrNO_2$

246.10 $gmol^{-1}$

To a solution of 2-(2-methoxyethoxy)aniline (**2.09**, 5.00 g, 29.9 mmol) in dry CH_3CN (200 mL) at 0 °C under N_2 was added *N*-bromosuccinimide (5.32 g, 30.0 mmol) in one portion. The mixture was then stirred at rt for 12 h. Reaction was quenched with water (50 mL) and extracted with CH_2Cl_2 (3 × 100 mL). The combined organic layers were washed with brine (100 mL), dried (Na_2SO_4) and concentrated under vacuum. Purification by silica gel column chromatography (EtOAc/hexane, 1:1) afforded the pure aryl bromide **2.18** as a dark red solid (6.64 g, 27.0 mmol, 90%).

FT-IR (neat) ν_{max} = 3357 (w), 2926 (w), 2877 (w), 1614 (m), 1500 (s), 1278 (m), 1219 (s), 1123 (m), 1086 (m), 934 (m), 850 (m), 741 (m) cm^{-1}

^{1}H NMR ($CDCl_3$, 400 MHz) δ = 6.92 (m, 2H, **3** & **5**), 6.60–6.62 (m, 1 H, **2**), 4.12–4.14 (m, 2 H, **7**), 3.74–3.77 (m, 2H, **8**), 3.45 (s, 3 H, **9**) ppm

^{13}C NMR ($CDCl_3$, 101 MHz) δ = 146.90 (C, **6**), 135.91 (C, **1**), 124.31 (CH, **3**), 115.77 and 115.99 (CH, **2** & **5**), 109.24 (C, **4**), 70.87 (CH_2, **8**), 68.33 (CH_2, **7**), 59.03 (CH_3, **9**) ppm

LRMS (ES$^+$) *m/z* = 248 [M(^{81}Br)+H]$^+$, 246 [M(^{79}Br)+H]$^+$

2,2'-((4-Bromo-2-(2-methoxyethoxy)phenyl)azanediyl) (2.15)

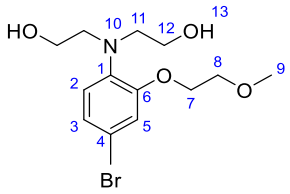

$C_{13}H_{20}BrNO_4$

334,21 $gmol^{-1}$

Method 1

A suspension of 4-bromo-2-(2-methoxyethoxy)aniline (**2.18**, 200 mg, 0.81 mmol), 2-bromoethanol (0.20 mL, 2.82 mmol), NaI (140 mg, 0.93 mmol) and $CaCO_3$ (200 mg, 1.99 mmol) in water (15 mL) was stirred 12 h at 60 °C. After cooling to rt, Na_2CO_3 (150 mg, 1.42 mmol) was added and the mixture was stirred for 40 min at 60 °C. The resulting solid was removed by filtration, and the aqueous layer saturated with NaCl prior to extraction EtOAc (3 × 10 mL). The combined organic phase was dried ($MgSO_4$) and concentrated under vacuum to give a brown oil. Purification by silica gel column chromatography (EtOAc, 100% to EtOAc/MeOH, 90:10) afforded 2,2'-((4-bromo-2-(2-methoxyethoxy)phenyl)azanediyl) (**2.15**) as a brown oil (170 mg, 0.51 mmol, 63%).

Method 2

To a solution of *N*,*N*-Di(2-hydroxyethyl)-2-(2-methoxyethoxy)aniline (**2.06**, 6.30 g, 24.68 mmol) in dry ACN (100 mL) at 0 °C under N_2 was added *N*-bromosuccinimide (4.39 g, 30.0 mmol) in one portion. The mixture was then stirred 12 h at rt. Water (50 mL) was added to the reaction, which was extracted with CH_2Cl_2 (3 × 50 mL). The combined organic layers were washed with brine (50 mL), dried (Na_2SO_4) and concentrated under vacuum. Purification by silica gel column chromatography (EtOAc, 100% to EtOAc/MeOH, 90:10) afforded 2,2'-((4-bromo-2-(2-methoxyethoxy)phenyl)azanediyl) (**2.15**) as a brown oil (7.09 g, 21.2 mmol, 86%).

Data for 2,2'-((4-bromo-2-(2-methoxyethoxy)phenyl)azanediyl) (**2.15**)

FT-IR (neat) ν_{max} = 3383 (w), 2925 (w), 2869 (w), 1594 (w), 1492 (m), 1445 (m), 1229 (m), 1049 (s), 926 (m), 744 (s) cm^{-1}

^{1}H NMR ($CDCl_3$, 400 MHz) δ = 6.93–7.07 (m, 3H, **2**, **3** & **5**), 4.01–4.11 (m, 2H, **7**), 3.67–3.72 (m, 2H, **8**), 3.43–3.49 (m, 4H, **12**), 3.37 (s, 3H, **9**), 3.07–3.17 (m, 4H, **11**) ppm

^{13}C NMR ($CDCl_3$, 101 MHz) δ = 155.28 (C, **6**), 138.65 (C, **1**), 126.08 and 124.91 (CH, **2** & **3**), 117.64 (C, **4**), 116.77 (CH, **5**), 70.50 (CH_2, **8**), 68.01 (CH_2, **7**), 59.67 (CH_2, **12**), 58.91 (CH_3, **9**), 57.10 (CH_2, **11**) ppm

LRMS (ES^+) *m/z* = 358 $[M(^{81}Br)+Na]^+$, 356 $[M(^{79}Br)+Na]^+$, 336 $[M(^{81}Br)+H]^+$, 334 $[M(^{79}Br)+H]^+$

16-(4-bromo-2-(2-methoxyethoxy)phenyl)-1,4,7,10,13-pentaoxa-16-azacyclooctadecane (2.13)

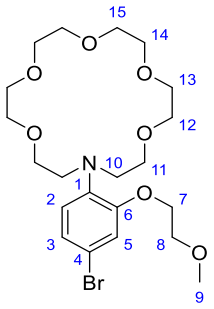

$C_{21}H_{34}BrNO_7$

492.41 $gmol^{-1}$

NaH (400 mg of a 60% dispersion in mineral oil, 10.0 mmol) was slowly added to a solution of 2,2'-((4-bromo-2-(2-methoxyethoxy)phenyl)azanediyl) (**2.18**, 1.00 g, 2.99 mmol) in dry THF (300 mL) under N_2 atm. The mixture was heated at reflux and tetraethylene glycol di(*p*-toluenesulfonate) (**2.11**, 1.51 g, 3.00 mmol) in dry THF (40 mL) was added dropwise using a syringe pump at 0.3 mL/min. The reaction was heated under reflux 12 h. After cooling to rt the precipitate was removed by filtration. The solvent was then removed under vacuum to give a brown oil. Purification by silica gel column chromatography ($CHCl_3$/MeOH, 90:10) afforded the pure product as a pale brown oil (768 mg, 1.56 mmol, 52%).

FT-IR (neat) ν_{max} = 2866 (m), 1495 (m), 1351 (w), 1242 (m), 1119 (s), 936 (w), 842 (w) cm^{-1}

^{1}H NMR ($CDCl_3$, 400 MHz) δ = 6.92-7.04 (m, 3H, **2**, **3** & **5**), 4.07–4.13 (m, 2H, **7**), 3.55-3.77 (m, 22H, **8**, **11**, **12**, **13**, **14** & **15**), 3.38–3.49 (m, 7H, **9** & **10**) ppm

^{13}C NMR ($CDCl_3$, 101 MHz) δ = 153.11 (C, **6**), 138.92 (C, **1**), 126.18 and 124.14 (CH, **2** & **3**), 116.82 (C & CH, **4** & **5**), 70.18–70.90 (CH_2, **11**, **12**, **13**, **14** & **15**), 69.54 (CH_2, **8**), 67.85 (CH_2, **7**), 58.98 (CH_3, **9**), 52.83 (CH_2, **10**) ppm

LRMS (ES^+) *m/z* = 516 $[M(^{81}Br)+Na]^+$, 514 $[M(^{79}Br)+Na]^+$, 494 $[M(^{81}Br)+H]^+$, 492 $[M(^{79}Br)+H]^+$

3-Nitro-1,8-naphthalic anhydride (2.19)

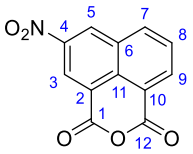

$C_{12}H_5NO_5$

243.17 gmol^{-1}

1,8-Naphthalic anhydride (5.00 g, 25.2 mmol) was dissolved in concentrated H_2SO_4 (20 mL) and cooled to 5 °C. Concentrated HNO_3 (1.70 g, 27.0 mmol) in concentrated H_2SO_4 (2.50 mL) was then added dropwise, and the mixture was stirred at rt for 90 min. The reaction was poured into a mixture of ice and water, and the resulting precipitate was filtered, washed with a large amount of water and recrystallized from glacial acetic acid to afford the pure nitrated product as a yellow solid (4.25 g, 17.5 mmol, 70%). Spectroscopic and physical data were consistent with reported values.[138]

M.P. 248 °C (Lit.[139] 247–249 °C)

FT-IR (neat) ν_{max} = 3689 (w), 3676 (w), 2361 (m), 1778 (s), 1749 (s), 1594 (m), 1532 (m), 1342 (m), 1292 (s), 1147 (m), 1082 (m), 1024 (s), 789 (s), 755 (m), 516 (m) cm^{-1}

^{1}H NMR (DMSO-d_6, 400 MHz) δ = 9.53 (d, J = 1.7 Hz, 1H, **3**), 8.93 (d, J = 1.7 Hz, 1H, **5**), 8.83 (d, J = 7.8 Hz, 1H, **7**), 8.71 (d, J = 7.8 Hz, 1H, **9**), 8.09 (t, J = 7.8 Hz, 1H, **8**) ppm

^{13}C NMR (DMSO-d_6, 101 MHz) δ = 160.23 (C, **12**), 159.97 (C, **1**), 146.24 (C, **4**), 137.67 (CH, **7**), 135.87 (CH, **9**), 132.09 (C, **11**), 131.29 (C, **6**), 131.07 (CH, **3**), 129.97 (CH, **8**), 124.66 (CH, **5**), 121.71 (C, **2**), 120.18 (C, **10**) ppm

LRMS (ES$^+$) m/z = 244 [M+H]$^+$

3-Amino-1,8-naphthalic anhydride (2.14)

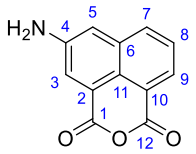

$C_{12}H_7NO_3$

213.19 $gmol^{-1}$

Method 1

A solution of $SnCl_2$ (4.00 g, 21.1 mmol) in concentrated HCl (3.50 mL) was added dropwise to a stirred solution of 3-nitro-1,8-naphthalic anhydride (**2.19**, 1.00 g, 4.11 mmol) in EtOH (5 mL). The resulting mixture was heated under reflux for 2 h, after cooling to rt the precipitated product was filtered and washed with water, EtOH and Et_2O. The solid was dried overnight under vacuum to afford the pure product as an orange powder. (631 mg, 2.96 mmol, 72%). Spectroscopic and physical data were consistent with reported values.[114]

Method 2

A suspension of 3-nitro-1,8-naphthalic anhydride (**2.19**, 1.00 g, 4.11 mmol) and Pd/C (100 mg of 5 wt %) in CH_3CN (50 mL) was placed under a H_2 atmosphere and stirred for 12 h. The reaction mixture was filtered through celite and concentrated *in vacuo* to yield the pure product as an orange powder (625 mg, 2.93 mmol, 71%). Spectroscopic and physical data were consistent with reported values.[114]

M.P. > 250 °C (Lit.[114] > 250 °C)

^{1}H NMR (DMSO-d_6, 400 MHz) δ = 8.06-8.11 (m, 2H, **7** & **9**), 7.94 (d, *J* = 2.0 Hz, 1H, **3**), 7.63 (t, *J* = 7.8 Hz, **8**), 7.34 (d, *J* = 2.0 Hz, **5**), 6.10 (s, 2H, N**H**$_2$) ppm

^{13}C NMR (DMSO-d_6, 101 MHz) δ = 160.87 and 160.74 (C, **1** & **12**), 148.02 (C, **4**), 133.45 (CH, **7**), 132.43 (CH, **9**), 127.13 and 127.01 (C, **6** & **11**), 122.95 and 122.71 (CH, **3** & **8**), 118.28 and 119.07 (C, **2** & **10**), 112.54 (CH, **5**) ppm

LRMS (ES^+) *m/z* = 214 $[M+H]^+$

3-Bromo-1,8-naphthalic anhydride (2.28)

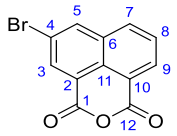

$C_{12}H_5BrO_3$

277.07 gmol^{-1}

To a solution of 1,8-naphthalic anhydride (1.00 g, 5.05 mmol) in concentrated H_2SO_4 (20 mL) at rt under N_2 was added *N*-bromosuccinimide (900 mg, 5.05 mmol) in one portion. The mixture was then stirred at rt overnight. The mixture was poured in iced water, the resulting solid was filtered off and washed water and Et_2O. Purification by recrystallisation from acetone to afford the brominated product as a white solid (633 mg, 2.28 mmol, 45%). Spectroscopic and physical data were consistent with reported values.[140]

M.P. > 250 °C (Lit.[140] > 250 °C)

FT-IR (neat) ν_{max} = 3064 (w), 1732 (s), 1583 (m), 1505 (w), 1415 (w), 1290 (m), 1226 (m), 1142 (s), 1004 (s), 781 (s), 511 (m) cm^{-1}

^{1}H NMR (DMSO-d_6, 400 MHz) δ = 8.84 (s, 1H, **3**), 8.43–8.58 (m, 3H, **5**, **7** & **9**), 7.95 (t, 1H, *J* = 7.8 Hz, **8**) ppm

^{13}C NMR (DMSO-d_6, 101 MHz) δ = 160.05 and 160.60 (C, **1** & **12**), 137.23 (CH, **3**), 133.12, 134.38 and 134.81 (CH, **5**, **7** & **9**), 133.14 (C, **6**), 129.19 (CH, **8**), 128.81 (C, **11**), 121.80 (C, **2**), 120.58 (C, **4**), 119.86 (C, **10**) ppm

5(6)-Carboxyfluorescein (1.07$_{a/b}$)

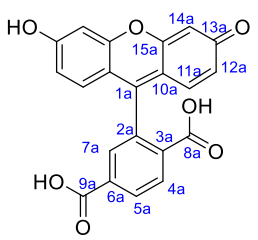

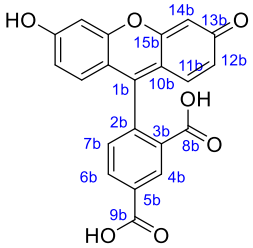

$C_{21}H_{12}O_7$

376.32 gmol^{-1}

Resorcinol (6.90 g, 62.7 mmol) and 1,2,4-benzenetricarboxylic anhydride (6.00 g, 31.2 mmol) were combined in CH_3SO_3H (50 mL) and stirred at 90 °C for 12 h. The reaction mixture was then poured into stirring iced water (450 mL), and the resulting suspension was filtered and washed with water. The solid was suspended in water (300 mL), filtered and dried under vacuum overnight to give an orange solid as the pure product (7.62 g, 20.3 mmol, 65%). Spectroscopic and physical data were consistent with reported values.[121]

M.P. > 250 °C (Lit.[121] > 250 °C)

FT-IR (neat) ν_{max} = 3045 (m), 1695 (w), 1580 (s), 1455 (s), 1363 (m), 1299 (s), 1233 (s), 1116 (s), 920 (m), 850 (m), 755 (m) cm^{-1}

RAMAN (neat) ν_{max} = 256, 320, 350, 373, 461, 411, 511, 601, 648, 762, 958, 976, 1086, 1135, 1173, 1315, 1377, 1412, 1447, 1514, 1637 cm^{-1}

^{1}H NMR (DMSO-d_6, 400 MHz) δ = 8.41 (s, 1H, **4**$_b$), 8.30 (d, J = 8.0 Hz, 1H, **6**$_b$), 8.23 (d, J = 8.1 Hz, 1H, **5**$_a$), 8.11 (d, J = 8.1 Hz, 1H, **4**$_a$), 7.66 (s, 1H, **7**$_a$), 7.40 (d, J = 8.0 Hz, 1H, **7**$_b$), 6.71 (s, 4H, **14**$_{a/b}$), 6.53–6.65 (m, 8H, **11**$_{a/b}$ & **12**$_{a/b}$) ppm

^{13}C NMR (DMSO-d_6, 101 MHz) δ = 167.91-167.89 (C, **8**$_{a/b}$), 166.10 (C, **9**$_{a/b}$), 159.93 (C, **15**$_{a/b}$), 155.84 (C, **2**$_b$), 152.36 (C, **2**$_a$), 152.09-151.99 (C, **13**$_{a/b}$), 137.31 (C, **6**$_a$), 136.13 (CH, **6**$_b$), 132.93 (C, **5**$_b$), 130.99 (CH, **5**$_a$), 129.64 (C, **3**$_a$), 129.37-129.32 (CH, **11**$_{a/b}$), 126.93 (C, **3**$_b$), 125.67 (CH, **4**$_b$), 125.44 (CH, **4**$_a$), 124.75 (CH, **7**$_b$), 124.61 (CH, **7a**), 112.91 (CH, **12**$_{a/b}$), 109.19-109.11 (C, **10**$_{a/b}$), 102.37 (CH, **14**$_{a/b}$) ppm

LRMS (ES$^+$) m/z = 477 [M+H]$^+$

5(6)-Carboxyfluorescein diacetate (2.35$_{a/b}$)

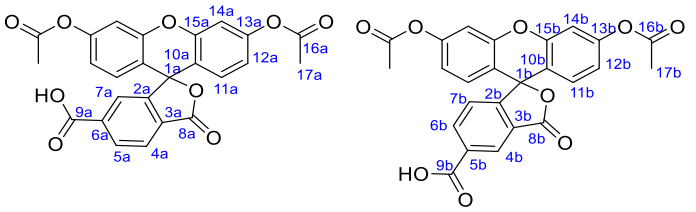

$C_{25}H_{16}O_9$

460.39 gmol^{-1}

To a solution of 5(6)-carboxyfluorescein (**1.07$_{a/b}$**, 5.26 g, 14.0 mmol) in Ac_2O (60 mL) was added pyridine (7.00 mL, 8.67 mmol) at rt. The reaction was stirred at 110 °C for 3 h, then the yellow solution was concentrated under vacuum. The residue was dissolved in EtOAc (100 mL) and washed with aqueous $KHSO_4$ (1 M, 3 × 50 mL), brine (50 mL), dried ($MgSO_4$) and concentrated under reduced pressure to give the mixture of diacetates as a yellow solid (6.33 g, 13.8 mmol, 100%). All data were obtained from the mixture of isomers, and the isomers were differenced in the analysis when possible. Spectroscopic and physical data were consistent with reported values.[122]

M.P. 154 °C (Lit.[122] 152–154 °C)

FT-IR (neat) ν_{max} = 1760 (m), 1420 (m), 1196 (s), 1153 (s), 1110 (m), 994 (m), 894 (m) cm^{-1}

^{1}H NMR (DMSO-d_6, 400 MHz) δ = 8.45 (s, 1H, **4$_b$**), 8.32 (dd, *J* = 8.1, 1.2 Hz, 1H, **6$_b$**), 8.27 (dd, *J* = 8.0, 1.0 Hz, 1H, **5$_a$**), 8.16 (d, *J* = 8 Hz, 1H, **4$_a$**), 7.83 (s, 1H, **7$_a$**), 7.54 (d, *J* = 8.1 Hz, 1H, **7$_b$**), 7.30 (s, 4H, **14$_{a/b}$**), 6.94–6.98 (m, 8H, **11$_{a/b}$** & **12$_{a/b}$**), 2.29 (s, 12H, **17$_{a/b}$**) ppm

^{13}C NMR (DMSO-d_6, 101 MHz) δ = 169.28 (C, **16$_{a/b}$**), 168.01 and 168.04 (C, **8$_{a/b}$**), 166.41 and 166.43 (C, **9$_{a/b}$**), 162.77 (C, **15$_{a/b}$**), 156.04 (C, **2$_b$**), 152.72 (C, **2$_a$**), 152.62 and 152.67 (C, **13$_{a/b}$**), 138.24 (C, **6$_a$**), 136.91 (CH, **6$_b$**), 133.80 (C, **5$_b$**), 131.83 (CH, **5$_a$**), 129.70 and 129.80 (CH, **11$_{a/b}$**), 129.37 (C, **3$_a$**), 126.69 (C, **3$_b$**), 126.34 (CH, **4$_b$**), 126.09 (CH, **4$_a$**), 125.11 and 125.18 (CH, **7$_{a/b}$**), 119.06 and 119.13 (CH, **12$_{a/b}$**), 116.00 and 116.12 (C, **10$_{a/b}$**), 110.97 (CH, **14$_{a/b}$**), 81.77 and 81.88 (C, **1$_{a/b}$**), 21.28 (CH_3, **17$_{a/b}$**) ppm

LRMS (ES$^+$) *m/z* = 461 [M+H]$^+$

5-Carboxyfluorescein diacetate *N*-succinimidyl ester and 6-carboxyfluorescein diacetate *N*-succinimidyl ester (2.38$_{a/b}$)

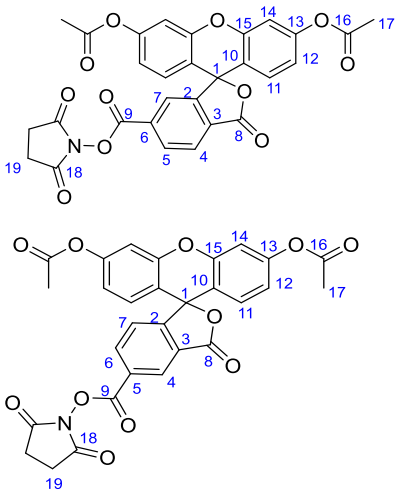

$C_{29}H_{19}NO_{11}$

557.47 gmol^{-1}

5(6)-Carboxyfluorescein diacetate (**2.35$_{a/b}$**, 6.33 g, 13.75 mmol) was dissolved in CH_2Cl_2 (100 mL), NHS (1.86 g, 16.2 mmol) was added and the mixture was stirred until it dissolved. DIC (2.48 mL, 16.01 mmol) was added in one portion, and the reaction was stirred for 30 min at rt. The organic layer was washed with water (2 × 50 mL), brine (50 mL), dried (Na_2SO_4) and concentrated to give a yellow solid. Separation of the isomers by silica gel column chromatography (EtOAc/toluene = 2:8) afforded 5-carboxy-fluorescein diacetate *N*-succinimidyl ester (2.50 g, 4.48 mmol, 33%) as white solid and 6-carboxy-fluorescein diacetate *N*-succinimidyl ester (1.26 g, 2.26 mmol, 22%) as white solid. Spectroscopic and physical data were consistent with reported values.[122]

Data for 6-carboxyfluorescein diacetate *N*-succinimidyl ester (2.38$_a$)

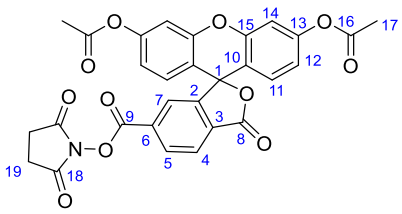

$C_{29}H_{19}NO_{11}$

557.47 gmol^{-1}

M.P. > 250 °C (Lit.[122] > 250 °C)

R_f 0.37 (EtOAc/toluene, 1:1)

FT-IR (neat) ν_{max} = 1771 (s), 1739 (s), 1608 (w), 1420 (m), 1188 (s), 1153 (s), 1111 (m), 1067 (m), 1012 (m), 892 (m), 730 (w) cm^{-1}

^{1}H NMR ($CDCl_3$, 400 MHz) δ = 8.41 (d, *J* = 7.9 Hz, 1H, **5**), 8.19 (d, *J* = 7.9 Hz, 1H, **4**), 7.94 (s, 1H, **7**), 7.15 (s, 2H, **14**), 6.76–6.92 (m, 4 H, **11** & **12**), 2.90 (br s, 4H, **19**), 2.33 (s, 6H, **17**) ppm

^{13}C NMR ($CDCl_3$, 101 MHz) δ = 168.66 (C, **18** & **16**), 167.42 (C, **8**), 160.49 (C, **9**), 152.96 (C, **2**), 152.42 (C, **15**), 151.57 (C, **13**), 132.13 (CH, **5**), 131.32 and 131.60 (C, **3** & **6**), 128.85 (C, **11**), 125.90 and 126.32 (CH, **4** & **7**), 118.10 (CH, **12**), 115.22 (C, **10**), 110.68 (CH, **14**), 82.31 (C, **1**), 25.62 (CH_2, **19**), 21.13 (CH_3, **17**) ppm

LRMS (ES^+) *m/z* = 558 $[M+H]^+$

Data for 5-carboxyfluorescein diacetate *N*-succinimidyl ester (2.38$_b$)

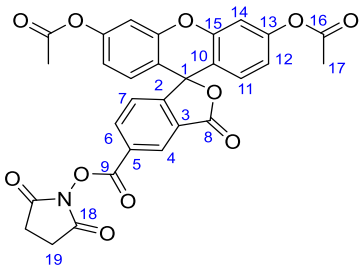

$C_{29}H_{19}NO_{11}$

557.47 $gmol^{-1}$

M.P. > 250 °C (Lit.[122] > 250 °C)

R_f 0.53 (EtOAc/toluene, 1:1)

FT-IR (neat) ν_{max} = 1777 (m), 1760 (m), 1731 (s), 1495 (w), 1421 (m), 1371 (w), 1198 (s), 1159 (s), 1111 (s), 1073 (m), 1008 (m), 861 (m), 740 (w) cm^{-1}

^{1}H NMR ($CDCl_3$, 400 MHz) δ = 8.83 (s, 1H, **4**), 8.43 (br d, *J* = 8.1 Hz, 1H, **6**), 7.38 (d, *J* = 8.1 Hz, 1H, **7**), 7.14 (s, 2H, **14**), 6.79–6.90 (m, 4H, **11** & **12**), 2.96 (br s, 4H, **19**), 2.33 (s, 6 H, **16**) ppm

^{13}C NMR ($CDCl_3$, 101 MHz) δ = 168.75 and 168.84 (C, **18** & **16**), 167.25 (C, **8**), 160.50 (C, **9**), 158.13 (C, **2**), 151.47 and 152.42 (C, **13** & **15**), 136.88 (CH, **6**), 128.85 (CH, **11**), 128.01 (CH, **4**), 127.62 (C, **3**), 127.14 (C, **5**), 125.08 (C, **7**), 118.09 (CH, **12**), 115.19 (C, **10**), 110.70 (CH, **14**), 82.04 (C, **1**),

25.69 (CH_2, **19**), 21.11 (CH_3, **17**) ppm

LRMS (ES^+) *m/z* = 558 $[M+H]^+$

2-(2,4-Dihydroxybenzoyl)terephthalic acid and 4-(2,4-dihydroxybenzoyl) isophthalic acid (2.47 and 2.48)

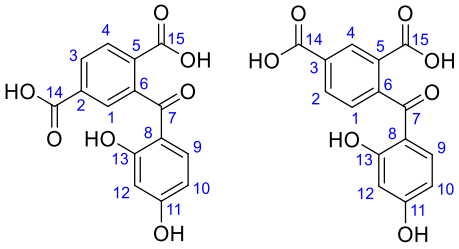

$C_{15}H_{10}O_7$

302.24 gmol^{-1}

5(6)-Carboxyfluorescein (**1.07**$_{a/b}$, 2.54 g, 6.75 mmol) was added to a solution of NaOH (20.0 g, 0.5 mol) in water (20 mL), and the mixture was heated at 80 °C for 12 h, during which time the solution became clear and almost colourless. The mixture was added to iced water (200 mL), then at 0 °C, aqueous HCl (12 M) was added slowly with stirring until a white precipitate formed (pH 1–2). The mixture was left at 5 °C overnight, filtered, and dried *in vacuo* to yield a crude mixture of isomers as an off-white solid (1:1). The solid was dissolved in EtOH (20 mL) and water was added (1 L). The solution was left for one week in an open Erlenmeyer flask. The precipitated crystals (pure 2-(2,4-dihydroxybenzoyl)terephthalic acid (**2.47**, 600 mg) were collected. The mother liquor was extracted with Et_2O, and the solvent evaporated to yield a mixture of isomer (2-(2,4-dihydroxybenzoyl)terephthalic acid (**2.47**) and 4-(2,4-dihydroxybenzoyl) isophthalic acid (**2.48**) in a ratio of 3:7, respectively. The solid recrystallised using the procedure described above, and the method repeated until a total separation of the isomers. The combined recrystallised material afforded 2-(2,4-dihydroxybenzoyl)terephthalic acid (**2.47**, 734 mg, 2.43 mmol, 36%). Evaporation of the Et_2O phases afford 4-(2,4-dihydroxybenzoyl) isophthalic acid (**2.48**, 530 mg, 1.76 mmol, 26%) a white solid. Spectroscopic and physical data were consistent with reported values.[121]

Data for 2-(2,4-dihydroxybenzoyl)terephthalic acid (2.47)

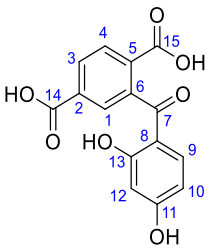

$C_{15}H_{10}O_7$

302.24 gmol^{-1}

M.P. > 250 °C (Lit.[121] > 250 °C)

FT-IR (neat) ν_{max} = 3426 (w), 3002 (w), 1687 (s), 1591 (s), 1498 (m), 1440 (m), 1219 (s), 1077 (m), 933 (m), 799 (s) cm^{-1}

^{1}H NMR (DMSO-d_6, 400 MHz) δ = 12.02 (s, 1H, −COO**H**), 8.00–8.24 (m, 2H, **3** & **4**), 7.85 (s, 1H, **1**), 6.99 (d, *J* = 7.7 Hz, 1H, **9**), 6.23–6.42 (m, 2H, **10** & **12**) ppm

^{13}C NMR (DMSO-d_6, 101 MHz) δ = 199.44 (C, **7**), 166.48 and 166.74 (C, **14** & **15**), 164.74 and 165.59 (C, **11** & **13**), 140.67 (C, **6**), 135.15 (CH, **9**), 133.80 and 134.31 (C, **2** & **5**), 130.82 and 130.89 (CH, **3** & **4**), 128.38 (CH, **1**), 113.61 (C, **8**), 108.90 (CH, **10**), 103.02 (CH, **12**) ppm

LRMS (ES^+) *m/z* = 303 $[M+H]^+$

Data for 4-(2,4-dihydroxybenzoyl) isophthalic acid (2.48)

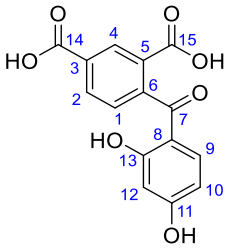

$C_{15}H_{10}O_7$

302.24 $gmol^{-1}$

M.P. > 250 °C (Lit.[121] > 250 °C)

FT-IR (neat) ν_{max} = 3426 (w), 3005 (w), 1681 (s), 1591 (s), 1494 (m), 1435 (m), 1219 (s), 1067 (m), 930 (m), 799 (s) cm^{-1}

^{1}H NMR (DMSO-d_6, 400 MHz) δ = 12.02 (s, 1H, −COO**H**), 8.52 (s, 1H, **4**), 8.23 (d, *J* = 7.6 Hz, 1H, **2**), 7.56 (d, *J* = 7.6 Hz, 1H, **1**), 6.96 (d, *J* = 8.6 Hz, 1H, **9**), 6.35 (s, 1H, **12**), 6.30 (d, *J* = 8.6 Hz, 1H, **10**) ppm

^{13}C NMR (DMSO-d_6, 101 MHz) δ = 199.75 (C, **7**), 166.43 and 166.54 (C, **14** & **15**), 164.44 and 165.59 (C, **11** & **13**), 144.27 (C, **6**), 135.08 (CH, **9**), 133.33 (CH, **2**), 130.24 and 132.32 (C, **3** & **5**), 131.20 (CH, **4**), 128.41 (CH, **1**),

113.61 (C, **8**), 108.91 (CH, **10**), 103.01 (CH, **12**) ppm

LRMS (ES$^+$) *m/z* = 303 [M+H]$^+$

5(6)-Carboxy-2′,7′-dichlorofluorescein (2.45$_{a/b}$)

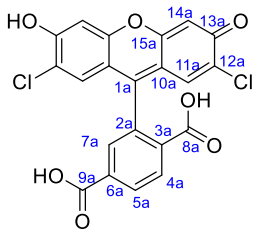

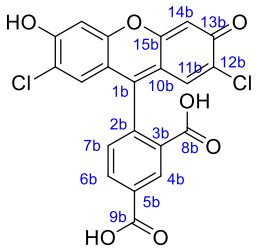

$C_{21}H_{10}Cl_2O_7$

445.20 gmol^{-1}

4-Chlororesorcinol (9.60 g, 66.4 mmol) and 1,2,4-benzenetricarboxylic anhydride (7.00 g, 36.4 mmol) were combined in CH_3SO_3H (50 mL) and stirred at 90 °C 12 h. The reaction mixture was then poured into stirring iced water (450 mL), and the resulting suspension was filtered and washed with water. The solid was suspended in water (300 mL), filtered and dried under vacuum overnight to give an orange solid as the pure product (10.9 g, 24.4 mmol, 67%). Spectroscopic and physical data were consistent with reported values.[73]

M.P. > 250 °C (Lit[73] > 250 °C)

FT-IR (neat) ν_{max} = 3066 (w), 1697 (m), 1577 (m), 1478 (m), 1267 (s), 1216 (s), 1044 (m), 952 (m), 878 (m), 842 (m), 755 (w) cm^{-1}

^{1}H NMR (DMSO-d_6, 400 MHz) δ = 11.09 (br s, 4H, −CO_2**H**), 8.41 (s, 1H, **4$_b$**), 8.31 (dd, J = 8.0, 1.4 Hz, 1H, **6$_b$**), 8.23 (dd, *J* = 8.0, 1.1 Hz, 1H, **5$_a$**), 8.10 (d, *J* = 8.0 Hz, 1H, **4$_a$**), 7.75 (s, 1H, **7$_a$**), 7.44 (d, *J* = 8.0 Hz, 1H, **7$_b$**), 6.91 (s, 4H, **14$_{a/b}$**), 6.77–6.80 (m, 4H, **11$_{a/b}$**) ppm

^{13}C NMR (DMSO-d_6, 101 MHz) δ = 168.00 and 167.96 (C, **8$_{a/b}$**), 166.48 (C, **9$_{a/b}$**), 155.72 (C, **15$_{a/b}$**), 155.50 (C, **2$_b$**), 152.24 (C, **2$_a$**), 150.55 and 150.48 (C, **13$_{a/b}$**), 137.92 (C, **6$_a$**), 136.74 (CH, **6$_b$**), 133.60 (C, **5$_b$**), 131.70 (CH, **5$_a$**), 129.79 (C, **3$_a$**), 128.93 and 128.82 (CH, **11$_{a/b}$**), 127.17 (C, **3$_b$**), 126.60 (CH, **4$_b$**), 126.15 (CH, **4$_a$**), 124.89 (CH, **7$_{a/b}$**), 116.87 and 116.79 (C, **12$_{a/b}$**), 110.38 and 110.32 (C, **10$_{a/b}$**), 104.18 and 104.14 (CH, **14$_{a/b}$**), 82.28 and 82.20 (C, **1$_{a/b}$**) ppm

LRMS (ES$^+$) *m/z* = 449 [M(^{37}Cl^{37}Cl)+H]$^+$, 447 [M(^{35}Cl^{37}Cl)+H]$^+$, 445 [M(^{35}Cl^{35}Cl)+H]$^+$

6-Carboxy-2´,7´-dichlorofluorescein diacetate, pyridinium Salt (2.51$_a$)

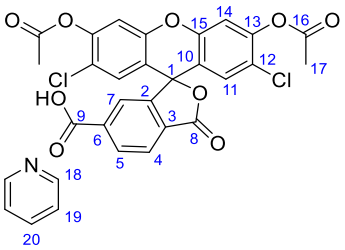

$C_{30}H_{19}Cl_2NO_9$

608.38 gmol^{-1}

5(6)-Carboxy-2′,7′-dichlorofluorescein (**2.45$_{a/b}$**, 12.0 g, 27.0 mmol) was stirred in Ac_2O (50 mL) and pyridine (2.70 mL, 33.4 mmol) and heated at reflux for 30 min. After cooling to rt the precipitate was collected by filtration, the mother liquor (containing 5-carboxy-2´,7´-dichlorofluorescein diacetate) was retained (see below). The solid was washed with water and Et_2O and dried under vacuum to yield the pure product as a white solid (4.80 g, 7.89 mmol, 29%). Spectroscopic and physical data were consistent with reported values.[73]

M.P. > 250 °C (Lit[73] > 250 °C)

FT-IR (neat) ν_{max} = 3040 (w), 1770 (s), 1603 (m), 1485 (m), 1439 (m), 1410 (m), 1192 (s), 1049 (m), 900 (m), 784 (m), 698 (s) cm^{-1}

RAMAN (neat) ν_{max} = 234, 267, 301, 348, 411, 546, 583, 650, 677, 735, 836, 863, 1015, 1169, 1219, 1262, 1279, 1319, 1380, 1625, 1771 cm^{-1}

^{1}H NMR ($CDCl_3$, 400 MHz) δ = 10.48 (br s, 1H, −CO_2**H**), 8.70 (d, *J* = 4.4 Hz, 2H, **18**), 8.43 (d, *J* = 8.0 Hz, 1H, **5**), 8.15 (d, *J* = 8.0 Hz, 1H, **4**), 7.92 (s, 1H, **7**), 7.85 (m, 1H, **20**), 7.39–7.50 (m, 2H, **19**), 7.18 (s, 2H, **14**), 6.88 (s, 2H, **11**), 2.37 (s, 6H, **17**) ppm

^{13}C NMR ($CDCl_3$, 101 MHz) δ = 167.85 (C, **9** & **16**) 167.74 (C, **8**), 152.00 (C, **2**), 149.70 (C, **15**), 148.61 (C, **13**), 147,46 (CH, **18**), 138.98 (C, **3**), 138.22 (CH, **20**), 132.19 (CH, **5**), 128.90 (CH, **11**), 128.58 (C, **6**), 125.65 (CH, **4**), 125.36 (CH, **7**), 124.59 (CH, **19**), 122.80 (C, **12**), 117.17 (C, **10**), 112.85 (CH, **14**), 80.69 (C, **1**), 20.61 (CH_3, **17**) ppm

LRMS (ES$^+$) *m/z* = 533 [M(^{37}Cl^{37}Cl)+H]$^+$, 531 [M(^{35}Cl^{37}Cl)+H]$^+$, 529 [M(^{35}Cl^{35}Cl)+H]$^+$

5-Carboxy-2´,7´-dichlorofluorescein diacetate (2.35$_b$)

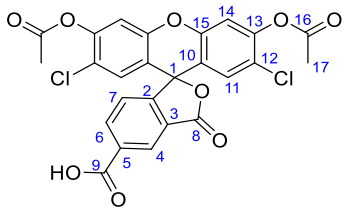

$C_{25}H_{14}Cl_2O_9$

529.28 gmol^{-1}

The mother liquor from the previous reaction was slowly added to water (150 mL), stirred for 10 min, and extracted with EtOAc (3 × 50 mL). The combined organics were washed with aqueous HCl (50 mL of 3%), brine (50 mL) and dried ($MgSO_4$). The solvent was evaporated to give a light brown solid residue, which was recrystallised from Et_2O to give the desired product as a pale yellow solid (3.90 g, 7.37 mmol, 27%). Spectroscopic and physical data were consistent with reported values.[73]

M.P. 179 °C (Lit.[73] 178–180 °C)

FT-IR (neat) ν_{max} = 3048 (w), 2937 (w), 1769 (s), 1700 (s), 1607 (m), 1479 (m), 1408 (s), 1183 (s), 1160 (s), 1025 (m), 892 (s), 700 (m) cm^{-1}

Raman (neat) ν_{max} = 231, 284, 315, 346, 387, 429, 477, 518, 544, 661, 681, 708, 736, 781, 906, 955, 999, 1069, 1115, 1162, 1257, 1271, 1318, 1415, 1623, 1781 cm^{-1}

^{1}H NMR ($CDCl_3$, 400 MHz) δ = 8.83 (s, 1H, **4**), 8.48 (dd, *J* = 8.0 Hz, 1.4 Hz, 1H, **6**), 7.35 (d, *J* = 8.0, 1H, **7**), 7.19 (s, 2H, **14**), 6.89 (s, 2H, **11**), 2.38 (s, 6H, **17**) ppm

^{13}C NMR ($CDCl_3$, 101 MHz) δ = 169.50 (C, **9**), 167.90 (C, **16**), 167.32 (C, **8**), 156.29 (C, **2**), 149.52 (C, **15**), 148.72 (C, **13**), 137.23 (CH, **6**), 132.19 (C, **3**), 128.75 (CH, **11**), 128.04 (CH, **4**), 126.27 (C, **5**), 124.47 (CH, **7**), 122.96 (C, **12**), 116.74 (C, **10**), 112.95 (CH, **14**), 80.60 (C, **1**), 20.58 (CH_3, **17**) ppm

LRMS (ES$^+$) *m/z* = 533 [M(^{37}Cl^{37}Cl)+H]$^+$, 531 [M(^{35}Cl^{37}Cl)+H]$^+$, 529 [M(^{35}Cl^{35}Cl)+H]$^+$

6-Carboxy-2´,7´-dichlorofluorescein diacetate, succinimidyl ester (2.52$_a$)

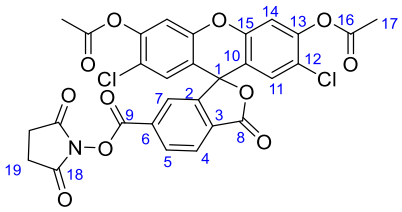

$C_{29}H_{17}Cl_2NO_{11}$

626.35 gmol^{-1}

6-Carboxy-2´,7´-dichlorofluorescein diacetate, pyridinium salt (**2.51$_a$**, 100 mg, 0.16 mmol) was dissolved in CH_2Cl_2 (10 mL), then NHS (27 mg, 0.23 mmol) was added and the mixture was stirred until it dissolved. DIC (40 µL, 0.23 mmol) was added in one portion, and the reaction was stirred 30 min at rt. The organic layer was washed with water (2 × 5 mL), brine (5 mL), dried (Na_2SO_4) and concentrated to give a yellow solid. Purification by silica gel column chromatography (EtOAc) afforded the pure product as yellow solid (100 mg, 0.16 mmol, 100 %).

M.P. > 250 °C

FT-IR (neat) ν_{max} = 3339 (w), 2968 (w), 1770 (s), 1734 (s), 1613 (m), 1479 (m), 1408 (m), 1368 (m), 1187 (s), 1160 (s), 1067 (m), 1024 (m), 894 (m), 696 (m), 643 (m) cm^{-1}

RAMAN (neat) ν_{max} = 237, 312, 416, 578, 680, 732, 866, 954, 1029, 1148, 1165, 1185, 1212, 1279, 1318, 1340, 1535, 1603, 1785, 1806 cm^{-1}

^{1}H NMR ($CDCl_3$, 400 MHz) δ = 8.43 (d, *J* = 8.0 Hz, 1H, **5**), 8.21 (d, *J* = 8.0 Hz, 1H, **4**), 7.94 (s, 1H, **7**), 7.19 (s, 2H, **14**), 6.86 (s, 2H, **11**), 2.89 (br s, 4H, **19**), 2.37 (s, 6H, **17**) ppm

^{13}C NMR ($CDCl_3$, 101 MHz) δ = 168.94 (C, **18**), 168.05 (C, **16**), 167.18 (C, **8**), 160.60 (C, **9**), 152.42 (C, **2**), 149.83 (C, **15**), 149.11 (C, **13**), 132.92 (CH, **5**), 132.29 (C, **3**), 130.88 (C, **6**), 129.07 (CH, **11**), 126.60 (CH, **4**), 126.41 (CH, **7**), 123.33 (C, **12**), 116.56 (C, **10**), 113.27 (CH, **14**), 81.17 (C, **1**), 25.88 (CH_2, **19**), 20.88 (CH_3, **17**) ppm

LRMS (ES$^+$) *m/z* = 652 [M(^{37}Cl^{37}Cl)+Na]$^+$, 650 [M(^{35}Cl^{37}Cl)+Na]$^+$, 648 [M(^{35}Cl^{35}Cl)+Na]$^+$, 630 [M(^{37}Cl^{37}Cl)+H]$^+$, 628 [M(^{35}Cl^{37}Cl)+H]$^+$, 626 [M(^{35}Cl^{35}Cl)+H]$^+$

5-Carboxy-2´,7´-dichlorofluorescein diacetate, succinimidyl ester (2.52$_b$)

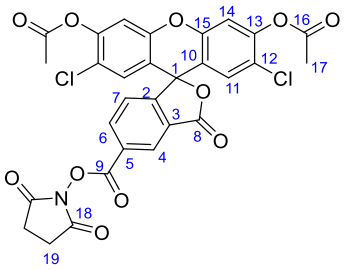

$C_{29}H_{17}Cl_2NO_{11}$

626.35 gmol^{-1}

5-Carboxy-2´,7´-dichlorofluorescein diacetate (**2.51$_b$**, 100 mg, 0.19 mmol) was dissolved in CH_2Cl_2 (10 mL), then NHS (27 mg, 0.23 mmol) was added and the mixture was stirred until it dissolved. DIC (40 µL, 0.23 mmol) was added in one portion, and the reaction was stirred 30 min at rt. The organic layer was washed with water (2 × 5 mL), brine (5 mL), dried (Na_2SO_4) and concentrated to give a yellow solid. Purification by silica gel column chromatography (EtOAc) afforded the pure product as yellow solid (118 mg, 0.19 mmol, 100%).

M.P. > 250 °C

FT-IR (neat) ν_{max} = 3340 (w), 2971 (w), 1735 (s), 1479 (m), 1408 (m), 1368 (m), 1159 (s), 1068 (m), 1009 (m), 894 (m), 696 (m) cm^{-1}

RAMAN (neat) ν_{max} = 415, 542, 626, 678, 710, 729, 754, 826, 866, 897, 1007, 1185, 1278, 1316, 1415, 1434, 1534, 1607, 1625, 1779, 1804, 1127, 1085 cm^{-1}

^{1}H NMR ($CDCl_3$, 400 MHz) δ = 8.85 (s, 1H, **4**), 8.48 (dd, *J* = 8.1,1.3 Hz, 1H, **6**), 7.40 (d, *J* = 8.1 Hz, 1H, **7**), 7.19 (s, 2H, **14**), 6.86 (s, 2H, **11**), 2.95 (br s, 4H, **19**), 2.37 (s, 6H, **17**) ppm

^{13}C NMR ($CDCl_3$, 101 MHz) δ = 168.75 (C, **18**), 167.85 (C, **16**), 166.68 (C, **8**), 160.34 (C, **9**), 156.98 (C, **2**), 149.62 (C, **15**), 148.88 (C, **13**), 137.34 (CH, **6**), 128.81 (CH, **11**), 128.37 (CH, **4**), 128.21 (C, **3**), 126.75 (C, **5**), 125.01 (CH, **7**), 123.13 (C, **12**), 116.38 (C, **10**), 113.04 (CH, **14**), 80.78 (C, **1**), 22.69 (CH_2, **19**), 20.60 (CH_3, **17**) ppm

LRMS (ES$^+$) *m/z* = 652 [M(^{37}Cl^{37}Cl)+Na]$^+$, 650 [M(^{35}Cl^{37}Cl)+Na]$^+$, 648 [M(^{35}Cl^{35}Cl)+Na]$^+$, 630 [M(^{37}Cl^{37}Cl)+H]$^+$, 628 [M(^{35}Cl^{37}Cl)+H]$^+$, 626

$[M(^{35}Cl^{35}Cl)+H]^+$

6-Carboxy-4',5'-bis(dipicolylamine)-2´,7´-dichlorofluorescein (2.61$_a$)

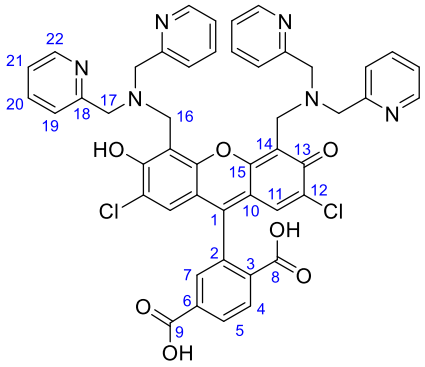

$C_{47}H_{36}Cl_2N_6O_7$

867.74 gmol^{-1}

A mixture of dipicolylamine (1.15 mL, 6.39 mmol) and paraformaldehyde (384 mg, 12.79 mmol) in CH_3CN (20 mL) was heated to reflux for 45 min. A solution of 6-Carboxy-2´,7´-dichlorofluorescein diacetate, pyridinium salt (**2.51$_a$**, 608 mg, 1.00 mmol) in CH_3CN (20 mL) was added to the reaction, and reflux was continued 12 h. After cooling to rt, a black residue was filtered off and the filtrate was evaporated to afford a red residue. The red residue was recrystallised from EtOH to afford the pure product as a pink solid (624 mg, 0.72 mmol, 72%). Spectroscopic and physical data were consistent with reported values.[73]

M.P. 216 °C (Lit.[73] 215–218 °C)

FT-IR (neat) ν_{max} = 3042 (w), 1764 (s), 1735 (s), 1599 (w), 1407 (m), 1159 (s), 1067 (m), 1008 (m), 895 (m), 698 (s) cm^{-1}

RAMAN (neat) ν_{max} = 218, 290, 408, 490, 587, 635, 706, 747, 843, 861, 927, 997, 1051, 1118, 1193, 1221, 1332, 1502, 1573, 1620, 1765 cm^{-1}

^{1}H NMR (DMSO-d_6, 400 MHz) δ = 8.55 (d, *J* = 4.2 Hz, 4H, **22**), 8.22 (d, *J* = 7.9 Hz, 1H, **5**), 8.08 (d, *J* = 7.9 Hz, 1H, **4**), 7.73–7.82 (m, 5H, **7** and **20**), 7.39 (d, *J* = 7.7 Hz, 4H, **19**), 7.25–7.31 (m, 4H, **21**), 6.62 (s, 2H, **11**), 4.16 (s, 4H, **16**), 4.01 (s, 8H, **17**) ppm

^{13}C NMR (DMSO-d_6, 101 MHz) δ = 168.03 (C, **8**), 166.64 (C, **9**), 157.78 (C, **18**), 156.28 (C, **15**), 154.61 (C, **2**), 149.09 (CH, **22**), 148.62 (C, **13**), 138.43 (C, **6**), 137.53 (CH, **20**), 131.65 (CH, **5**), 129.79 (C, **3**), 127.13 (CH, **11**), 126.05 (CH, **4**), 125.24 (CH, **7**), 123.65 (CH, **19**), 123.03 (CH, **21**), 116.85 (C, **12**), 112.37 (C, **14**), 109.76 (C, **10**), 59.07 (CH_2, **17**), 49.33 (CH_2, **16**) ppm

LRMS (ES$^+$) *m/z* = 871 [M(^{37}Cl^{37}Cl)+H]$^+$, 869 [M(^{35}Cl^{37}Cl)+H]$^+$, 867 [M(^{35}Cl^{35}Cl)+H]$^+$

5-Carboxy-4',5'-bis(dipicolylamine)-2´,7´-dichlorofluorescein (2.61$_b$)

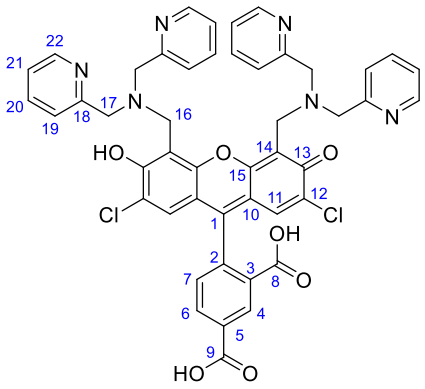

$C_{47}H_{36}Cl_2N_6O_7$

867.74 gmol^{-1}

A mixture of dipicolylamine (1.15 mL, 6.39 mmol) and paraformaldehyde (384 mg, 12.8 mmol) in CH_3CN (20 mL) was heated to reflux for 45 min. A solution of 5-carboxy-2´,7´-dichlorofluorescein diacetate (**2.51$_b$**, 529 mg, 1.00 mmol) in CH_3CN (20 mL) was added to the reaction, and reflux was continued 12 h. After cooling to rt, a black residue was filtered off and the filtrate was evaporated to afford a red residue. The red residue was recrystallised from EtOH to afford the pure product as a pink solid (528 mg, 0.61 mmol, 61%). Spectroscopic and physical data were consistent with reported values.[73]

M.P. 194 °C (Lit.[73] 195 °C)

FT-IR (neat) ν_{max} = 3057 (w), 2851 (w), 1764 (s), 1590 (s), 1432 (s), 1279 (m), 1208 (s), 1115 (m), 855 (m), 756 (s) cm^{-1}

RAMAN (neat) ν_{max} = 293, 330, 414, 488, 540, 637, 702, 747, 830, 1011, 1052, 1190, 1233, 1340, 1503, 1571, 1599, 1626, 1766 cm^{-1}

^{1}H NMR (DMSO-d_6, 400 MHz) δ = 8.55 (d, *J* = 4.4 Hz, 4H, **22**), 8.40 (s, 1H, **4**), 8.32 (d, *J* = 8.1 Hz, 1H, **6**), 7.77 (td, *J* = 7.7, 1.4 Hz, 4H, **20**), 7.45 (d, *J* = 8.1 Hz, 1H, **7**), 7.38 (br d, *J* = 7.7, 4H, **19**), 7.28 (m, 4H, **21**), 6.67 (s, 2H, **11**), 4.16 (s, 4H, **16**), 4.01 (s, 8H, **17**) ppm

^{13}C NMR (DMSO-d_6, 101 MHz) δ = 167.24 (C, **8**), 165.84 (C, **9**), 157.07 (C, **18**), 155.39 (C, **15**), 154.42 (C, **2**), 148.41 (C, **22**), 147.87 (C, **13**), 136.86 (CH, **20**), 135.97 (C, **6**), 133.25 (C, **3**), 126.55 (CH, **11**), 125.83 (C & CH, **4** & **5**), 124.47 (C, **7**), 122.93 (CH, **19**), 122.37 (CH, **21**), 116.13 (C, **12**), 111.67 (C, **14**), 108.98 (C, **10**), 58.23 (CH_2, **17**), 48.53 (CH_2, **16**) ppm

LRMS (ES$^+$) *m/z* = 871 [M(^{37}Cl^{37}Cl)+H]$^+$, 869 [M(^{35}Cl^{37}Cl)+H]$^+$, 867 [M(^{35}Cl^{35}Cl)+H]$^+$

6-Carboxy-4',5'-bis(morpholin)-2´,7´-dichlorofluorescein (2.60$_a$)

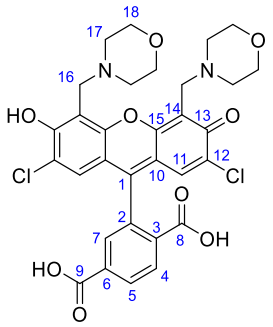

$C_{31}H_{28}Cl_2N_2O_9$

643.47 gmol^{-1}

A mixture of morpholine (0.55 mL, 6.39 mmol) and paraformaldehyde (384 mg, 12.8 mmol) in CH_3CN (20 mL) was heated to reflux for 45 min. A solution of 6-carboxy-2´,7´-dichlorofluorescein diacetate, pyridinium salt (**2.51$_a$**, 608 mg, 1.00 mmol) in CH_3CN (20 mL) was added to the reaction, and reflux was continued overnight. After cooling to rt, a black residue was filtered off and the filtrate was evaporated to afford a red residue. The red residue was recrystallised from EtOH to afford the pure product as a bright red solid (630 mg, 0.98 mmol, 98%).

M.P. > 250 °C

FT-IR (neat) ν_{max} = 3372 (w), 2995 (w), 2945 (w), 1570 (m), 1457 (s), 1356 (s), 1263 (s), 1100 (s), 1044 (s), 945 (m), 760 (w) cm^{-1}

^{1}H NMR (DMSO-d_6, 400 MHz) δ = 8.21 (br d, J = 8.1 Hz, 1H, **5**), 8.13 (br d, J = 8.1 Hz, **4**), 7.76 (s, 1H, **7**), 6.72 (s, 2H, **11**), 4.12 (br s, 4H, **16**), 3.70 (br s, 8H, **17**), 2.80 (br s, 8H, **18**) ppm

^{13}C NMR (DMSO-d_6, 101 MHz) δ = 167.06 and 167.48 (C, **8** & **9**), 151.82 (C, **2**), 137.70 (C, **6**), 132.61 (CH, **5**), 131.37 (C, **3**), 130.67 (CH, **4**), 128.20 (CH, **7**), 127.00 (CH, **11**), 122.36 (C, **12**), 109.11 (C, **14**), 107.79 (C, **10**), 80.66 (C, **1**), 65.15 (CH_2, **18**), 52.31 (CH_2, **17**), 52.02 (CH_2, **16**) ppm (*C_{13} and C_{15} not observed)*

LRMS (ES$^+$) *m/z* = 647 [M(^{37}Cl^{37}Cl)+H]$^+$, 645 [M(^{35}Cl^{37}Cl)+H]$^+$, 643 [M(^{35}Cl^{35}Cl)+H]$^+$

HRMS (ES$^+$) For $C_{31}H_{29}Cl_2N_2O_9^+$ calculated 643.1245, found 643.1248 Da

5-Carboxy-4',5'-bis(morpholin)-2´,7´-dichlorofluorescein (2.60$_b$)

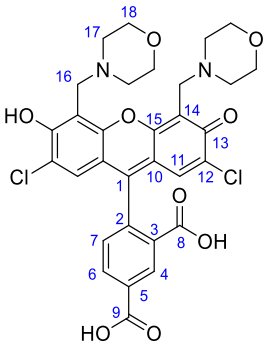

$C_{31}H_{28}Cl_2N_2O_9$

643.47 gmol^{-1}

A mixture of morpholine (0.55 mL, 6.39 mmol) and paraformaldehyde (384 mg, 12.8 mmol) in CH_3CN (20 mL) was heated to reflux for 45 min. A solution of 5-Carboxy-2´,7´-dichlorofluorescein diacetate (**2.51$_b$**, 529 mg, 1.00 mmol) in CH_3CN (20 mL) was added, and reflux was continued 12 h. After cooling to rt, a black residue was filtered off and the filtrate was evaporated to afford a red residue. The red residue was recrystallised from EtOH to afford the pure product as a bright pink solid (598 mg, 0.93 mmol, 93%).

M.P. > 250 °C

FT-IR (neat) ν_{max} = 3373 (w), 2989 (w), 2941 (w), 1568 (m), 1455 (s), 1359 (s), 1262 (s), 1100 (s), 1046 (s), 949 (m), 781 (w) cm^{-1}

^{1}H NMR (DMSO-d_6, 400 MHz) δ = 8.49 (s, 1H, **4**) 8.25 (d, *J* = 7.9 Hz, 1H, **6**), 7.41 (d, *J* = 7.9 Hz, 1H, **7**), 6.74 (s, 2H, **11**), 4.13 (s, 4H, **16**), 3.70 (s, 8H, **18**), 2.83 (s, 8H, **17**) ppm

^{13}C NMR (DMSO-d_6, 101 MHz) δ = 166.85 and 167.50 (C, **8** & **9**), 151.18 (C, **2**), 134.81 (C, **3**), 133.95 (CH, **6**), 130.06 (C, **5**), 128.77 (CH, **4**), 127.56 (CH, **7**), 127.18 (CH, **11**), 116.38 (C, **12**), 109.01 and 109.20 (C, **10** & **14**), 81.07 (C, **1**), 65.82 (CH_2, **18**), 57.78 (CH_2, **16** & **17**) ppm (*C_{13} and C_{15} not observed)*

LRMS (ES$^+$) *m/z* = 647 [M(^{37}Cl^{37}Cl)+H]$^+$, 645 [M(^{35}Cl^{37}Cl)+H]$^+$, 643 [M(^{35}Cl^{35}Cl)+H]$^+$

HRMS (ES$^+$) For $C_{31}H_{29}Cl_2N_2O_9^+$ calculated 643.1245, found 643.1241 Da

6-Carboxy-4',5'-bis(1-aza-18-crown-6)-2´,7´-dichlorofluorescein (2.62)

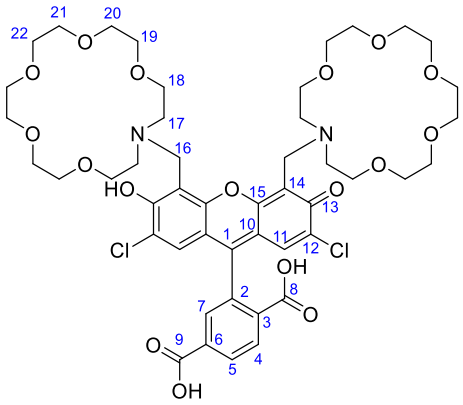

$C_{47}H_{60}Cl_2N_2O_{17}$

995.89 $gmol^{-1}$

A mixture of 1-aza-18-crown-6 (420 mg, 1.59 mmol) and paraformaldehyde (96 mg, 3.20 mmol) in CH_3CN (10 mL) was heated to reflux for 45 min. A solution of 6-Carboxy-2´,7´-dichlorofluorescein diacetate, pyridinium salt (**2.51**, 150 mg, 0.25 mmol) in CH_3CN (10 mL) was added, and reflux was continued 12 h. After cooling to rt the solvent was evaporated to afford a red residue. The red residue was recrystallised from EtOH to afford the pure product as a bright pink solid (180 mg, 0.18 mmol, 72%).

M.P. > 250 °C

FT-IR (neat) ν_{max} = 3451 (w), 2869 (m), 1569 (s), 1464 (s), 1350 (s), 1280 (s), 1089 (s), 947 (m) cm^{-1}

RAMAN (neat) ν_{max} = 280, 490, 582, 609, 743, 847, 926, 1101, 1188, 1304, 1336, 1505, 1578, 1633 cm^{-1}

^{1}H NMR ($CDCl_3$, 400 MHz) δ = 8.31 (d, *J* = 7.8 Hz, 1H, **5**), 7.98 (d, *J* = 7.8 Hz, 1H, **4**), 7.81 (s, 1H, **7**), 6.62 (s, 2H, **11**), 3.58–3.76 (m, 44H, **16**, **18**, **19**, **20**, **21** & **22**), 2.94–3.18 (m, 8H, **17**), ppm

^{13}C NMR ($CDCl_3$, 101 MHz) δ = 169.28 and 170.96 (C, **8** & **9**), 156.49 (C, **15**), 153.29 (C, **2**), 147.71 (C, **13**), 144.92 (C, **6**), 131.24 (CH, **5**), 128.04 (C, **3**), 127.69 (CH, **11**), 124.92 (CH, **7**), 124.52 (CH, **4**), 117.17 (C, **12**), 109.61 and 109.87 (C, **10** & **14**), 82.56 (C, **1**), 68.79–70.86 (CH_2, **19**, **20**, **21** & **22**), 66.94 (CH_2, **18**), 53.96 (CH_2, **17**), 48.23 (CH_2, **16**) ppm

LRMS (ES$^+$) *m/z* = 1000 [M(^{37}Cl^{37}Cl)+H]$^+$, 998 [M(^{35}Cl^{37}Cl)+H]$^+$, 996 [M(^{35}Cl^{35}Cl)+H]$^+$

HRMS (ES$^+$) For $C_{47}H_{61}(^{35}Cl^{35}Cl)N_2O_{17}^+$ calculated 995.3342, found 995.3315 Da

6-Carboxy-4',5'-bis(dipicolylamine)-2´,7´-dichlorofluorescein, succinimidyl ester (2.64$_a$)

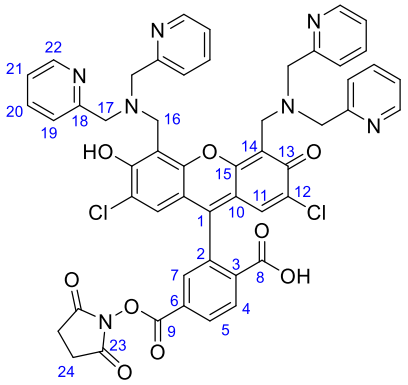

$C_{51}H_{39}Cl_2N_7O_9$

964.81 gmol^{-1}

6-Carboxy-4',5'-bis(dipicolylamine)-2´,7´-dichlorofluorescein (**2.61$_a$**, 100 mg, 0.12 mmol) was dissolved in CH_2Cl_2 (7 mL), then NHS (14 mg, 0.12 mmol) was added and the mixture was stirred until it dissolved. DIC (20 µL, 0.12 mmol) was added in one portion, and the reaction was stirred 30 min at rt. The solvent was evaporated and the red residue was recrystallised from EtOH to yield the pure product as a pale pink solid (110 mg, 0.11 mmol, 95%).

M.P. > 250 °C

FT-IR (neat) ν_{max} = 3374 (w), 2944 (w), 1708 (s), 1572 (m), 1467 (m), 1363 (m), 1285 (m), 1217 (m), 1073 (w) cm^{-1}

RAMAN (neat) ν_{max} = 282, 408, 488, 585, 633, 712, 747, 858, 996, 1049, 1104, 1201, 1340, 1529, 1575, 1638, 1777 cm^{-1}

^{1}H NMR ($CDCl_3$, 400 MHz) δ = 8.59 (br s, 4H, **22**), 8.42 (d, *J* = 7.6 Hz, 1H, **5**), 8.18 (d, *J* = 7.6 Hz, 1H, **4**), 7.92 (s, 1H, **7**), 7.65 (br s, 4H, **20**), 7.36 (br d, 4H, **19**), 7.19 (br s, 4H, **21**), 6.60 (s, 2H, **11**), 4.21 (br s, 4H, **16**), 4.01 (s, 8H, **17**), 2.87 (br s, 4H, **24**) ppm

^{13}C NMR ($CDCl_3$, 101 MHz) δ = 168.62 (C, **23**), 167.32 (C, **8**), 160.62 (C, **9**), 157.52 (C, **18**), 156.32 (C, **15**), 152.33 (C, **2**), 148.71 (CH, **22**), 148.48 (C, **13**), 137.12 (CH, **20**), 132.14 (C, **4**), 131.98 (C, 3), 131.41 (C, **6**), 127.54 (CH, **11**), 126.30-125.91 (CH, **7** & **5**), 123.32 (CH, **19**), 122.48 (CH, **21**), 118.01 (C, **12**), 111.85 (C, **14**), 108.53 (C, **10**), 83.86 (C, **1**), 59.26 (CH_2, **17**), 49.32 (CH_2, **16**), 25.58 (CH_2, **24**) ppm

LRMS (ES$^+$) *m/z* = 990 [M(^{37}Cl^{37}Cl)+Na]$^+$, 998 [M(^{35}Cl^{37}Cl)+Na]$^+$, 990 [M(^{35}Cl^{35}Cl)+Na]$^+$, 968 [M(^{37}Cl^{37}Cl)+H]$^+$, 966 [M(^{35}Cl^{37}Cl)+H]$^+$, 964 [M(^{35}Cl^{35}Cl)+H]$^+$

HRMS (ES$^+$) For $C_{51}H_{40}(^{35}Cl^{35}Cl)N_7O_9^+$ calculated 964.2259, found 964.2245 Da

5-Carboxy-4',5'-bis(dipicolylamine)-2´,7´-dichlorofluorescein, succinimidyl ester (2.64$_b$)

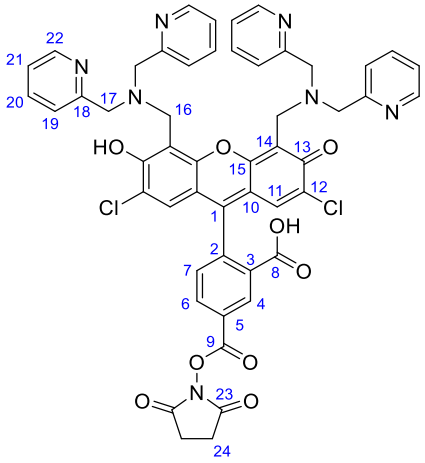

$C_{51}H_{39}Cl_2N_7O_9$

964.81 gmol^{-1}

5-Carboxy-4',5'-bis(dipicolylamine)-2´,7´-dichlorofluorescein (**2.61$_b$**, 100 mg, 0.12 mmol) was dissolved in CH_2Cl_2 (7 mL), then NHS (14 mg, 0.12 mmol) was added and the mixture was stirred until it dissolved. DIC (20 µL, 0.12 mmol) was added in one portion, and the reaction was stirred 30 min at rt. The solvent was evaporated and the red residue was recrystallised from EtOH to yield the pure product as a pale pink solid (106 mg, 0.11 mmol, 92%).

M.P. > 250 °C

FT-IR (neat) ν_{max} = 3060 (w), 3010 (w), 2859 (w), 1773 (m), 1741 (s), 1592 (m), 1432 (m), 1363 (m), 1281 (m), 1201 (m), 1070 (w), 911 (w), 730 (m) cm^{-1}

RAMAN (neat) ν_{max} = 286, 411, 488, 639, 696, 747, 826, 997, 1051, 1112, 1202, 1343, 1529, 1573, 1635, 1775, 1807 cm^{-1}

^{1}H NMR ($CDCl_3$, 400 MHz) δ = 8.83 (s, 1H, **4**), 8.60 (d, *J* = 4.3 Hz, 4H, **22**), 8.44 (d, *J* = 8.1 Hz, 1H, **6**), 7.66 (t, 7.1 Hz, 4H, **20**), 7.33–7.39 (m, 5H, **7** & **19**), 7.15–7.24 (m, 4H, **21**), 6.62 (s, 2H, **11**), 4.21 (s, 4H, **16**), 3.95–4.21 (m, 8H, **17**), 2.95 (s, 4H, **24**) ppm

^{13}C NMR ($CDCl_3$, 101 MHz) δ = 168.73 (C, **23**), 167.11 (C, **8**), 160.55 (C, **9**), 157.56 (C, **18**), 156.33 (C, **15**), 153.57 (C, **2**), 148.73 (CH, **22**), 148.48 (C, **13**), 137.17 (CH, **20**), 136.78 (CH, **6**), 128.08 (CH, **4**), 127.94 and 127.55 (C, **3** & **5**), 127.47 (CH, **11**), 125.03 (CH, **7**), 123.24 (CH, **19**), 122.50 (CH, **21**), 118.01 (C, **12**), 111.95 (C, **14**), 108.71 (C, **10**), 83.64 (C, **1**), 59.12

(CH_2, **17**), 49.22 (CH_2, **16**), 25.68 (CH_2, **24**) ppm

LRMS (ES^+) *m/z* = 990 [M($^{37}Cl^{37}Cl$)+Na]$^+$, 998 [M($^{35}Cl^{37}Cl$)+Na]$^+$, 990 [M($^{35}Cl^{35}Cl$)+Na]$^+$, 968 [M($^{37}Cl^{37}Cl$)+H]$^+$, 966 [M($^{35}Cl^{37}Cl$)+H]$^+$, 964 [M($^{35}Cl^{35}Cl$)+H]$^+$

HRMS (ES^+) For $C_{51}H_{40}(^{35}Cl^{35}Cl)N_7O_9^+$ calculated 964.2259, found 964.2247 Da

6-Carboxy-4',5'-bis(morpholin)-2´,7´-dichlorofluorescein, succinimidyl ester (2.63$_a$)

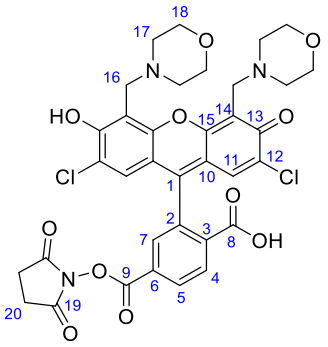

$C_{35}H_{31}Cl_2N_3O_{11}$

740.54 gmol^{-1}

6-Carboxy-4',5'-bis(morpholin)-2´,7´-dichlorofluorescein (**2.60$_a$**, 150 mg, 0.23 mmol) was dissolved in CH_2Cl_2 (10 mL), then NHS (27 mg, 0.23 mmol) was added and the mixture was stirred until it dissolved. DIC (36 µL, 0.23 mmol) was added in one portion, and the reaction was stirred 30 min at rt. The solvent was evaporated and the red residue was recrystallised from EtOH to yield the pure product as a pale red solid (160 mg, 0.22 mmol, 94%).

M.P. > 250 °C

FT-IR (neat) ν_{max} = 3438 (w), 2962 (w), 2855 (w), 1769 (m), 1740 (s), 1572 (m), 1466 (s), 1399 (m), 1276 (s), 1210 (s), 1117 (m), 913 (w), 729 (m) cm^{-1}

RAMAN (neat) ν_{max} = 280, 487, 592, 748, 668, 942, 1105, 1194, 1311, 1339, 1503, 1533, 1576, 1637 cm^{-1}

^{1}H NMR ($CDCl_3$, 400 MHz) δ = 8.42 (d, *J* = 8.1 Hz, 1H, **5**), 8.20 (d, *J* = 8.1 Hz, 1H, **4**), 7.89 (s, 1H, **7**), 6.63 (s, 2H, **11**), 4.01-4.09 (m ,4H, **16**), 3.84 (br s, 8H, **18**), 2.91 (br s, 4H, **20**), 2.75 (br s, 8H, **17**) ppm

^{13}C NMR ($CDCl_3$, 101 MHz) δ = 168.68 (C, **19**), 167.16 (C, **8**), 160.59 (C, **9**), 156.29 (C, **15**), 152.33 (C, **2**), 147.55 (C, **13**), 132.25 (C, **6**), 131.58 and 131.55 (C & CH, **3** & **4**), 127.66 (CH, **11**), 126.08 (CH, **5** & **7**), 117.76 (C, **12**), 109.01 (C, **14**), 108.32 (C, **10**), 82.91 (C, **1**), 66.48 (CH_2, **18**), 55.00 (CH_2, **16**), 53.18 (CH_2, **17**), 25.60 (CH_2, **20**) ppm

LRMS (ES$^+$) *m/z* = 744 [M(^{37}Cl^{37}Cl)+H]$^+$, 742 [M(^{35}Cl^{37}Cl)+H]$^+$, 740 [M(^{35}Cl^{35}Cl)+H]$^+$

HRMS (ES$^+$) For $C_{35}H_{32}(^{35}Cl^{35}Cl)N_3O_{11}^+$ calculated 740.1414, found 740.1425 Da

5-Carboxy-4',5'-bis(morpholin)-2´,7´-Dichlorofluorescein, succinimidyl ester (2.63b)

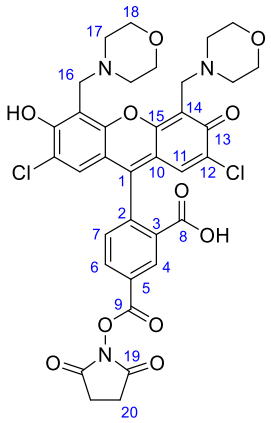

$C_{35}H_{31}Cl_2N_3O_{11}$

740.54 $gmol^{-1}$

5-Carboxy-4',5'-bis(morpholin)-2´,7´-dichlorofluorescein (**2.60b**, 150 mg, 0.23 mmol) was dissolved in CH_2Cl_2 (10 mL), then NHS (27 mg, 0.23 mmol) was added and the mixture was stirred until it dissolved. DIC (36 µL, 0.23 mmol) was added in one portion, and the reaction was stirred 30 min at rt. The solvent was evaporated and the red residue was recrystallised from EtOH to yield the pure product as a pale red solid (154 mg, 0.21 mmol, 91%).

M.P. > 250 °C

FT-IR (neat) ν_{max} = 3382 (w), 2962 (w), 2855 (w), 2611 (w), 1736 (w), 1706 (w), 1570 (m), 1459 (s), 1358 (s), 1274 (s), 1194 (m), 1067 (m), 887 (w), cm^{-1}

RAMAN (neat) ν_{max} = 408, 480, 588, 668, 698, 746, 873, 920, 1081, 1108, 1190, 1305, 1340, 1506, 1533, 1582, 1638 cm^{-1}

^{1}H NMR ($CDCl_3$, 400 MHz) δ = 8.85 (s, 1H, **4**), 8.48 (d, *J* = 7.9 Hz, 1H, **6**), 7.36 (d, *J* = 7.9 Hz, 1H, **7**), 6.62 (s, 2H, **11**), 4.01–4.14 (m, 4H, **16**), 3.85 (br s, 8H, **18**), 2.96 (br s, 4H, **20**), 2.74 (br s, 8H, **17**) ppm

^{13}C NMR ($CDCl_3$, 101 MHz) δ = 168.77 (C, **19**), 168.83 (C, **8**) 160.44 (C, **9**),156.39 (C, **15**), 154.62 (C, **2**), 147.79 (C, **13**), 136.84 (CH, **6**), 128.19 (CH, **4**), 127.97 and 127.77 (C, **3** & **5**), 127.52 (CH, **11**), 124.85 (CH, **7**), 117.70 (C, **12**), 109.20 (C, **14**), 108.37 (C, **10**), 83.00 (C, **1**), 66.43 (CH_2, **18**), 54.96 (CH_2, **16**), 53.13 (CH_2, **17**), 25.65 (CH_2, **20**) ppm

LRMS (ES$^+$) *m/z* = 744 [M(^{37}Cl^{37}Cl)+H]$^+$, 742 [M(^{35}Cl^{37}Cl)+H]$^+$, 740 [M(^{35}Cl^{35}Cl)+H]$^+$

HRMS (ES$^+$) For $C_{35}H_{32}(^{35}Cl^{35}Cl)N_3O_{11}^+$ calculated 740.1414, found 740.1425 Da

Preparation and modification of the surfaces

Electrodeposition of mesoporous silica[104]

All the experiments were carried out in plastic glassware to avoid any interaction with silica. Aqueous $NaNO_3$ (20 mL of 0.10 M, 2.00 mmol) was mixed with ethanol (20 mL); the solution was adjusted to pH 3 with HCl aqueous (0.20 M). Tetraethyl orthosilicate (0.90 mL, 4.03 mmol) was added and the solution was stirred for 90 min at rt. Cetrimonium bromide (0.47 g, 1.29 mmol) was added and the limpid solution stirred for 30 min. A three-electrode electrochemical cell was used, provided with a saturated calomel electrode (SCE) reference and a large (7 cm^2) stainless steel as counter. The working electrode was a glass coated ITO (slide or coverslip). A constant potential of −1.3 V was applied for 20 s, then the substrates were washed immediately with deionized water and dried in the oven at 130 °C overnight. The samples were then immersed in HCl-ethanol solution (0.10 M) for 5 min in order to remove all the surfactant. The deposits were then washed with ethanol and dried at 130 °C for 4 h. A thin white film was observed on the ITO surface. Characterisation by grazing incidence small angle x-ray scattering was in accordance with the literature.[104]

Electrodeposition of flat silica

All the experiments were carried out in plastic glassware to avoid any interaction with silica. Aqueous $NaNO_3$ (0.10 M, 20 mL, 2.00 mmol) was mixed with ethanol (20 mL); the solution was adjusted to pH 3 with HCl aqueous (0.20 M). Tetraethyl orthosilicate (0.90 mL, 4.03 mmol) was added and the solution was stirred for 90 min at rt. A three-electrode Electrochemical cell was used, provided with a saturated calomel electrode (SCE) reference and a large (7 cm^2) stainless steel as counter. The working electrode was a glass coated ITO (slide or coverslip). A constant potential of −1.3 V was applied for 20 s, then the substrates were washed immediately with deionized water and dried in the oven at 130 °C overnight. The deposits were then washed with ethanol and dried at 130 °C for 4 h. A thin white film was observed on the ITO surface. Characterisation by grazing incidence small angle x-ray scattering.

Addition of the linker

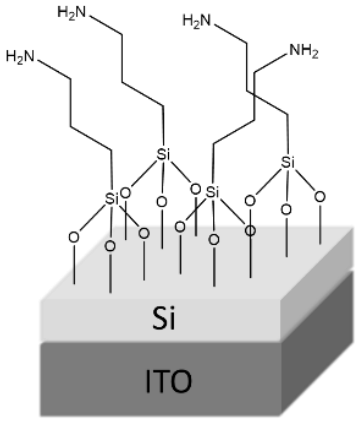

The samples of silica deposited on ITO were attached on a cap, to avoid any destruction from stirring, and immersed in a vial with a solution of APTES (0.01 mM) in EtOH (20 mL), the mixture was stirred at rt overnight. The samples were washed with EtOH and dried overnight at 130 °C. Characterisation was performed by grazing incidence small angle x-ray scattering.

Addition of the probes

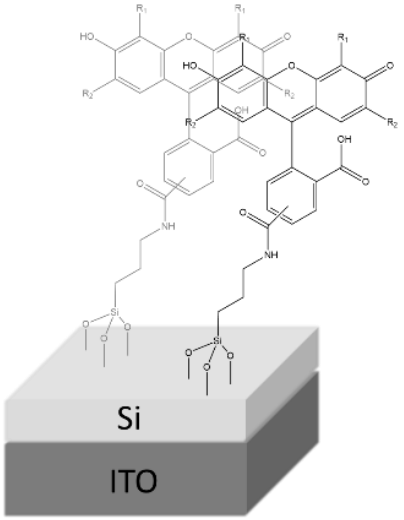

The modified silica sample was immersed in a solution of the probes (0.01 mM of **2.38$_a$**, **2.38$_b$**, **2.52$_a$**, **2.52$_b$**, **2.63$_a$**, **2.63$_b$**, **2.64$_a$** or **2.64$_b$**) in aqueous NaOH (0.05 M), and the mixture was stirred at rt overnight. The sample was washed with water and EtOH, then dried overnight at 130 °C. Characterisation was performed using Raman spectroscopy.

Modification of the surface with anthraquinone-2-carboxylic acid

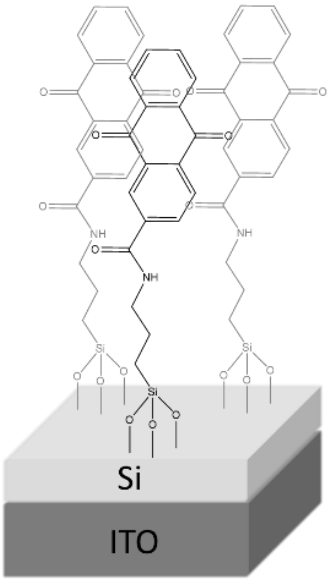

The modified silica was immersed in a solution of anthraquinone-2-carboxylic acid (25 mM), DCC (100 mM) and NHS (60 mM) in DMF. The mixture was stirred overnight and then washed with NaOH (0.1 M) and water, then the substrate was dried overnight at 130 °C.

Characterisation of the surfaces

Cyclic voltammetry of $Ru^{2+/3+}$

The cyclic voltammograms were recorded in a solution of $NaNO_3$ (0.1 M) and $[Ru(NH_3)_6]^{3+}$ (1 mM) from −0.5 V to 0.2 V *vs.* SCE at a scan rate of 0.05 $V.s^{-1}$. An ITO substrate at different stage of modification was used as working electrode.

Cyclic voltammetry of modified ITO substrate with 6-carboxyfluorescein diacetate *N*-succinimidyl ester and anthraquinone-2-carboxylic acid

The cyclic voltammograms were recorded in a tris buffer solution (pH 7.4, 50 mM) from −0.5 V to 0.2 V *vs.* SCE at a scan rate of 0.05 $V.s^{-1}$. ITO modified substrates were used as working electrode.

Raman spectroscopy

6-carboxyfluorescein substrate 2.69_a

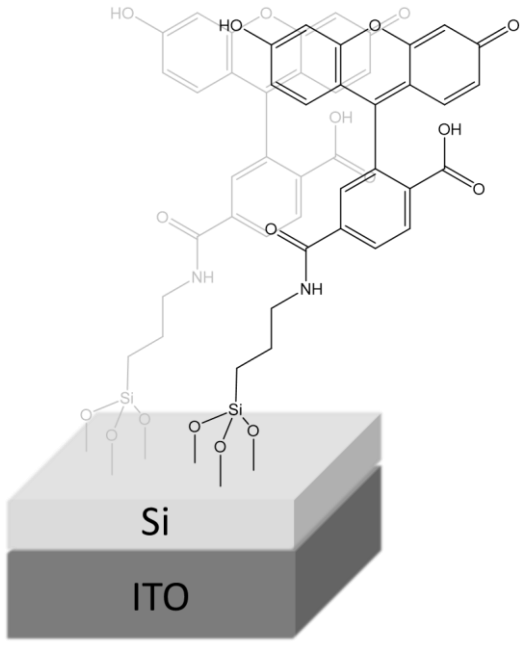

2.69_a

Raman shift: 305, 447, 529, 726, 806, 876, 994, 1051, 1103, 1241, 1302, 1357, 1420, 1575, 1899 cm^{-1}

5-carboxyfluorescein substrate 2.69$_b$

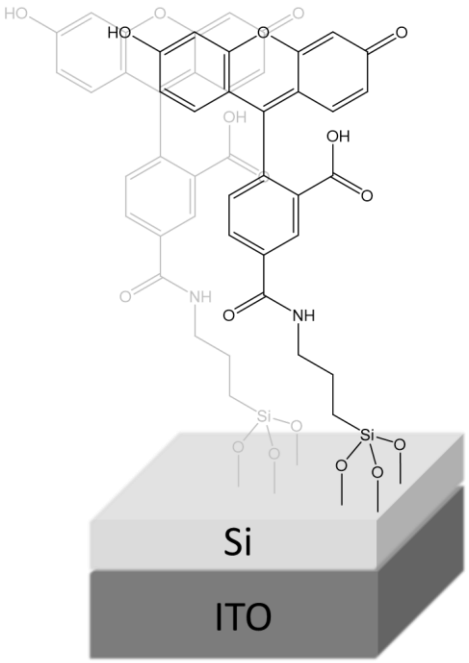

2.69$_b$

Raman shift: 221, 258, 293, 333, 380, 442, 490, 540, 571, 623, 671, 715, 755, 850, 897, 971, 1014, 1113, 1234, 1250, 1289, 1331, 1621, 1781, 1804, 732, 1172 cm^{-1}

6-Carboxy-2´,7´-Dichlorofluorescein substrate 2.70$_a$

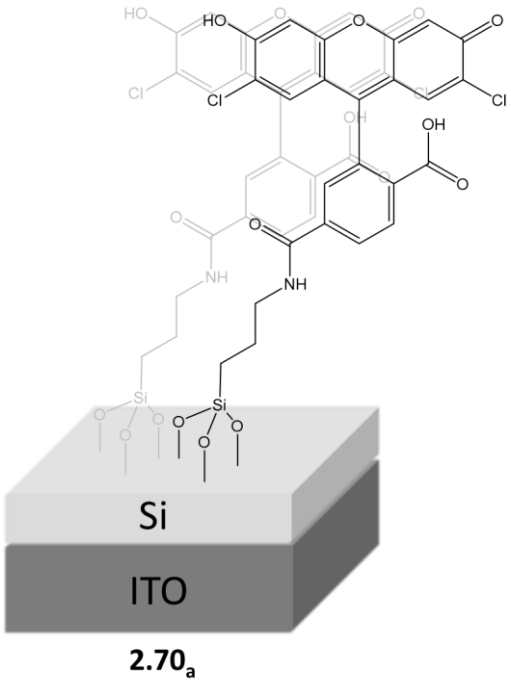

2.70$_a$

Raman shift: 306, 445, 521, 633, 727, 806, 878, 993, 1046, 1100, 1236, 1312, 1354, 1417, 1575 cm^{-1}

5-Carboxy-2´,7´-Dichlorofluorescein substrate 2.70$_b$

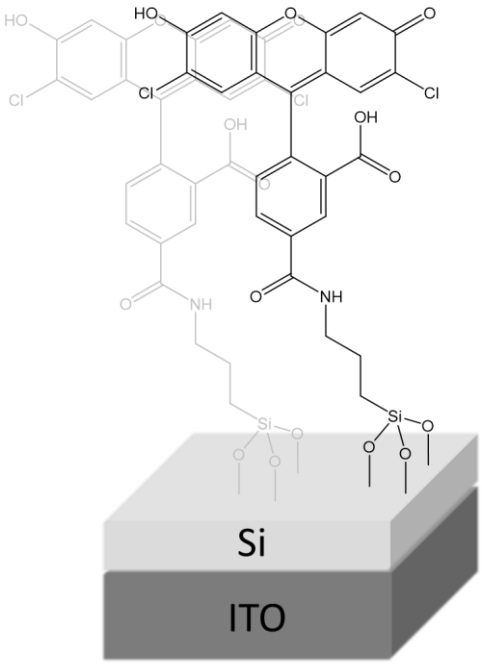

2.70$_b$

Raman shift: 450, 529, 632, 729, 805, 879, 993, 1049, 1101, 1239, 1357, 1417, 1572 cm^{-1}

6-Carboxy-4',5'-bis(Dipicolylamine)-2´,7´-Dichlorofluorescein substrate 2.72$_a$

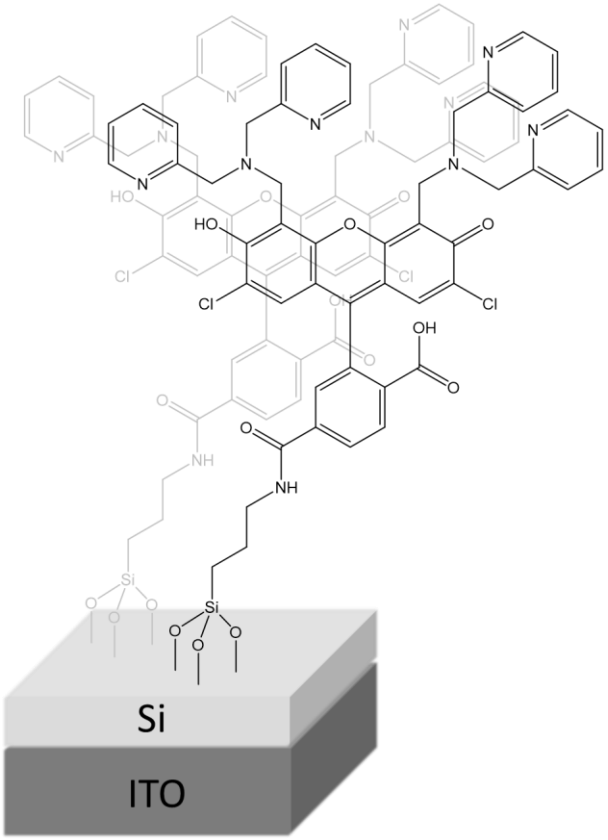

2.72$_a$

Raman shift: 305, 447, 528, 635, 729, 803, 878, 994, 1049, 1095, 1178, 1239, 1359, 1423, 1512, 1569, 1663, 1880, 2249, 2452 cm^{-1}

5-Carboxy-4',5'-bis(Dipicolylamine)-2´,7´-Dichlorofluorescein substrate 2.72$_b$

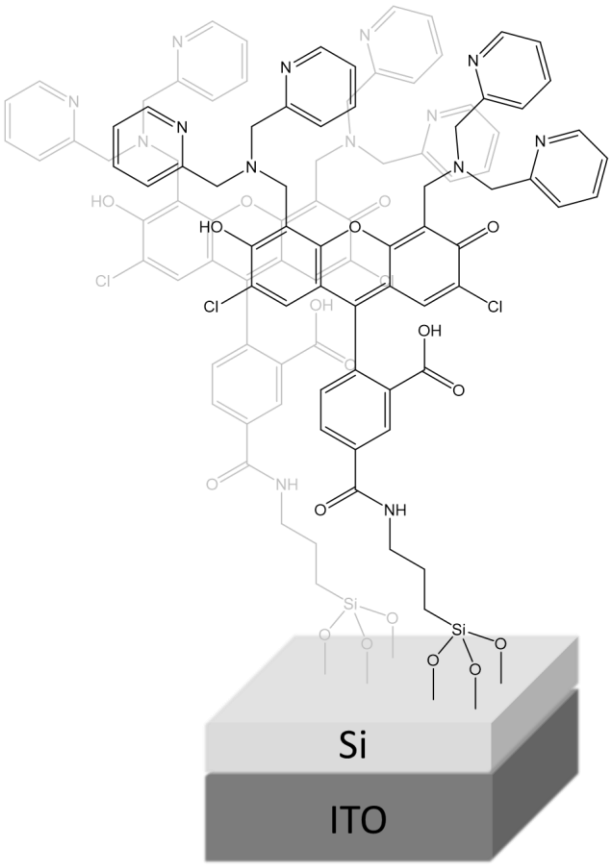

2.72$_b$

Raman shift: 312, 447, 528, 725, 803, 843, 880, 996, 1053, 1103, 1235, 1355, 1420, 1510, 1569, 1698, 1893, 2267, 2468 cm^{-1}

6-Carboxy-4',5'-bis(morpholin)-2´,7´-Dichlorofluorescein substrate 2.71$_a$

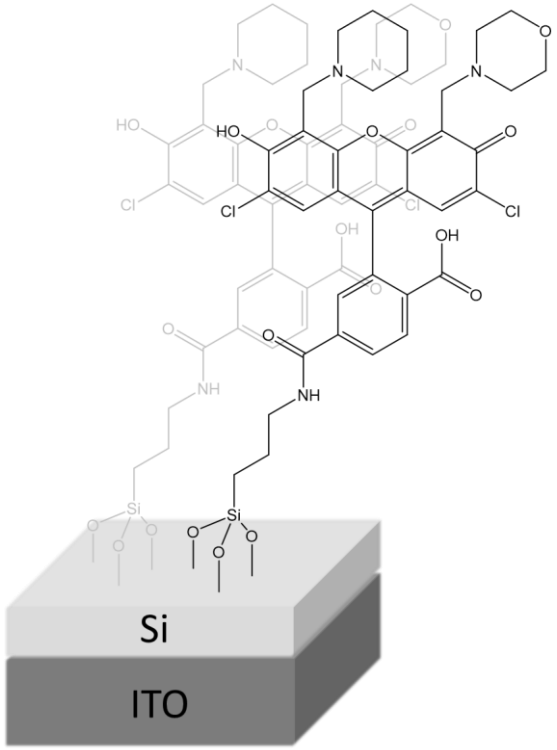

2.71$_a$

Raman shift: 285, 419, 482, 590, 673, 698, 744, 872, 920, 1107, 1193, 1308, 1373, 1504, 1535, 1641, 1580, 1883 cm^{-1}

5-Carboxy-4',5'-bis(morpholin)-2´,7´-Dichlorofluorescein substrate 2.71$_b$

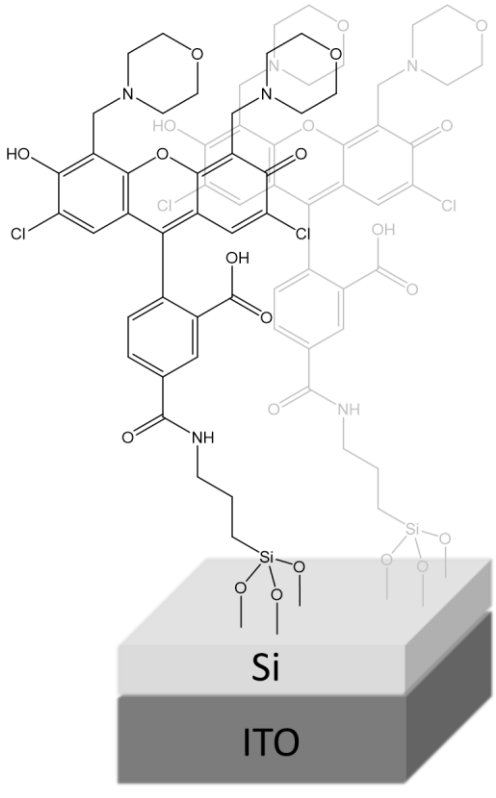

2.71$_b$

Raman shift: 287, 418, 487, 591, 671, 749, 764, 871, 922, 1105, 1193, 1310, 1342, 1374, 1505, 1580, 1636 cm^{-1}

Fluorescent experiments

Spectroscopic Measurements

All glassware was washed sequentially with deionized water and ethanol and oven dried before use. Purified water was obtained from a Millipore Milli-Q water purification system. Fluorophore stock solutions in DMSO were made up to concentrations of 1 mM and kept at 4 °C in 2 mL aliquots. Portions were diluted to the required concentrations immediately prior to each experiment. Fluorescence and absorption data were measured in HEPES buffer (50 mM, pH 7.5, KCl or NaBr 100 mM) except for the fluorescein standard in quantum yield measurements. Fluorescence spectra were measured from 475 nm to 650 nm.

Determination of pK_a in solution

A 1 mM stock solution of the fluorophore was diluted with 20 mL of an aqueous solution of KCl (100 mM) and EDTA (1 mM) to a final concentration of 1 μM. The pH was brought to 11.0 with aqueous KOH (45% w/v), then gradually monitored and lowered to pH 2, the fluorescence spectrum was recorded at different pH. The integrated emission area was normalized, plotted as a function of pH, and fitted to an equation using Origin. This procedure was applied to all the prepared fluorophores except for the potassium probe where NaBr was used instead of KCl.

Determination of pK_a on the surface

An aqueous solution of KCl (100 mM) and EDTA (1 mM) was brought to pH 11.0 with aqueous KOH (45% w/v), then gradually monitored and lowered to pH 2. 3 mL of the solution was kept on the side at different pH. The modified surface was immersed in the 3 mL samples previously prepared and an emission spectrum was recorded at each pH. The integrated emission area was normalized, plotted as a function of pH, and fitted to an equation using Origin. This procedure was applied to all the prepared fluorophores except for the potassium probe where NaBr was used instead of KCl.

Determination of extinction coefficient for the pH probes

Fluorophore stock was titrated in 3 mL HEPES buffer; the absorption was measured at each concentration (0–15 μM). The absorbance at the maximum was plotted as a function of concentration, and the slope was taken as the extinction coefficient. The procedure was repeated using 1.9 mL portions HEPES buffer containing 100 μL aliquots of $ZnCl_2$(10 mM) solution for the zinc probe and 100 μL of KCl (10 mM) for the potassium probe.

Determination of extinction coefficient of the zinc probe

Fluorophore stock was titrated in 3 mL HEPES buffer; the absorption was measured at each concentration (0–15 μM). The absorbance at the maximum was plotted as a function of concentration, and the slope was taken as the extinction coefficient. The procedure was repeated using 1.9 mL portions HEPES buffer containing 100 μL aliquots of $ZnCl_2$(10 mM) solution for the zinc probe and 100 μL of KCl (10 mM) for the potassium probe.

Determination of extinction coefficient of the potassium probe

Fluorophore stock was titrated in 3 mL HEPES buffer; the absorption was measured at each concentration (0–15 μM). The absorbance at the maximum was plotted as a function of concentration, and the slope was taken as the extinction coefficient. The procedure was repeated using 1.9 mL portions HEPES buffer containing 100 μL aliquots of μL of KCl (10 mM).

Relative determination of fluorescence quantum yield

An absorption spectrum was measured for the sample (*A* as a function of wavelength); if necessary to minimize possible reabsorption effects, dilute the dye solution until the absorbance reaches a maximum value of 0.1 at the longest wavelength absorption band. Fluorescein (0.1 μM in 0.1 M NaOH) was chosen as quantum yield standard, its absorption spectrum was measured. Excitation wavelength was chosen such that the sample and the standard are excited at an almost plateau-like region of their absorption spectra or at least at a wavelength with little slope in the absorption spectrum. Fluorescence spectrometer was chosen with settings such that the sample and the standard can be measured with identical instrument settings (excitation wavelength, slit widths of excitation and emission monochromator, scan speed, integration time). The fluorescence spectrum of each was then recorded, exciting at the wavelength determined by UV-vis spectral comparison. The photoluminescence quantum yield was calculated according to the following equation:

$$\Phi_{\mathrm{f,x}} = \Phi_{\mathrm{f,st}} \cdot \frac{F_{\mathrm{x}}}{F_{\mathrm{st}}} \cdot \frac{f_{\mathrm{st}}}{f_x} \cdot \frac{n_{\mathrm{x}}^2(\lambda_{\mathrm{em}})}{n_{\mathrm{st}}^2(\lambda_{\mathrm{em}})}$$

Φ_{f}: quantum yield; F: Integral of photon flux; f: absorption factor; n: refractive index of the solvent; x: sample; st: standard.

With $\Phi_{\mathrm{f,st}} = 0.95$ and $n_{\mathrm{x}}^2(\lambda_{\mathrm{em}}) = n_{\mathrm{st}}^2(\lambda_{\mathrm{em}})$

Metal ion selectivity of the zinc probes

The fluorescence spectrum of a 3 mL aliquot of 1 μM fluorophore excited at 512 nm was acquired by itself, after addition of a 4 μL ($CaCl_2$, $MgCl_2$, 1.00 M) or 10 μL (NaCl 2.00 M, $MnSO_4$, $CoCl_2$, $NiCl_2$, $CuCl_2$, $CdCl_2$10 mM) aliquot of metal stock solution, and after addition

of a 10 µL aliquot of $ZnCl_2$ (10 mM). The integrated emission of each spectrum was normalized to that of the metal-free control spectrum.

Limit of detection for the zinc probe in solution

To a 3 mL solution of the fluorophore (1 µM) was added $ZnCl_2$ at different concentration (0.2–2 µM), every 0.2 µM emission spectra were recorded. The integrated emission spectra were normalized and plotted as function of the concentration of $ZnCl_2$.

Limit of detection for the zinc probe on the surface

To the modified surface in the buffer solution was added $ZnCl_2$ at different concentrations (0.2–2.0 nM), every 0.2 nM emission spectra were recorded. The integrated emission spectra were normalized and plotted as function of the concentration of $ZnCl_2$

Limit of detection for the potassium probe in solution

To a 3 mL solution of the fluorophore (1 µM) was added KCl at different concentration (0.2–2.0 µM), every 0.2 µM emission spectra were recorded. The integrated emission spectra were normalized and plotted as function of the concentration of $ZnCl_2$.

Limit of detection for the potassium probe on the surface

To the modified surface in the buffer solution was added $ZnCl_2$ at different concentrations (0.2–2.0 nM), every 0.2 nM emission spectra were recorded. The integrated emission spectra were normalized and plotted as function of the concentration of $ZnCl_2$.

Chapter 5 References

1. Steiner, R. A.; Oehme, M.; Ammann, D.; Simon, W., *Analytical Chemistry* **1979,** *51* (3), 351-353.

2. Han, J.; Burgess, K., *Chem. Rev.* **2010,** *110* (5), 2709-2728.

3. Roos, A.; Boron, W. F., *Physiol. Rev.* **1981,** *61* (2), 296-434.

4. Rui, W.; Chunwei, Y.; Fabiao, Y.; Lingxin, C., *TRAC Trends in Analytical Chemistry* **2010,** *29* (9), 1004-1013.

5. Progatzky, F.; Dallman, M. J.; Lo Celso, C., *Interface Focus* **2013,** *3* (3).

6. Fellenz, M. P.; Gerweck, L. E., *Radiation Research* **1988,** *116* (2), 305-312.

7. Hansen, G.; Johansen, C. L.; Marten, G.; Wilmes, J.; Jespersen, L.; Arneborg, N., *Applied Microbiology and Biotechnology* **2016,** *100* (13), 5965-5976.

8. Teisseyre, A.; Mozrzymas, J., *Journal of Physiology and Pharmacology* **2006,** *57* (1), 131-147.

9. Lardner, A., *Journal of Leukocyte Biology* **2001,** *69* (4), 522-530.

10. Enger, E., *Concepts in Biology*. 10th ed.; McGraw Hill: 2003.

11. Kinkel, H.; Baumann, K. H.; Cepek, M., *Marine Micropaleontology* **2000,** *39* (4), 87-112.

12. Bach, L. T.; Mackinder, L. C. M.; Schulz, K. G.; Wheeler, G.; Schroeder, D. C.; Brownlee, C.; Riebesell, U., *New Phytologist* **2013,** *199* (1), 121-134.

13. Lim, N. C.; Schuster, J. V.; Porto, M. C.; Tanudra, M. A.; Yao, L.; Freake, H. C.; Bruckner, C., *Inorganic Chemistry* **2005,** *44* (6), 2018-2030.

14. von Dassow, P.; van den Engh, G.; Iglesias-Rodriguez, D.; Gittins, J. R., *Journal of Plankton Research* **2012,** *34* (12), 1011-1027.

15. Hutchins, D. A., *Nature* **2011,** *476* (7358), 41-42.

16. Cheng, C. J.; Kuo, E.; Huang, C. L., *Seminars in Nephrology* **2013,** *33* (3), 237-247.

17. Frederickson, C. J., *International Review of Neurobiology* **1989,** *31*, 145-238.

18. Takeda, A.; Tamano, H.; Ogawa, T.; Takada, S.; Nakamura, M.; Fujii, H.; Ando, M., *Hippocampus* **2014,** *24* (11), 1404-1412.

19. Hey, J. G.; Chu, X. P.; Seeds, J.; Simon, R. P.; Xiong, Z. G., *Stroke* **2007,** *38* (2), 670-673.

20. Higashi, Y.; Aratake, T.; Shimizu, S.; Shimizu, T.; Nakamura, K.; Tsuda, M.; Yawata, T.; Ueba, T.; Saito, M., *Scientific Reports* **2017,** *7*, 13.

21. Frederickson, C. J.; Giblin, L. J.; Krezel, A.; McAdoo, D. J.; Muelle, R. N.; Zeng, Y.; Balaji, R. V.; Masalha, R.; Thompson, R. B.; Fierke, C. A.; Sarvey, J. M.; de Valdenebro, M.; Prough, D. S.; Zornow, M. H., *Experimental Neurology* **2006,** *198* (2), 285-293.

22. King, M.; Kopelman, R., *Sensors and Actuators B-Chemical* **2003,** *90* (1-3), 76-81.

23. Behrendt, J. M.; Nagel, D.; Chundoo, E.; Alexander, L. M.; Dupin, D.; Hine, A. V.; Bradley, M.; Sutherland, A. J., *PLoS One* **2013,** *8* (3), e50713.

24. Xu, H.; Aylott, J. W.; Kopelman, R.; Miller, T. J.; Philbert, M. A., *Analytical Chemistry* **2001,** *73* (17), 4124-4133.

25. Urano, Y.; Asanuma, D.; Hama, Y.; Koyama, Y.; Barrett, T.; Kamiya, M.; Nagano, T.; Watanabe, T.; Hasegawa, A.; Choyke, P. L.; Kobayashi, H., *Nature Medicine* **2009,** *15* (1), 104-109.

26. Callan, J. F.; de Silva, A. P.; Magri, D. C., *Tetrahedron* **2005,** *61* (36), 8551-8588.

27. Fei, X. N.; Gu, Y. C., *Progress in Natural Science-Materials International* **2009,** *19* (1), 1-7.

28. Zhang, X. X.; Wang, Z.; Yue, X.; Ma, Y.; Kiesewetter, D. O.; Chen, X., *Molecular Pharmaceutics* **2013,** *10* (5), 1910-1907.

29. Liu, W.; Sun, R.; Ge, J. F.; Xu, Y. J.; Xu, Y.; Lu, J. M.; Itoh, I.; Ihara, M., *Analytical Chemistry* **2013,** *85* (15), 7419-7425.

30. Cao, L. X.; Li, X. Y.; Wang, S. Q.; Li, S. Y.; Li, Y.; Yang, G. Q., *Chemical Communications* **2014,** *50* (63), 8787-8790.

31. Tian, M. Z.; Peng, X. J.; Fan, J. L.; Wang, J. Y.; Sun, S. G., *Dyes and Pigments* **2012,** *95* (1), 112-115.

32. Lavis, L. D.; Chao, T. Y.; Raines, R. T., *ACS Chemical Biology* **2006,** *1* (4), 252-260.

33. Asanuma, D.; Takaoka, Y.; Namiki, S.; Takikawa, K.; Kamiya, M.; Nagano, T.; Urano, Y.; Hirose, K., *Angewandte Chemie-International Edition* **2014,** *53* (24), 6085-6089.

34. Jokic, T.; Borisov, S. M.; Saf, R.; Nielsen, D. A.; Kuhl, M.; Klimant, I., *Analytical Chemistry* **2012,** *84* (15), 6723-6730.

35. Baruah, M.; Qin, W.; Basaric, N.; De Borggraeve, W. M.; Boens, N., *Journal of Organic Chemistry* **2005,** *70* (10), 4152-4157.

36. Hecht, M.; Fischer, T.; Dietrich, P.; Kraus, W.; Descalzo, A. B.; Unger, W. E.; Rurack, K., *ChemistryOpen* **2013,** *2* (1), 25-38.

37. Yue, Y. K.; Huo, F. J.; Lee, S.; Yin, C. X.; Yoon, J., *Analyst* **2017,** *142* (1), 30-41.

38. Yin, J.; Hu, Y.; Yoon, J., *Chemical Society Reviews* **2015,** *44* (14), 4619-4644.

39. Robertson, T. A.; Bunel, F.; Roberts, M. S., *Cells* **2013,** *2* (3), 591-606.

40. Adamczyk, M.; Chan, C. M.; Fino, J. R.; Mattingly, P. G., *J Org Chem* **2000,** *65* (2), 596-601.

41. Diwu, Z.; Twu, J. J.; Yi, G.; Lavis, L. D.; Chen, Y.-W.; Cassutt, K. J. US 6800765, **2004**.

42. Ge, F. Y.; Chen, L. G., *Journal of Fluorescence* **2008,** *18* (3-4), 741-747.

43. Ou, B. X.; Hampsch-Woodill, M.; Prior, R. L., *Journal of Agricultural and Food Chemistry* **2001,** *49* (10), 4619-4626.

44. Sjoback, R.; Nygren, J.; Kubista, M., *Spectrochimica Acta Part A : Molecular and Biomolecular Spectroscopy* **1995,** *51* (6), 7-21.

45. Bradley, M.; Alexander, L.; Duncan, K.; Chennaoui, M.; Jones, A. C.; Sanchez-Martin, R. M., *Bioorganic and Medicinal Chemistry Letters* **2008,** *18* (1), 313-307.

46. Hammond, V. J.; Aylott, J. W.; Greenway, G. M.; Watts, P.; Webster, A.; Wiles, C., *Analyst* **2008,** *133* (1), 71-5.

47. Nooney, R. I.; McCormack, E.; McDonagh, C., *Analytical and Bioanalytical Chemistry* **2012,** *404* (10), 2807-2818.

48. Tusa, J. K.; He, H. R., *Journal of Materials Chemistry* **2005,** *15* (27-28), 2640-2647.

49. Messerli, M. A.; Collis, L. P.; Smith, P. J. S., *Biophysical Journal* **2009,** *96* (4), 1597-1605.

50. Yu, J. C.; Zhang, L. Q.; Xu, X.; Liu, S. Q., *Analytical Chemistry* **2014,** *86* (21), 10741-10748.

51. Zhang, S.; Zhang, R. B.; Ma, B. J.; Qiu, J. C.; Li, J. H.; Sang, Y. H.; Liu, W.; Liu, H., *Rsc Advances* **2016,** *6* (48), 41999-42007.

52. Yu, B. R.; Wang, B. Y.; Guo, S. W.; Zhang, Q.; Zheng, X. R.; Lei, H. T.; Liu, W. S.; Bu, W. F.; Zhang, Y.; Chen, X., *Chemistry-a European Journal* **2013,** *19* (15), 4922-4930.

53. Hirata, T.; Terai, T.; Yamamura, H.; Shirnonishi, M.; Komatsu, T.; Hanaoka, K.; Ueno, T.; Imaizumi, Y.; Nagano, T.; Urano, Y., *Analytical Chemistry* **2016,** *88* (5), 2693-2700.

54. Zhou, X. F.; Su, F. Y.; Tian, Y. Q.; Youngbull, C.; Johnson, R. H.; Meldrum, D. R., *Journal of the American Chemical Society* **2011,** *133* (46), 18530-18533.

55. de Silva, A. P.; Gunaratne, H. Q. N.; Gunnlaugsson, T.; Huxley, A. J. M.; McCoy, C. P.; Rademacher, J. T.; Rice, T. E., *Chemical Reviews* **1997,** *97* (5), 1515-1566.

56. de Silva, A. P.; Moody, T. S.; Wright, G. D., *Analyst* **2009,** *134* (12), 2385-2393.

57. Pearson, A. J.; Xiao, W. J., *Journal of Organic Chemistry* **2003,** *68* (13), 5361-+.

58. Liou, C. C.; Brodbelt, J. S., *Journal of the American Society for Mass Spectrometry* **1992,** *3* (5), 543-548.

59. Subhodip, S.; Pinkisaha, S.; Shyam Sundar, M.; Anirban, P.; Maitrayee Basu, R.; Sanjib, G., *Journal of Chemical Sciences* **2007,** *119* (2), 175-183.

60. Harootunian, A. T.; Kao, J. P.; Eckert, B. K.; Tsien, R. Y., *Journal of Biological Chemistry* **1989,** *264* (32), 19458-19467.

61. Meuwis, K.; Boens, N.; De Schryver, F. C.; Gallay, J.; Vincent, M., *Biophysical journal.* **1995,** *68* (6), 2469-2473.

62. He, H. R.; Mortellaro, M. A.; Leiner, M. J. P.; Fraatz, R. J.; Tusa, J. K., *Journal of the American Chemical Society* **2003,** *125* (6), 1468-1469.

63. Xianfeng, Z.; Fengyu, S.; Weimin, G.; Yanqing, T.; Youngbull, C.; Johnson, R. H.; Meldrum, D. R., *Biomaterials* **2011,** *32* (33), 8574-8583.

64. He, H.; Mortellaro, M. A.; Leiner, M. J.; Young, S. T.; Fraatz, R. J.; Tusa, J. K., *Analytical Chemistry* **2003,** *75* (3), 549-555.

65. Carpenter, R. D.; Verkman, A. S., *European Journal of Organic Chemistry* **2011,** *2011* (7), 1242-1248.

66. Ast, S.; Schwarze, T.; Muller, H.; Sukhanov, A.; Michaelis, S.; Wegener, J.; Wolfbeis, O. S.; Korzdorfer, T.; Durkop, A.; Holdt, H. J., *Chemistry* **2013,** *19* (44), 14911-14917.

67. Ast, S.; Fischer, T.; Muller, H.; Mickler, W.; Schwichtenberg, M.; Rurack, K.; Holdt, H. J., *Chemistry* **2013,** *19* (9), 2990-3005.

68. Carter, K. P.; Young, A. M.; Palmer, A. E., *Chemistry Review* **2014,** *114* (8), 4564-4601.

69. Kiyose, K.; Kojima, H.; Urano, Y.; Nagano, T., *Journal of the American Chemical Society* **2006,** *128* (20), 6548-6549.

70. Nolan, E. M.; Lippard, S. J., *Accounts of Chemical Research* **2009,** *42* (1), 193-203.

71. Komatsu, K.; Urano, Y.; Kojima, H.; Nagano, T., *Journal of the American Chemical Society* **2007,** *129* (44), 13447-13454.

72. Zhang, X. A.; Hayes, D.; Smith, S. J.; Friedle, S.; Lippard, S. J., *Journal of the American Chemical Society* **2008,** *130* (47), 15788-15789.

73. Woodroofe, C. C.; Masalha, R.; Barnes, K. R.; Frederickson, C. J.; Lippard, S. J., *Chemistry and Biology* **2004,** *11* (12), 1659-1666.

74. Buccella, D.; Horowitz, J. A.; Lippard, S. J., *Journal of American Chemical Society* **2011,** *133* (11), 4101-4114.

75. Webster, A.; Compton, S. J.; Aylott, J. W., *Analyst* **2005,** *130* (2), 163-170.

76. Schwarze, T.; Muller, H.; Ast, S.; Steinbruck, D.; Eidner, S.; Geissler, F.; Kumke, M. U.; Holdt, H. J., *Chemistry Communication* **2014,** *50* (91), 14167-14170.

77. Xu, H.; Aylott, J. W.; Kopelman, R., *Analyst* **2002,** *127* (11), 1471-1477.

78. Budd, P. M.; Makhseed, S. M.; Ghanem, B. S.; Msayib, K. J.; Tattershall, C. E.; McKeown, N. B., *Materials Today* **2004,** *7* (4), 40-46.

79. Chang, F.; Zhou, J.; Chen, P.; Chen, Y. L.; Jia, H. H.; Saad, S. M. I.; Gao, Y.; Cao, X.; Zheng, T., *Asia-Pacific Journal of Chemical Engineering* **2013,** *8* (4), 618-626.

80. Navrotsky, A.; Trofymluk, O.; Levchenko, A. A., *Chemical Reviews* **2009,** *109* (9), 3885-3902.

81. Izaak, T. I.; Vodyankina, O. V., *Russian Chemical Reviews* **2009,** *78* (1), 77-88.

82. Wang, B. J.; Prinsen, P.; Wang, H. Z.; Bai, Z. S.; Wang, H. L.; Luque, R.; Xuan, J., *Chemical Society Reviews* **2017,** *46* (3), 855-914.

83. Yang, X. Y.; Chen, L. H.; Li, Y.; Rooke, J. C.; Sanchez, C.; Su, B. L., *Chemical Society Reviews* **2017,** *46* (2), 481-558.

84. Zhang, P. F.; Zhang, J. S.; Dai, S., *Chemistry-a European Journal* **2017,** *23* (9), 1986-1998.

85. Innocenzi, P.; Malfatti, L.; Carboni, D., *Nanoscale* **2015,** *7* (30), 12759-12772.

86. Liu, L.; Yuan, Z. Y., *Progress in Chemistry* **2014,** *26* (5), 756-771.

87. Liang, C. D.; Li, Z. J.; Dai, S., *Angewandte Chemie-International Edition* **2008,** *47* (20), 3696-3717.

88. Bae, E. J.; Choi, W. B.; Jeong, K. S.; Chu, J. U.; Park, G. S.; Song, S.; Yoo, I. K., *Advanced Materials* **2002,** *14* (4), 277-279.

89. Deng, X. H.; Chen, K.; Tuysuz, H., *Chemistry of Materials* **2017,** *29* (1), 40-52.

90. Ren, Y.; Ma, Z.; Bruce, P. G., *Chemical Society Reviews* **2012,** *41* (14), 4909-4927.

91. Choi, K. S.; McFarland, E. W.; Stucky, G. D., *Advanced Materials* **2003,** *15* (23), 2018-2021.

92. Mahoney, L.; Koodali, R. T., *Materials* **2014,** *7* (4), 2697-2746.

93. Hoffmann, F.; Cornelius, M.; Morell, J.; Froba, M., *Angewandte Chemie-International Edition* **2006,** *45* (20), 3216-3251.

94. Melde, B. J.; Johnson, B. J.; Charles, P. T., *Sensors* **2008,** *8* (8), 5202-5228.

95. Dian, J.; Konecny, M.; Broncova, G.; Krondak, M.; Matolinova, I., *International Journal of Electrochemical Science* **2013,** *8* (2), 1559-1572.

96. Li, W.; Ding, L.; Wang, Q.; Su, B., *Analyst* **2014,** *139* (16), 3926-3931.

97. Vila, N.; Ghanbaja, J.; Aubert, E.; Walcarius, A., *Angewandte Chemie-International Edition* **2014,** *53* (11), 2945-2950.

98. Kresge, C. T.; Leonowicz, M. E.; Roth, W. J.; Vartuli, J. C.; Beck, J. S., *Nature* **1992,** *359* (6397), 710-712.

99. Berlier, G.; Gastaldi, L.; Ugazio, E.; Miletto, I.; Iliade, P.; Sapino, S., *Journal of Colloid Interface Science* **2013,** *393*, 109-118.

100. Nandiyanto, A. B. D.; Kim, S. G.; Iskandar, F.; Okuyama, K., *Microporous and Mesoporous Materials* **2009,** *120* (3), 447-453.

101. Edler, K. J.; Roser, S. J., *International Reviews in Physical Chemistry* **2001,** *20* (3), 387-466.

102. Hench, L. L.; West, J. K., *Chemical Reviews* **1990,** *90* (1), 33-72.

103. Walcarius, A.; Sibottier, E.; Etienne, M.; Ghanbaja, J., *Nature Materials* **2007,** *6* (8), 602-608.

104. Robertson, C.; Beanland, R.; Boden, S. A.; Hector, A. L.; Kashtiban, R. J.; Sloan, J.; Smith, D. C.; Walcarius, A., *Physical Chemistry Chemical Physics* **2015,** *17* (6), 4763-4770.

105. Herzog, G.; Sibottier, E.; Etienne, M.; Walcarius, A., *Faraday Discuss* **2013,** *164*, 259-273.

106. Walcarius, A., *Electroanalysis* **2008,** *20* (7), 711-738.

107. Walcarius, A., *Analytical Bioanalytical Chemistry* **2010,** *396* (1), 261-272.

108. Walcarius, A., *Chemical Society Reviews* **2013,** *42* (9), 4098-4140.

109. Lu, H. T., *Colloid Journal* **2013,** *75* (3), 311-318.

110. Wu, J. B.; Ling, L. X.; Xie, J. B.; Ma, G. Z.; Wang, B. J., *Chemical Physics Letters* **2014,** *591*, 227-232.

111. Gun'ko, V. M.; Voronina, O. E.; Voronin, E. F.; Zarko, V. I.; Pakhlov, E. M.; Leboda, R.; Skubiszewska-Zieba, J.; Janusz, W.; Chikowski, S., *Polish Journal of Chemistry* **2005,** *79* (11), 1787-1804.

112. Goux, A.; Etienne, M.; Aubert, E.; Lecomte, C.; Ghanbaja, J.; Walcarius, A., *Chemistry of Materials* **2009,** *21* (4), 731-741.

113. Liu, Y. G.; Lu, Y. S.; Prashad, M.; Repic, J.; Blacklock, T. J., *Advanced Synthesis & Catalysis* **2005,** *347* (2-3), 217-219.

114. MacGregor, K. A.; Robertson, M. J.; Young, K. A.; von Kleist, L.; Stahlschmidt, W.; Whiting, A.; Chau, N.; Robinson, P. J.; Haucke, V.; McCluskey, A., *Journal of Medicinal Chemistry* **2014,** *57* (1), 131-143.

115. Klapars, A.; Antilla, J. C.; Huang, X. H.; Buchwald, S. L., *Journal of the American Chemical Society* **2001,** *123* (31), 7727-7729.

116. Vrba, Z., *Collection of Czechoslovak Chemical Communications* **1981,** *46* (1), 92-100.

117. Baeten, M.; Maes, B. U. W., *Advances in Organometallic Chemistry, 67*, **2017**; 401-481.

118. Guo, X.; Rao, H. H.; Fu, H.; Jiang, Y. Y.; Zhao, Y. F., *Advanced Synthesis & Catalysis* **2006,** *348* (15), 2197-2202.

119. Chinchilla, R.; Najera, C., *Chemical Society Reviews* **2011,** *40* (10), 5084-5121.

120. Li, X. L.; Lin, Y. J.; Yuan, Y. K.; Liu, K.; Qian, X. H., *Tetrahedron* **2011,** *67* (12), 2299-2304.

121. Hammershoj, P.; Kumar, E. K. P.; Harris, P.; Andresen, T. L.; Clausen, M. H., *European Journal of Organic Chemistry* **2015,** (33), 7301-7309.

122. Brunet, A.; Aslam, T.; Bradley, M., *Bioorganic & Medicinal Chemistry Letters* **2014,** *24* (14), 3186-3188.

123. Kim, H. N.; Swamy, K. M. K.; Yoon, J., *Tetrahedron Letters* **2011,** *52* (18), 2340-2343.

124. Swamy, K. M. K.; Kim, H. N.; Soh, J. H.; Kim, Y.; Kim, S. J.; Yoon, J., *Chemical Communications* **2009,** (10), 1234-1236.

125. Ishii, Y.; Nishiwaki, Y.; Al-zubaidi, A.; Kawasaki, S., *Journal of Physical Chemistry* **2013,** *117* (35), 18120-18130.

126. Kishor, R.; Ghoshal, A. K., *Chemical Engineering Journal* **2015,** *262*, 882-890.

127. Luo, G. F.; Chen, W. H.; Liu, Y.; Zhang, J.; Cheng, S. X.; Zhuo, R. X.; Zhang, X. Z., *Journal of Materials Chemistry B* **2013,** *1* (41), 5723-5732.

128. Compton, R. G.; Mason, D.; Unwin, P. R., *Journal of the Chemical Society-Faraday Transactions I* **1988,** *84*, 483-489.

129. Celiktas, A.; Ghanem, M. A.; Bartlett, P. N., *Journal of Electroanalytical Chemistry* **2012,** *670*, 42-49.

130. Chretien, J. M.; Ghanem, M. A.; Bartlett, P. N.; Kilburn, J. D., *Chemistry-a European Journal* **2008,** *14* (8), 2548-2556.

131. Ghanem, M. A.; Kocak, I.; Al-Mayouf, A.; AlHoshan, M.; Bartlett, P. N., *Electrochimica Acta* **2012,** *68*, 74-80.

132. Wang, L. L.; Roitberg, A.; Meuse, C.; Gaigalas, A. K., *Spectrochimica Acta Part a-Molecular and Biomolecular Spectroscopy* **2001,** *57* (9), 1781-1791.

133. Massou, S.; Albigot, R.; Prats, M., *Biochemical Education* **2000,** *28* (3), 171-173.

134. Wurth, C.; Grabolle, M.; Pauli, J.; Spieles, M.; Resch-Genger, U., *Nature Protocols* **2013,** *8* (8), 1535-1550.

135. Song, L. L.; Hennink, E. J.; Young, I. T.; Tanke, H. J., *Biophysical Journal* **1995,** *68* (6), 2588-2600.

136. Armarego, W. L. F.; Chai, C. L. L., *Purification of Laboratory Chemicals, 6th Edition* **2009**, 1-743.

137. Davila, J.; Chassepot, A.; Longo, J.; Boulmedais, F.; Reisch, A.; Frisch, B.; Meyer, F.; Voegel, J. C.; Mesini, P. J.; Senger, B.; Metz-Boutigue, M. H.; Hemmerle, J.; Lavalle, P.; Schaaf, P.; Jierry, L., *Journal of the American Chemical Society* **2012,** *134* (1), 83-86.

138. Ares, J. J.; Kador, P. F.; Miller, D. D., *Journal of Medicinal Chemistry* **1986,** *29* (11), 2384-2389.

139. Montgomery, J. A.; Shortnacy, A. T.; Carson, D. A.; Secrist, J. A., *Journal of Medicinal Chemistry* **1986,** *29* (11), 2389-2392.

140. Kogiso, T.; Yamamoto, K.; Suemune, H.; Usui, K., *Organic & Biomolecular Chemistry* **2012,** *10* (15), 2934-2936.